

# Toxicity mechanisms, exposure, toxicokinetic and risk assessment aspects of metals, toxic for animals and humans, volume II

**Edited by**

Fatma Mohamady El-Demerdash, Alex Boye,  
Michel Mansur Machado, Yanzhu Zhu, Xinwei Li and Xu Yang

**Published in**

Frontiers in Pharmacology



#### FRONTIERS EBOOK COPYRIGHT STATEMENT

The copyright in the text of individual articles in this ebook is the property of their respective authors or their respective institutions or funders. The copyright in graphics and images within each article may be subject to copyright of other parties. In both cases this is subject to a license granted to Frontiers.

The compilation of articles constituting this ebook is the property of Frontiers.

Each article within this ebook, and the ebook itself, are published under the most recent version of the Creative Commons CC-BY licence. The version current at the date of publication of this ebook is CC-BY 4.0. If the CC-BY licence is updated, the licence granted by Frontiers is automatically updated to the new version.

When exercising any right under the CC-BY licence, Frontiers must be attributed as the original publisher of the article or ebook, as applicable.

Authors have the responsibility of ensuring that any graphics or other materials which are the property of others may be included in the CC-BY licence, but this should be checked before relying on the CC-BY licence to reproduce those materials. Any copyright notices relating to those materials must be complied with.

Copyright and source acknowledgement notices may not be removed and must be displayed in any copy, derivative work or partial copy which includes the elements in question.

All copyright, and all rights therein, are protected by national and international copyright laws. The above represents a summary only. For further information please read Frontiers' Conditions for Website Use and Copyright Statement, and the applicable CC-BY licence.

ISSN 1664-8714  
ISBN 978-2-83251-436-8  
DOI 10.3389/978-2-83251-436-8

## About Frontiers

Frontiers is more than just an open access publisher of scholarly articles: it is a pioneering approach to the world of academia, radically improving the way scholarly research is managed. The grand vision of Frontiers is a world where all people have an equal opportunity to seek, share and generate knowledge. Frontiers provides immediate and permanent online open access to all its publications, but this alone is not enough to realize our grand goals.

## Frontiers journal series

The Frontiers journal series is a multi-tier and interdisciplinary set of open-access, online journals, promising a paradigm shift from the current review, selection and dissemination processes in academic publishing. All Frontiers journals are driven by researchers for researchers; therefore, they constitute a service to the scholarly community. At the same time, the *Frontiers journal series* operates on a revolutionary invention, the tiered publishing system, initially addressing specific communities of scholars, and gradually climbing up to broader public understanding, thus serving the interests of the lay society, too.

## Dedication to quality

Each Frontiers article is a landmark of the highest quality, thanks to genuinely collaborative interactions between authors and review editors, who include some of the world's best academicians. Research must be certified by peers before entering a stream of knowledge that may eventually reach the public - and shape society; therefore, Frontiers only applies the most rigorous and unbiased reviews. Frontiers revolutionizes research publishing by freely delivering the most outstanding research, evaluated with no bias from both the academic and social point of view. By applying the most advanced information technologies, Frontiers is catapulting scholarly publishing into a new generation.

## What are Frontiers Research Topics?

Frontiers Research Topics are very popular trademarks of the *Frontiers journals series*: they are collections of at least ten articles, all centered on a particular subject. With their unique mix of varied contributions from Original Research to Review Articles, Frontiers Research Topics unify the most influential researchers, the latest key findings and historical advances in a hot research area.

Find out more on how to host your own Frontiers Research Topic or contribute to one as an author by contacting the Frontiers editorial office: [frontiersin.org/about/contact](https://frontiersin.org/about/contact)

# Toxicity mechanisms, exposure, toxicokinetic and risk assessment aspects of metals, toxic for animals and humans, volume II

## Topic editors

Fatma Mohamady El-Demerdash — Alexandria University, Egypt

Alex Boye — University of Cape Coast, Ghana

Michel Mansur Machado — Federal University of Pampa, Brazil

Yanzhu Zhu — Chinese Academy of Agricultural Sciences (CAAS), China

Xinwei Li — Jilin University, China

Xu Yang — Henan Agricultural University, China

## Citation

El-Demerdash, F. M., Boye, A., Machado, M. M., Zhu, Y., Li, X., Yang, X., eds. (2023).

*Toxicity mechanisms, exposure, toxicokinetic and risk assessment aspects of metals, toxic for animals and humans, volume II*. Lausanne: Frontiers Media SA.

doi: 10.3389/978-2-83251-436-8

## Table of contents

- 05 **Editorial: Toxicity mechanisms, exposure, toxicokinetic and risk assessment aspects of metals, toxic for animals and humans, Volume II**  
Yanzhu Zhu, Fatma M. El-Demerdash, Xu Yang, Alex Boye, Michel Mansur Machado and Xinwei Li
- 07 **Strontium Regulates the Proliferation and Differentiation of Isolated Primary Bovine Chondrocytes via the TGF $\beta$ /SMAD Pathway**  
Siqi Liu, Bingyu Shen, Juan J. Loor, Qianming Jiang, Yang Yuan, Yezi Kong, Panpan Tan, Fangyuan Zeng, Chenxu Zhao, Xiaoyan Zhu and Jianguo Wang
- 19 **Immunomodulatory Effect of Ginsenoside Rb2 Against Cyclophosphamide-Induced Immunosuppression in Mice**  
Siwen Zheng, Housheng Zheng, Rui Zhang, Xiangmin Piao, Junnan Hu, Yanzhu Zhu and Yingping Wang
- 29 **The Combination of *Tamarindus indica* and Coenzyme Q10 can be a Potential Therapy Preference to Attenuate Cadmium-Induced Hepatorenal Injury**  
Amany Abdelnaby, Nabila Abdel-Aleem, Ayman Mansour, Afaf Abdelkader, Amany N. Ibrahim, Safwa M. Sorour, Enas Elgendy, Heba Bayoumi, Shaymaa M. Abdelrahman, Samah F. Ibrahim, Ilhaam Alsaati and Ahmed Abdeen
- 43 **Alleviating effect of quercetin on cadmium-induced oxidative damage and apoptosis by activating the Nrf2-keap1 pathway in BRL-3A cells**  
Jicang Wang, Ke Wang, Lulu Ding, Pengli Zhao, Cai Zhang, Hongwei Wang, Zijun Yang and Zongping Liu
- 55 **Protective effect of quercetin on cadmium-induced renal apoptosis through cyt-c/caspase-9/caspase-3 signaling pathway**  
Ruxue Huang, Lulu Ding, Ying Ye, Ke Wang, Wenjing Yu, Bingzhao Yan, Zongping Liu and Jicang Wang
- 66 **Proteomics unite traditional toxicological assessment methods to evaluate the toxicity of iron oxide nanoparticles**  
Junyuan Han, Yongzhang Tian, Minghan Wang, Yajuan Li, Jiye Yin, Wensheng Qu, Changhui Yan, Rigao Ding, Yongbiao Guan and Quanjun Wang
- 83 **Progress on the efficacy and mechanism of action of panax ginseng monomer saponins treat toxicity**  
Xinyi Wang, Rongcan Wang, Yongfei Qiao and Yali Li

- 90 **White adipose tissue as a target for cadmium toxicity**  
Sarrah Mohammed Attia, Sandra Concepcion Das,  
Kavitha Varadharajan and Hamda A. Al-Naemi
- 99 **Selenium-enriched yeast modulates the metal  
bioaccumulation, oxidant status, and inflammation in  
copper-stressed broiler chickens**  
Ola A. Habotta, Xiaoyan Wang, Hamzah Othman,  
Abdulrahman A. Aljali, Mahmoud Gewaily, Mahmoud Dawood,  
Asmaa Khafaga, Amr I. Zaineldin, Rajeev K. Singla, Bairong Shen,  
Heba I. Ghamry, Eman Elhussieny, Amany El-Mleeh, Samah F. Ibrahim  
and Ahmed Abdeen



## OPEN ACCESS

EDITED AND REVIEWED BY  
Ursula Gundert-Remy,  
Charité Universitätsmedizin Berlin,  
Germany

## \*CORRESPONDENCE

Yanzhu Zhu,  
✉ zyzhu@126.com

## SPECIALTY SECTION

This article was submitted to  
Predictive Toxicology,  
a section of the journal  
Frontiers in Pharmacology

RECEIVED 24 November 2022

ACCEPTED 21 December 2022

PUBLISHED 11 January 2023

## CITATION

Zhu Y, El-Demerdash FM, Yang X, Boye A,  
Machado MM and Li X (2023), Editorial:  
Toxicity mechanisms, exposure,  
toxicokinetic and risk assessment aspects  
of metals, toxic for animals and humans,  
Volume II.  
*Front. Pharmacol.* 13:1107327.  
doi: 10.3389/fphar.2022.1107327

## COPYRIGHT

© 2023 Zhu, El-Demerdash, Yang, Boye,  
Machado and Li. This is an open-access  
article distributed under the terms of the  
[Creative Commons Attribution License](#)  
(CC BY). The use, distribution or  
reproduction in other forums is permitted,  
provided the original author(s) and the  
copyright owner(s) are credited and that  
the original publication in this journal is  
cited, in accordance with accepted  
academic practice. No use, distribution or  
reproduction is permitted which does not  
comply with these terms.

# Editorial: Toxicity mechanisms, exposure, toxicokinetic and risk assessment aspects of metals, toxic for animals and humans, Volume II

Yanzhu Zhu <sup>1\*</sup>, Fatma M. El-Demerdash <sup>2</sup>, Xu Yang <sup>3</sup>,  
Alex Boye <sup>4</sup>, Michel Mansur Machado <sup>5</sup> and Xinwei Li <sup>6</sup>

<sup>1</sup>Jilin Agriculture Science and Technology College, Jilin, Jilin Province, China, <sup>2</sup>Environmental Studies Department, Institute of Graduate Studies and Research, Alexandria University, Alexandria, Egypt, <sup>3</sup>College of Veterinary Medicine, Henan Agricultural University, Zhengzhou, Henan Province, China, <sup>4</sup>Department of Medical Laboratory Science, School of Allied Health Sciences, College of Health and Allied Sciences, University of Cape Coast, Cape Coast, Ghana, <sup>5</sup>Universidade Federal do Pampa, Uruguaiana, Brazil, <sup>6</sup>Key Laboratory of Zoonosis, Ministry of Education, College of Veterinary Medicine, Jilin University, Changchun, Jilin Province, China

## KEYWORDS

toxicity mechanisms, toxicity exposure, toxicokinetic, risk assessment, metals

## Editorial on the Research Topic

[Toxicity mechanisms, exposure, toxicokinetic and risk assessment aspects of metals, toxic for animals and humans, Volume II](#)

Pollutants such as copper (Cu), cadmium (Cd), iron oxide nanoparticles (IONPs), and cyclophosphamide (CTX) exert toxicity on all animal species in the ecosystem (Gioia et al., 2011). Cu is an essential trace element in various cellular processes, but excessive levels of Cu are markedly harmful. Cd can exert toxic effects on various microorganisms, plants, and animals in very low quantities. As the first generation of nanomaterials, IONPs can cure iron deficiency in chronic kidney disease. CTX induces immunosuppression; however, the underlying mechanisms of these pollutants need to be further explored.

Quercetin (Que), Panax ginseng C. A. Meyer (PG), Tamarindus indica (TM), coenzyme Q10 (CoQ), strontium (Sr), and selenium-enriched yeast (SeY) have the potential to be used in the treatment of the toxicity. Que is a special subclass of flavonoid and a powerful antioxidant. PG has a variety of ginsenosides that show diverse biological effects on various diseases. As a traditional medicine, TM has anti-inflammatory and analgesic effects. CoQ10 plays a key role in mitochondrial bioenergetics and exerts a natural antioxidant effect. Selenium is a micronutrient that is essential for the proper functioning of all organisms. High doses of Sr induce alterations in mineralization.

Many researchers have focused on this field and have obtained important findings. Habotta et al. reported that SeY reduces the hepatic and renal damage induced by Cu in broiler chickens, and it can be used as a potential feed supplement (Wang et al.). Wang et al. found that ginsenosides alleviate exogenous toxicity and reduce drug toxicities and they could potentially be used as a treatment for toxicity (Han et al.). Han et al. revealed that IONPs accumulated in the macrophage lysosomes and the spleen eliminate the IONPs in the systemic circulation (Attia et al.). Attia et al. found that Cd damages the adipocyte function (Huang et al.). Attia et al. found that Que could alleviate kidney damage and renal-cell apoptosis induced by Cd (Wang et al.). Wang et al. found that QE has an antioxidant effect in BRL-3A cells (Abdelnaby et al.). Abdelnaby et al. found that hepatorenal damage

induced by Cd is alleviated by TM or CoQ supplementation (Zheng et al.). Zheng et al. found that immunosuppression in mice induced by CTX could be treated by ginsenoside Rb2 (Liu et al.). Liu et al. found that primary chondrocyte proliferation is promoted by Sr, but primary chondrocyte differentiation is inhibited by Sr (Liu et al.).

This special issue provides new ideas for the application of Que, PG, TM, CoQ, SeY, and Sr in the prevention and treatment of Cu, Cr, IONPs, and CTX toxicity.

## Author contributions

YZ, FE, XY, AB, MM, and XL contributed to this topic.

## Conflict of interest

The authors declare that the research was conducted in the absence of any commercial or financial relationships that could be construed as a potential conflict of interest.

## Publisher's note

All claims expressed in this article are solely those of the authors and do not necessarily represent those of their affiliated organizations, or those of the publisher, the editors and the reviewers. Any product that may be evaluated in this article, or claim that may be made by its manufacturer, is not guaranteed or endorsed by the publisher.



# Strontium Regulates the Proliferation and Differentiation of Isolated Primary Bovine Chondrocytes *via* the TGF $\beta$ /SMAD Pathway

Siqi Liu<sup>1†</sup>, Bingyu Shen<sup>1†</sup>, Juan J. Loo<sup>2</sup>, Qianming Jiang<sup>2</sup>, Yang Yuan<sup>1</sup>, Yezi Kong<sup>1</sup>, Panpan Tan<sup>1</sup>, Fangyuan Zeng<sup>1</sup>, Chenxu Zhao<sup>1</sup>, Xiaoyan Zhu<sup>1</sup> and Jianguo Wang<sup>1\*</sup>

<sup>1</sup>College of Veterinary Medicine, Northwest A&F University, Xianyang, China, <sup>2</sup>Department of Animal Sciences, Division of Nutritional Sciences, University of Illinois, Urbana, IL, United States

## OPEN ACCESS

### Edited by:

Yanzhu Zhu,  
Chinese Academy of Agricultural  
Sciences (CAAS), China

### Reviewed by:

Chuang Xu,  
Heilongjiang Bayi Agricultural  
University, China  
Mei-zhou Huang,  
The Affiliated Hospital of Southwest  
Medical University, China

### \*Correspondence:

Jianguo Wang  
jgwang0625@nwsuaf.edu.cn

<sup>†</sup>These authors share first authorship

### Specialty section:

This article was submitted to  
Predictive Toxicology,  
a section of the journal  
Frontiers in Pharmacology

**Received:** 21 April 2022

**Accepted:** 13 May 2022

**Published:** 27 May 2022

### Citation:

Liu S, Shen B, Loo JJ, Jiang Q,  
Yuan Y, Kong Y, Tan P, Zeng F,  
Zhao C, Zhu X and Wang J (2022)  
Strontium Regulates the Proliferation  
and Differentiation of Isolated Primary  
Bovine Chondrocytes *via* the TGF $\beta$ /  
SMAD Pathway.  
Front. Pharmacol. 13:925302.  
doi: 10.3389/fphar.2022.925302

The present study evaluated the effects of strontium (Sr) on proliferation and differentiation of chondrocytes isolated from dairy cows, and whether Sr exerts its effects *via* transforming growth factor  $\beta$  (TGF $\beta$ ) signaling. The chondrocytes were isolated from patellar cartilage from newborn Holstein bull calves ( $n = 3$ , 1 day old,  $38.0 \pm 2.8$  kg, fasting) within 15 min after euthanasia, and treated with different concentrations of Sr (0, 0.1, 1, and 10  $\mu\text{g/ml}$ , as SrCl<sub>2</sub>·6H<sub>2</sub>O). After pretreatment with or without activin receptor-like kinase 5 (ALK5) inhibitor (10  $\mu\text{M}$  SB-505124) for 4 h, chondrocytes were incubated with Sr for another 4 h. Overall effects of Sr were evaluated relative to NaCl as the control. In contrast, the 1  $\mu\text{g/ml}$  Sr-treated group served as the control to determine effects of preincubating with SB-505124. Western blot and qRT-PCR were used for measuring expression of proliferation-, differentiation-, and TGF $\beta$ 1-responsive factors. Data were analyzed using one-way ANOVA in GraphPad Prism 7.0. Incubation with all doses of Sr increased TGF $\beta$ 1/ALK5-induced SMAD3 phosphorylation, and at 10  $\mu\text{g/ml}$  it inhibited ALK1-induced SMAD1/5/9 phosphorylation. Expression of mRNA and protein of the proliferation-responsive factors type II Collagen  $\alpha$ 1 (COL2A1) and aggrecan (ACAN) was induced by Sr at 1  $\mu\text{g/ml}$ . In contrast, Sr at 10  $\mu\text{g/ml}$  inhibited the expression of differentiation-responsive factors type X Collagen  $\alpha$ 1 (COL10A1) and secreted phosphoprotein 1 (SPP1), and at 1  $\mu\text{g/ml}$  it had the same effect on alkaline phosphatase (ALPL) mRNA and protein levels. Cells were stained with PI/RNase Staining buffer to assess cell cycle activity using flow-cytometry. Incubation with Sr at 1 and 10  $\mu\text{g/ml}$  induced an increase in the number of cells in the S-phase, leading to an increase in the proliferation index. Incubation with SB-505124 inhibited phosphorylation of SMAD3. Abundance of ACAN and COL2A1 mRNA and protein was lower when cells were pre-incubated with SB-505124. Overall, data indicated that Sr promotes proliferation and inhibits differentiation of primary chondrocytes by directing TGF $\beta$ 1 signaling towards SMAD3 phosphorylation rather than SMAD1/5/9 phosphorylation. Whether these effects occur *in vivo* remains to be determined and could impact future application of Sr as an experimental tool in livestock.

**Keywords:** strontium, bovine chondrocyte, proliferation and differentiation, TGF $\beta$ , Smad3

## INTRODUCTION

Strontium (Sr) belongs to the second major group of elements, along with Ca and Mg (Pilmane et al., 2017). Although present in trace amounts in the body, similar to Ca, Sr is also a bone-seeking element due to its similar physicochemical properties. Most of the Sr entering the body is absorbed by bones and teeth (Nielsen, 2004). The function of Sr in the context of bone relates to its role in promoting osteoblast-mediated bone formation and inhibiting osteoclast-mediated bone resorption (Querido et al., 2016).

In ruminants, it is well-established that Ca absorption from the gastrointestinal tract, Ca reabsorption from the kidney and mobilization of skeletal Ca stores help maintain Ca concentrations in the blood (Hernandez-Castellano et al., 2020). Thus, because Ca levels in the blood do not reflect intestinal absorption capacity, protocols for using Sr as a surrogate marker have been developed (Milsom et al., 1987; Khan et al., 2013). Studies with cows and sheep have reported a close correlation between the absorption rates of oral Sr and radioactive Ca, indicating that the Sr concentrations in the blood measured orally can serve as an index for Ca absorption capacity of the gastrointestinal tract of dairy cows and sheep (Hyde and Fraser, 2014; Hyde et al., 2019). Although these studies have provided information on the use of Sr, it is unknown to what extent (if any) Sr can affect other tissues in the body.

The transforming growth factor  $\beta$  (TGF $\beta$ ) superfamily comprises more than forty members including TGF $\beta$ , activin, and bone morphogenetic protein (BMP) (Chen et al., 2012) all of which play pivotal roles in the metabolism, differentiation, proliferation, and survival of chondrocytes (van Caam et al., 2016; Woods et al., 2021). SMAD family member (SMAD)-dependent signaling is a classical pathway of the TGF $\beta$  family and it involves binding of TGF $\beta$  to its tetrameric receptor comprised of activin receptor-like kinase 5 (ALK5) and TGF $\beta$  type II kinase receptor dimers. As a result, the signal delivered into cells induces subsequent phosphorylation of the receptor-SMAD components, SMAD2 and SMAD3 (Zhu et al., 2016; Thielen et al., 2019). These receptor-SMAD complex binds to the common-SMAD, SMAD4, to trigger nuclear translocation of this whole complex to regulate gene transcription. Together with the

phosphorylation of SMAD1/5/9 *via* ALK1, these events (at least in non-ruminants) regulate cartilage and bone development as well as homeostasis (Wu et al., 2016).

A previous study reported that Sr can regulate proliferation and differentiation of chondrocytes in rats by promoting the expression of TGF $\beta$ 1 and TGF $\beta$ 2 (Kong et al., 2018). However, it is unknown if Sr can mediate the TGF $\beta$  pathway to regulate chondrocyte proliferation and differentiation in the bovine. Thus, the main objective of the present study was to determine *in vitro* the effect of Sr on proliferation and differentiation of bovine chondrocytes *via* the TGF $\beta$  signaling pathway.

## MATERIALS AND METHODS

### Ethics Statement

This study was conducted at one of the experimental farms of Northwest A&F University (Shaanxi Province, China) in Western China (106°55'57"E, 34°48'41"N). The protocol was approved by the Animal Welfare and Research Ethics Committee at Northwest A&F University (Permit Number: 2021049), Shaanxi, People's Republic of China.

### Animals and Tissue Collection

Tissue was isolated from newborn Holstein bull calves ( $n = 3$ ;  $38.0 \pm 2.8$  kg BW). At each of 3 consecutive d, within 15 min after euthanasia by a veterinarian with barbiturate, patellar cartilage was separated from the articular knee of each calf through surgical patellar excision. Patellar cartilage was then washed three times with 0.1% PBS and within 1 h transported to the laboratory on ice.

### Isolation and Culture of Bovine Primary Chondrocytes

Primary chondrocytes were isolated from patellar cartilage from each calf and cultured individually. Methods for isolation of chondrocytes were described in a previous study (Wang et al., 2013). Briefly, the cartilage was sliced into thin slices and

**TABLE 1** | Sequences of the primers used in this study.

Gene <sup>a</sup>	NCBI reference sequence	Product length (bp)	Forward primer	Reverse primer
ALK5	NM_001130916	323	TTCOGTGAGGCGAGAGATT	GCAATACAGCAAGTTCATT
TGF $\beta$ 1	NM_001166068	159	GACACCAACTACTGCTTCA	ATCCAGGCTCCAGATGTAA
SERPINE1	NM_174137.2	381	GGCTCAGACCAACAAGTT	TTCACCTCAATCTTCACCTT
ID1	NM_001097568.2	73	GCTCCGCTCAGCACTCTCAA	GATCGTCCGCTGGAACACA
ALK1	NM_001083479.1	109	ACAACACAGTGCTGCTCAGACA	TGCTCGTGGTAGTGCGTGAT
COL2A1	NM_001001135.3	299	GTGGAAGAGCGGAGACTA	GGTAGGTGATGTTCTGAGAG
ACAN	NM_173981	155	CGGAAGTGAGTGGAGAGT	GGTGGTCTGATGACAATA
ALPL	NM_176858.2	163	AACACAAGCACTCTCACTAT	GCCATCTCTACCATCTCAG
COL10A1	NM_174634.1	184	AGCTGAGATCATGCTGCCAC	CTCTCCTCTCAGTGATACACCTTT
SPP1	NM_174187	158	AGAGGAGGACTTCACATCA	TCAGATTGGAATGCTTGTTC
VEGFA	NM_001316955	270	CCTTGCTGCTTACCTTC	TGGTGATGTTGAACTCCTC
GAPDH	NM_001034034	117	CCTGCCAAGTATGATGAGAT	AGTGTGCGCTGTTGAAGTC

<sup>a</sup>ALK5, activin receptor-like kinase 5; TGF $\beta$ 1, transforming growth factor  $\beta$ ; SERPINE1, Serpin family E member 1; ID1, inhibitor of DNA binding 1; ALK1, activin receptor-like kinase 1; COL2A1, type II Collagen  $\alpha$ 1; ACAN, aggrecan; ALPL, ALKaline phosphatase; COL10A1, type X Collagen  $\alpha$ 1; SPP1, secreted phosphoprotein 1; VEGFA, vascular endothelial growth factor.

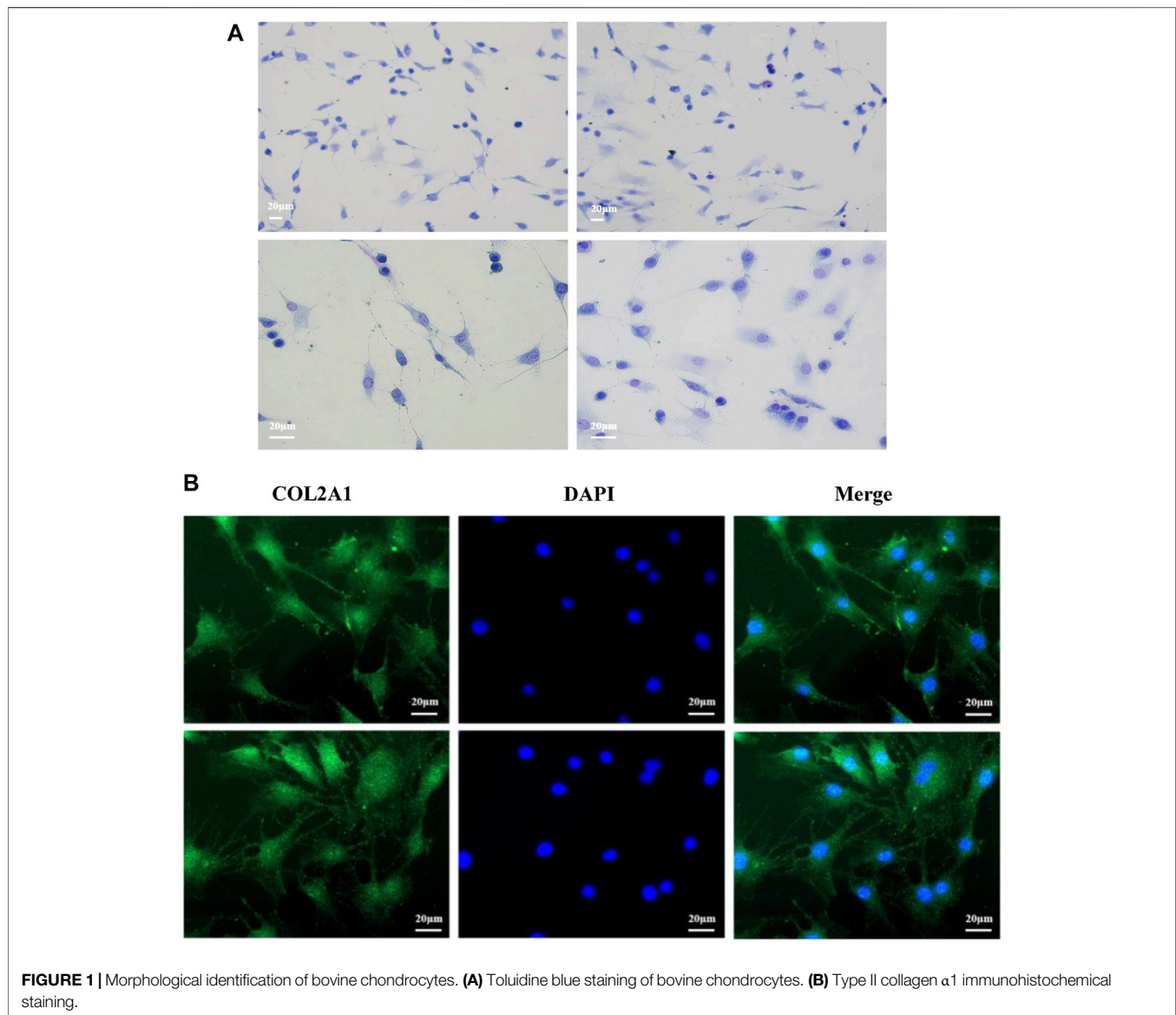


**FIGURE 1** | Morphological identification of bovine chondrocytes. **(A)** Toluidine blue staining of bovine chondrocytes. **(B)** Type II collagen  $\alpha 1$  immunohistochemical staining.

incubated with 0.25% collagenase type II (1761015, Sigma, United States) at 37°C in 5% CO<sub>2</sub> for 18 h. Cells were collected by passing through a 100-mesh filter and then centrifuged at 400 × g for 10 min with at least three washes. Chondrocytes were then cultured in a 60 mm culture dish (704001, Nest, China) in DMEM/High-glucose (12800017, Gibco, United States) with 10% fetal bovine serum (FB15015, Clark, United States) at 5 × 10<sup>5</sup> cells/mL in a humidified atmosphere of 5% CO<sub>2</sub> in air at 37°C. The culture medium was replaced regularly every 2 days. When the growth density of the cells reached about 80–90% confluence, cells were passaged using a 0.25% trypsin digestion solution (T1186, Gentihold, China). Cells from second passage were then used for further experiments.

For experiments, cells were treated with a solution of Sr chloride (SrCl<sub>2</sub>·6H<sub>2</sub>O, V900279, Sigma, United States) dissolved in 0.9% NaCl at different concentrations. In

ruminants, the maximum concentration of Sr used to measure level of Ca absorption from blood is 1 μg/ml (Hyde et al., 2019). Thus, 1 μg/ml was set as the medium-dose group. Doses of 0.1 μg/ml and 10 μg/ml were used as low- and high-dose groups. Cells were cultured for 4 h and 0.9% NaCl was used as a control. To inhibit ALK5 kinase activity, we had another set of cells cultured with the ALK5 inhibitor SB-505124 (HY-13521, MedChemExpress, United States) at a concentration of 10 μM (Vogt et al., 2011; van Caam et al., 2017) for 4 h before treated with 1 μg/ml Sr. 1 μg/ml Sr-treated group served as a control.

### Toluidine Blue Staining and Immunofluorescence Staining

Second passage cells on glass coverslips were washed twice using PBS, stained with toluidine blue O (G3660, Solarbio, Beijing,

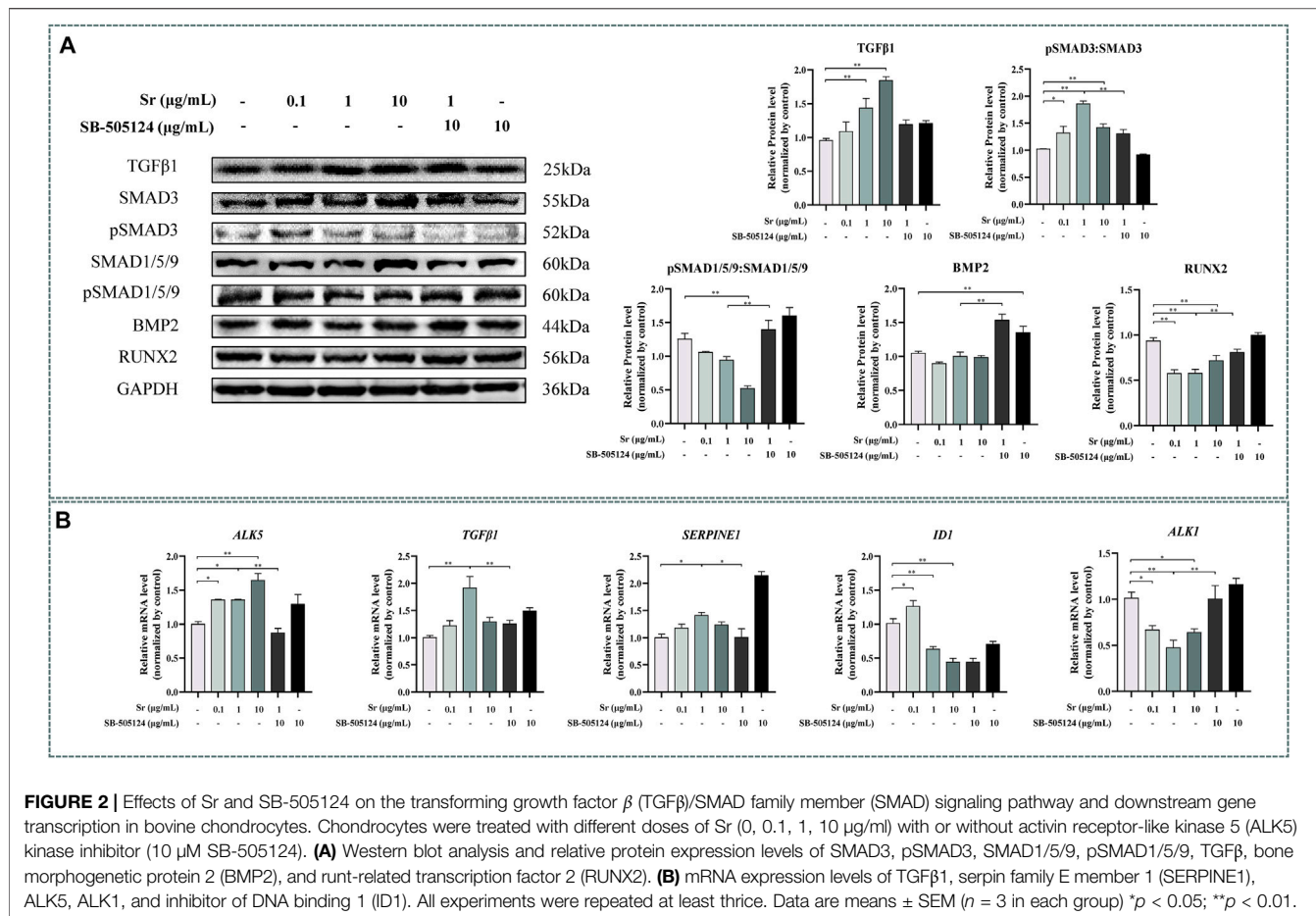


**FIGURE 2 |** Effects of Sr and SB-505124 on the transforming growth factor  $\beta$  (TGF $\beta$ )/SMAD family member (SMAD) signaling pathway and downstream gene transcription in bovine chondrocytes. Chondrocytes were treated with different doses of Sr (0, 0.1, 1, 10  $\mu$ g/ml) with or without activin receptor-like kinase 5 (ALK5) kinase inhibitor (10  $\mu$ M SB-505124). **(A)** Western blot analysis and relative protein expression levels of SMAD3, pSMAD3, SMAD1/5/9, pSMAD1/5/9, TGF $\beta$ , bone morphogenetic protein 2 (BMP2), and runt-related transcription factor 2 (RUNX2). **(B)** mRNA expression levels of TGF $\beta$ 1, serpin family E member 1 (SERPINE1), ALK5, ALK1, and inhibitor of DNA binding 1 (ID1). All experiments were repeated at least thrice. Data are means  $\pm$  SEM ( $n = 3$  in each group) \* $p < 0.05$ ; \*\* $p < 0.01$ .

China) for 5 min. Equal amounts of distilled water were then added and allowed to stand for 15 min. After washing twice with PBS, cells were observed and photographed using a microscope (Carl Zeiss GmbH, Jena, Germany).

Second passage cells on glass coverslips were rinsed three times using PBS and fixed with 4% paraformaldehyde for 30 min. After washing three times with PBS, cells were treated with 0.1% Triton X-100 diluted in PBS for 15 min at 37°C, and blocked with 5% BSA in PBS for 20 min. COL2A1 antibody (COL2A1, AF6528, Beyotime Biotechnology, China) was incubated overnight at 4°C, the glass coverslips rinsed and then incubated with Goat Anti-Rabbit IgG H&L (ab150077, Alexa Fluor 488) for 4 h at 37°C. Cell nuclei were counterstained with DAPI (C1002, Beyotime Biotechnology, China). Lastly, glass coverslips were observed and photographed using a fluorescence microscope (Carl Zeiss GmbH, Jena, Germany).

## Total RNA Extraction, Primer Design, and qRT-PCR

Total RNA was extracted using Trizol reagent (15596026, Invitrogen, Carlsbad, United States) following manufacturer's protocols. Concentration and purity of RNA were checked with a NanoDrop 2000C (Thermo Scientific, Waltham, MA, United States). Samples had an optical density ratio at 260/

280 nm  $> 1.9$  and  $< 2.2$ . Reverse transcription of the total RNA was conducted using SuperScript™ RT reagent kit (RR047A, TaKaRa, Japan). All primers used were designed with Primer Premier 6 (Premier Biosoft, United States) based on GenBank data. Primer sequences are listed in **Table 1**. The housekeeping gene *GAPDH* was used as an internal control. Quantitative real-time polymerase chain reaction (qRT-PCR) was performed using the 2  $\times$  M5 HiPer SYBR Premix EsTaq (MF787-01, Meisbio, China).

## Protein Extraction and Western Blotting

Total protein was extracted from chondrocytes using the radioimmunoprecipitation assay Lysis Buffer (P0013B, Beyotime Biotechnology, China), and concentration measured with the BCA Protein Assay Kit (P0012, Beyotime Biotechnology, China). Then, 50  $\mu$ g protein were separated on a 10% or 8% bisacrylamide gel and transferred to a PVDF membrane (IPVH00010, Millipore, United States). Membranes were blocked with 5% skimmed milk or BSA solution in TBS-T buffer for 2 h, and incubated overnight at 4°C with antibodies including type II Collagen  $\alpha$ 1 (COL2A1, 1:1000, AF6528, Beyotime Biotechnology, China), aggrecan (ACAN, 1:500, NB110-6524, Novusbio biologicals, United States), type X Collagen  $\alpha$ 1 (COL10A1, 1:500, bs0554R, Bioss biotechnology, China), Osteopontin (OPN, 1:1000, also called SPP1, secreted

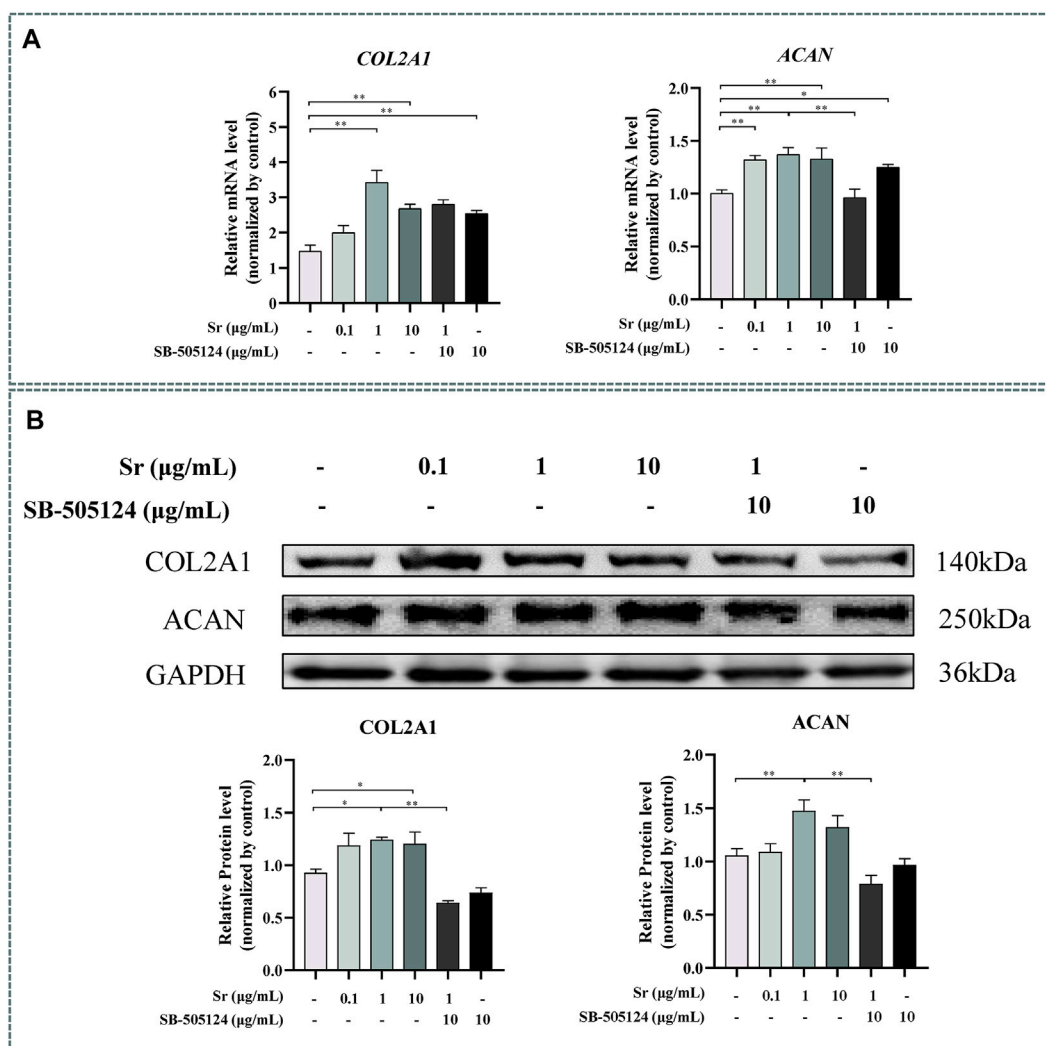


**FIGURE 3 |** Effects of Sr and SB-505124 on proliferation-related factors in bovine chondrocytes. Chondrocytes were treated with different doses of Sr (0, 0.1, 1, 10 μg/ml) with or without activin receptor-like kinase 5 (ALK5) kinase inhibitor (10 μM SB-505124). **(A)** Relative mRNA expression levels of type II Collagen α1 (COL2A1) and aggrecan (ACAN). **(B)** Western blot and protein expression levels of COL2A1 and ACAN. All experiments were repeated at least thrice. Data are means ± SEM ( $n = 3$  in each group) \* $p < 0.05$ ; \*\* $p < 0.01$ .

phosphoprotein 1, bs0019R, Bioss biotechnology, China), vascular endothelial growth factor (VEGFA, 1:1000, NB110-2381ss, Novus Bio biologicals, United States), alkaline phosphatase (ALPL, 1:1000, DF6225, Affinity, United States), SMAD3 (1:500, NB100-56479ss, Novusbio biologicals, United States), pSMAD3 (1:1000, 9520T, Cell Signaling Technology, United States), SMAD1/5/9 (1:1000, AF0614, Affinity, United States), pSMAD1/5/9 (1:1000, 13820T, Cell Signaling Technology, United States) and runt-related transcription factor 2 (RUNX2, 1:1000, AF5189, Affinity, United States). Blots were incubated for 2 h in a horseradish peroxidase (HPR)-conjugated secondary antibody at 25°C. Membranes were detected using a chemiluminescence (ECL) system (ProteinSimple, Santa Clara, CA, United States). Results were analyzed using the ImageJ software (Media Cybernetics, Bethesda, MD, United States).

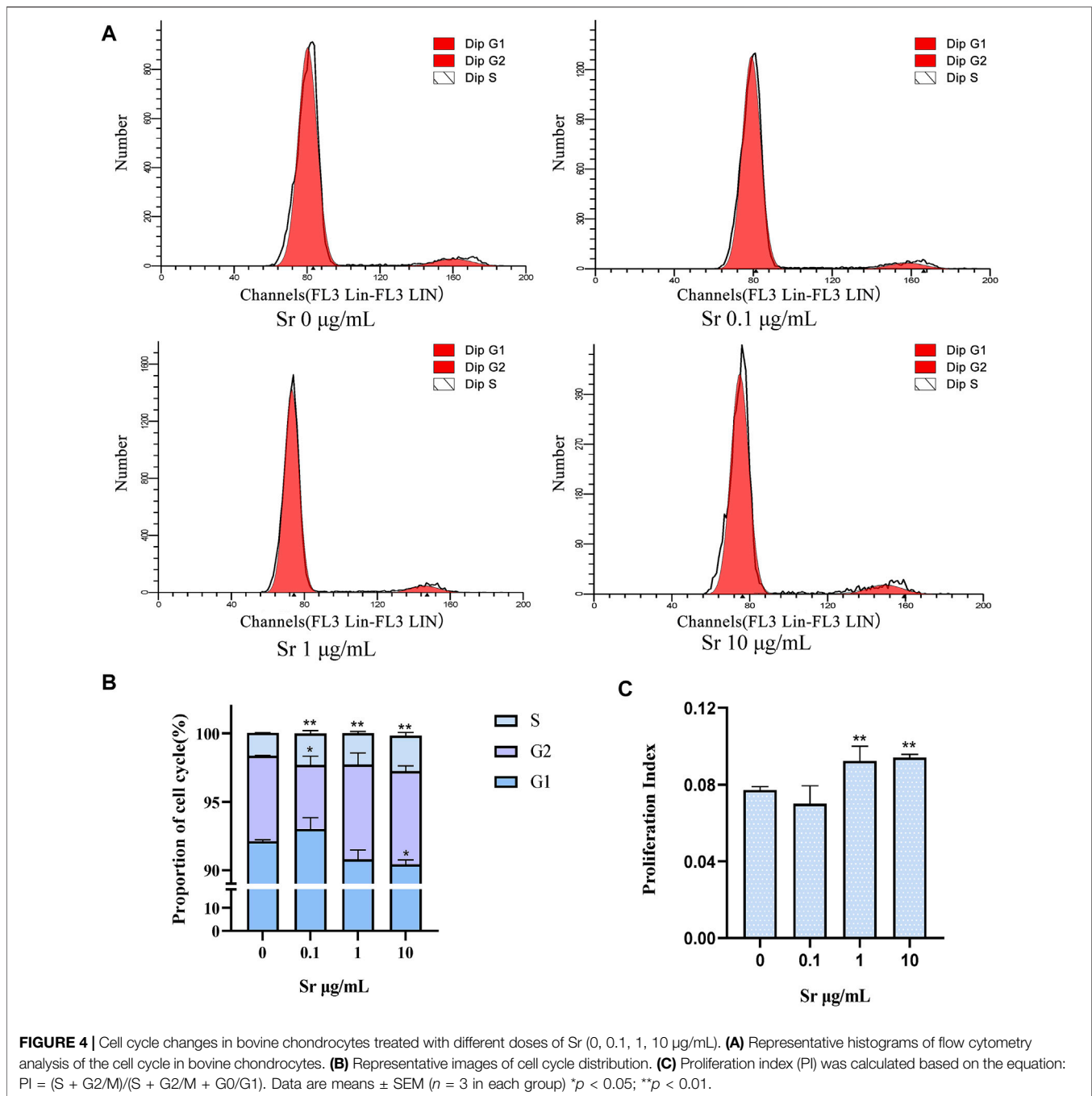
## Flow Cytometry

Cells were collected and stained with PI/RNase Staining Buffer (BD pharmingen) to measure cell cycle activity determined by flow cytometry (Coulter-XL). Data were analyzed in ModFit 3.0 (Verity Software House, ME, United States) and the proliferation index (PI) was calculated using the following equations (Ming et al., 2019):

$$PI = (S + G2/M) / (S + G2/M + G0/G1)$$

## Coomassie Blue Staining of the Cytoskeleton

Second passage cells in a 35 mm culture dish were cultured at a density of  $5.0 \times 10^4$  cells/mL. After treatment, cells were washed three times with 0.1% PBS and 1% TritonX-100 was added to each



dish for incubation in a humidified 37°C incubator for 15 min. The dish was washed three times with buffer M (60 mM imidazole, 50 mM KCl, 0.5 mM MgCl<sub>2</sub>, 0.1 mM EDTA, 1 mM EGTA, 1 mM β-mercaptoethanol, pH7.5) to stabilize the cytoskeleton. Cells were then fixed in 3% glutaraldehyde for 30 min and washed three times with 0.1% PBS after fixation, followed by addition of 0.2% Coomassie blue R<sub>250</sub> for 30 min. Cells were washed with running water and observed and photographed using a microscope (Carl Zeiss GmbH, Jena, Germany).

## Statistical Analysis

Each experiment was repeated at least 3 times on consecutive days. The data were analyzed using the GraphPad Prism 7.0 (GraphPad Software Inc., United States) software. All data are reported as means  $\pm$  SEM. For data with dose-response effects to Sr, comparisons among groups were performed using one-way ANOVA with Dunnett's multiple comparison test with 0.9% NaCl as the control group. For data with effects of preincubation with SB-505124, comparisons among groups were performed

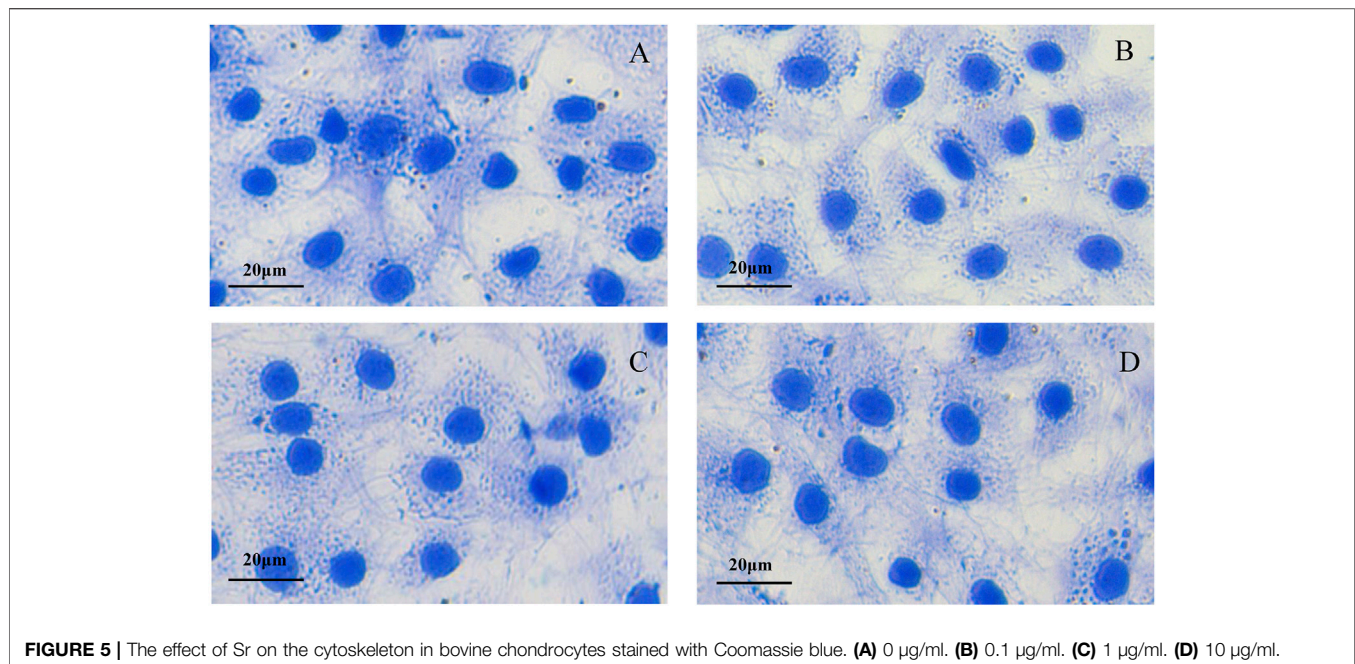


**FIGURE 5 |** The effect of Sr on the cytoskeleton in bovine chondrocytes stained with Coomassie blue. (A) 0 µg/ml. (B) 0.1 µg/ml. (C) 1 µg/ml. (D) 10 µg/ml.

using one-way ANOVA with Dunnett's multiple comparison test with 1 µg/ml Sr as the control.  $p < 0.05$  was considered significant.

## RESULTS

### Morphological Identification of Bovine Chondrocytes

Primary bovine chondrocytes were identified by Toluidine blue staining and type II collagen immunofluorescence staining. Chondrocytes were stained purple by toluidine blue (Figure 1A), and Type II collagen in chondrocytes stained green (type II collagen immunofluorescence). The nuclei stained blue when incubated with DAPI (Figure 1B). Together, these results indicated isolated cells from articular cartilage were chondrocytes.

### Strontium Promotes Proliferation and Inhibits Differentiation of Chondrocytes via TGFβ/SMAD3

Exogenous Sr upregulated expression of TGFβ1 at both the transcriptional and protein level (Figure 2). Compared with the control, pSMAD3:SMAD3 ratio was higher (Figure 2A,  $p < 0.05$ ) and the pSMAD1/5/9:SMAD1/5/9 ratio lower ( $p < 0.01$ ) with each dose of Sr. Exogenous Sr did not alter BMP2 ( $p = 0.27$  at 0.1 µg/ml;  $p = 0.97$  at 1 µg/ml;  $p = 0.92$  at 10 µg/ml, Figure 2A). Compared with the control, abundance of the key transcription factor RUNX2, regulated by pSMAD3 and pSMAD1/5/9, was decreased with each dose of Sr (Figure 2A,  $p < 0.01$ ).

As evident from Figure 1B, abundance of the SMAD3-dependent genes *TGFβ1* and *ALK5* increased upon treatment with Sr at all doses

( $p < 0.05$ ). Serpin family E member 1 (*SERPINE1*), another SMAD3-dependent gene, was greater with 1 µg/ml ( $p < 0.05$ ). In contrast to the SMAD3-dependent genes, the abundance of inhibitor of DNA binding 1 (*ID1*) and *ALK1*, both SMAD1/5/9-dependent genes, decreased in all Sr-treated groups compared with the control ( $p < 0.05$ ).

### Strontium Promotes Proliferation of Chondrocytes

Both *COL2A1* and *ACAN* were upregulated by treating with Sr and reached the highest level in the 1 µg/ml group ( $p < 0.01$ ) (Figure 3A). The upregulation of *COL2A1* and *ACAN* was also confirmed at the protein level (Figure 3B), with upregulation of *COL2A1* in the 1 and 10 µg/ml groups ( $p < 0.05$ ) while *ACAN* was upregulated in the 1 µg/ml group ( $p < 0.01$ ).

Compared with the control, treatment with Sr led to a remarkable increase in cells at the S-phase from 1.66 to 2.31% in the 0.1 µg/ml group to 2.27 and 2.59% in the 1 µg/ml and 10 µg/ml group (Figures 4A,B). Treatment with 10 µg Sr/mL decreased the number of cells in the G1 phase and 0.1 µg/ml Sr decreased cells in the G2 phase cells (Figures 4A,B). The proliferation index was higher in cells treated with 1 and 10 µg/ml Sr (Figure 4C). Culture with Sr had no effect on the cytoskeleton (Figure 5).

### Strontium Inhibits Differentiation of Chondrocytes

Western blotting indicated that Sr treatment downregulated ALPL expression at a concentration of 1 and 10 µg/ml Sr ( $p < 0.05$ , Figure 6A). Expression of *COL10A1* decreased in the 10 µg/ml treatment group, and expression of *SPP1* decreased in 1 and 10 µg/ml Sr groups ( $p < 0.01$ , Figure 6A). Compared with the

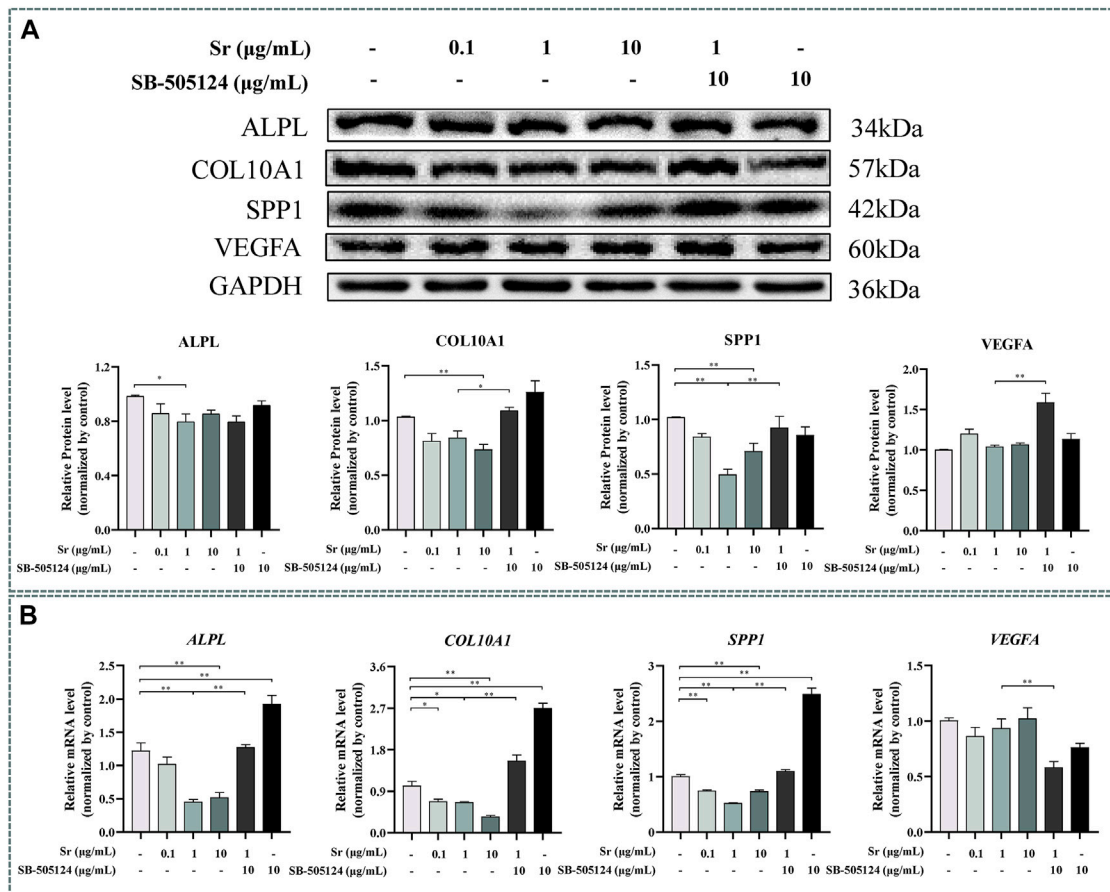


**FIGURE 6** | Effects of Sr and SB-505124 on differentiation-related factors in bovine chondrocytes. Chondrocytes were treated with different doses of Sr (0, 0.1, 1, 10 µg/ml) with or without activin receptor-like kinase 5 (ALK5) kinase inhibitor (10 µM SB-505124). **(A)** Western blot and protein expression levels of secreted phosphoprotein 1 (SPP1), alkaline phosphatase (ALPL), vascular endothelial growth factor (VEGFA), and type X Collagen α1 (COL10A1). **(B)** mRNA expression levels of SPP1, ALPL, VEGFA, and COL10A1. All experiments were repeated at least thrice. Data are means ± SEM ( $n = 3$  in each group) \* $p < 0.05$ ; \*\* $p < 0.01$ .

control, there was no effect of Sr on the expression of VEGFA. However, qPCR results revealed a marked downregulation of *ALPL* upon treatment with Sr at 1 µg/ml and 10 µg/ml ( $p < 0.01$ , **Figure 6B**). Both *COL10A1* and *SPP1* decreased in all Sr-treated groups ( $p < 0.05$ , **Figure 6B**). Dose of Sr had no effect on *VEGFA* expression.

## Strontium-Induced SMAD3 Phosphorylation

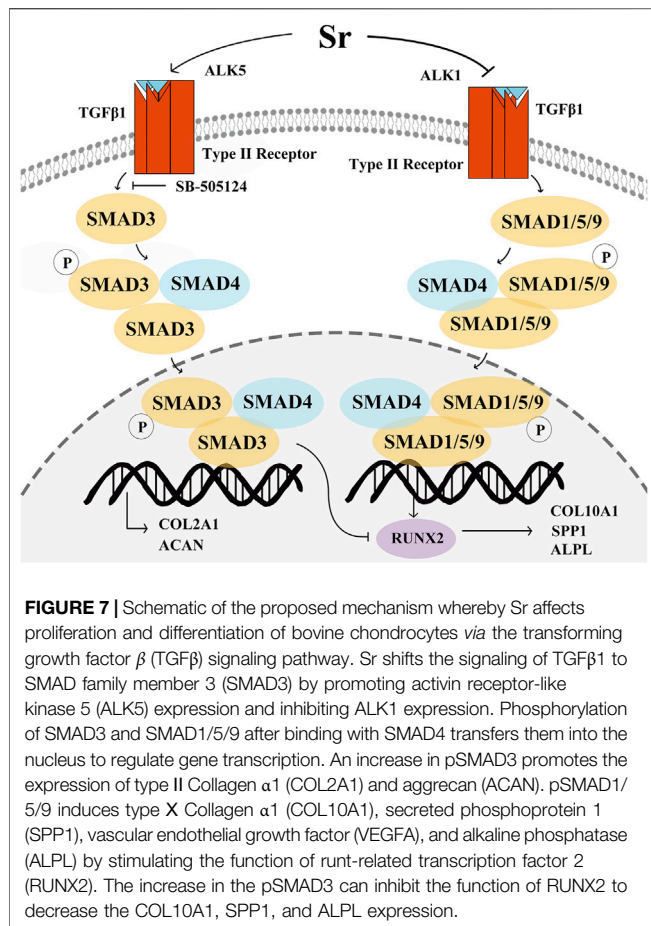
Pre-incubation with SB-505124 inhibited Sr-induced SMAD3 phosphorylation and promoted Sr-induced SMAD1/5/9 phosphorylation ( $p < 0.01$ , **Figure 2A**). SB-505124 inhibited mRNA expression of the SMAD3-dependent genes *TGFβ1*, *ALK5*, and *SERPINE1* ( $p < 0.05$ , **Figure 2B**). Although there was no significant change in *ID1* ( $p = 0.48$ ), SB-505124 increased mRNA expression of *ALK1* ( $p < 0.01$ , **Figure 2B**).

Expression of *ACAN* mRNA decreased ( $p < 0.01$ , **Figure 3A**) while protein abundance of *ACAN* and *COL2A1* decreased at the protein level when cells were pre-incubated with SB-505124 ( $p < 0.01$ , **Figure 3B**). Abundance of *ALPL*, *COL10A1*, and *SPP1*

mRNA all increased ( $p < 0.01$ , **Figure 6B**) while protein expression of *COL10A1* and *SPP1* also increased ( $p < 0.05$ , **Figure 6A**).

## DISCUSSION

Some studies have reported that Sr absorption could be used as a surrogate indicator for evaluating Ca absorption in the gastrointestinal tract in dairy cows and sheep (Hyde and Fraser, 2014; Hyde et al., 2019). However, the last few decades have witnessed studies on the effect of Sr in the cartilage and chondrocyte. For instance, Sr can reduce cartilage degeneration and promote ECM production in the ovariectomized rats (Mierzwa et al., 2017). Strontium gluconate was increased mRNA expression of *COL2A1* and *ACAN* in the osteoarthritic rat model (Hu et al., 2020). Thus, these studies provided some evidence for a role of Sr on the regulation of proliferation and differentiation of the cartilage. Unlike rodents, the role of Sr and the underlying molecular mechanisms on proliferation and differentiation of



chondrocytes in ruminants are not well known. Further, whether Sr regulates chondrocyte proliferation and differentiation *via* the TGF $\beta$  pathway remains unclear. The present study demonstrated that Sr promoted TGF $\beta$ 1/ALK5-induced SMAD3 phosphorylation and inhibited ALK1-induced SMAD1/5/9 phosphorylation. Sr promoted the expression of the proliferation-responsive factors COL2A1 and ACAN while inhibiting the expression of differentiation-responsive factors COL10A1, SPP1, and ALPL both at the mRNA and protein levels.

In non-ruminants, TGF $\beta$ 1 is well-known to regulate proliferation and differentiation of chondrocytes (Wu et al., 2016). It plays an anti-hypertrophic role *via* the most classical ALK5/SMAD2/3-dependent pathway (Thielen et al., 2019), and several studies have reported that TGF $\beta$ 1 also induces the SMAD1/5/9-dependent pathway *via* ALK1 (Chen et al., 2012; Charlier et al., 2019; Thielen et al., 2019). These two pathways have antagonistic functions in the chondrocytes (Finsson et al., 2008). For instance, a study in human chondrocytes reported that TGF $\beta$ 1 could induce SMAD2 phosphorylation *via* ALK5 and SMAD1/5/9 phosphorylation *via* ALK1 (Finsson et al., 2010). It was also demonstrated that phosphorylation of SMAD2 increased the expression of COL2A1. Zhang et al. (2017) working with newborn mice reported that TGF $\beta$  regulated SMAD1/5/9 phosphorylation

*via* the ALK1 in pulmonary artery smooth muscle cells and fibroblasts.

The significant increase of TGF $\beta$ 1 levels in response to 1  $\mu$ g/ml and 10  $\mu$ g/ml Sr provided direct evidence that this mineral can affect TGF $\beta$  signaling. Furthermore, the present study determined that Sr, at a low concentration (i.e., 0.1  $\mu$ g/ml), altered the pSMAD3:SMAD3 and the pSMAD1/5/9:SMAD1/5/9 ratio in a way that underscores its potential regulatory role of the TGF $\beta$ 1 pathway. Such an effect is important in the context of biological responses that this mineral can induced in the bovine. For instance, Sr-containing  $\alpha$ -calcium sulfate hemihydrate promoted osteogenic differentiation through TGF $\beta$ 1-induced SMAD2/3 phosphorylation (Liu et al., 2019). In addition, in one of our previous studies we demonstrated that Sr can activate TGF $\beta$ 1 signaling in rat chondrocytes (Kong et al., 2018). Overall, the results of the present study were consistent with the functional link between Sr and TGF $\beta$  signaling.

Existing studies have demonstrated that SMAD3 can be regulated by TGF $\beta$  through ALK5 (Li et al., 2005). This mechanism was confirmed in the present study when pre-treating chondrocytes with SB-505124 (Byfield et al., 2004; Vogt et al., 2011), the inhibitor of ALK5-mediated SMAD3 phosphorylation, inhibited SMAD3 phosphorylation in the co-treated group. Hellingman et al. (2011) reported that blocking SMAD2/3 with SB-505124 decreased abundance of COL2A1, which our results confirmed that COL2A1 and ACAN significantly decreased in the co-treatment group. In non-ruminants, BMP2, 4, 6, 7, and 9 are well-known to regulate SMAD1/5/9 *via* ALK1 (Li et al., 2004; Dexheimer et al., 2016). In addition, TGF $\beta$  also regulates SMAD1/5/9 *via* both ALK1 and ALK5 (Finsson et al., 2008; van Caam et al., 2017). Taking all these into account, although the present study did not detect effects of Sr on BMP2, any potential effects on BMP4, 6, 7, and 9 on the SMAD1/5/9 pathway cannot be excluded. Additional studies are needed to identify the mechanism whereby Sr can affect this pathway.

Previous studies in non-ruminants have reported that SMAD3-dependent genes such as TGF $\beta$ 1, SERPINE1, and ALK5 (van Caam et al., 2015) are upregulated in response to Sr. *ID1* and *ALK1* are well-known SMAD1/5/9-dependent genes in non-ruminants (Ehrichtiou et al., 2010). Thus, the downregulation of *ID1* and *ALK1* at doses of 1 and 10  $\mu$ g/ml Sr were in line with results demonstrating that Sr activated the SMAD3-dependent pathway while inhibiting the SMAD1/5/9-dependent pathway, the latter being a response already demonstrated in murine chondrocytes (Ehrichtiou et al., 2010).

The differentiation and maturation of chondrocytes in non-ruminants is positively regulated, at least *in vitro*, by RUNX2 (Komori, 2018). This transcription factor promotes the expression of hypertrophy makers such as COL10A1, SPP1, VEGFA, and ALPL (Komori, 2017). Several studies reported a closed relationship between RUNX2 and SMAD proteins, and demonstrated that SMAD1/5/9 promotes chondrocyte maturation by stimulating the RUNX2 function, with SMAD3 serving to counteract RUNX2 (Wu et al., 2016; Yu et al., 2019). In the current study, the downregulation of RUNX2 in response to

Sr was consistent with the downregulation of COL10A1 and SPP1. From these responses we speculate that SMAD3 and SMAD1/5/9 could at least partly regulate chondrocyte maturation *via* RUNX2. Support for this idea arises from data indicating that macrophages stimulated by 10 ng/ml IL-4 induced hypertrophy of human chondrocytes by promoting COL10A1 and RUNX2 (Ferrao Blanco et al., 2021). A role for RUNX2 on controlling hypertrophy of the tibial growth plate also was demonstrated in broilers (Wang et al., 2021). Overall, the present results were consistent with previous data.

The structural proteins COL2A1 and ACAN are upregulated in the proliferating zone during cartilage maturation, and when chondrocytes undergo hypertrophy, the proteins VEGFA, SPP1, COL10A1, and ALPL are secreted (Kronenberg, 2003; Kozhemyakina et al., 2015; Charlier et al., 2019; Vimalraj, 2020). In our previous study with rat primary chondrocytes there was a dose-dependent upregulation in COL2A1 with 1, 3 and 5 mM Sr (Wang et al., 2013). The fact that Sr promoted the expression of COL2A1 and ACAN at both mRNA and protein levels along with an increase in the PI suggested that Sr could promote chondrocyte proliferation in the bovine. Similarly, these results were also in agreement with data in human primary chondrocytes demonstrating that Sr chondroitin sulfate markedly upregulated the expression of COL2A1 and ACAN (Ma et al., 2017). The TGF $\beta$  co-receptor Cripto promoted COL10A1 by inducing SMAD1/5/9 signaling in ATDC5 cells and immortalized C28/12 human chondrocytes (Garcia de Vinuesa et al., 2021). A role for ALPL in the maturation and mineralization as well as the inhibitory effect of Sr on SPP1, COL10A1, and ALPL was reported in murine chondrocytes (Ehriouchi et al., 2020). Thus, together, available data suggest a mechanistic function for the systemic supply of Sr on fundamental aspects of chondrocyte development (Figure 7).

Similar to non-ruminants, Sr promotes SMAD3 phosphorylation and transcription of its downstream genes *via* the TGF $\beta$ 1/ALK5 pathway, including COL2A1 and ACAN, both of which are key factors in the proliferation of chondrocytes. Differentiation of chondrocytes is controlled by Sr *via* decreasing the ALK1-induced SMAD1/5/9 phosphorylation and transcription of SPP1, COL10A1, and ALPL, all of which are key factors in differentiation. Overall, Sr activates TGF $\beta$ 1-

signaling towards phosphorylation of SMAD3 and, as such, systemic availability of this mineral can directly affect chondrocyte biology in dairy cattle.

## DATA AVAILABILITY STATEMENT

The original contributions presented in the study are included in the article/**Supplementary Material**, further inquiries can be directed to the corresponding author.

## ETHICS STATEMENT

The animal study was reviewed and approved by Animal Welfare and Research Ethics Committee at Northwest A&F University. Written informed consent was obtained from the owners for the participation of their animals in this study.

## AUTHOR CONTRIBUTIONS

SL and BS contributed to conception and design of the study, performed the experiments and wrote original draft. JL and QJ contributed to manuscript revision and editing. YY performed immunocytochemistry experiments. YK, PT, and FZ performed the statistical analysis. CZ and XZ designed the study. JW edited the manuscript.

## FUNDING

This study was supported by funds from the National Natural Science Foundation of China (No. 31873032 and No. 32102742).

## SUPPLEMENTARY MATERIAL

The Supplementary Material for this article can be found online at: <https://www.frontiersin.org/articles/10.3389/fphar.2022.925302/full#supplementary-material>

## REFERENCES

- Blaney Davidson, E. N., Remst, D. F., Vitters, E. L., van Beuningen, H. M., Blom, A. B., Goumans, M. J., et al. (2010). Increase in ALK1/ALK5 Ratio as a Cause for Elevated MMP-13 Expression in Osteoarthritis in Humans and Mice. *J. Immunol.* 182 (12), 7937–7945. doi:10.4049/jimmunol.109006810.4049/jimmunol.0803991
- Charlier, E., Deroyer, C., Ciregia, F., Malaise, O., Neuville, S., Plener, Z., et al. (2019). Chondrocyte Dedifferentiation and Osteoarthritis (OA). *Biochem. Pharmacol.* 165, 49–65. doi:10.1016/j.bcp.2019.02.036
- Chen, G., Deng, C., and Li, Y. P. (2012). TGF- $\beta$  and BMP Signaling in Osteoblast Differentiation and Bone Formation. *Int. J. Biol. Sci.* 8 (2), 272–288. doi:10.7150/ijbs.2929
- DaCosta Byfield, S., Major, C., Laping, N. J., and Roberts, A. B. (2004). SB-505124 Is a Selective Inhibitor of Transforming Growth Factor-Beta Type I Receptors

ALK4, ALK5, and ALK7. *Mol. Pharmacol.* 65 (3), 744–752. doi:10.1124/mol.65.3.744

- Dexheimer, V., Gabler, J., Bomans, K., Sims, T., Omlor, G., and Richter, W. (2016). Differential Expression of TGF- $\beta$  Superfamily Members and Role of Smad1/5/9-Signalling in Chondral versus Endochondral Chondrocyte Differentiation. *Sci. Rep.* 6, 36655. doi:10.1038/srep36655
- Ehriouchi, D., Bernabei, I., Chobaz, V., Castelblanco, M., Hügle, T., So, A., et al. (2020). CD11b Signaling Prevents Chondrocyte Mineralization and Attenuates the Severity of Osteoarthritis. *Front. Cell Dev. Biol.* 8, 611757. doi:10.3389/fcell.2020.611757
- Ferrao Blanco, M. N., Bastiaansen-Jenniskens, Y. M., Chambers, M. G., Pittsillides, A. A., Narcisi, R., and van Osch, G. J. V. M. (2021). Effect of Inflammatory Signaling on Human Articular Chondrocyte Hypertrophy: Potential Involvement of Tissue Repair Macrophages. *Cartilage* 13, 168S–174S. doi:10.1177/19476035211021907

- Finsson, K. W., Parker, W. L., Chi, Y., Hoemann, C. D., Goldring, M. B., Antoniou, J., et al. (2010). Endoglin Differentially Regulates TGF- $\beta$ -Induced Smad2/3 and Smad1/5 Signaling and its Expression Correlates with Extracellular Matrix Production and Cellular Differentiation State in Human Chondrocytes. *Osteoarthr. Cartil.* 18 (11), 1518–1527. doi:10.1016/j.joca.2010.09.002
- Finsson, K. W., Parker, W. L., ten Dijke, P., Thorikay, M., and Philip, A. (2008). ALK1 Opposes ALK5/Smad3 Signaling and Expression of Extracellular Matrix Components in Human Chondrocytes. *J. Bone Min. Res.* 23 (6), 896–906. doi:10.1359/jbmr.080209
- García de Vinuesa, A., Sanchez-Duffhues, G., Blaney-Davidson, E., van Caam, A., Lodder, K., Ramos, Y., et al. (2021). Cripto Favors Chondrocyte Hypertrophy via TGF- $\beta$  SMAD1/5 Signaling during Development of Osteoarthritis. *J. Pathol.* 255 (3), 330–342. doi:10.1002/path.5774
- Hellingman, C. A., Davidson, E. N., Koevoet, W., Vitters, E. L., van den Berg, W. B., van Osch, G. J., et al. (2011). Smad Signaling Determines Chondrogenic Differentiation of Bone-Marrow-Derived Mesenchymal Stem Cells: Inhibition of Smad1/5/8P Prevents Terminal Differentiation and Calcification. *Tissue Eng. Part A* 17 (7-8), 1157–1167. doi:10.1089/ten.TEA.2010.0043
- Hernández-Castellano, L. E., Hernandez, L. L., and Bruckmaier, R. M. (2020). Review: Endocrine Pathways to Regulate Calcium Homeostasis Around Parturition and the Prevention of Hypocalcemia in Periparturient Dairy Cows. *Animal* 14 (2), 330–338. doi:10.1017/S1751731119001605
- Hu, P., Du, J., Zhang, S., Wang, T., Li, J., Chen, G., et al. (2020). Oral Administration of Strontium Gluconate Effectively Reduces Articular Cartilage Degeneration through Enhanced Anabolic Activity of Chondrocytes and Chondrogenic Differentiation of Mesenchymal Stromal Cells. *Biol. Trace Elem. Res.* 193 (2), 422–433. doi:10.1007/s12011-019-01711-9
- Hyde, M. L., and Fraser, D. R. (2014). *In Vivo* measurement of the Absorption of Strontium in the Rumen and Small Intestine of Sheep as an Index of Calcium Absorption Capacity. *Br. J. Nutr.* 112 (5), 718–724. doi:10.1017/S0007114514001500
- Hyde, M. L., Wilkens, M. R., and Fraser, D. R. (2019). *In Vivo* measurement of Strontium Absorption from the Rumen of Dairy Cows as an Index of Calcium Absorption Capacity. *J. Dairy Sci.* 102 (6), 5699–5705. doi:10.3168/jds.2018-16052
- Khan, A. H., Rohra, D. K., Saghir, S. A., Udani, S. K., Wood, R. J., and Jabbar, A. (2013). No Change in Calcium Absorption in Adult Pakistani Population before and after Vitamin D Administration Using Strontium as Surrogate. *Osteoporos. Int.* 24 (3), 1057–1062. doi:10.1007/s00198-012-2007-9
- Komori, T. (2017). Roles of Runx2 in Skeletal Development. *Adv. Exp. Med. Biol.* 962, 83–93. doi:10.1007/978-981-10-3233-2\_6
- Komori, T. (2018). Runx2, an Inducer of Osteoblast and Chondrocyte Differentiation. *Histochem. Cell Biol.* 149 (4), 313–323. doi:10.1007/s00418-018-1640-6
- Kong, Y., Guo, Y., Zhang, J., Zhao, B., and Wang, J. (2018). Strontium Promotes Transforming Growth Factors  $\beta$ 1 and  $\beta$ 2 Expression in Rat Chondrocytes Cultured *In Vitro*. *Biol. Trace Elem. Res.* 184 (2), 450–455. doi:10.1007/s12011-017-1208-7
- Kozhemyakina, E., Lassar, A. B., and Zelzer, E. (2015). A Pathway to Bone: Signaling Molecules and Transcription Factors Involved in Chondrocyte Development and Maturation. *Development* 142 (5), 817–831. doi:10.1242/dev.105536
- Kronenberg, H. M. (2003). Developmental Regulation of the Growth Plate. *Nature* 423 (6937), 332–336. doi:10.1038/nature01657
- Li, T.-F., Darowish, M., Zuscik, M. J., Chen, D., Schwarz, E. M., Rosier, R. N., et al. (2004). Smad3-Deficient Chondrocytes Have Enhanced BMP Signaling and Accelerated Differentiation. *J. Bone Min. Res.* 21, 4–16. doi:10.1359/JBMR.050911
- Li, T. F., O'Keefe, R. J., and Chen, D. (2005). TGF-beta Signaling in Chondrocytes. *Front. Biosci.* 10, 681–688. doi:10.2741/1563
- Liu, Z., Yu, Z., Chang, H., Wang, Y., Xiang, H., Zhang, X., et al. (2019). Strontium-containing  $\alpha$ -calcium Sulfate Hemihydrate Promotes Bone Repair via the TGF- $\beta$ /Smad Signaling Pathway. *Mol. Med. Rep.* 20 (4), 3555–3564. doi:10.3892/mmr.2019.10592
- Ma, F. B., Liu, N., Hu, N., Wen, C. Y., and Tang, B. (2017). Synthesis of Strontium Chondroitin Sulfate and the Evaluation of its Capability to Attenuate Osteoarthritis. *Carbohydr. Polym.* 170, 217–225. doi:10.1016/j.carbpol.2017.04.067
- Madej, W., van Caam, A., Blaney Davidson, E., Buma, P., and van der Kraan, P. M. (2016). Unloading Results in Rapid Loss of TGF $\beta$  Signaling in Articular Cartilage: Role of Loading-Induced TGF $\beta$  Signaling in Maintenance of Articular Chondrocyte Phenotype? *Osteoarthr. Cartil.* 24, 1807–1815. doi:10.1016/j.joca.2016.05.018
- Mierzwa, A. G. H., Campos, J. F., Jesus, M. F., Nader, H. B., Lazaretti-Castro, M., and Reginato, R. D. (2017). Different Doses of Strontium Ranelate and Mechanical Vibration Modulate Distinct Responses in the Articular Cartilage of Ovariectomized Rats. *Osteoarthr. Cartil.* 25 (7), 1179–1188. doi:10.1016/j.joca.2017.02.793
- Milsom, S., Ibbertson, K., Hannan, S., Shaw, D., and Pybus, J. (1987). Simple Test of Intestinal Calcium Absorption Measured by Stable Strontium. *Br. Med. J. Clin. Res. Ed.* 295 (6592), 231–234. doi:10.1136/bmj.295.6592.231
- Ming, J., Wu, S., You, T., Wang, X., Yu, C., Luo, P., et al. (2019). Histone Deacetylation in the Promoter of P16 Is Involved in Fluoride-Induced Human Osteoblast Activation via the Inhibition of Sp1 Binding. *Biol. Trace Elem. Res.* 188 (2), 373–383. doi:10.1007/s12011-018-1413-z
- Pilmame, M., Salma-Ancane, K., Loca, D., Locs, J., and Berzina-Cimdina, L. (2017). Strontium and Strontium Ranelate: Historical Review of Some of Their Functions. *Mater. Sci. Eng. C Mater. Biol. Appl.* 78, 1222–1230. doi:10.1016/j.msec.2017.05.042
- Pors Nielsen, S. (2004). The Biological Role of Strontium. *Bone* 35 (3), 583–588. doi:10.1016/j.bone.2004.04.026
- Querido, W., Rossi, A. L., and Farina, M. (2016). The Effects of Strontium on Bone Mineral: A Review on Current Knowledge and Microanalytical Approaches. *Micron* 80, 122–134. doi:10.1016/j.micron.2015.10.006
- Thielen, N. G. M., van der Kraan, P. M., and van Caam, A. P. M. (2019). TGF $\beta$ /BMP Signaling Pathway in Cartilage Homeostasis. *Cells* 8 (9), 969. doi:10.3390/cells8090969
- van Caam, A., Blaney Davidson, E., Garcia de Vinuesa, A., van Geffen, E., van den Berg, W., Goumans, M. J., et al. (2015). The High Affinity ALK1-Ligand BMP9 Induces a Hypertrophy-like State in Chondrocytes that Is Antagonized by TGF $\beta$ 1. *Osteoarthr. Cartil.* 23 (6), 985–995. doi:10.1016/j.joca.2015.02.007
- van Caam, A., Madej, W., Garcia de Vinuesa, A., Goumans, M. J., ten Dijke, P., Blaney Davidson, E., et al. (2017). TGF $\beta$ 1-induced SMAD2/3 and SMAD1/5 Phosphorylation Are Both ALK5-kinase-dependent in Primary Chondrocytes and Mediated by TAK1 Kinase Activity. *Arthritis Res. Ther.* 19 (1), 112. doi:10.1186/s13075-017-1302-4
- Vimalraj, S. (2020). Alkaline Phosphatase: Structure, Expression and its Function in Bone Mineralization. *Gene* 754, 144855. doi:10.1016/j.gene.2020.144855
- Vogt, J., Traynor, R., and Sapkota, G. P. (2011). The Specificities of Small Molecule Inhibitors of the TGF $\beta$  and BMP Pathways. *Cell. Signal.* 23 (11), 1831–1842. doi:10.1016/j.cellsig.2011.06.019
- Wang, C. Y., Xia, W. H., Wang, L., and Wang, Z. Y. (2021). Manganese Deficiency Induces Avian Tibial Dyschondroplasia by Inhibiting Chondrocyte Proliferation and Differentiation. *Res. Vet. Sci.* 140, 164–170. doi:10.1016/j.rvsc.2021.08.018
- Wang, J., Zhu, X., Liu, L., Shi, X., Yin, L., Zhang, Y., et al. (2013). Effects of Strontium on Collagen Content and Expression of Related Genes in Rat Chondrocytes Cultured *In Vitro*. *Biol. Trace Elem. Res.* 153 (1-3), 212–219. doi:10.1007/s12011-013-9640-9
- Woods, S., Humphreys, P. A., Bates, N., Richardson, S. A., Kuba, S. Y., Brooks, I. R., et al. (2021). Regulation of TGF $\beta$  Signaling by TRPV4 in Chondrocytes. *Cells* 10 (4), 726. doi:10.3390/cells10040726
- Wu, M., Chen, G., and Li, Y. P. (2016). TGF- $\beta$  and BMP Signaling in Osteoblast, Skeletal Development, and Bone Formation, Homeostasis and Disease. *Bone Res.* 4, 16009. doi:10.1038/boneres.2016.9
- Yu, X., Shen, G., Ren, H., Zhang, Z., Shang, Q., Zhao, W., et al. (2019). Tgfb-Induced Factor Homeobox 2 Blocks Osteoblastic Differentiation through Targeting pSmad3/HDAC4/H4ac/Runx2 axis. *J. Cell. Physiol.* 234 (11), 21284–21293. doi:10.1002/jcp.28733

- Zhang, H., Du, L., Zhong, Y., Flanders, K. C., and Roberts, J. D. (2017). Transforming Growth Factor- $\beta$  Stimulates Smad1/5 Signaling in Pulmonary Artery Smooth Muscle Cells and Fibroblasts of the Newborn Mouse through ALK1. *Am. J. Physiol. Lung Cell Mol. Physiol.* 313 (3), L615–L627. doi:10.1152/ajplung.00079.2017
- Zhu, Y., Hu, C., Zheng, P., Miao, L., Yan, X., Li, H., et al. (2016). Ginsenoside Rb1 Alleviates Aluminum Chloride-Induced Rat Osteoblasts Dysfunction. *Toxicol.* 368–369, 183–188. doi:10.1016/j.tox.2016.07.014

**Conflict of Interest:** The authors declare that the research was conducted in the absence of any commercial or financial relationships that could be construed as a potential conflict of interest.

**Publisher's Note:** All claims expressed in this article are solely those of the authors and do not necessarily represent those of their affiliated organizations, or those of the publisher, the editors and the reviewers. Any product that may be evaluated in this article, or claim that may be made by its manufacturer, is not guaranteed or endorsed by the publisher.

Copyright © 2022 Liu, Shen, Loo, Jiang, Yuan, Kong, Tan, Zeng, Zhao, Zhu and Wang. This is an open-access article distributed under the terms of the Creative Commons Attribution License (CC BY). The use, distribution or reproduction in other forums is permitted, provided the original author(s) and the copyright owner(s) are credited and that the original publication in this journal is cited, in accordance with accepted academic practice. No use, distribution or reproduction is permitted which does not comply with these terms.



# Immunomodulatory Effect of Ginsenoside Rb2 Against Cyclophosphamide-Induced Immunosuppression in Mice

Siwen Zheng<sup>1,2†</sup>, Housheng Zheng<sup>1,2†</sup>, Rui Zhang<sup>1,2</sup>, Xiangmin Piao<sup>1,2</sup>, Junnan Hu<sup>2</sup>, Yanzhu Zhu<sup>3,4\*</sup> and Yingping Wang<sup>1,2\*</sup>

## OPEN ACCESS

### Edited by:

Eleonore Fröhlich,  
Medical University of Graz, Austria

### Reviewed by:

Dirlei Nico,  
Federal University of Rio de Janeiro,  
Brazil  
Yinshi Sun,  
Institute of Special Animal and Plant  
Sciences (CAAS), China  
Xiaoying Wang,  
Tianjin University of Traditional  
Chinese Medicine, China  
Ting Shen,  
Huaiyin Normal University, China

### \*Correspondence:

Yanzhu Zhu  
zyzzu@126.com  
Yingping Wang  
wangyingping@jlan.edu.cn

<sup>†</sup>These authors have contributed  
equally to this work and share first  
authorship

### Specialty section:

This article was submitted to  
Predictive Toxicology,  
a section of the journal  
Frontiers in Pharmacology

Received: 23 April 2022

Accepted: 31 May 2022

Published: 24 June 2022

### Citation:

Zheng S, Zheng H, Zhang R, Piao X,  
Hu J, Zhu Y and Wang Y (2022)  
Immunomodulatory Effect of  
Ginsenoside Rb2 Against  
Cyclophosphamide-Induced  
Immunosuppression in Mice.  
*Front. Pharmacol.* 13:927087.  
doi: 10.3389/fphar.2022.927087

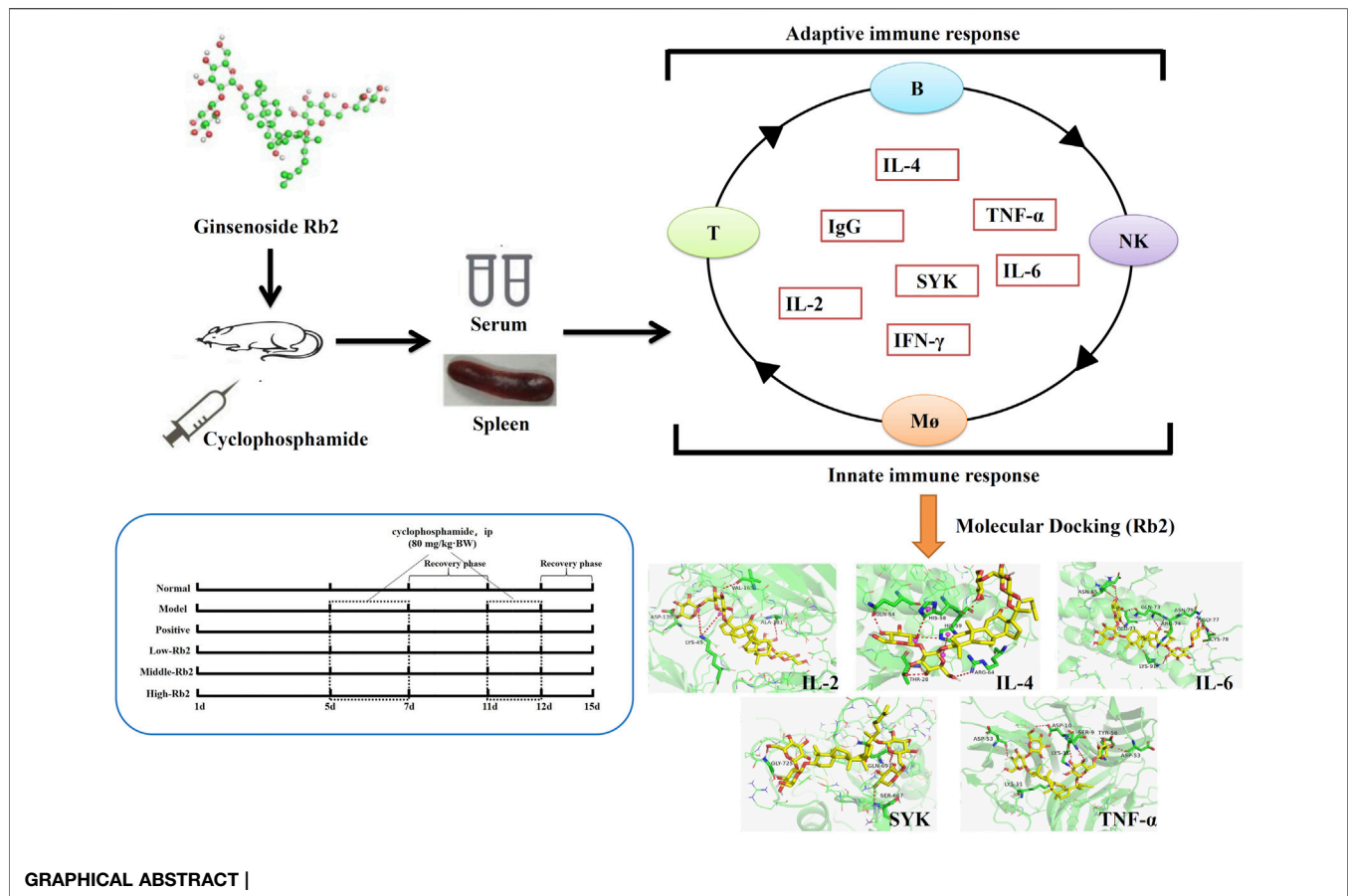
<sup>1</sup>National and Local Joint Engineering Research Center for Ginseng Breeding and Development, Changchun, China, <sup>2</sup>College of Chinese Medicinal Materials, Jilin Agricultural University, Changchun, China, <sup>3</sup>Institute of Special Animal and Plant Sciences, Chinese Academy of Agricultural Sciences, Changchun, China, <sup>4</sup>Animal Science and Technology College, Jilin Agriculture Science and Technology University, Jilin, China

Ginsenoside Rb2 (Rb2), a fundamental saponin produced and isolated from ginseng (*Panax ginseng* C.A. Meyer), has a wide range of biological actions. The objective of this investigation was to see if ginsenoside Rb2 has any immunomodulatory properties against cyclophosphamide (CTX)-induced immunosuppression. For the positive control group, levamisole hydrochloride (LD) was used. We discovered that intraperitoneal injection of Rb2 (5, 10, 20 mg/kg) could relieve CTX-induced immunosuppression by enhanced immune organ index, reduced the pathological characteristics of immunosuppression, promoted natural killer (NK) cells viability, improved cell-mediated immune response, boosted the IFN- $\gamma$  (Interferon-gamma), TNF- $\alpha$  (Tumor necrosis factor-alpha), IL-2 (Interleukin-2), and IgG (Immunoglobulin G), as well as macrophage activity like carbon clearance and phagocytic index. Rb2 significantly elevated the mRNA expression of IL-4 (Interleukin-4), SYK (Tyrosine-protein kinase-SYK), IL-2, TNF- $\alpha$ , and IL-6 (Interleukin-6) in the spleen of CTX-injected animals. Molecular docking results showed that Rb2 had excellent binding properties with IL-4, SYK, IL-2, TNF, and IL-6, indicating the target protein might be strongly correlated with the immunomodulatory effect of Rb2. Taken together, ginsenoside Rb2 can improve the immune function that is declined in CTX-induced immunosuppressed mice, the efficacy maybe due to the regulation of related cytokine and mRNA expression.

**Keywords:** ginsenoside Rb2, cyclophosphamide, side effect, immunosuppression, immune regulation

## INTRODUCTION

Cancer is internationally recognized as one of the most dangerous diseases that endanger human life and development. Chemotherapy is the main method to treat cancer. It is based on the prevention of rapid cell proliferation, which is a feature of malignant cells. Unfortunately, normal cells with quick proliferation rates, such as lymphocytes, bone marrow, and hair follicles, are also affected (Pérez-Herrero and Fernández-Medarde, 2015; Kondo et al., 2019). CTX (cyclophosphamide) is a well-known anticancer medication that is still used to treat hematological malignancies and a variety of epithelial tumors (Ahlmann and Hempel, 2016; Hughes et al., 2018). However, its treatment is often



accompanied by serious side effects (Chow et al., 2017; Yang et al., 2020; Zhang et al., 2020). Immunosuppression induced by CTX is the main side effect of clinical chemotherapy. When a patient's immune function is harmed by chemotherapy, the risk of secondary infection and immunodeficiency rises, which may result in serious morbidity and mortality problems (Yoo et al., 2020). *Lactobacillus plantarum* NCU116 was found to be capable of reversing immunosuppression caused by CTX (Xie et al., 2016), and *Paecilomyces sinensis* glycopeptides demonstrated excellent immunostimulatory capabilities (Zhen-Yuan Zhu et al., 2016).

Ginseng is one of the most widely used traditional herbal medicines, with a medical history dating back thousands of years (Ji et al., 2020). Numerous investigations into the impact of the systemic immune function of ginseng have been conducted (Riaz et al., 2019; Ratan et al., 2021). Ginsenosides are the main bioactive components in ginseng that have a variety of pharmacological actions, including the treatment of cardiovascular diseases (Kim, 2018; Irfan et al., 2020), antioxidant (Oh et al., 2015), anticancer (Wanderi et al., 2016), immune (Kang and Min, 2012; Chen et al., 2019) and osteoblast growth regulation (Yanzhu Zhu et al., 2016). Ginsenoside Rb2 (Rb2) is a highly abundant dammarane-type ginsenoside (Hong et al., 2019). Rb2 inhibits metabolic syndrome in mice such as diabetes mellitus and hyperlipidemia (Lee et al., 2011; Hong et al., 2019). Rb2 reduces the number of metastatic nodules in liver, lung

and kidney of mice with colon cancer (Phi et al., 2018; Dai et al., 2019). Moreover, Rb2 protects bone marrow-derived mesenchymal stem cells from dexamethasone-induced apoptosis by increasing the GPR120-mediated Ras-ERK1/2 signaling pathway, and up-regulates GPR120 expression in lipopolysaccharide (LPS)-stimulated RAW264.7 macrophages to boost the anti-inflammatory efficacy of -3 fatty acid (Gao et al., 2015; Huang et al., 2017). Oral administration of ginsenoside Rb2 protects mice from the lethal infection of Japanese hemoagglutinating virus (Yoo et al., 2013). Thus, Rb2 is expected to be an anti-viral immune adjuvant.

The aim of this research was to explore the role of Rb2 in the immunosuppression caused by CTX. To assess the beneficial effects of ginsenoside Rb2, organ index and pathological features of spleen, splenocyte proliferation, carbon clearance, NK cell activities, mRNA expression of immune-related genes (in spleen) and cytokines (in serum) were also determined. This result will illustrate the role of Rb2 in the prevention of CTX-induced immunosuppressive effects.

## MATERIALS AND METHODS

### Reagents and Animals

Jilin University (Changchun, China) provided us with ginsenoside Rb2 (purity >98%). Jiangsu Shengdi

Pharmaceutical Co., Ltd. (Jiangsu China) was the source of CTX. Levamisole hydrochloride (LD) was bought from Sigma (St. Louis, MO). YAC-1 cell lines (Chinese Academy of Sciences, China) were stored by our lab. CCK-8, RPMI 1640 medium, ConA (canavalin A), LPS, Red Blood Cell Lysis Buffer, Hank's solution, Triton X-100 and fetal bovine serum (FBS) were obtained from Beijing Solarbio Science & Technology Co., Ltd. Gibco (BRL Co. Ltd., Gaithersburg, MD, United States). IFN- $\gamma$  (Interferon-gamma), TNF- $\alpha$  (Tumor necrosis factor-alpha), IL-2 (Interleukin-2) and IgG (Immunoglobulin G) kits were bought from Lengtong Bioscience Co., Ltd. (Shanghai, China). Reverse transcription kit and qPCR kit were obtained from Trans Biotechnology Co., Ltd. (Beijing, China).

Changchun Institute of Biological Products Co. Ltd. provided one hundred and twenty male BALB/c mice (SPF level, License No. SCXK (Ji)-2017-0005). For at least a week before use, the mice were maintained in plastic cages with 12-h light/dark cycles and a relative humidity of 55% at a temperature of  $23 \pm 2^\circ\text{C}$ . They were fed a conventional laboratory diet and had unrestricted access to water. The guiding principle was followed during the care and use of mice. The experiment was approved by the Laboratory Animal Ethics Committee of Jilin Agricultural University (Permit No. 20200923002). The experiment was repeated three times independently, and the detection of each indicator was repeated three times by different experimenters.

## Animals and Experiments Design

Six groups ( $n = 20$  BALB/c mice) were prepared after a 7-day acclimation period: normal group, low-dose Rb2 administration group (5 mg/kg), middle-dose Rb2 administration group (10 mg/kg), high-dose Rb2 administration group (20 mg/kg), model group, positive group. Normal saline was given to both normal and model mice. LD (100 mg/kg) was given to the animals in the positive control group. Except for the mice in the positive group, which were administered intragastrically, the animals in other groups were administered by intraperitoneal injection. After the experiment commenced, the mice were administered for 15 consecutive days. Except for normal mice, the mice were administered with CTX (80 mg/kg) through intraperitoneal injection for three consecutive days on the 5th day and two consecutive days on the 11th day. Sixty mice ( $n = 10$ ) were weighed individually after 24 h, while the other sixty mice were used in a carbon clearance test. The mice were euthanized by intraperitoneal injection of pentobarbital (150 mg/kg) (Alibolandi et al., 2017), and the serum was collected and centrifuged twice at 4000 rpm for 10 min. The livers and spleens were collected and weighed. The spleen indexes were computed as:  $\text{index} = \text{spleen weight (g)} \times 1000/\text{body weight (g)}$ . Extra spleen samples were stored in liquid nitrogen after a small quantity of spleen samples were used for tissue biopsies. Spleen samples were preserved in buffered formaldehyde at 10% (V/V), embedded in paraffin, and sectioned for histological analysis (Meng et al., 2019). 4  $\mu\text{m}$  thick slices were stained with hematoxylin and eosin (HE) and captured by a microscope (OLYMPUS BX 53, Olympus Co., Tokyo, Japan).

**TABLE 1** | Primer sequences (5'-3') used for qRT-PCR.

Gene	Forward sequence	Reverse sequence
IL-2	TACAGCGGAAGCACAGCAG	CGCAGAGGTCCAAGTTCATC
IL-4	AACGAGGTCACAGGAGAAGG	TGGAAGCCCTACAGACAAGC
IL-6	CGGAGAGGAGACTTCACAGAG	CATTTCACGATTTCCAGAG
SYK	CAGCTGGAGGATCGGAGAAC	CCATGGAACCGGGCATCTT

## Preparation of Spleen-Derived Lymphocyte Populations

After 24 h, the mice were euthanized by intraperitoneal injection of pentobarbital (150 mg/kg) (Alibolandi et al., 2017), and disinfected with ethanol for 3 min. The spleen was taken to the clean bench. Splenic cell suspension was prepared following the method (Singh et al., 2016). The connective tissue on the spleen was removed. 3 ml Hank's was added and ground with a 10 ml syringe core. The cell suspension was screened by a 70- $\mu\text{m}$ -cell-sieve, centrifugation was performed subsequently, and Red Cell Lysis Buffer was added for 3 min. Then RPMI 1640 culture medium containing 10% FBS was used to wash them twice, so as to prepare a uniform cell suspension. Spleen cell suspension was counted and checked for viability using trypan blue staining.

## Lymphocyte Proliferation

This experiment was performed as previously described (Jang et al., 2016). The CCK-8 assay was used to evaluate ConA and LPS-induced T and B splenic lymphocyte proliferation. Trypan blue staining revealed more than 95% viable cells, and the cell concentration of the cell suspension was  $1 \times 10^6/\text{ml}$ . Con A (5 g/ml) or LPS (10 g/ml) was added to each well of 96-well plates before seeding spleen cells (100  $\mu\text{l}$ ). The control group consisted of spleen cells cultured in RPMI 1640 medium. The spleen cells were cultured for 48 h at  $37^\circ\text{C}$  in 5%  $\text{CO}_2$ . After a 48-h incubation time, 10  $\mu\text{l}$  CCK-8 chromogenic agent was supplied to each well and incubated for three additional hours. A microplate reader was used to measure the absorbance at 450 nm. The detection was repeated three times by different experimenters.

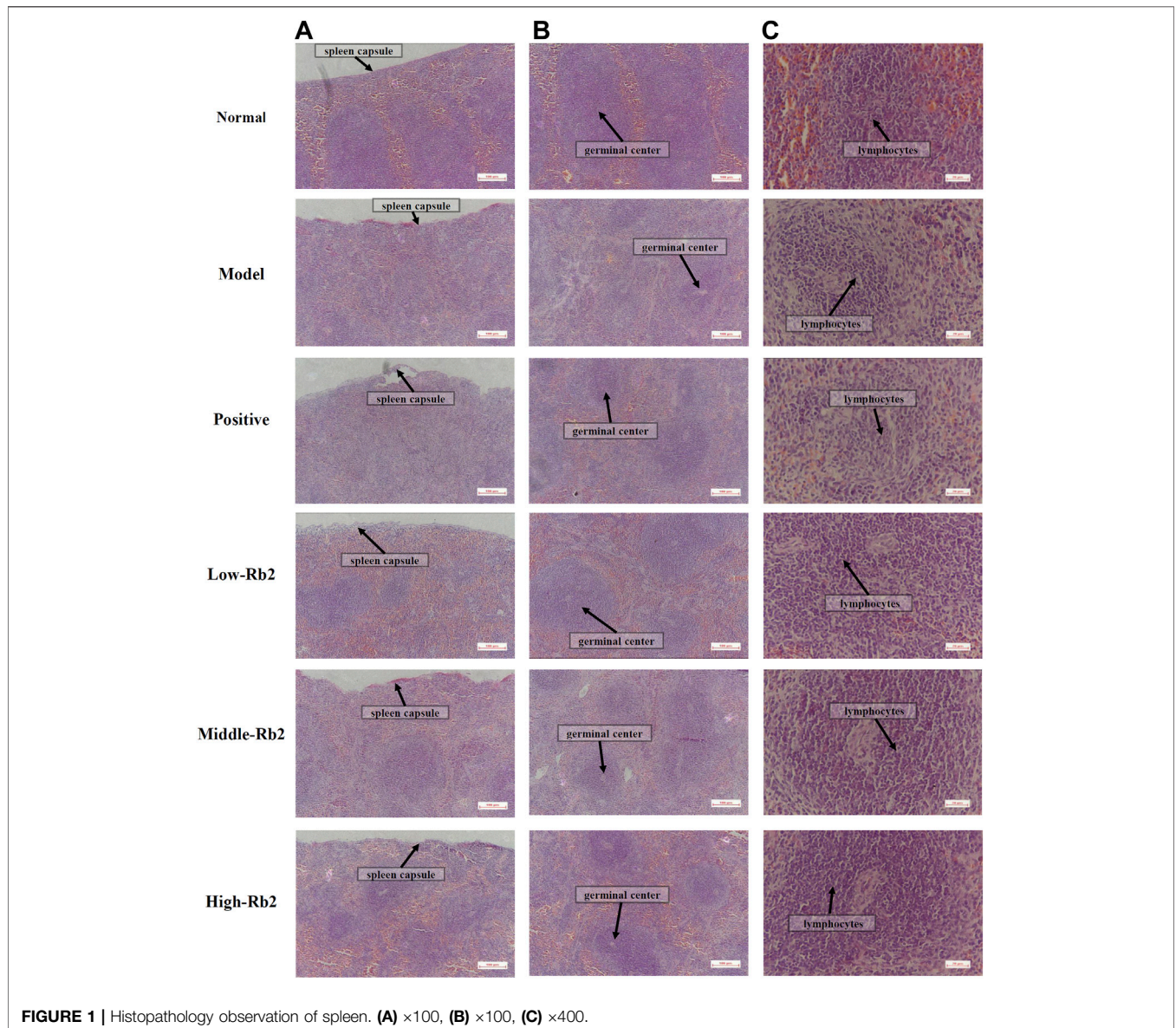
## Determination of Natural Killer Cell Activity

Lactate dehydrogenase (LDH) release test was used to measure NK cell activity (Hwang et al., 2022). NK cells were employed to treat pre-cultured YAC-1 cells. The concentration of target cells was adjusted to  $4 \times 10^5$  cells per milliliter. Splenocytes from mice's spleens were used as a source of effector cells, and the cell concentration was controlled to  $2 \times 10^7$  cells per milliliter using RPMI 1640 media containing 10% FBS.

Effector cells were co-cultured with target cells (100  $\mu\text{l}$ ) at a 50:1 ratio in an U-shaped 96-well plate. For the experiment, two controls were used: a spontaneous control and a maximum spontaneous control. As a spontaneous control, target cells (100  $\mu\text{l}$ ) and RPMI1640 medium (100  $\mu\text{l}$ ) were added to the natural target cells release well. A maximal spontaneous control was created by adding target cells (100  $\mu\text{l}$ ) and Triton X-100 (100  $\mu\text{l}$ , 2.5%, v/v) to the maximum releasing well. Plates

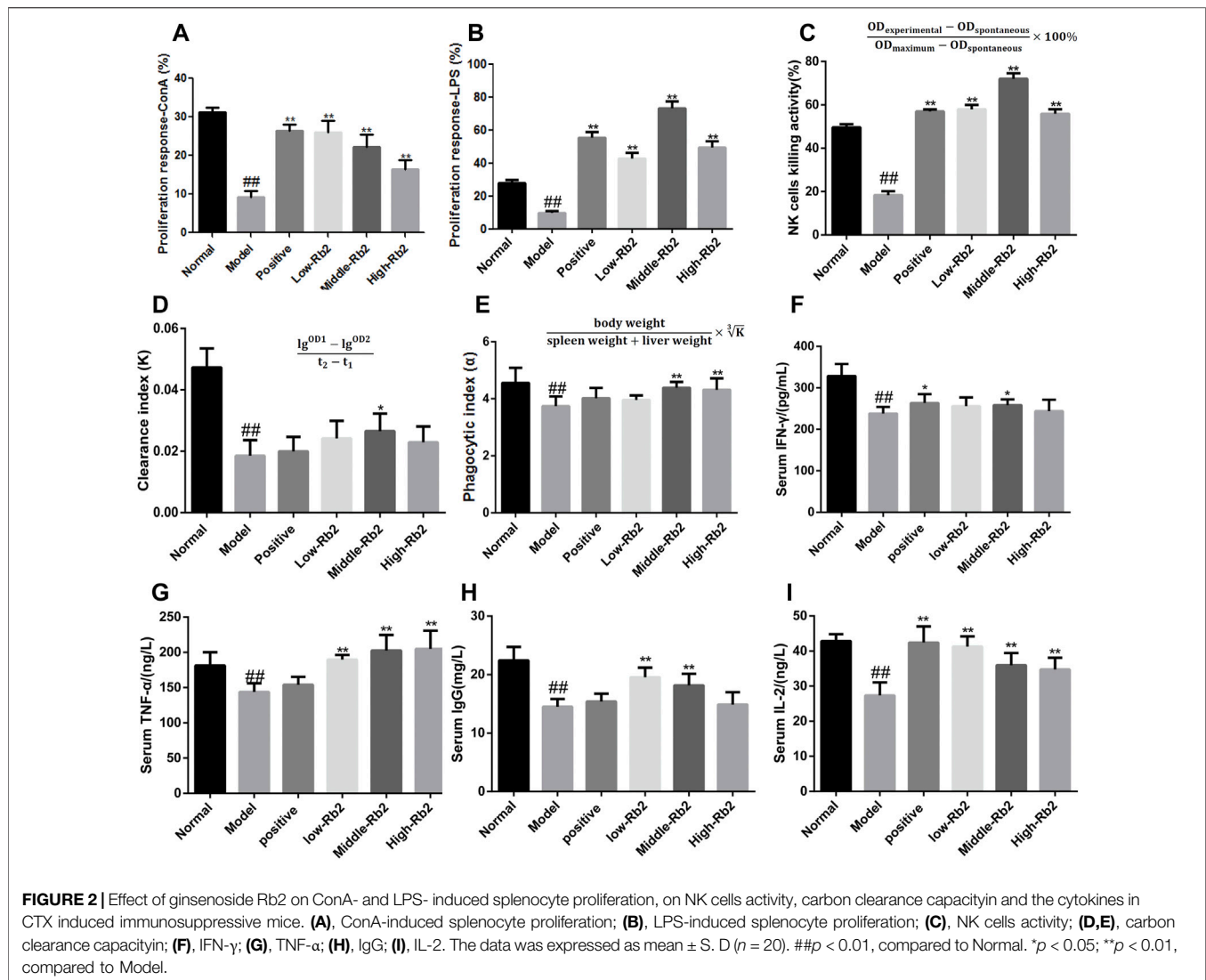
**TABLE 2** | Effect of ginsenoside Rb2 on body weight and spleen indices in mice (mean  $\pm$  S.D.,  $n = 10$ ).

Group	Dose (mg/kg)	Initial body weight (g)	Final body weight (g)	Spleen index (mg/g)
Normal	-	26.77 $\pm$ 1.64	28.95 $\pm$ 1.16	5.53 $\pm$ 0.91
Model	-	27.00 $\pm$ 1.67	23.81 $\pm$ 2.66 <sup>##</sup>	2.14 $\pm$ 0.31 <sup>##</sup>
Positive	100 (LD)	27.92 $\pm$ 1.10	26.89 $\pm$ 1.50*	3.46 $\pm$ 0.89**
Low-Rb2	5	26.58 $\pm$ 1.57	23.99 $\pm$ 2.20	3.00 $\pm$ 0.89*
Middle-Rb2	10	26.84 $\pm$ 1.93	26.92 $\pm$ 1.49*	3.57 $\pm$ 0.66**
High-Rb2	20	27.38 $\pm$ 1.98	26.12 $\pm$ 2.43	3.86 $\pm$ 0.50**



were incubated at 37°C for 4 h in a 5% CO<sub>2</sub> incubator before being centrifuged for 5 min at 900 g. Supernatant (100  $\mu$ l) was transferred to a new plate, followed by 100  $\mu$ l of LDH matrix solution and 30  $\mu$ l of 1 M HCL in each well. Finally, at 490 nm, the

absorbance value was determined by an automatic microplate reader (BioTek Epoch, BioTek, Winooski, VT, United States). The detection was repeated three times by different experimenters.



## Carbon Clearance Test

Chen's approach was used to conduct the carbon clearance test (Chen et al., 2019). Each mouse (six groups,  $n = 10$ ) received an intravenous injection of 4 times diluted India ink at a dose of 100  $\mu$ l/10 g. After 2 min ( $t_1$ ) and 10 min ( $t_2$ ), 20  $\mu$ l blood was collected from the retinal venous plexuses and mixed with 2 ml of 0.1%  $\text{Na}_2\text{CO}_3$  at once. The absorbance was measured at 600 nm in an ELISA reader. Mice were euthanized by cervical dislocation (Karimi et al., 2018), and their spleen and liver were removed and weighed. Phagocytic index  $\alpha$  was used to express the carbon clearance ability of the mice. The detection was repeated three times by different experimenters.

## Measurement of Immune-Related Cytokines in the Serum

The serum was obtained before the animals were euthanized (ip., Pentobarbital, 150 mg/kg) and centrifuged twice at 4000 rpm for 10 min. The manufacturer's instructions were followed to assess

the levels of IL-2, TNF- $\alpha$ , IFN- $\gamma$ , and IgG in the serum using mouse enzyme-linked immunosorbent assay kit. The detection was repeated three times by different experimenters.

## qRT-PCR Analysis

The reverse transcription method was based on the instructions of the kit. The dose of reactants was adjusted according to the concentration of total RNA extracted from tissues. After successful reverse transcription, samples were stored at  $-80^\circ\text{C}$ . The functional gene expression was determined by the TransStart Top Green qPCR SuperMix (+dye II) method in QuantStudio<sup>®</sup> three real-time quantitative PCR system.  $2^{-\Delta\Delta\text{CT}}$  approach was used to obtain the mRNA relative expression. The primer sequences of the target gene and housekeeper gene determined in this study are shown in Table 1. The detection was repeated three times by different experimenters.

## Molecular Docking

In order to explore the binding site and binding force between Rb2 and IL2, IL-4, IL-6, Syk, and TNF, we used molecular docking

technology. The steps of molecular docking were as follows: download the protein structure and preprocess, download the ligand structure and preprocess, conduct molecular docking, calculate the binding score, and visualize the docking results (Ferdian et al., 2020). Canonical SMILES notations of Rb2 were retrieved from PubChem Databases in NCBI (National Library of Medicine) and PDB structure files was created by ChemOffice 2017. Protein structures for SYK (PDB ID: 2mc1), TNF (PDB ID: 2tnf), IL-2 (PDB ID: 4YUE), IL-4 (PDB ID: 2B8U), and IL-6 (PDB ID: 2I3Y) were available from the Protein Data Bank. The Lamarckian genetic process was used to convert the format and find the active pocket with AutoDockTools-1.5.6 (Molecular Graphics Laboratory, The Scripps Research Institute, La Jolla, CA, United States). The pretreated protein ligands and protein receptors were docked with Autodock-Vina (Molecular Graphics Laboratory, The Scripps Research Institute, La Jolla, CA, United States) for three times independently. Docking log files yielded the lowest binding energy. The mean of binding energy was calculated from three independent dockings. Selected dockings were visualized with PyMol software (Schrodinger, LLC, New York, NY, United States).

## Statistical Analysis

Experimental data were analyzed utilizing Graphpad Prism 7.0 (GraphPad Software Inc., La Jolla, CA, United States). The data were presented as means  $\pm$  S.D. One-way ANOVA with *t*-tests for post hoc analysis was used to assess the differences between the groups. If the difference was less than 0.05, it was regarded as significant, and if it was less than 0.01, it was considered extremely significant.  $\#p < 0.01$ , compared to Normal.  $*p < 0.05$ ;  $**p < 0.01$ , compared to Model.

## RESULTS

### Body Weight and Spleen Index

As indicated in **Table 2**, CTX-induced immunosuppression resulted in significant weight loss of the body and spleen indexes. However, the mice with different doses of Rb2 showed significantly larger spleen indices than the CTX group ( $p < 0.05$ ). When compared to the CTX group, the body weight of the positive control and middle-Rb2 groups improved significantly ( $p < 0.05$ ). It indicates that ginsenoside Rb2 restored the spleen indices and the body weight in the mice with CTX.

### Histopathological Alterations

The spleen histopathology was examined with H&E staining to further analyze the effect of Rb2. The spleen capsule was damaged, the germinal center was distributed, and the number of lymphocytes was lowered and sparse in the model group (**Figure 1**). The damage to the spleen was relieved to varying degrees after Rb2 treatment compared to the model, the spleen capsule was intact, and the germinal center was integrated. The lymphocytes had increased considerably, and they were tightly packed together. The findings showed that Rb2 reduces CTX-induced spleen damage in mice.

### Splenic Lymphocytes Proliferation

T and B lymphocyte proliferation in response to mitogens or antigens has traditionally been used as an immunological

measure to assess lymphocyte responsiveness. ConA-induced cellular proliferation was used to assess T lymphocyte immunity, while LPS-induced B cell activation was used to identify B lymphocyte immunity. In the model group, the proliferation index of splenic lymphocytes to ConA (**Figure 2A**) and LPS (**Figure 2B**) was considerably lower than the normal control group ( $p < 0.05$ ). The proliferation index of splenic lymphocytes in immunosuppressed mice was considerably increased after treatment with Rb2 compared to the model group ( $p < 0.05$ ). Rb2 was found to be involved in the splenic T and B lymphocytes proliferation in immunosuppressed mice induced by CTX.

### Natural Killer Cell Activity

LDH release test was used to assess NK cell activity. **Figure 2C** demonstrates that the model group's NK cell activity was dramatically reduced to 18% ( $p < 0.01$ ) compared to the normal control group. Compared to the model group, the activity of NK cells in the positive group, the low-Rb2 group, the middle-Rb2 group and the high-Rb2 group was significantly increased to 57, 58, 72, and 56%, respectively. It indicates that Rb2 boosts cell immunological function in mice with CTX.

### Effects of Ginsenoside Rb2 on Carbon Clearance

To investigate the influence of Rb2 on macrophage activation, carbon clearance assays were performed. The CTX-treated group had a considerably lower phagocytic index  $\alpha$  than the normal control group ( $p < 0.01$ ) (**Figures 2D,E**). Pretreatment with Rb2 dramatically reversed the inhibitory effect of CTX. The values in the middle-Rb2 ( $p < 0.05$ ) and high-Rb2 groups ( $p < 0.01$ ) were considerably higher than those in the model group, suggesting that Rb2 can improve macrophage function in immunosuppressed mice caused by CTX.

### Cytokines

To explore the immunomodulatory effects of Rb2 on cytokines, IFN- $\gamma$ , TNF- $\alpha$ , IL-2, and IgG levels in serum were assessed. As shown in **Figures 2F-I**, the levels of immune-related cytokines in the model were considerably lower ( $p < 0.01$ ) than the control. The IFN- $\gamma$  content in the positive and middle-Rb2 group was substantially higher compared to the model ( $p < 0.05$ ), whereas that in the low-Rb2 and high-Rb2 groups exerted an increased trend. The content of TNF- $\alpha$  and IL-2 in the three Rb2 administration groups was significantly enhanced ( $p < 0.01$ ). IgG content in the low and middle groups was enormously improved ( $p < 0.01$ ), but IgG was not significantly regulated in high group.

### The Levels of Immune-Related Gene Expression

Compared with the control, CTX significantly reduced the above-mentioned relative gene expression levels (**Figures 3A-E**) in the model ( $p < 0.01$ ). The relative expression of IL-4, TNF- $\alpha$ , IL-2, SYK, and IL-6 was promoted after treatment with Rb2.

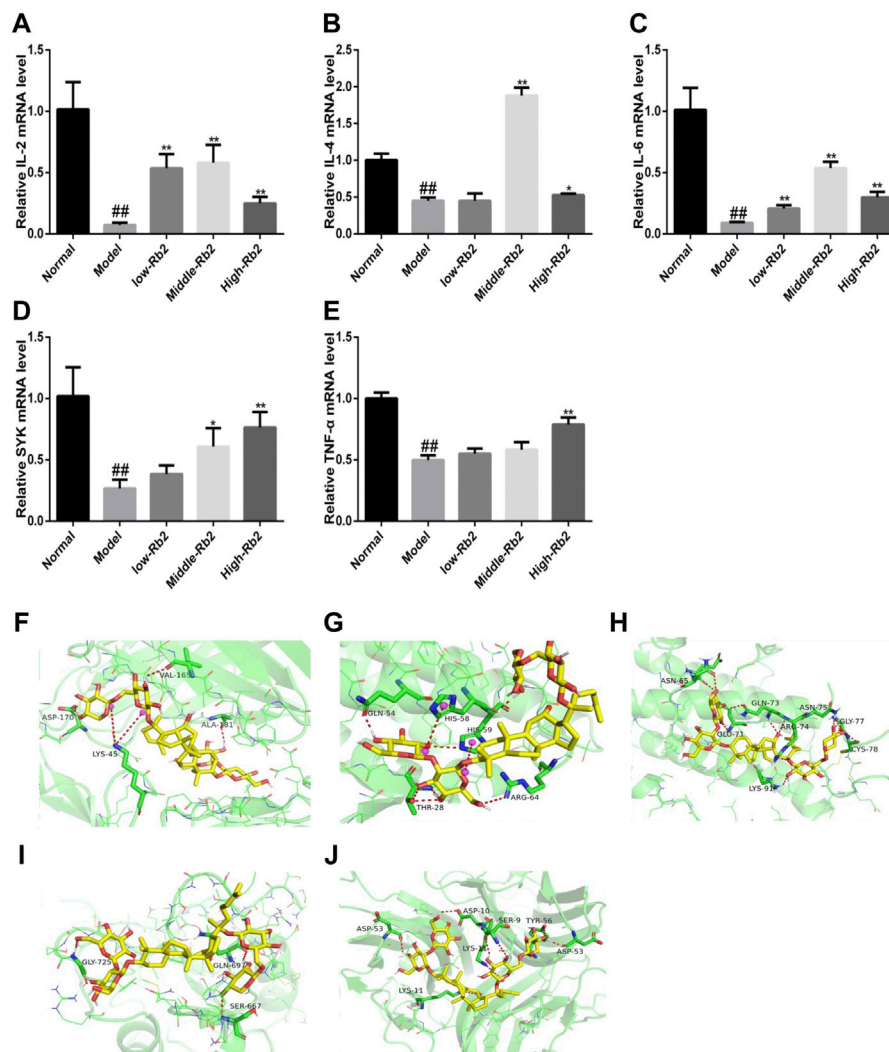


**FIGURE 3 |** The relative gene expression of cytokines in spleen. **(A)**, IL-2; **(B)**, IL-4; **(C)**, IL-6; **(D)**, SYK; **(E)**, TNF- $\alpha$ . ## $p < 0.01$ , compared to Normal. \*\* $p < 0.01$ , compared to Model. **(F)** Docking of Rb2 (yellow) into the binding site of mouse IL-2 (PDB code: 4yue, green); **(G)** Docking of Rb2 (yellow) into the binding site of mouse IL-4 (PDB code: 2b8u, green); **(H)** Docking of Rb2 (yellow) into the binding site of mouse IL-6 (PDB code: 2l3y, green); **(I)** Docking of Rb2 (yellow) into the binding site of mouse SYK (PDB code: 2mc1, green); **(J)** Docking of Rb2 (yellow) into the binding site of mouse TNF (PDB code: 2tnf, green).

## Docking Results

In order to investigate the binding pattern and the active site cavity of Rb2 and IL-4, SYK, IL-2, TNF, and IL-6, molecular docking was accomplished by AutoDockTools-1.5.6 and AutoDock vina. The lowest binding energies for TNF, IL-4, SYK, IL-2, and IL-6 were  $-7.7$ ,  $-7.3$ ,  $-7.6$ ,  $-9.8$  and  $-8.3$  kcal/mol, respectively. The result indicates that Rb2 has a higher affinity for IL-2 than the other proteins. Molecular docking investigations of Rb2 on IL-2 (**Figure 3F**) revealed hydrogen bonding interactions as well as a salt bridge with the amino acid residues around the binding site. Rb2 binds with IL-2 by forming three hydrogen bonds as illustrated in **Figure 3F** (amino acid residues ASP-170, VAL-165 and ALA-180), and the salt bridge was evident with amino acid residues LYS-45 (2 bonds). Hydrogen bonds between Rb2 and IL-4 were formed with

amino acid residues GLN-54, THR-28 (3 bonds) and ARG-64, and the salt bridge was evident with amino acid residues HIS-58 and HIS-59. The binding interactions of Rb2 on IL-6 have been shown in the form of hydrogen bonds in molecular docking studies. The amino acid residues ASN-65 (2 bonds), GLU-71, GLN-73 (2 bonds), ARG-74, LYS-91, ASN-75 (2 bonds), GLY-77 (2 bonds), and CYS-78 were identified as forming hydrogen bonds with Rb2 (**Figure 3H**). Rb2 binds to SYK via hydrogen bonds. The amino acid residues GLY-725, GLN-697, and SER-667 (**Figure 3I**) were all discovered to form hydrogen bonds with Rb2. Additionally, Rb2 was found to interact with TNF by forming hydrogen bonds with amino acid residues ASP10, SER-9 (2 bonds), TYP-56, ASP-53 (2 bonds), and LSP-11, and the salt bridge was evident with amino acid residues LYS-11 (**Figure 3J**).

## DISCUSSION

Almost all chemotherapeutic medicines are toxic, and chemotherapy has substantial and often fatal adverse effects, such as severe nausea, myelosuppression, and immunosuppression (Ngulde et al., 2020). CTX is an immunosuppressant that is frequently used in clinical chemotherapy for malignant tumors. The proliferation of T and B was inhibited by CTX through disrupting with DNA and RNA activities (Johnson et al., 2012). Ginseng is well known for its immune-boosting properties. The modulation of the immune system has been extensively described in terms of preserving immune system homeostasis and increasing resistance to disease or pathogenic attacks (Lee et al., 2015; Iqbal and Rhee, 2020).

Ginsenosides (Re, Rg3, Rg1, Rb1, Rb2) are the major bioactive constituents of ginseng, which dramatically amplify immune function in mice (Song et al., 2010; Park et al., 2011; Wang et al., 2014). Combining CTX with ginsenosides can improve the anti-cancer activity of CTX. The enhancing effects were responsible for the increase in anti-cancer immunity (Chen et al., 2017; Zhu et al., 2021). The immune system, which consists of innate and adaptive immunity, is the human's ultimate defense against infectious illnesses, tumor and cancer growth. In this investigation, we used a variety of assays to assess the effects of Rb2 on immune responses. The tests showed that Rb2 improved cellular, macrophage phagocytosis and NK cell activity in animals that had been given CTX, reducing the negative effects of immune suppression. The immunomodulatory effect of Rb2 is due, at least in part, to the related cytokine regulation and mRNA expression.

Spleen indices can reveal information about an organism's immunological activity and prognosis. In this study, the spleen weight was increased in the Rb2 groups compared to the model and control group. The adaptive immune response's key cell component is the lymphocyte. T and B lymphocyte proliferation in response to mitogen or antigen is a common immunological measure used to evaluate lymphocyte response. In general, T lymphocyte immunity can be detected using ConA-induced cell proliferation, whereas B lymphocyte immunity may be detected using LPS-induced B cell activation (Monmai et al., 2017; Liu et al., 2018). It indicated that ginsenoside Rb2 reversed the effect of CTX on splenic T and B lymphocyte proliferation.

Macrophages and NK cells play an important role in the anti-microbial response (Bihl et al., 2011; Orange, 2013; Shapouri-Moghaddam et al., 2018). Macrophages regulate innate immune protection against pathogens, as well as adaptive immunological responses. Macrophages are well-known for being highly secretory cells. Macrophages coordinate the immune response by secreting a variety of cytokines in response to stimulation. In numerous experiments, ginseng extracts were found to increase macrophage phagocytic activity. In the innate immune system, NK cells are a type of cytotoxic lymphocyte that fights freshly formed malignant cells and infected cells. After being stimulated, macrophages begin phagocytosis and produce a variety of effector molecules, including NO, to protect the host from damage (Kovacevic et al., 2017). NK cells participate in immune surveillance by destroying non-specific target cells and releasing IFN- $\gamma$ . Further, NK cells activate macrophages to eliminate phagocytized microorganisms (O'Sullivan et al., 2015). Thus, macrophages and NK cells are contributing to tumor

monitoring and pathogen clearance (Cerwenka and Lanier, 2016). In our experiment, Rb2 can improve macrophage and NK cell function, indicating that it could improve cell immunological function.

Innate and acquired immunity against microbial invasion, as well as the formation and activation of effector cells, also rely on cytokines. They are tiny signaling molecules produced by a variety of cells that help to mediate immune responses. Innate immunity is regulated by IL-10, TNFs, IL-12, and IL-6, which are produced by macrophages and NK cells. IFN- $\gamma$ , IL-2, TNF- $\beta$ , IL-12 were secreted by Th1 cells, and IL-10, IL-4, IL-13, and IL-5 were secreted by Th2 cells. Th1 and Th2 cells differ in the cytokines they secrete, which determines their differentiation and biological roles. IL-2 is a major immune factor secreted by Th cells. Combined with IL-2R, IL-2 can stimulate immune cell proliferation while inhibiting malignant cell division (Wang et al., 2005; Sockolosky et al., 2018). Moreover, IL-2 enhances the activity of NK cells like interferon. Thus, IFN- $\gamma$  production is increased (Ferlazzo et al., 2004; Wang et al., 2012). IL-2 can also promote B cell differentiation and IgG secretion from naive B cells stimulated by IL-21 (Berglund et al., 2013). IFN- $\gamma$  is an effective activator of macrophages. After CTX exposure, the Rb2 treated groups had significantly improved NK cell activity, which could be associated with greater amounts of IL-2. According to the findings, Rb2 reversed the significant depression caused by CTX by increasing the levels of IFN- $\gamma$ , TNF- $\alpha$ , IL-2, and IgG.

IL-4, IL-2, and IL-6 have been shown in numerous studies to stimulate immune cell activity and boost overall immunity. In immunosuppressed mice, Rb2 was observed to boost the mRNA expression of IL-2, SYK, IL-4, TNF- $\alpha$ , and IL-6. SYK is a protein tyrosine kinase that is found in hematopoietic cells in large amounts (Toyabe et al., 2010). They activated immunological receptors and downstream signaling to control cell proliferation, differentiation and phagocytosis (Siegel et al., 2006). Molecular docking is a popular computational approach for researching intermolecular interactions between molecular. From molecular docking study, it was found that IL-4, IL-2, SYK, IL-6, and TNF exhibited enough favorable interactions with Rb2. Hence, the results confirmed that Rb2 can enhance immune activity through regulating the production of IL-2, SYK, IL-4, TNF, and IL-6 in CTX-induced immunosuppressed mice.

## CONCLUSION

The current findings showed that ginsenoside Rb2 reversed CTX-induced spleen damage, increased splenic T and B lymphocyte proliferation, improved macrophage function and NK cell activity, and increased cytokine production and mRNA expression. It suggests that ginsenoside Rb2 reversed CTX-induced immunosuppression in the mice.

## DATA AVAILABILITY STATEMENT

The original contributions presented in the study are included in the article/supplementary materials, further inquiries can be directed to the corresponding authors.

## ETHICS STATEMENT

The animal study was reviewed and approved by Jilin Agricultural University.

## AUTHOR CONTRIBUTIONS

Conceptualization, YW; data curation and formal analysis, HZ and XP; methodology and validation, SZ and RZ; supervision, XP

## REFERENCES

- Ahlmann, M., and Hempel, G. (2016). The Effect of Cyclophosphamide on the Immune System: Implications for Clinical Cancer Therapy. *Cancer Chemother. Pharmacol.* 78 (4), 661–671. doi:10.1007/s00280-016-3152-1
- Alibolandi, M., Abnous, K., Mohammadi, M., Hadizadeh, F., Sadeghi, F., Taghavi, S., et al. (2017). Extensive Preclinical Investigation of Polymersomal Formulation of Doxorubicin versus Doxil-Mimic Formulation. *J. Control Release* 264, 228–236. doi:10.1016/j.jconrel.2017.08.030
- Berglund, L. J., Avery, D. T., Ma, C. S., Moens, L., Deenick, E. K., Bustamante, J., et al. (2013). IL-21 Signalling via STAT3 Primes Human Naive B Cells to Respond to IL-2 to Enhance Their Differentiation into Plasmablasts. *Blood* 122, 3940–3950. doi:10.1182/blood-2013-06-506865
- Bihl, F., Germain, C., Luci, C., and Braud, V. M. (2011). Mechanisms of NK Cell Activation: CD4(+) T Cells Enter the Scene. *Cell. Mol. Life Sci.* 68 (21), 3457–3467. doi:10.1007/s00018-011-0796-1
- Cerwenka, A., and Lanier, L. L. (2016). Natural Killer Cell Memory in Infection, Inflammation and Cancer. *Nat. Rev. Immunol.* 16 (2), 112–123. doi:10.1038/nri.2015.9
- Chen, G., Li, H., Gao, Y., Zhang, L., and Zhao, Y. (2017). Flavored Black Ginseng Exhibited Antitumor Activity via Improving Immune Function and Inducing Apoptosis. *Food Funct.* 8 (5), 1880–1889. doi:10.1039/c6fo01870j
- Chen, L. X., Qi, Y. L., Qi, Z., Gao, K., Gong, R. Z., Shao, Z. J., et al. (2019). A Comparative Study on the Effects of Different Parts of Panax Ginseng on the Immune Activity of Cyclophosphamide-Induced Immunosuppressed Mice. *Molecules* 24 (6), 1096. doi:10.3390/molecules24061096
- Chow, L. W. C., Biganzoli, L., Leo, A. D., Kuroi, K., Han, H. S., Patel, J., et al. (2017). Toxicity Profile Differences of Adjuvant Docetaxel/cyclophosphamide (TC) between Asian and Caucasian Breast Cancer Patients. *Asia. Pac. J. Clin. Oncol.* 13 (6), 372–378. doi:10.1111/ajco.12682
- Dai, G., Sun, B., Gong, T., Pan, Z., Meng, Q., and Ju, W. (2019). Ginsenoside Rb2 Inhibits Epithelial-Mesenchymal Transition of Colorectal Cancer Cells by Suppressing TGF- $\beta$ /Smad Signaling. *Phytomedicine* 56, 126–135. doi:10.1016/j.phymed.2018.10.025
- Ferdian, P. R., Elfirta, R. R., Emilia, Q., and Ikhwan, A. Z. N. (2020). Inhibitory Potential of Black Seed (*Nigella Sativa* L.) Bioactive Compounds towards Main Protease of SARS-CoV-2: In Silico Study. *Ann. Bogor.* 24 (2), 81–94. doi:10.14203/ann.bogor.2020.v24.n2.81-94
- Ferlazzo, G., Thomas, D., Lin, S. L., Goodman, K., Morandi, B., Muller, W. A., et al. (2004). The Abundant NK Cells in Human Secondary Lymphoid Tissues Require Activation to Express Killer Cell Ig-like Receptors and Become Cytolytic. *J. Immunol.* 172, 1455–1462. doi:10.4049/jimmunol.172.3.1455
- Gao, B., Huang, Q., Jie, Q., Zhang, H. Y., Wang, L., Guo, Y. S., et al. (2015). Ginsenoside-Rb2 Inhibits Dexamethasone-Induced Apoptosis through Promotion of GPR120 Induction in Bone Marrow-Derived Mesenchymal Stem Cells. *Stem Cells Dev.* 24 (6), 781–790. doi:10.1089/scd.2014.0367
- Hong, Y., Lin, Y., Si, Q., Yang, L., Dong, W., and Gu, X. (2019). Ginsenoside Rb2 Alleviates Obesity by Activation of Brown Fat and Induction of Browning of White Fat. *Front. Endocrinol. (Lausanne)* 10, 153. doi:10.3389/fendo.2019.00153
- Huang, Q., Wang, T., and Wang, H. Y. (2017). Ginsenoside Rb2 Enhances the Anti-inflammatory Effect of  $\omega$ -3 Fatty Acid in LPS-Stimulated RAW264.7 Macrophages by Upregulating GPR120 Expression. *Acta. Pharmacol. Sin.* 38 (2), 192–200. doi:10.1038/aps.2016.135

and YW; writing—original draft, SZ and HZ; writing—review and editing, SZ, JH and YZ.

## FUNDING

This research was supported by the Project of the Jilin Province Department of Science and Technology, China (No. 20210401123YY).

- Hughes, E., Scurr, M., Campbell, E., Jones, E., Godkin, A., and Gallimore, A. (2018). T-cell Modulation by Cyclophosphamide for Tumour Therapy. *Immunology* 154 (1), 62–68. doi:10.1111/imm.12913
- Hwang, Y. P., Lee, G. H., Pham, T. H., Kim, M. Y., Kim, C. Y., Lee, S. Y., et al. (2022). Immune-Enhancing Effect of Submerged Culture of Ceriporia Lacerata Mycelia on Cyclophosphamide-Induced Immunosuppressed Mice and the Underlying Mechanisms in Macrophages. *Int. J. Mol. Sci.* 23 (2), 597. doi:10.3390/ijms23020597
- Iqbal, H., and Rhee, D. K. (2020). Ginseng Alleviates Microbial Infections of the Respiratory Tract: a Review. *J. Ginseng Res.* 44 (2), 194–204. doi:10.1016/j.jgr.2019.12.001
- Irfan, M., Kim, M., and Rhee, M. H. (2020). Anti-platelet Role of Korean Ginseng and Ginsenosides in Cardiovascular Diseases. *J. Ginseng Res.* 44 (1), 24–32. doi:10.1016/j.jgr.2019.05.005
- Jang, M., Lim, T. G., Ahn, S., Hong, H. D., Rhee, Y. K., Kim, K. T., et al. (2016). Immune-enhancing Effects of a High Molecular Weight Fraction of *Cynanchum Wilfordii* Hemsley in Macrophages and Immunosuppressed Mice. *Nutrients* 8 (10), 600. doi:10.3390/nu8100600
- Ji, X., Hou, C., Shi, M., Yan, Y., and Liu, Y. (2020). An Insight into the Research Concerning Panax Ginseng C. A. Meyer Polysaccharides: A Review. *Food Rev. Int.*, 1–17. doi:10.1080/87559129.2020.1771363
- Johnson, L. A., Malayappan, B., Tretyakova, N., Campbell, C., MacMillan, M. L., Wagner, J. E., et al. (2012). Formation of Cyclophosphamide Specific DNA Adducts in Hematological Diseases. *Pediatr. Blood Cancer.* 58 (5), 708–714. doi:10.1002/pbc.23254
- Kang, S., and Min, H. (2012). Ginseng, the 'Immunity Boost': The Effects of Panax Ginseng on Immune System. *J. Ginseng Res.* 36 (4), 354–368. doi:10.5142/jgr.2012.36.4.354
- Karimi, G., Hassanzadeh-Josan, S., Memar, B., Esmaeili, S. A., and Riahi-Zanjani, B. (2018). Immunomodulatory Effects of Silymarin after Subacute Exposure to Mice: A Tiered Approach Immunotoxicity Screening. *J. Pharmacopuncture* 21 (2), 90–97. doi:10.3831/KPI.2018.21.011
- Kim, J. H. (2018). Pharmacological and Medical Applications of Panax Ginseng and Ginsenosides: a Review for Use in Cardiovascular Diseases. *J. Ginseng Res.* 42 (3), 264–269. doi:10.1016/j.jgr.2017.10.004
- Kondo, T., Fujioka, M., Fujisawa, S., Sato, K., Tsuda, M., Miyagishima, T., et al. (2019). Clinical Efficacy and Safety of First-Line Nilotinib Therapy and Evaluation of the Clinical Utility of the FRET-Based Drug Sensitivity Test. *Int. J. Hematol.* 110 (4), 482–489. doi:10.1007/s12185-019-02696-w
- Kovacevic, Z., Sahni, S., Lok, H., Davies, M. J., Wink, D. A., and Richardson, D. R. (2017). Regulation and Control of Nitric Oxide (NO) in Macrophages: Protecting the "professional Killer Cell" from its Own Cytotoxic Arsenal via MRP1 and GSTP1. *Biochim. Biophys. Acta Gen. Subj.* 1861 (5), 995–999. doi:10.1016/j.bbagen.2017.02.021
- Lee, K. T., Jung, T. W., Lee, H. J., Kim, S. G., Shin, Y. S., and Whang, W. K. (2011). The Antidiabetic Effect of Ginsenoside Rb2 via Activation of AMPK. *Arch. Pharm. Res.* 34 (7), 1201–1208. doi:10.1007/s12272-011-0719-6
- Lee, J. S., Lee, Y. N., Lee, Y. T., Hwang, H. S., Kim, K. H., Ko, E. J., et al. (2015). Ginseng Protects against Respiratory Syncytial Virus by Modulating Multiple Immune Cells and Inhibiting Viral Replication. *Nutrients* 7 (2), 1021–1036. doi:10.3390/nu7021021
- Liu, N., Dong, Z., Zhu, X., Xu, H., and Zhao, Z. (2018). Characterization and Protective Effect of Polygonatum Sibiricum Polysaccharide against Cyclophosphamide-Induced Immunosuppression in Balb/c Mice. *Int. J. Biol. Macromol.* 107 (1), 796–802. doi:10.1016/j.ijbiomac.2017.09.051

- Meng, M., Wang, H., Li, Z., Guo, M., and Hou, L. (2019). Protective Effects of Polysaccharides from *Cordyceps Gunnii* Mycelia against Cyclophosphamide-Induced Immunosuppression to TLR4/TRAF6/NF- $\kappa$ B Signalling in BALB/c Mice. *Food Funct.* 10 (6), 3262–3271. doi:10.1039/c9fo00482c
- Monmai, C., Park, S. H., You, S., and Park, W. J. (2017). Immuno-enhancement Effect of Polysaccharide Extracted from *Stichopus Japonicus* on Cyclophosphamide-Induced Immunosuppression Mice. *Food Sci. Biotechnol.* 27 (2), 565–573. doi:10.1007/s10068-017-0248-2
- Ngulde, S. I., Sandabe, U. K., Abounader, R., Zhang, Y., and Hussaini, I. M. (2020). Activities of Some Medicinal Plants on the Proliferation and Invasion of Brain Tumor Cell Lines. *Adv. Pharmacol. Pharm. Sci.* 2020, 3626879. doi:10.1155/2020/3626879
- O'Sullivan, T. E., Sun, J. C., and Lanier, L. L. (2015). Natural Killer Cell Memory. *Immunity* 43 (4), 634–645. doi:10.1016/j.immuni.2015.09.013
- Oh, S. J., Kim, K., and Lim, C. J. (2015). Ginsenoside Rb2 Attenuates UV-B Radiation-Induced Reactive Oxygen Species and Matrix Metalloproteinase-2 through Upregulation of Antioxidant Components in Human Dermal Fibroblasts. *Pharmacology* 96 (1–2), 32–40. doi:10.1159/000431154
- Orange, J. S. (2013). Natural Killer Cell Deficiency. *J. Allergy Clin. Immunol.* 132 (3), 515–525. doi:10.1016/j.jaci.2013.07.020
- Park, D., Bae, D. K., Jeon, J. H., Lee, J., Oh, N., Yang, G., et al. (2011). Immunopotential and Antitumor Effects of a Ginsenoside Rg<sub>3</sub>-Fortified Red Ginseng Preparation in Mice Bearing H460 Lung Cancer Cells. *Environ. Toxicol. Pharmacol.* 31 (3), 397–405. doi:10.1016/j.etap.2011.01.008
- Pérez-Herrero, E., and Fernández-Medarde, A. (2015). Advanced Targeted Therapies in Cancer: Drug Nanocarriers, the Future of Chemotherapy. *Eur. J. Pharm. Biopharm.* 93 (1), 52–79. doi:10.1016/j.ejpb.2015.03.018
- Phi, L. T. H., Wijaya, Y. T., Sari, I. N., Yang, Y. G., Lee, Y. K., and Kwon, H. Y. (2018). The Anti-metastatic Effect of Ginsenoside Rb2 in Colorectal Cancer in an EGFR/SOX2-dependent Manner. *Cancer Med.* 7 (11), 5621–5631. doi:10.1002/cam4.1800
- Ratan, Z. A., Youn, S. H., Kwak, Y. S., Han, C. K., Haidere, M. F., Kim, J. K., et al. (2021). Adaptogenic Effects of Panax Ginseng on Modulation of Immune Functions. *J. Ginseng Res.* 45 (1), 32–40. doi:10.1016/j.jgr.2020.09.004
- Riaz, M., Rahman, N. U., Zia-Ul-Haq, M., Jaffar, H. Z. E., and Manea, R. (2019). Ginseng: A Dietary Supplement as Immune-Modulator in Various Diseases. *Trends Food Sci. Technol.* 83, 12–30. doi:10.1016/j.tifs.2018.11.008
- Shapouri-Moghaddam, A., Mohammadian, S., Vazini, H., Taghadosi, M., Esmaili, S. A., Mardani, F., et al. (2018). Macrophage Plasticity, Polarization, and Function in Health and Disease. *J. Cell Physiol.* 233 (9), 6425–6440. doi:10.1002/jcp.26429
- Siegel, R., Kim, U., Patke, A., Yu, X., Ren, X., Tarakhovsky, A., et al. (2006). Nontranscriptional Regulation of SYK by the Coactivator OCA-B Is Required at Multiple Stages of B Cell Development. *Cell* 125 (4), 761–774. doi:10.1016/j.cell.2006.03.036
- Singh, V. K., Dwivedi, P., Chaudhary, B. R., and Singh, R. (2016). Gymnemic Acid Stimulates *In Vitro* Splenic Lymphocyte Proliferation. *Phytother. Res.* 30 (2), 341–344. doi:10.1002/ptr.5514
- Sockolovsky, J. T., Trotta, E., Parisi, G., Picton, L., Su, L. L., Le, A. C., et al. (2018). Selective Targeting of Engineered T Cells Using Orthogonal IL-2 Cytokine-Receptor Complexes. *Science* 359 (6379), 1037–1042. doi:10.1126/science.aar3246
- Song, X., Chen, J., Sakwivatkul, K., Li, R., and Hu, S. (2010). Enhancement of Immune Responses to Influenza Vaccine (H3N2) by Ginsenoside Re. *Int. Immunopharmacol.* 10 (3), 351–356. doi:10.1016/j.intimp.2009.12.009
- Toyabe, S., Watanabe, A., Harada, W., Karasawa, T., and Uchiyama, M. (2010). Specific Immunoglobulin E Responses in ZAP-70-Deficient Patients Are Mediated by Syk-dependent T-Cell Receptor Signalling. *Immunology* 103 (2), 164–171. doi:10.1046/j.1365-2567.2001.01246.x
- Wanderi, C., Kim, E., Chang, S., Choi, C., and Choi, K. (2016). Ginsenoside 20(S)-Protopanaxadiol Suppresses Viability of Human Glioblastoma Cells via Down-Regulation of Cell Adhesion Proteins and Cell-Cycle Arrest. *Anticancer Res.* 36 (3), 925–932.
- Wang, X., Rickert, M., and Garcia, K. C. (2005). Structure of the Quaternary Complex of Interleukin-2 with its Alpha, Beta, and Gamma Receptors. *Science* 310, 1159–1163. doi:10.1126/science.1117893
- Wang, R., Jaw, J. J., Stutzman, N. C., Zou, Z., and Sun, P. D. (2012). Natural Killer Cell-Produced IFN- $\gamma$  and TNF- $\alpha$  Induce Target Cell Cytolysis through Up-Regulation of ICAM-1. *J. Leukoc. Biol.* 91 (2), 299–309. doi:10.1189/jlb.0611308
- Wang, Y., Liu, Y., Zhang, X. Y., Xu, L. H., Ouyang, D. Y., Liu, K. P., et al. (2014). Ginsenoside Rg1 Regulates Innate Immune Responses in Macrophages through Differentially Modulating the NF- $\kappa$ B and PI3K/Akt/mTOR Pathways. *Int. Immunopharmacol.* 23 (1), 77–84. doi:10.1016/j.intimp.2014.07.028
- Xie, J., Nie, S., Yu, Q., Yin, J., Xiong, T., Gong, D., et al. (2016). *Lactobacillus Plantarum* NCU116 Attenuates Cyclophosphamide-Induced Immunosuppression and Regulates Th17/Treg Cell Immune Responses in Mice. *J. Agric. Food Chem.* 64, 1291–1297. doi:10.1021/acs.jafc.5b06177
- Yang, S., Wang, X., Duan, C., and Zhang, J. (2020). A Novel Approach Combining Metabolomics and Molecular Pharmacology to Study the Effect of Gei Herba on Mouse Hematopoietic Function. *Biomed. Pharmacother.* 129, 110437. doi:10.1016/j.biopha.2020.110437
- Yanzhu Zhu, Y., Hu, C., Zheng, P., Miao, L., Yan, X., Li, H., et al. (2016). Ginsenoside Rb1 Alleviates Aluminum Chloride-Induced Rat Osteoblasts Dysfunction. *Toxicology* 368–369, 183–188. doi:10.1016/j.tox.2016.07.014
- Yoo, J., Jung, Y., Ahn, J. H., Choi, Y. J., Lee, K. H., and Hur, S. (2020). Incidence and Clinical Course of Septic Shock in Neutropenic Patients during Chemotherapy for Gynecological Cancers. *J. Gynecol. Oncol.* 31 (5), e62. doi:10.3802/jgo.2020.31.e62
- Yoo, Y. C., Lee, J., Park, S. R., Nam, K. Y., Cho, Y. H., and Choi, J. E. (2013). Protective Effect of Ginsenoside-Rb2 from Korean Red Ginseng on the Lethal Infection of Haemagglutinating Virus of Japan in Mice. *J. Ginseng Res.* 37 (1), 80–86. doi:10.5142/jgr.2013.37.80
- Zhang, Y., Ouyang, X., You, S., Zou, H., Shao, X., Zhang, G., et al. (2020). Effect of Human Amniotic Epithelial Cells on Ovarian Function, Fertility and Ovarian Reserve in Primary Ovarian Insufficiency Rats and Analysis of Underlying Mechanisms by mRNA Sequencing. *Am. J. Transl. Res.* 12 (7), 3234–3254.
- Zhen-Yuan Zhu, Z. Y., Meng, M., Sun, H., Li, Y., Ren, Y. Y., and Zhang, Y. (2016). Immunostimulatory Activity of Glycopeptides from *Paeclomyces Sinensis* under Normal and Cyclophosphamide Induced Immunosuppressive Conditions in Mice Models. *Food Funct.* 7, 3566–3576. doi:10.1039/c6fo00667a
- Zhu, H., He, Y. S., Ma, J., Zhou, J., Kong, M., Wu, C. Y., et al. (2021). The Dual Roles of Ginsenosides in Improving the Anti-tumor Efficiency of Cyclophosphamide in Mammary Carcinoma Mice. *J. Ethnopharmacol.* 265, 113271. doi:10.1016/j.jep.2020.113271

**Conflict of Interest:** The authors declare that the research was conducted in the absence of any commercial or financial relationships that could be construed as a potential conflict of interest.

The reviewer YS declared a shared affiliation with the author YZ to the handling editor at the time of review.

**Publisher's Note:** All claims expressed in this article are solely those of the authors and do not necessarily represent those of their affiliated organizations, or those of the publisher, the editors and the reviewers. Any product that may be evaluated in this article, or claim that may be made by its manufacturer, is not guaranteed or endorsed by the publisher.

Copyright © 2022 Zheng, Zheng, Zhang, Piao, Hu, Zhu and Wang. This is an open-access article distributed under the terms of the Creative Commons Attribution License (CC BY). The use, distribution or reproduction in other forums is permitted, provided the original author(s) and the copyright owner(s) are credited and that the original publication in this journal is cited, in accordance with accepted academic practice. No use, distribution or reproduction is permitted which does not comply with these terms.



# The Combination of *Tamarindus indica* and Coenzyme Q10 can be a Potential Therapy Preference to Attenuate Cadmium-Induced Hepatorenal Injury

Amany Abdelnaby<sup>1</sup>, Nabila Abdel-Aleem<sup>2</sup>, Ayman Mansour<sup>1</sup>, Afaf Abdelkader<sup>3,4\*</sup>, Amany N. Ibrahim<sup>5</sup>, Safwa M. Sorour<sup>5</sup>, Enas Elgendy<sup>6</sup>, Heba Bayoumi<sup>6</sup>, Shaymaa M. Abdelrahman<sup>7</sup>, Samah F. Ibrahim<sup>8</sup>, Ilhaam Alsaati<sup>9</sup> and Ahmed Abdeen<sup>2,4,10\*</sup>

<sup>1</sup>Department of Biotechnology, Animal Health Research Institute, Agricultural Research Center, Giza, Egypt, <sup>2</sup>Department of Forensic Medicine and Toxicology, Faculty of Veterinary Medicine, Benha University, Toukh, Egypt, <sup>3</sup>Department of Forensic Medicine and Clinical Toxicology, Faculty of Medicine, Benha University, Benha, Egypt, <sup>4</sup>Center of Excellence in Screening of Environmental Contaminants (CESEC), Benha University, Toukh, Egypt, <sup>5</sup>Department of Pharmacology, Faculty of Medicine, Benha University, Benha, Egypt, <sup>6</sup>Histology and Cell Biology Department, Faculty of Medicine, Benha University, Benha, Egypt, <sup>7</sup>Medical Biochemistry and Molecular Biology Department, Faculty of Medicine, Benha University, Benha, Egypt, <sup>8</sup>Department of Clinical Sciences, College of Medicine, Princess Nourah bint Abdulrahman University, Riyadh, Saudi Arabia, <sup>9</sup>Department of Basic Sciences, College of Medicine, Princess Nourah bint Abdulrahman University, Riyadh, Saudi Arabia, <sup>10</sup>Department of Biochemistry, Faculty of Veterinary Medicine, South Valley University, Qena, Egypt

## OPEN ACCESS

### Edited by:

Fatma Mohamady El-Demerdash,  
Alexandria University, Egypt

### Reviewed by:

Qudratullah Kalwar,  
Lanzhou Institute of Husbandry and  
Pharmaceutical Sciences (CAAS),  
China

Rohit Sharma,  
Banaras Hindu University, India

### \*Correspondence:

Afaf Abdelkader  
afaf.abdelkader@fmed.bu.edu.eg  
Ahmed Abdeen  
ahmed.abdeen@fvtm.bu.edu.eg

### Specialty section:

This article was submitted to  
Predictive Toxicology,  
a section of the journal  
Frontiers in Pharmacology

Received: 26 May 2022

Accepted: 23 June 2022

Published: 08 August 2022

### Citation:

Abdelnaby A, Abdel-Aleem N, Mansour A, Abdelkader A, Ibrahim AN, Sorour SM, Elgendy E, Bayoumi H, Abdelrahman SM, Ibrahim SF, Alsaati I and Abdeen A (2022) The Combination of *Tamarindus indica* and Coenzyme Q10 can be a Potential Therapy Preference to Attenuate Cadmium-Induced Hepatorenal Injury. *Front. Pharmacol.* 13:954030. doi: 10.3389/fphar.2022.954030

Cadmium (Cd) is a hazardous environmental pollutant that menaces human and animal health and induces serious adverse effects in various organs, particularly the liver and kidneys. Thus, the current study was designed to look into the possible mechanisms behind the ameliorative activities of *Tamarindus indica* (TM) and coenzyme Q10 (CoQ) combined therapy toward Cd-inflicted tissue injury. Male Wistar rats were categorized into seven groups: Control (received saline only); TM (50 mg/kg); CoQ (40 mg/kg); Cd (2 mg/kg); (Cd + TM); (Cd + CoQ); and (Cd + TM + CoQ). All the treatments were employed once daily *via* oral gavage for 28 consecutive days. The results revealed that Cd exposure considerably induced liver and kidney damage, evidenced by enhancement of liver and kidney function tests. In addition, Cd intoxication could provoke oxidative stress evidenced by markedly decreased glutathione (GSH) content and catalase (CAT) activity alongside a substantial increase in malondialdehyde (MDA) concentrations in the hepatic and renal tissues. Besides, disrupted protein and lipid metabolism were noticed. Unambiguously, TM or CoQ supplementation alleviated Cd-induced hepatorenal damage, which is most likely attributed to their antioxidant and anti-inflammatory contents. Interestingly, when TM and CoQ were given in combination, a better restoration of Cd-induced liver and kidney damage was noticed than was during their individual treatments.

**Keywords:** cadmium, *Tamarindus indica*, coenzyme Q10, antioxidants, hepatorenal damage, oxidative stress

## INTRODUCTION

Cadmium (Cd) is one of the most harmful of environmental and industrial pollutants that endangers human and animal health (Balali-Mood et al., 2021). It is ubiquitously existent in the environment, naturally or *via* pollution (van Gerwen et al., 2022). Contaminated water, food, and air (particularly cigarette smoke) are the most inevitable sources of exposure to Cd (Abdeen et al., 2019). Alarmingly, Cd is poorly excreted out from the body and therefore has the ability to

accumulate in various tissues, mainly the kidneys and liver (Taghavizadeh Yazdi et al., 2021; Wang et al., 2021).

It is well documented that Cd has a high affinity to sulfhydryl thiol-containing cellular macromolecules, such as antioxidant components and metallothioneins (MTs), a cysteine-rich protein important for the detoxification of Cd (Wang et al., 2021). The Cd-MT complex is generated and accumulates in liver and kidney cells, causing Cd sequestration in the target site and consequently disrupting cellular redox hemostasis. A building body of studies has shown that oxidative damage is deemed to be the principal mechanism of Cd-induced tissue damage (Abdeen et al., 2019; de Anicésio and Monteiro, 2022). Cd promotes mitochondrial deterioration leading to reduction in ATP synthesis and incremented reactive oxygen species (ROS) generation (Mirkov et al., 2021). As a result, mitochondrial dysfunction, peroxidation of membrane lipid (LPO), protein misfolding, DNA oxidation, and ultimately, overture of apoptotic pathways are instigated (Abdeen et al., 2019; Mirkov et al., 2021; Elgazzar et al., 2022).

*Tamarindus indica* (TM) is commonly known as tamarind, which grows naturally in tropical and subtropical regions (Asad et al., 2022). Many studies have been published the benefits of TM as a natural antioxidant and on its ability to scavenge ROS, which are attributed to its high flavonoid and phenolic contents (Maria et al., 2011; Escalona-Arranz et al., 2016; Devi et al., 2020; Kengaiah et al., 2020). Accordingly, an ample number of literature have reported that TM could exert a hepatorenal protection against a variety of environmental toxicants and drugs, such as toxicities caused by fluoride (Ranjan et al., 2009), carbon tetrachloride (Atawodi et al., 2013), ethanol (Ghoneim and Eldahshan, 2012), antitubercular drugs (Amir et al., 2016), and gentamicin (Khader et al., 2019).

Coenzyme Q10 (CoQ) is a natural antioxidant molecule present in all biological membranes of living organisms (Sangsefidi et al., 2020; Abdeen et al., 2020). CoQ is predominantly found in high energy-demanding cells such as the hepatocytes and renal cells, where the mitochondria are plentiful. It is an integral constituent of the mitochondrial electron transport chain and essential in ATP synthesis (Sangsefidi et al., 2020). Additionally, as a part of the intracellular antioxidant system, CoQ has a substantial free radical scavenging capability, which assists in maintaining the mitochondrial membrane potential and in mitigating LPO; thereby, the oxidative stress is quenched (Gutierrez-Mariscal et al., 2020). The antioxidant potency of CoQ has been documented against oxidative harm done to the liver and kidneys triggered by cisplatin (Fatima et al., 2013), doxorubicin (El-Sheikh et al., 2012), piroxicam (Abdeen et al., 2020), gentamicin (Upaganlawar et al., 2006), and acetaminophen (Fouad and Jresat, 2011).

Considering the antioxidant potential of TM and CoQ on quenching the generated ROS and promoting the cellular antioxidant capacity at the levels of the mitochondria and cytoplasm, we anticipated that supplementing both the agents might mitigate Cd-stimulated oxidative stress and enhance

tissue remodeling. Hereby, the current research evaluates their palliative capability on Cd-prompted hepatorenal oxidative stress. Biomarkers of the liver and kidneys, lipid profiles, oxidative state, and histopathological alterations were all investigated.

## MATERIALS AND METHODS

### Botanical Material and *Tamarindus indica* Extract Preparation

*T. indica* seeds were gained from the local market (Cairo, Egypt). The seeds were removed manually from their coats, then rinsed and dried at 40°C for 24 h in the dark. Next, the seeds were processed into a powder using a lab blender. Twenty-five grams of dried and smashed seeds were placed in a conical flask and steeped for 3 days at room temperature in 500 ml of anhydrous ethanol, stirring constantly. The obtained extract was filtered before being roto-evaporated, after which the extract paste was freeze-dried. Finally, the TM extract was diluted in saline and thoroughly mixed with vortex before use.

### Phytochemical Profiling of *Tamarindus indica* Extract Using Gas Chromatography–Mass Spectrometer

The phytochemical constituents of TM were identified by GC/MS analysis (GC-Trace Ultra-ISQ mass spectrometer, Thermo-Scientific, Austin, United States) as previously described by our group (Abdeen et al., 2021).

### Assessment of Total Phenolic Content and Total Flavonoid Content

The TPC and TFC of TM were calculated by a colorimetric technique in accordance with the Žilić et al. (2012) technique.

### ABTS<sup>+</sup> and 2,2-Diphenyl-1-Picrylhydrazyl Radical-Scavenging Efficacy

The scavenging capability of the robust free radicals—2,2-diphenyl-1-picrylhydrazyl (DPPH<sup>•</sup>) and 2,20-azino-bis(3-ethylbenzothiazoline-6-sulphonate) (ABTS<sup>+</sup>)—was assessed according to the Hwang and Thi (2014) method.

### Animals and Ethical Endorsement

From the Center of Laboratory Animal, Faculty of Veterinary Medicine at Benha University, Egypt, 42 Wistar Albino rats (130–150 g) were obtained. Two weeks prior to the incipience of the trial, the rats were housed and accustomed to get adjusted to the environmental conditions (25 ± 2°C) and were supplied balanced pellets and water *ad libitum*. All animal experimentation steps were incongruent with the guidelines set by the ethical committee established in the Faculty of Veterinary Medicine, Benha University (approval no: BUFVTM130222).

## Design of the Trial

Subsequent to acclimation, the animals were sorted into seven equable groups (six rats in each group): Control group—the rats were given normal saline as a vehicle; TM group—TM seed extract (50 mg/kg b.wt) was given to the rats (Sundaram et al., 2014); CoQ group—animals received coenzyme Q10 (CoQ; 40 mg/kg b.wt) (Abdeen et al., 2020); Cd group—the rats received cadmium chloride (CdCl<sub>2</sub>; 2 mg/kg b.wt) (Abdeen et al., 2019); Cd + TM group—the rats were given TM and CdCl<sub>2</sub>; Cd + CoQ group—the rats were administered CoQ and CdCl<sub>2</sub>; and Cd + TM + CoQ group—animals were treated with TM, CoQ, and CdCl<sub>2</sub> at the same abovementioned dosages. TM and CoQ were given 1 h foregoing to CdCl<sub>2</sub>. All of the remedies were given orally once daily for 28 sequent days. CoQ capsules (Coenzyme Q10<sup>®</sup>, 30 mg) were bought from MEPACO-MediFood, Egypt. While, CdCl<sub>2</sub> was got from the Central Drug House (P) Ltd., New Delhi, India.

## Sampling

At the end of the experiment, the rats were euthanized under isoflurane inhalation anesthesia. Then, blood samples were immediately sampled from the inferior vena cava, centrifuged for 15 min at 2,000g for serum separation, and stored at -20°C for biochemical investigations. To dislodge blood clots, liver and kidney tissues were swiftly harvested and permeated in ice-cold saline. After that, each tissue sample was separated into two halves, one of which was kept in a 10% buffered formalin solution for further histological analysis, while the other part was treated as shown later for the oxidative cascade and biomarkers evaluation.

## Serum Biochemical Indices

Serum alanine aminotransferase (ALT), aspartate aminotransferase (AST), alkaline phosphatase (ALP) enzymatic activities and BUN, creatinine, total protein, albumin, globulin, and lipid profile (cholesterol and triglycerides) were estimated using chemical kits bought from Laboratory Bio-diagnostics Co., Cairo, Egypt. All the procedures were executed in conformity with the manufacturer's guidelines.

## Preparation of Tissue Homogenates and Oxidative Cascade Analysis

Using a sonicator homogenizer, 1 g of each tissue was homogenized in 5 ml of ice-cold buffer (50 Mm potassium phosphate, pH 7.5, 1 Mm EDTA). Aliquots of tissue homogenates were spun at 4,000 rpm in a cooling centrifuge for 20 min, and the supernatant was frozen at -20°C till further assessment of the oxidative parameters. Oxidative cascade was achieved by measuring the catalase (CAT) activity and malondialdehyde (MDA) and reduced-glutathione (GSH) levels utilizing special diagnostic kits procured from Laboratory Bio-diagnostic Co.

## Histopathological Inspection

Following proper fixation (10% buffered formalin for 24 h at 25°C), the liver and kidney tissue specimens were rinsed with

running water for 10 min before dehydrating with successive ethanol dilutions. They were cleared up in xylene solution after that and the tissue specimens were embedded in paraffin at 60°C, then cut into 5- $\mu$ m-thick sections and stained with H&E to examine the histoarchitectural changes. As previously described by our group, an ordinal scoring system was used to grade the histopathological changes in the liver and kidneys (Abdeen et al., 2021). The scores were graded from 0 to 3 for describing normal (score = 0), mild (score = 1), moderate (score = 2), and severe (score = 3) affections.

## Statistical Analyses

Statistical tests were performed using SPSS software (version 21.0; SPSS Inc., Chicago, IL, United States). Comparisons of the various data sets were done using one-way ANOVA followed by the Duncan's *post hoc* test. The values are displayed as mean  $\pm$  SD. Statistically significant values were designated at  $p \leq 0.05$ . To determine the contribution of all the variables, the "Factoextra" and "FactoMineR" packages were installed in RStudio under R version 4.0.2 to perform the multivariate principal component analysis (PCA). RStudio and MetaboAnalyst software were used for data visualization.

## RESULTS

### Gas Chromatography–Mass Spectrometer Fragmentation Pattern of *Tamarindus indica* Seeds Extract

The GC/MS approach was used to identify the chemical components of TM by matching the retention time of the constitutes exemplified in the mass spectra with those obtained from the renowned compounds stored in the spectrometry database libraries. The chromatogram depicted in **Figure 1** expounds the mass spectrum pattern of TM, with ten distinct peaks at 3.66, 19.98, 21.38, 24.88, 25.58, 27.10, 28.64, 30.65, 31.17, and 31.82 m/z. The most predominating compounds, which conquered the largest peak area were epoxygedunin (32.24%) followed by caryophyllene (17.91%), ethyl iso-allocholate (11.85%), 9-octadecenoic acid (11.37%), cholesta-8,24-dien-3-ol, 4-methyl-, (3 $\beta$ ,4 $\alpha$ )- (6.54%), isochiapiin B (6.21%), 10,13-octadecadienoic acid, methyl ester (4.63%), tribehenin (3.91%), retinol (3.48%), and hexadecanoic acid, 2,3-dihydroxypropyl ester (1.87%). These specified compounds elucidated that TM is an enriched source of antioxidant and hydrogen donor compounds, explicating its ability to combat many disorders (**Table 1**).

### Total Phenolic Content, Total Flavonoid Content, and Free Radical Scavenging Potential of *Tamarindus indica*

**Table 2** shows that TPC and TFC had average levels of 611.08 mg of gallic acid equivalent (GAE)/g and 179.08 mg catechin equivalent (CE)/g, respectively. Following that, DPPH<sup>•</sup> and ABTS<sup>+</sup> were used to

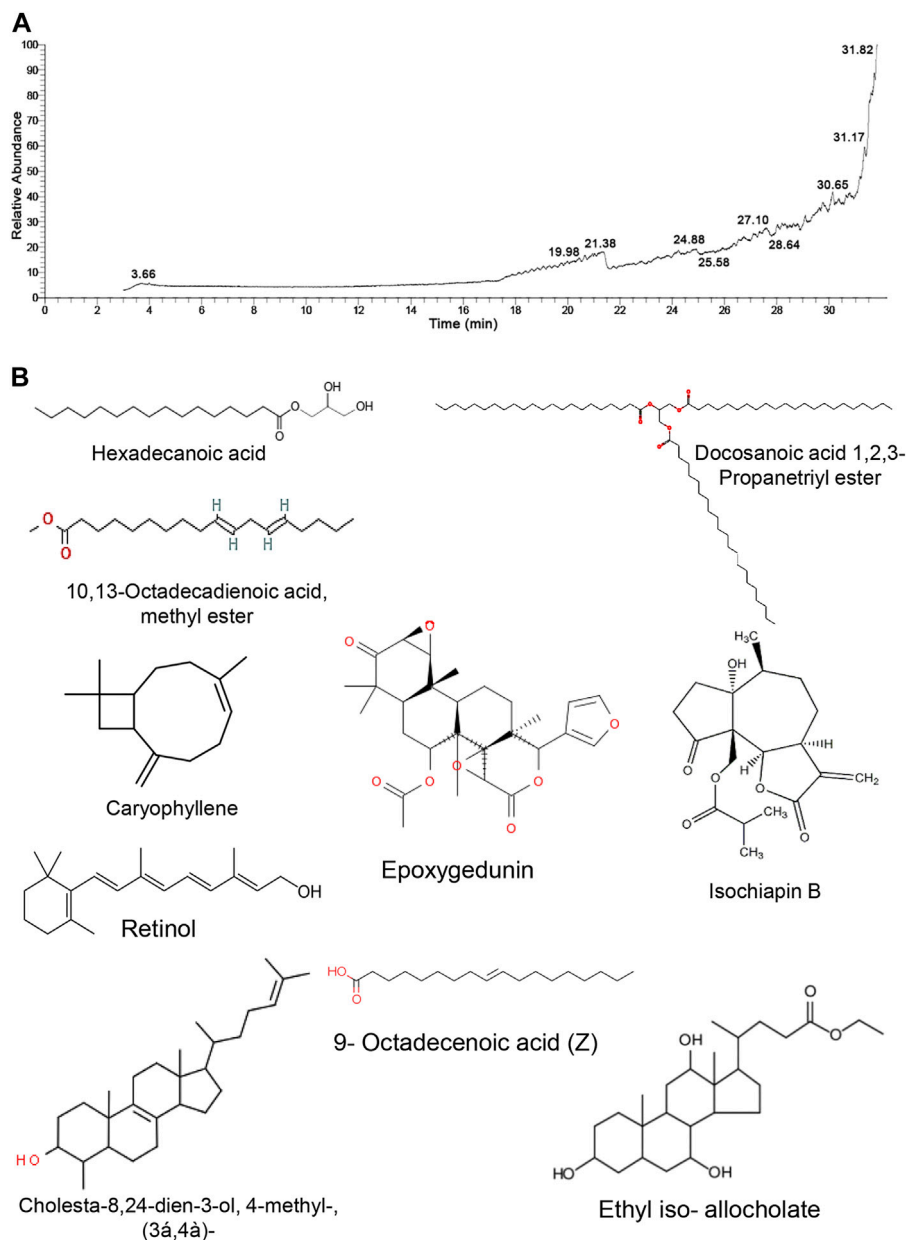


**FIGURE 1** | GC/MS analysis of *Tamarindus indica* seeds extract. **(A)** GC/MS chromatogram pattern of TM exhibits the abundance of distinct phytochemical constituents isolated at various retention times. **(B)** Chemical construction of the identified phytochemicals.

evaluate the antioxidant capabilities of the discovered phenolic and flavonoid components. Intriguingly, the gained data elucidated the strong antioxidant activity of TM with average scavenging capacities of 1813.62 and 1703.27 mg TE/g for DPPH<sup>•</sup> and ABTS<sup>+</sup> radicals, respectively (Table 2).

### Serum Biochemical Assays

As shown in Figures 2, 3, Cd treatment resulted in liver and kidney impairment, as documented by marked increases in the serum indices of AST, ALT, ALP, creatinine, and BUN, as well as marked decreases in albumin, total protein, and globulin levels

when compared to the Control. We also noticed dramatic increases in cholesterol and triglyceride levels (Figure 3). These findings reveal that Cd poisoning affected lipid metabolism. By contrast, when Cd-exposed rats were given TM or CoQ, the harmful effects of Cd were reduced, as evidenced by a significant improvement in the lipid profile and adjustment of all hepatorenal biomarker levels. As both the medicines (TM and CoQ) were coadministered with Cd, there were notable improvements in hepatic and renal functions and lipid metabolisms when compared to their individual treatments.

**TABLE 1 |** Phytochemical compounds identified in extract of *Tamarindus indica* seeds by GC-MS analysis.

No	Chemical name	Phytochemical compounds	RT (min)	Peak area %	Chemical formula	MW
1	Hexadecanoic acid, 2,3-dihydroxypropyl ester	Glycerol palmitate	3.66	1.87	C <sub>19</sub> H <sub>38</sub> O <sub>4</sub>	330
2	10,13-Octadecadienoic acid, methyl ester	Fatty acids methyl esters	19.98	4.63	C <sub>19</sub> H <sub>34</sub> O <sub>2</sub>	294
3	Caryophyllene	Sesquiterpene	21.38	17.91	C <sub>15</sub> H <sub>24</sub>	204
4	Retinol	Vit A	24.88	3.48	C <sub>20</sub> H <sub>30</sub> O	286
5	Cholesta-8,24-dien-3-ol, 4-methyl-, (3β,4α)-	Steroids and derivatives	25.58	6.54	C <sub>28</sub> H <sub>46</sub> O	398
6	Isochiapin B	Terpenoid compounds (sesquiterpene lactone)	27.10	6.21	C <sub>19</sub> H <sub>22</sub> O <sub>6</sub>	346
7	Docosanoic acid 1,2,3-propanetriyl ester (Tribehenin)	Glycerol tribehenate fatty acid	28.64	3.91	C <sub>68</sub> H <sub>134</sub> O <sub>6</sub>	1,058
8	9-Octadecenoic acid (Z)	Oleic acid	30.65	11.37	C <sub>18</sub> H <sub>34</sub> O <sub>2</sub>	282
9	Ethyl iso-allochololate	Steroid derivatives	31.17	11.85	C <sub>26</sub> H <sub>44</sub> O <sub>5</sub>	436
10	Epoxygedunin	Saponin/steroids	31.82	32.24	C <sub>26</sub> H <sub>34</sub> O <sub>8</sub>	498

MW, molecular weight; RT, retention time.

**TABLE 2 |** Antioxidant contents and activities of ethanolic extract of *Tamarindus indica* seeds.

	ABTS <sup>+</sup> (mg TE/g)	DPPH <sup>•</sup> (mg TE/g)	TFC (mg CE/g)	TPC (mg GAE/g)
Replicate1	1711.45	1801.29	179	612.5
Replicate2	1,695.53	1817.14	180	610
Replicate3	1702.81	1822.42	178.25	610.75
Mean ± SE	1703.27 ± 4.61	1813.62 ± 6.36	179.08 ± 0.51	611.08 ± 0.74

TE; trolox equivalent; CE, catechin equivalent; GAE, gallic acid equivalent. Data are expressed as the mean ± SE.

## Antioxidant and Peroxidation Indices

Lipid peroxidation biomarker (MDA) and antioxidant enzyme capacity (CAT and GSH) upon Cd, TM, or CoQ treatment are illustrated in **Figure 4**. As explicated, Cd exposure negatively impacted the cellular oxidative state through drastic increment in the MDA levels with an outstanding depletion in CAT activity and GSH level in the liver and renal tissues when compared to the Control. TM or CoQ treatment notably amended hepatorenal oxidative harm prompted by Cd exposure. The overall data revealed a refinement of the oxidative status in the Cd + TM + CoQ group when compared to the Cd + TM or Cd + CoQ group, suggesting that the synchronous use of TM and CoQ has robust synergistic antioxidant advantages against Cd intoxication.

## Histopathological Findings

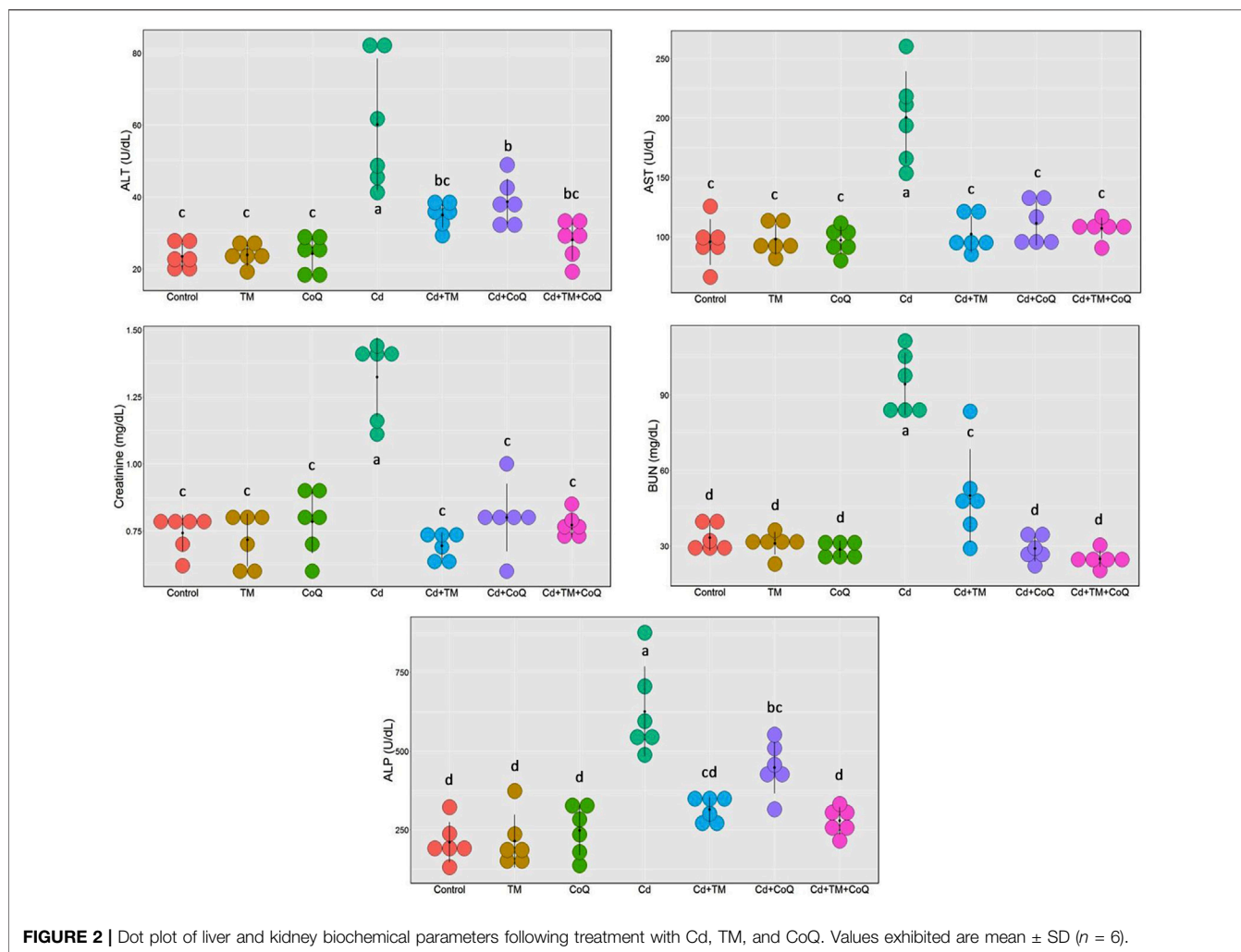
To corroborate the formerly noted observations, the morphological derangement in the hepatic and renal tissues upon Cd, TM, or CoQ administration was evaluated. The hepatic histological inspection of the Control, TM-treated, and CoQ-treated groups exposed normal construction of liver lobule (uniform polyhedral hepatocytes, well-organized sinusoids, and portal veins) as displayed in **Figures 5A–C**, respectively. On the contrary, the Cd-intoxicated rats showed a loss of hepatic architecture with the proliferation of bile ducts, centrilobular vacuolation of hepatocytes' cytoplasm and diffuse fatty changes "signet cell" (accumulation of fat droplet within the hepatocyte). Besides, portal blood vessel congestion and tremendous leukocyte leakage were also spotted (**Figures 5D1,D2**). With the concurrent use of Cd, TM, or CoQ, the portal region showed minimal lymphocytic spillage and fatty changes when compared to Cd-untreated rats (**Figures 5E,F**). Fortunately, when Cd was used

synchronously with TM and CoQ, the hepatic architecture mostly reverted to normal with very mild fatty changes (**Figures 5G,H**).

In relation to the kidney sections, the Control, TM-, and CoQ-treated animals (**Figures 6A–C**, respectively) exhibited no histopathological alterations, with a normal arrangement of the renal parenchyma exhibited by the normal appearance of glomerular tuft, Bowman's capsule, and tubules. However, the Cd-intoxicated group showed perturbation of renal architecture, desquamation of the apical epithelia of proximal and distal tubules along with cytoplasmic vacuolation. Dense inflammatory cellular infiltration was also noted (**Figures 6D1,D2**). Nevertheless, combining the treatment of Cd and TM or CoQ culminated in a moderate recovery of histological findings with an improvement of renal architecture as evidenced by mild hydropic changes in the form of vacuolated cytoplasm in some renal tubules (**Figures 6E,F**). Interestingly, when Cd was used simultaneously with both TM and CoQ, the renal architecture was restored close to normal (**Figures 5G,H**). The data obtained from the histopathological scoring revealed mitigation of Cd-induced tissue injury in animals co-treated with TM or CoQ, with better improvements when both TM and CoQ were combined. The histopathological findings corroborated the biochemical results, implying that the TM and CoQ supplementation had a considerable impact on Cd-inflicted hepatorenal injury (**Figures 5H, 6H**).

## Principal Component Analysis and Hierarchical Clustering Heatmap

All of the studied parameters (creatinine, BUN, ALT, AST, ALP, cholesterol, triglycerides, total protein, albumin,

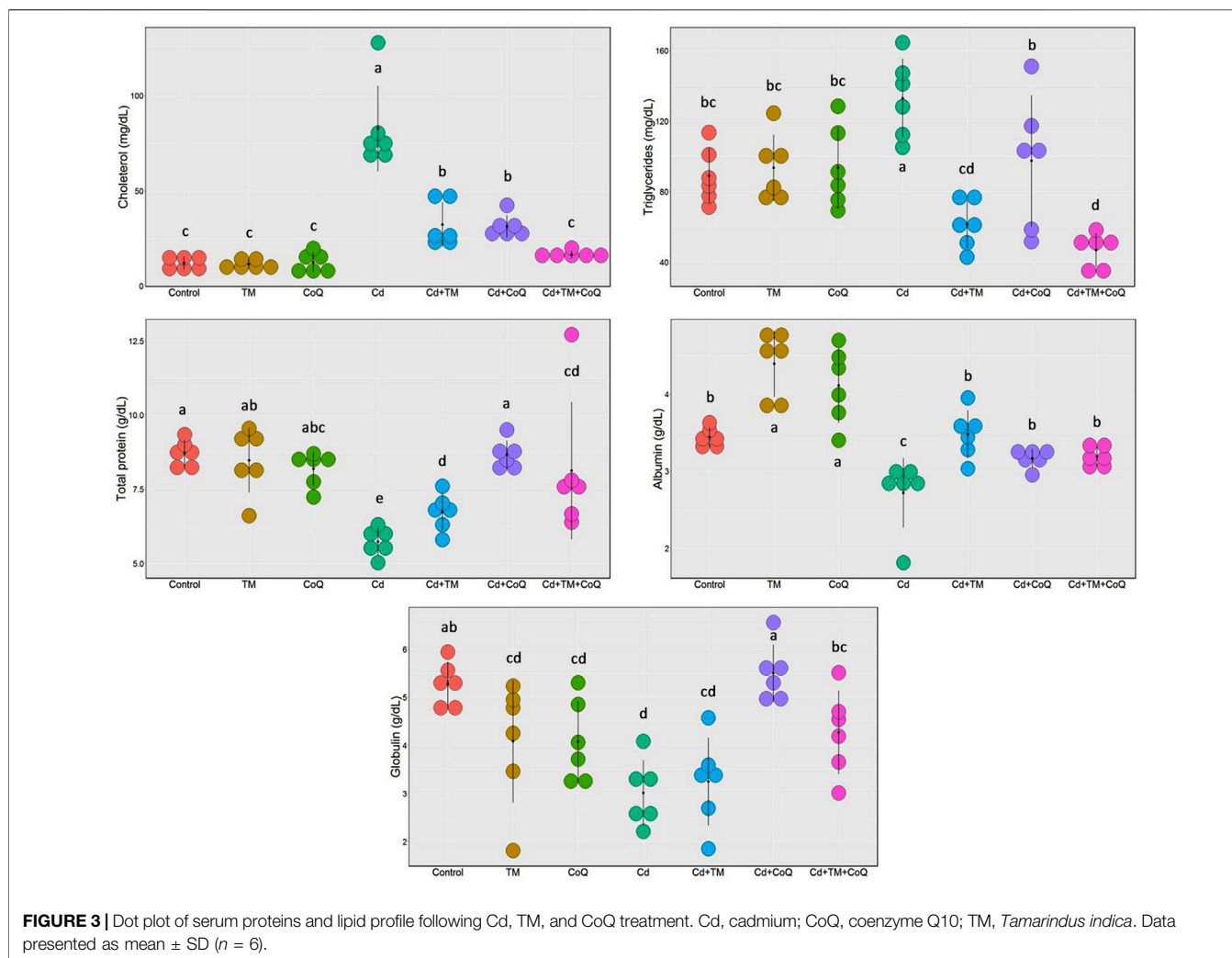


globulin, MDA, GSH, and CAT) contributed mostly along the two major dimensional components (Dim1 and Dim2), accounting for 74% of the total variation. As shown in **Figure 7**, Dim1 differentiated the majority of investigated factors, resulting in a larger proportion of variance (64.5%), while Dim2 captured the smaller proportion of variation (9.5%). The PCA score plot revealed that the Control, TM, CoQ, Cd + TM, Cd + CoQ, and Cd + TM + CoQ groups were clustered together on the left side and segregated from those subjected to Cd intoxication (**Figure 7A**). In the PCA loading plot, creatinine, BUN, ALT, AST, ALP, cholesterol, triglycerides, and MDA were positively associated with the Cd group. On the other hand, total protein, albumin, globulin, GSH, and CAT were positively linked with the Control, TM, CoQ, Cd + TM, Cd + CoQ, and Cd + TM + CoQ groups (**Figure 7B**). Alongside the PCA, the clustering heatmap depicted in **Figure 7C** provides intuitive visualization of all the data sets, which summarizes the concentration values of all measured biochemical parameters in response to different treatments. These data show how the Cd-treated group exhibited more injury than the other groups.

## DISCUSSION

Cd is a prevalent nonbiodegradable environmental pollutant that threatens human and animal health (Wang et al., 2021). Cd has a long half-life, and once absorbed through the plasma membrane's calcium channel, it builds up in the body permanently due to its binding to the cytoplasm and nuclear molecules. Cd accumulation in the tissues triggers early oxidative stress and various pathological conditions, particularly in the liver and kidneys (Larregle et al., 2008; Cabral et al., 2021). Oxidative distress is renowned for being initiated when the produced ROS, such as superoxide anions ( $O_2^{\bullet-}$ ), hydroxyl radicals ( $OH^{\bullet}$ ), and hydrogen peroxide ( $H_2O_2$ ), overrides the endogenous antioxidant's capacity (Abdeen et al., 2019). Thereafter, tissue injury is elicited *via* provoking a cascade of complex mechanisms, such as the enhancement of LPO, protein misfolding, mitochondrial perturbation, depleted ATP production, and DNA damage (Abdel Moneim et al., 2014; Aboubakr et al., 2021a; Wang et al., 2021).

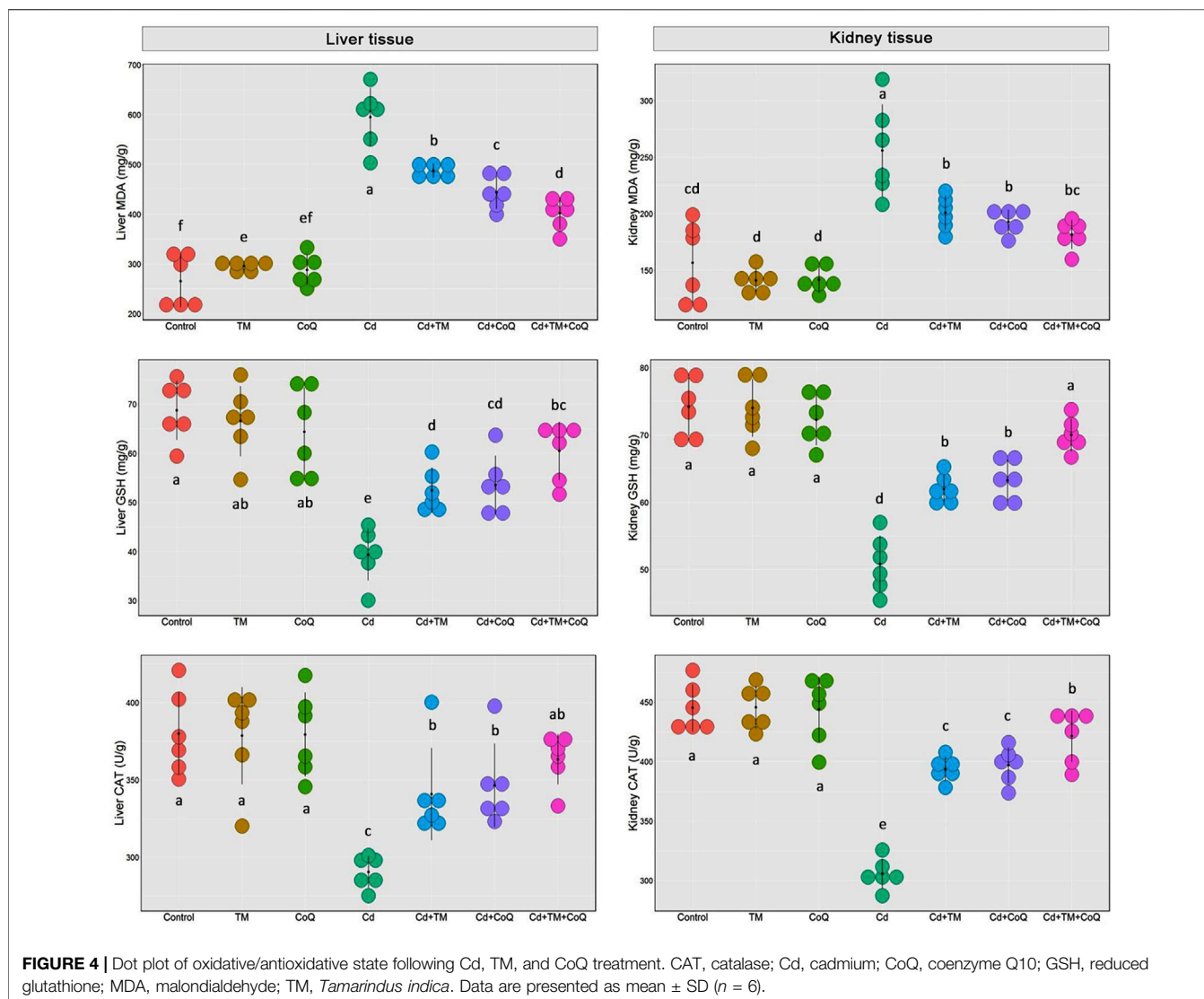
Consequently, the current findings exhibited noteworthy oxidative stress following Cd exposure, as elucidated by



significant declines in the GSH concentration and CAT activity in both the liver and kidney tissues. These findings align with formerly published studies (Abdel Moneim et al., 2014; El-boshy et al., 2014; Abdeen et al., 2019). GSH is the major sovereign antioxidant abundantly available in all biological systems since it functions as a nonenzymatic antioxidant by directly scavenging ROS (Abdel-Daim et al., 2021). Cd interacts exclusively with the SH content of the GSH, forming a GSH-Cd complex which is less readily reabsorbed in renal epithelial cells than the Cd-MT complex (Abdeen et al., 2019). The presented findings are in conformity with various former reports proposing that the reduced levels of GSH in the liver and kidneys upon Cd intoxication might enhance their vulnerability to the ROS damaging effect (Renugadevi and Prabu, 2010; Samarghandian et al., 2015; Aboubakr et al., 2021b). In addition to GSH, CAT is another endogenous antioxidant that is necessary for decomposing  $H_2O_2$  into  $H_2O$  and  $O_2$ ; therefore, it conserves the cell from oxidative harm caused by the oxygen species. Thus, in a condition when CAT activity is depleted by Cd-induced overproduction of ROS, Fenton's reaction is accelerated and plentiful amounts of  $OH^\bullet$  are produced

(Abdeen et al., 2019). The  $OH^\bullet$  molecule is the most damaging radical among other ROS, which strongly destroys the lipid membranes, triggering LPO and increasing MDA (LPO marker) levels (Renugadevi and Prabu, 2010).

Alarming, besides the damaging effect of ROS, MDA has the competence to make chaotic binding with other subcellular molecules, such as proteins and nucleic acids, speeding up the oxidative cascade, making matters worse (Uddin et al., 2021). Consistently, the current investigation revealed enhanced LPO after Cd exposure, which is indicated by marked increases in MDA tissue levels. It has been reported that when the hepatocyte loses its membrane integrity, the membrane permeability is increased, contributing in the escaping of hepatic enzymes (ALT, AST, and ALP) into the circulation, increasing their blood levels (Abdeen et al., 2021). As shown in the current study, Cd intoxication could dramatically enhance the activities of ALT, AST, and ALP. The histopathological examination vividly mirrored the biochemical findings on the liver sections. Additionally, the activation of the von Kupffer cells and neutrophil recruitment in our study has also been embroiled in the Cd hepatotoxic process. Wang et al. (2021) and Abdeen



et al. (2019) have corroborated the hepatotoxic damage in Cd-intoxicated rats.

In other words, histological analysis showed the presence of LPO in renal cell membranes, as seen by the disintegrating apical membrane, which caused tubular dysfunction as exhibited by marked increases in BUN and creatinine levels. There is strong evidence that the proximal tubules' sensitivity to ROS-induced oxidative damage is due to their high mitochondrial content. Surprisingly, according to the current histological study, the proximal tubules were the most affected areas of the kidneys following Cd intoxication. These findings are consistent with our prior research, which indicates the vulnerability of the cortical region to oxidative degradation caused by different insults such as gentamicin (Abdeen et al., 2021), cefepime (Aboubakr et al., 2021a), and aflatoxins B<sub>1</sub> (Abdel-Daim et al., 2021). Therefore, it is strongly assumed that mitochondria constitutes a potential subcellular target for Cd (Gobe and Crane, 2010). Furthermore, this work shows substantial reductions in albumin and globulin serum levels which in turn affect the total protein levels after Cd

exposure. These reductions might be attributed to the Cd-induced inhibition of protein synthesis due to oxidative stress, endoplasmic reticulum stress, and DNA oxidation, which ended up suppressing mRNA transcription and translation processes in the hepatocytes (El-boshy et al., 2014; Aboubakr et al., 2021a). Our histopathological findings confirm the occurrence of hepatic degenerative changes in response to Cd intoxication. Moreover, the renal reabsorption defects caused by Cd were another condemned mechanism for excessive protein loss in the urine, reducing their serum levels (Abdeen et al., 2020).

Moreover, we observed disruption of lipid metabolism, as seen by raised serum cholesterol and triglyceride levels, implying the presence of liver injury following Cd poisoning, as evidenced by the fatty buildup in hepatocytes shown in our histological findings. Our data are in agreement with those obtained by Larregle et al. (2008), who found that Cd exposure accelerated fat degeneration in isolated rat hepatocytes. It is evident that Cd affects the amount of lipids in various organs. We anticipate that the hypertriglyceridemia

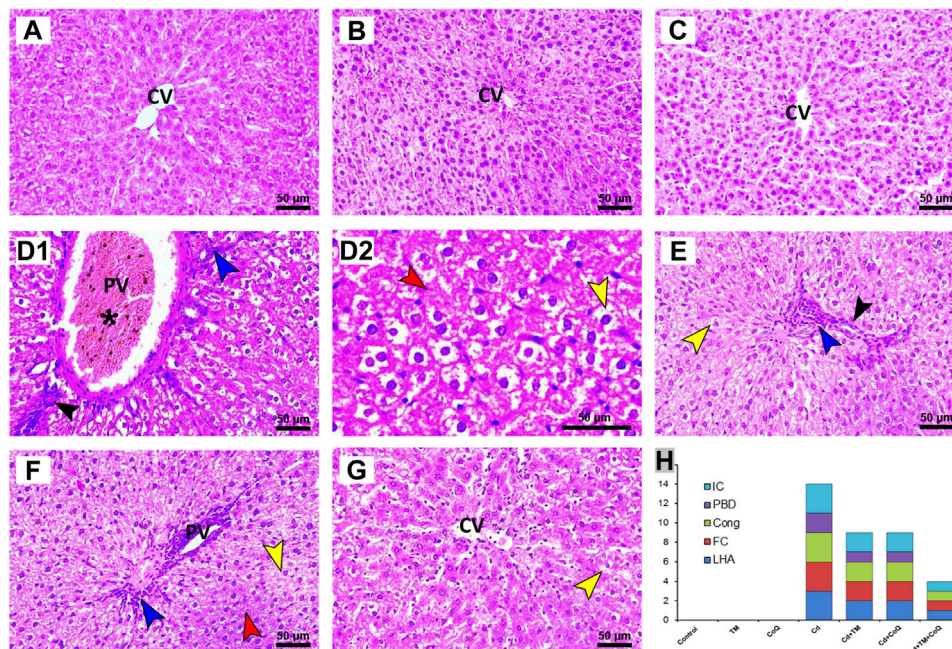


**FIGURE 5 |** Histopathology of liver tissue in Control and Cd-, TM-, and CoQ-treated groups. Nearly normal hepatic architectures were observed in Control (A), TM-treated (B), and CoQ-treated (C) rats. Cd (D1): liver section of Cd-treated group showing severe congestion of portal vein (asterisk), proliferation of bile duct (black arrow), and dense portal inflammation (blue arrow). Loss of hepatic architecture (red arrow) and severe fatty changes were also detected in Cd (D2). Cd + TM (E) and Cd + CoQ (F): dramatic improvement of hepatic architecture observed when Cd was co-administered with TM or CoQ, indicated by mild fatty changes (yellow arrow), portal inflammation (blue arrow), and proliferation of bile duct (black arrow). Cd + TM + CoQ (G): rats treated synchronously with Cd and both TM and CoQ revealed hepatic architecture reverted to normal with very mild fatty changes. (H) Ordinal scoring of recorded histopathological alterations in the liver tissue. (Cong; congestion; CV, central vein; FC, fatty changes; IC, inflammatory cell infiltration; LHA, loss of hepatic architecture; PBD, proliferation of bile duct; PV, portal vein; scale bar = 50  $\mu$ m.)

and hypercholesterolemia noticed in Cd-treated animals were attributed to the reduced activity of plasma lipoprotein lipase, a pivotal enzyme, in their breakdown (Larregle et al., 2008). Besides, Cd inhibits cholesterol uptake by macrophage, which is crucial in cholesterol metabolism (Ramirez and Gimenez, 2003). Taken together, all the aforementioned mechanisms promote fatty liver induction. These data are in congruence with Kim et al. (2018), who demonstrated a noteworthy rise in cholesterol and triglyceride levels after Cd intoxication in a zebrafish model.

In addition, our results are in harmony with those of Samarghandian et al. Larregle et al. (2008) elucidated that Cd exposure adversely disrupted the lipid profile through LPO. Worse, elevated cholesterol levels were frequently cited as a factor that hastens the deposition of Cd (Türkcan et al., 2015). Additionally, dyslipidemia is reported to promote mitochondrial instability and excess production of ROS, thereby oxidative stress exacerbates the deleterious sequels (Gutierrez-Mariscal et al., 2020).

GC/MS was used to identify the *T. indica* plant in the current study. The GC/MS chromatogram revealed that saponin, terpenoids, steroids, oleic acid, fatty acids methyl esters, vitamin A, and glyceryl palmitate were the most ubiquitous constituents in the TM seed extract (Table 1).

Notably, these secondary metabolites evince diverse therapeutic potential, mainly antioxidant (S et al., 2021; Atawodi et al., 2013), anti-inflammatory (Mushtaq et al., 2021), and antihyperlipidemic (Velu et al., 2018) properties. The presence of these phytochemicals is in congruence with that reported in preceding studies those screened the prime constituents of *T. indica* seeds (S et al., 2021; Mushtaq et al., 2021; Sadiq et al., 2016). Furthermore, the current investigation has proven the antioxidant potential of TM by the presence of remarkable levels of phenols (611.08 mg GAE/g), flavonoids (179.08 mg CE/g), and increments of free radicals scavenging activity (according to DPPH<sup>•</sup> and ABTS<sup>+</sup> assays), supporting the findings of prior investigations (Rebaya et al., 2015). The phenolic compounds can be deemed the cornerstone of TM's antioxidant potentiality, depending on their chemical architectures, particularly the number and location of the OH groups, the nature of exchange on the aromatic rings, and double bonds those enable the delocalization of free electrons. They have the potential to transform unpaired electrons to paired ones *via* donating hydrogen atom (H<sup>+</sup>) to them which is crucial for free radicals neutralization and stability, therefore conferring the phenolic molecules their scavenging capability (Yeasmen and Islam, 2015).

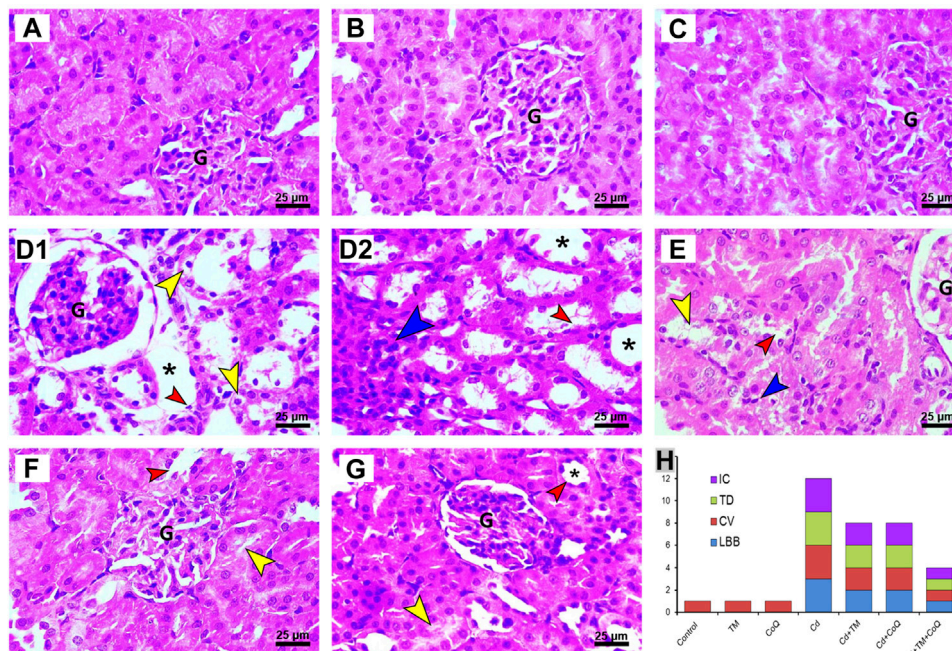


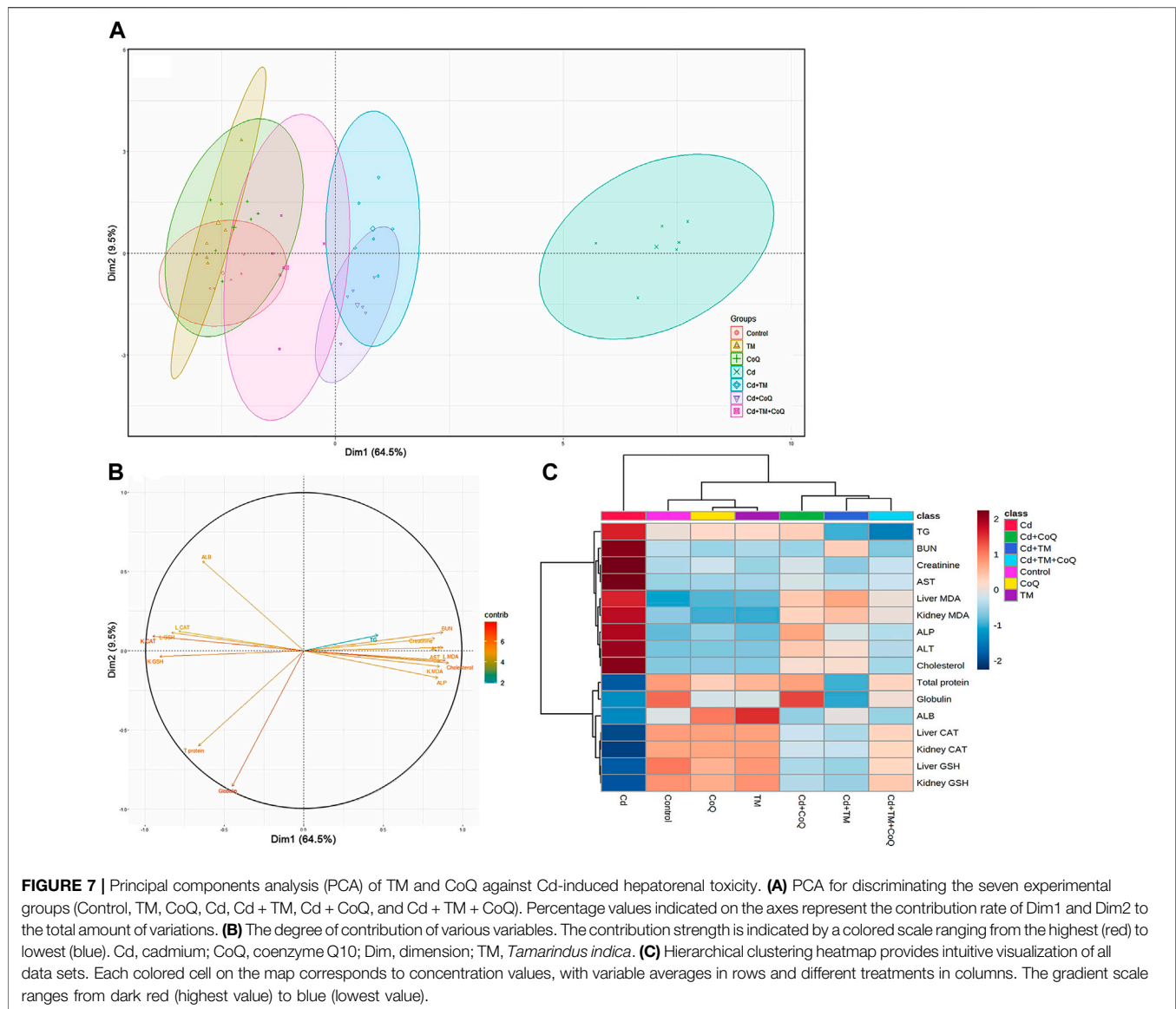
**FIGURE 6** | Histopathology of kidney tissue in Control and Cd-, TM-, and CoQ-treated groups. Normal nephrons were observed in Control (A), TM-treated (B), and CoQ-treated (C) rats. Cd (D1 and D2): kidney section of Cd-treated group showing loss of normal renal architecture with loss of brush border (red arrow), vacuolated cytoplasm (yellow arrow) in the epithelial lining of renal tubules, dense inflammatory cell infiltration (blue arrow), and severe tubular dilation (asterisk). Cd + TM (E) and Cd + CoQ (F): dramatic improvement of renal architecture was observed when Cd was co-administered with TM or CoQ, indicated by mild lesions in certain renal tubules. Cd + TM + CoQ (G): rats treated synchronously with Cd and both TM and CoQ, expounded that renal tubules were reverted close to normal. (H) Ordinal scoring of recorded histopathological alterations in the renal tissue. (CV, cytoplasmic vacuolation; G, glomerular tuft; IC, inflammatory cell infiltration; LBB, loss of brush border; TD, tubular dilatation; H&E, hematoxylin and eosin; scale bar = 25  $\mu$ M.)

Moreover, the OH group has the potential to detoxify the ROS, including mainly  $\text{HO}^\bullet$  radicals aiding in protecting the membrane lipids from the  $\text{HO}^\bullet$ -induced LPO. Several reports have revealed a robust correlation between the antioxidant power of plants and phenolic contents (Abdeen et al., 2021). In particular, saponins (epoxygedunin), representing the largest proportion among other constituents of TM (32.24%) in the current study, are well known for their potent antioxidant and chelating activities. Saponins are reported to assist the renovation of mitochondrial function and suppress inflammatory responses (Wang et al., 2021). Likewise, saponins have the capability to scavenge the superoxide radical through the xanthine and xanthine oxidase pathway (Fu et al., 2009).

CoQ is a unique lipid-soluble *de novo*-created antioxidant that confers molecular stability to the membrane phospholipid bilayer (Hernández-Camacho et al., 2018). The most significant and relevant activity of CoQ is associated with the high antioxidant capability of its coexisting redox states (ubiquinone, semi-ubiquinone, and ubiquinol), which function on the electron transport chain (Abdeen et al., 2020). The antioxidant properties of CoQ is located behind its efficiency of inhibiting the electron loss along the electron transport chain, besides its role in the recycling of other antioxidants such as vitamin C and vitamin

E (Hernández-Camacho et al., 2018; Gutierrez-Mariscal et al., 2020).

Interestingly, the ongoing experiment suggests that treatment with TM or CoQ could potentially attenuate Cd-induced hepatorenal damage, as seen by remarkable improvements in liver and kidney functions, lipid metabolism, and oxidative/antioxidative state. We also noticed a refinement of histological alterations after TM and CoQ supplementations confirming their ameliorative properties. Our findings are in harmony with antecedent reports that TM could protect rat liver from carbon tetrachloride-induced injury (Atawodi et al., 2013). Another report elucidated the enhancement of antioxidative enzyme activities in the liver and kidneys following CoQ supplement in a piroxicam-intoxicated rat (Abdeen et al., 2020). Besides the antioxidant properties, TM and CoQ have antihyperlipidemic (Velu et al., 2018; Gutierrez-Mariscal et al., 2020) and anti-inflammatory (Abdeen et al., 2020; Mushtaq et al., 2021; da Silveira e Sá Rde et al., 2015) capabilities, which supposedly play a role in restoring serum cholesterol and triglyceride levels and obscuring lymphocytic infiltrates as indicated in our histopathology results, respectively. There are various mechanisms by which CoQ serves lipid metabolism such as boosting fatty acid oxidation and inhibiting the oxidation of low-density lipoprotein, the primary carrier of blood



cholesterol, which is implicated in the cumulation of cholesterol (Gutierrez-Mariscal et al., 2020). Intriguingly, saponins in TM cause hypolipidemia by inhibiting HMG-CoA reductase, a crucial enzyme in the cholesterol biosynthetic pathway (Velu et al., 2018). Furthermore, caryophyllene, another essential ingredient of TM, preferentially binds to the cannabinoid type-2 receptor, modulating the inflammatory processes and exerting considerable cannabimimetic anti-inflammatory effects. Caryophyllene can also modulate the release of proinflammatory cytokines (da Silveira e Sá Rde et al., 2015).

We employed multivariate PCA for analyzing the role of TM, CoQ, and Cd interventions on liver and kidney tissues. The PCA displays each experimental group's pathway in space spanned by biochemical and oxidative stress markers. The data obtained by PCA exhibit how Cd

exposure causes a detrimental shift in the measured parameters, rendering these animals differentiated from the other treated groups by about 64.5%. In this work, both single-variate and PCA demonstrated that increasing the antioxidant activity alleviated the detrimental effects of Cd in rats co-treated with TM and/or CoQ, while PCA1 revealed that GSH levels and CAT activities significantly alleviated the damaging effects of Cd. Interestingly, PCA found that administering TM and CoQ together was more effective than using them separately against Cd-induced hepatorenal damage. In addition to the PCA, the clustering heatmap provides intuitive visualization of the concentration values that could potentially discriminate the Cd-exposed group from other treatments.

Overall, combining TM and CoQ supplementation provided superior hepatorenal protection against Cd

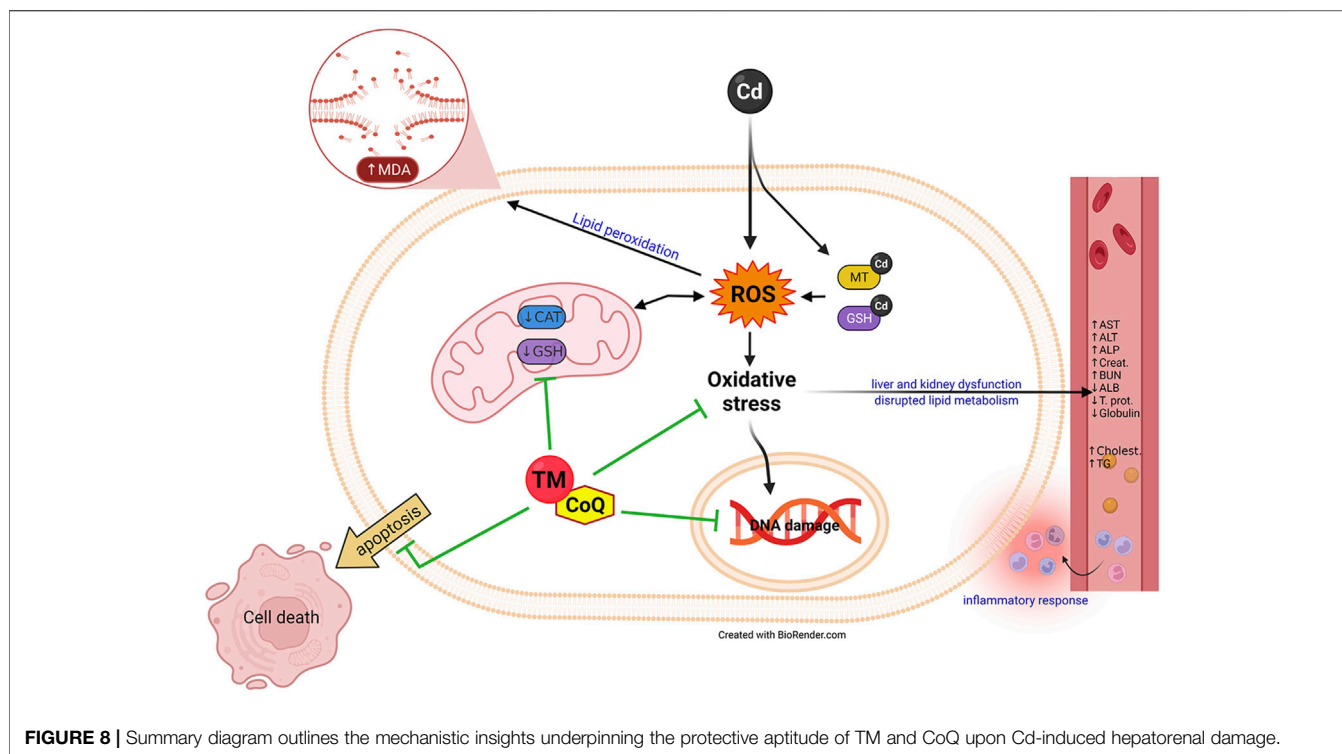


**FIGURE 8 |** Summary diagram outlines the mechanistic insights underpinning the protective aptitude of TM and CoQ upon Cd-induced hepatorenal damage.

toxicity than did either of the supplements alone. These might be because of their potent ROS-scavenging activity, enhancing the cellular antioxidant system, improving lipid metabolism, and suppressing the inflammatory response. The mechanistic insights underpinning the preemptive potential of TM and CoQ against Cd-induced hepatorenal injury are summarized in **Figure 8**.

## CONCLUSION

Cd could evoke notable hepatorenal damage, as demonstrated by higher levels of function biomarkers, changes in lipid and protein metabolism, and changes in oxidative status. TM and CoQ have the capacity to protect hepatocytes and renal cells from Cd-induced damage by combating oxidative distress, which can be because of their antioxidant and anti-inflammatory activities. In Cd-intoxicated animals, supplementing with TM or CoQ only reduces the severity of injury. When both therapies are used together, they produce greater results than when used separately. We expected that supplementing with TM and CoQ would help prevent Cd-induced tissue damage.

## DATA AVAILABILITY STATEMENT

The original contributions presented in the study are included in the article/Supplementary Material, and further inquiries can be directed to the corresponding authors.

## ETHICS STATEMENT

The animal study was reviewed and approved by the Ethical Committee, Faculty of Veterinary Medicine, Benha University (approval no: BUFVTM130222).

## AUTHOR CONTRIBUTIONS

AmA: conceptualization, data curation, formal analysis, investigation, methodology, software, and writing—original draft. NA-A: conceptualization, data curation, formal analysis, supervision, validation, and writing—review and editing. AM: conceptualization, data curation, formal analysis, supervision, validation, and writing—review and editing. AfA: formal analysis, investigation, methodology, software, writing—original draft, and writing—review and editing. AI: data curation, formal analysis, investigation, methodology, software, visualization, and writing—original draft. SS: data curation, formal analysis, investigation, methodology, software, visualization, and writing—original draft. EE: data curation, formal analysis, investigation, methodology, software, visualization, and writing—original draft. HB: data curation, formal analysis, investigation, methodology, software, visualization, and writing—original draft. SA: investigation, methodology, software, visualization, and writing—original draft. SI: funding acquisition, resources, software, validation, visualization, writing—original draft, and writing—review and editing. IA: Data curation, Software, Validation, Visualization, Writing—original draft. AhA: conceptualization, data curation, formal analysis, funding acquisition, investigation, methodology, project administration,

resources, software, supervision, validation, visualization, and writing—review and editing.

## FUNDING

This work was partially supported by STDF (grant no. 31290) and Princess Nourah bint Abdulrahman University Researchers Supporting Project number (PNURSP 2022R127), Princess Nourah bint Abdulrahman University, Riyadh, Saudi Arabia.

## REFERENCES

- Abdeen, A., Abou-Zaid, O. A., Abdel-Maksoud, H. A., Aboubakr, M., Abdelkader, A., Abdelnaby, A., et al. (2019). Cadmium Overload Modulates Piroxicam-Regulated Oxidative Damage and Apoptotic Pathways. *Environ. Sci. Pollut. Res. Int.* 26, 25167–25177. doi:10.1007/s11356-019-05783-x
- Abdeen, A., Abdelkader, A., Elgazzar, D., Aboubakr, M., Abdulah, O. A., Shoghy, K., et al. (2020). Coenzyme Q10 Supplementation Mitigates Piroxicam-Induced Oxidative Injury and Apoptotic Pathways in the Stomach, Liver, and Kidney. *Biomed. Pharmacother.* 130, 110627. doi:10.1016/j.biopha.2020.110627
- Abdeen, A., Samir, A., Elkomy, A., Aboubaker, M., Habotta, O. A., Gaber, A., et al. (2021). The Potential Antioxidant Bioactivity of Date Palm Fruit against Gentamicin-Mediated Hepato-Renal Injury in Male Albino Rats. *Biomed. Pharmacother.* 143, 112154. doi:10.1016/j.biopha.2021.112154
- Abdel Moneim, A. E., Bauomy, A. A., Diab, M. M., Shata, M. T., Al-Olayan, E. M., and El-Khadragy, M. F. (2014). The Protective Effect of *Physalis Peruviana* L. Against Cadmium-Induced Neurotoxicity in Rats. *Biol. Trace Elem. Res.* 160 (3), 392–399. doi:10.1007/s12011-014-0066-9
- Abdel-Daim, M. M., Abdeen, A., Jalouli, M., Abdelkader, A., Megahed, A., Alkahtane, A., et al. (2021). Fucoidan Supplementation Modulates Hepato-Renal Oxidative Stress and DNA Damage Induced by Aflatoxin B1 Intoxication in Rats. *Sci. Total Environ. [Internet]* 768 (xxxx), 144781. doi:10.1016/j.scitotenv.2020.144781
- Aboubakr, M., Abdelkader, A., Habotta, O. A., Adel, N., Emam, M. A., Abdelhiee, E. Y., et al. (2021). Cefepime and Diclofenac Sodium Combined Treatment-Potentiates Multiple Organ Injury: Role of Oxidative Damage and Disrupted Lipid Metabolism. *J. Biochem. Mol. Toxicol.* 35 (12), e22929. doi:10.1002/jbt.22929
- Aboubakr, M., Elshafae, S. M., Abdelhiee, E. Y., Fadl, S. E., Soliman, A., Abdelkader, A., et al. (2021). Antioxidant and Anti-inflammatory Potential of Thymoquinone and Lycopene Mitigate the Chlorpyrifos-Induced Toxic Neuropathy. *Pharm. [Internet]* 1 (II), 1–16. doi:10.3390/ph14090940
- Amir, M., Khan, M. A., Ahmad, S., Akhtar, M., Mujeeb, M., Ahmad, A., et al. (2016). Ameliorating Effects of *Tamarindus indica* Fruit Extract on Anti-tubercular Drugs Induced Liver Toxicity in Rats. *Nat. Prod. Res.* 30 (6), 715–719. doi:10.1080/14786419.2015.1039001
- Asad, S., Kabir, F., Alam, S., Richi, F. T., Anny, I. P., Nesa, M. L., et al. (2022). *In Vitro* Analysis Provides New Insights into the Pharmacological Actions of Methanol Extract of Seeds of *Tamarindus indica* L. And its Kupchan Fractions. *Bangla Pharma J.* 25 (1), 9–15. doi:10.3329/bpj.v25i1.57835
- Atawodi, S. E., Liman, M. L., and Onyike, E. O. (2013). Antioxidant Effects of *Tamarindus indica* Following Acute and Chronic Carbon Tetrachloride Induced Liver Injury. *Int. J. Agric. Biol.* 15 (3), 410–418.
- Balali-Mood, M., Naseri, K., Tahergorabi, Z., Khazdair, M. R., and Sadeghi, M. (2021). Toxic Mechanisms of Five Heavy Metals: Mercury, Lead, Chromium, Cadmium, and Arsenic. *Front. Pharmacol.* 12, 643972. doi:10.3389/fphar.2021.643972
- Cabral, M., Garçon, G., Touré, A., Bah, F., Dewaele, D., Bouhsina, S., et al. (2021). Renal Impairment Assessment on Adults Living Nearby a Landfill: Early Kidney Dysfunction Biomarkers Linked to the Environmental Exposure to Heavy Metals. *Toxicol. Rep.* 8 (January), 386–394. doi:10.1016/j.toxrep.2021.02.009

## ACKNOWLEDGMENTS

The authors are grateful for the resources provided by the Science and Technology Development Fund, Egypt (STDF grant no. 31290). The acknowledgment is also extended to the Princess Nourah bint Abdulrahman University Researchers Supporting Project number (PNURSP 2022R127), Princess Nourah bint Abdulrahman University, Riyadh, Saudi Arabia. The Department of Veterinary Forensic Medicine and Toxicology, Benha University, is also acknowledged for providing all necessary facilities for this research.

- da Silveira e Sá Rde, C., Andrade, L. N., and de Sousa, D. P. (2015). Sesquiterpenes from Essential Oils and Anti-inflammatory Activity. *Nat. Prod. Commun.* 10 (10), 1767–1774.
- de Anicésio, É. C. A., and Monteiro, F. A. (2022). Potassium Reduces Oxidative Stress in *Tanzania guinea* Grass under Cadmium Toxicity. *Environ. Sci. Pollut. Res.* 29 (1), 1184–1198. doi:10.1007/s11356-021-15620-9
- Devi, B., and Boruah, T. (2020). “Antioxidants in Fruits: Properties and Health Benefits,” in *Antioxidants in Fruits: Properties and Health Benefits*. Editors G. A. Nayik and A. Gull (Singapore Pte: Springer Nature Singapore).
- El-boshy, M. E., Risha, E. F., Abdelhamid, F. M., Mubarak, M. S., and Hadda, T. B. (2014). Protective Effects of Selenium against Cadmium Induced. *J. Trace Elem. Med. Biol.* 1, 1.
- Elgazzar, D., Aboubakr, M., Bayoumi, H., Ibrahim, A. N., Sorour, S. M., El-hewaity, M., et al. (2022). Tigecycline and Gentamicin-Combined Treatment Enhances Renal Damage: Oxidative Stress, Inflammatory Reaction and Apoptosis Interplay. *Pharmaceuticals* 15 (6), 736. doi:10.3390/ph15060736
- El-Sheikh, A. A., Morsy, M. A., Mahmoud, M. M., Rifaai, R. A., and Abdelrahman, A. M. (2012). Effect of Coenzyme-Q10 on Doxorubicin-Induced Nephrotoxicity in Rats. *Adv. Pharmacol. Sci.* 2012, 981461. doi:10.1155/2012/981461
- Escalona-Arranz, J. C., Perez-Rosés, R., Rodriguez-Amado, J., Morris-Quevedo, H. J., Mwasi, L. B., Cabrera-Sotomayor, O., et al. (2016). Antioxidant and Toxicological Evaluation of a *Tamarindus indica* L. Leaf Fluid Extract. *Nat. Prod. Res.* 30 (4), 456–459. doi:10.1080/14786419.2015.1019350
- Fatima, S., Alsheikh, Y. A., and Almohaimeed, N. H. (2013). Protective Effect of Coenzyme Q10 (Coq10) and Epigallocatechin Gallate (Eccg) against Cisplatin-Induced Acute Renal Failure in Rats: 2nd Int Conf Biosci. *Biochem. Pharm. Sci.* 10, 95–98.
- Fouad, A. A., and Jresat, I. (2011). Hepatoprotective Effect of Coenzyme Q10 in Rats with Acetaminophen Toxicity. *Environ. Toxicol. Pharmacol.* 33 (2), 158–167. doi:10.1016/j.etap.2011.12.011
- Fu, X. J., Liu, H. B., Wang, P., and Guan, H. S. (2009). A Study on the Antioxidant Activity and Tissues Selective Inhibition of Lipid Peroxidation by Saponins from the Roots of *Platycodon Grandiflorum*. *Am. J. Chin. Med.* 37 (5), 967–975. doi:10.1142/S0192415X09007375
- Ghoneim, A., and Eldahshan, O. (2012). Antiapoptotic Effects of Tamarind Leaves against Ethanol-Induced Rat Liver Injury. *J. Pharm. Pharmacol.* 64 (3), 430–438. doi:10.1111/j.2042-7158.2011.01418.x
- Gobe, G., and Crane, D. (2010). Mitochondria, Reactive Oxygen Species and Cadmium Toxicity in the Kidney. *Toxicol. Lett.* 198 (1), 49–55. doi:10.1016/j.toxlet.2010.04.013
- Gutierrez-Mariscal, F. M., de Larriva, A. P. A., Limia-Perez, L., Romero-Cabrera, J. L., Yubero-Serrano, E. M., and López-Miranda, J. (2020). Coenzyme Q10 Supplementation for the Reduction of Oxidative Stress: Clinical Implications in the Treatment of Chronic Diseases. *Int. J. Mol. Sci.* 21 (21), 1–19. doi:10.3390/ijms21217870
- Hernández-Camacho, J. D., Bernier, M., López-Lluch, G., and Navas, P. (2018). Coenzyme Q10 Supplementation in Aging and Disease. *Front. Physiol. [Internet]* 9 (February), 1–11. doi:10.3389/fphys.2018.00044
- Hwang, E. S., and Thi, N. D. (2014). Effects of Extraction and Processing Methods on Antioxidant Compound Contents and Radical Scavenging Activities of Laver (*Porphyra Tenera*). *Prev. Nutr. Food Sci.* 19, 40–48. doi:10.3746/pnf.2014.19.1.040

- Kengaijah, J., Nandish, S. K. M., Ramachandriah, C., Chandramma, S., Shivaiah, A., Vishalakshi, G. J., et al. (2020). Protective Effect of Tamarind Seed Coat Ethanol Extract on Eryptosis Induced by Oxidative Stress. *Biochem. (Mosc)* 85 (1), 119–129. doi:10.1134/S0006297920010113
- Khader, S. A., Abdl-Mutaleb, M., and Khadrah, A. (2019). Effect of Tamarind and Carob in Treatment of Kidney Functions Induced-Gentamicin in Rats. *J. Home Econ. [Internet]* 29 (4), 2019.
- Larregle, E. V., Varas, S. M., Oliveros, L. B., Martinez, L. D., Antón, R., Marchevsky, E., et al. (2008). Lipid Metabolism in Liver of Rat Exposed to Cadmium. *Food Chem. Toxicol.* 46 (5), 1786–1792. doi:10.1016/j.fct.2008.01.018
- Maria, D., Luzia, M., and Jorge, N. (2011). Antioxidant Activity, Fatty Acid Profile and Tocopherols of *Tamarindus indica* L. Seeds. *Food Sci. Technol. (Campinas)* 2010 (004428), 497–501. doi:10.1590/S0101-20612011000200034
- Mirkov, I., Popov Aleksandrov, A., Ninkov, M., Tucovic, D., Kulas, J., Zeljkovic, M., et al. (2021). Immunotoxicology of Cadmium: Cells of the Immune System as Targets and Effectors of Cadmium Toxicity. *Food Chem. Toxicol.* 149 (December 2020), 112026. doi:10.1016/j.fct.2021.112026
- Mushtaq, A., Hanif, M. A., Zahid, M., Rashid, U., Mushtaq, Z., Zubair, M., et al. (2021). Production and Evaluation of Fractionated Tamarind Seed Oil Methyl Esters as a New Source of Biodiesel. *Energies* 14 (21), 1–13. doi:10.3390/en14217148
- Ramirez, D. C., and Gimenez, M. S. (2003). Induction of Redox Changes, Inducible Nitric Oxide Synthase and Cyclooxygenase-2 by Chronic Cadmium Exposure in Mouse Peritoneal Macrophages. *Toxicol. Lett.* 145 (2), 121–132. doi:10.1016/s0378-4274(03)00237-6
- Ranjan, R., Swarup, D., Patra, R. C., and Chandra, V. (2009). *Tamarindus indica* L. And *Moringa Oleifera* M. Extract Administration Ameliorates Fluoride Toxicity in Rabbits. *Indian J. Exp. Biol.* 47 (11), 900–905.
- Rebaya, A., Belghith, S. I., Baghdikian, B., Leddet, V. M., Mabrouki, F., Olivier, E., et al. (2015). Total Phenolic, Total Flavonoid, Tannin Content, and Antioxidant Capacity of *Halimium Halimifolium* (Cistaceae). *J. Appl. Pharm. Sci.* 5 (1), 052–057. doi:10.7324/JAPS.2015.50110
- Renugadevi, J., and Prabu, S. M. (2010). Cadmium-induced Hepatotoxicity in Rats and the Protective Effect of Naringenin. *Exp. Toxicol. Pathol.* 62 (2), 171–181. doi:10.1016/j.etp.2009.03.010
- S, O. Z., Iyadunni, A., A, A. I., A, A. J., and I, U. D. (2021). Black Velvet Tamarind: Phytochemical Analysis, Antiradical and Antimicrobial Properties of the Seed Extract for Human Therapeutic and Health Benefits. *J. Phytopharm.* 10 (4), 249–255. doi:10.31254/phyto.2021.10406
- Sadiq, I. S., Duruminiya, N. I., Balogun, J. B., Kwada, D., and Izuagie, T. (2016). Nutritional and Anti-nutritional Value of Tamarind Fruit (*Tamarindus indica*). *Int. J. Appl. Res. Technol.* 5 (3), 50–56.
- Samarghandian, S., Azimi-Nezhad, M., Shabestari, M. M., Azad, F. J., Farkhondeh, T., and Bafandeh, F. (2015). Effect of Chronic Exposure to Cadmium on Serum Lipid, Lipoprotein and Oxidative Stress Indices in Male Rats. *Interdiscip. Toxicol.* 8 (3), 151–154. doi:10.1515/intox-2015-0023
- Sangsefidi, Z. S., Yaghoubi, F., Hajihmadi, S., and Hosseinzadeh, M. (2020). The Effect of Coenzyme Q10 Supplementation on Oxidative Stress: A Systematic Review and Meta-Analysis of Randomized Controlled Clinical Trials. *Food Sci. Nutr.* 8, 1766–1776. doi:10.1002/fsn3.1492
- Sundaram, M. S., Hemshekhar, M., Thushara, R. M., Santhosh, M. S., Kumar, S. K., Paul, M., et al. (2014). Tamarind Seed Extract Mitigates the Liver Oxidative Stress in Arthritic Rats. *Food Funct.* 5 (3), 587–597. doi:10.1039/c3fo60381d
- Taghavizadeh Yazdi, M. E., Amiri, M. S., Nourbakhsh, F., Rahnama, M., Forouzanfar, F., Mousavi, S. H., et al. (2021). Bio-indicators in Cadmium Toxicity: Role of HSP27 and HSP70. *Environ. Sci. Pollut. Res.* 28 (21), 26359–26379. doi:10.1007/s11356-021-13687-y
- Türkcan, A., Scharinger, B., Grabmann, G., Keppler, B. K., Laufer, G., Bernhard, D., et al. (2015). Combination of Cadmium and High Cholesterol Levels as a Risk Factor for Heart Fibrosis. *Toxicol. Sci.* 145 (2), 360–371. doi:10.1093/toxsci/kfv057
- Uddin, M. J., Kim, E. H., Hannan, M. A., and Ha, H. (2021). Pharmacotherapy against Oxidative Stress in Chronic Kidney Disease: Promising Small Molecule Natural Products Targeting Nrf2-Ho-1 Signaling. *Antioxidants (Basel)* 10 (2), 1–26. doi:10.3390/antiox10020258
- Upaganlawar, A., Farswan, M., Rathod, S., and Balaraman, R. (2006). Modification of Biochemical Parameters of Gentamicin Nephrotoxicity by Coenzyme Q10 and Green Tea in Rats. *Indian J. Exp. Biol.* 44 (May), 416–418.
- van Gerwen, M., Alerte, E., Alsen, M., Little, C., Sinclair, C., and Genden, E. (2022). The Role of Heavy Metals in Thyroid Cancer: A Meta-Analysis. *J. Trace Elem. Med. Biol.* 69, 126900. doi:10.1016/j.jtemb.2021.126900
- Velu, G., Palanichamy, V., and Rajan, A. P. (2018). Phytochemical and Pharmacological Importance of Plant Secondary Metabolites in Modern Medicine. *Bioorg. Phase Nat. Food Overv.* 1, 135–156. doi:10.1007/978-3-319-74210-6\_8
- Wang, M., Chen, Z., Song, W., Hong, D., Huang, L., and Li, Y. (2021). A Review on Cadmium Exposure in the Population and Intervention Strategies against Cadmium Toxicity. *Bull. Environ. Contam. Toxicol.* 106 (1), 65–74. doi:10.1007/s00128-020-03088-1
- Yeasmen, N., and Islam, M. (2015). Ethanol as a Solvent and Hot Extraction Technique Preserved the Antioxidant Properties of Tamarind (*Tamarindus indica*) Seed. *J. Adv. Vet. Anim. Res.* 2 (3), 332–337. doi:10.5455/javar.2015.b103
- Žilić, S., Serpen, A., Akilloğlu, G., Janković, M., and Gökmen, V. (2012). Distributions of Phenolic Compounds, Yellow Pigments and Oxidative Enzymes in Wheat Grains and Their Relation to Antioxidant Capacity of Bran and Debranned Flour. *J. Cereal Sci.* 56 (3), 652–658. doi:10.1016/j.jcs.2012.07.014

**Conflict of Interest:** The authors declare that the research was conducted in the absence of any commercial or financial relationships that could be construed as a potential conflict of interest.

**Publisher's Note:** All claims expressed in this article are solely those of the authors and do not necessarily represent those of their affiliated organizations, or those of the publisher, the editors, and the reviewers. Any product that may be evaluated in this article, or claim that may be made by its manufacturer, is not guaranteed or endorsed by the publisher.

Copyright © 2022 Abdelnaby, Abdel-Aleem, Mansour, Abdelkader, Ibrahim, Sorour, Elgendy, Bayoumi, Abdelrahman, Ibrahim, Alsaati and Abdeen. This is an open-access article distributed under the terms of the Creative Commons Attribution License (CC BY). The use, distribution or reproduction in other forums is permitted, provided the original author(s) and the copyright owner(s) are credited and that the original publication in this journal is cited, in accordance with accepted academic practice. No use, distribution or reproduction is permitted which does not comply with these terms.



## OPEN ACCESS

## EDITED BY

Yanzhu Zhu,  
Chinese Academy of Agricultural  
Sciences (CAAS), China

## REVIEWED BY

Hao Lu,  
Northwest A&F University, China  
Miao Long,  
Shenyang Agricultural University, China  
Xu Wang,  
Huazhong Agricultural University, China

## \*CORRESPONDENCE

Jicang Wang,  
wangjicang@126.com

<sup>†</sup>These authors share first authorship

## SPECIALTY SECTION

This article was submitted to Predictive  
Toxicology,  
a section of the journal  
Frontiers in Pharmacology

RECEIVED 15 June 2022

ACCEPTED 14 July 2022

PUBLISHED 11 August 2022

## CITATION

Wang J, Wang K, Ding L, Zhao P,  
Zhang C, Wang H, Yang Z and Liu Z  
(2022), Alleviating effect of quercetin on  
cadmium-induced oxidative damage  
and apoptosis by activating the Nrf2-  
keap1 pathway in BRL-3A cells.  
*Front. Pharmacol.* 13:969892.  
doi: 10.3389/fphar.2022.969892

## COPYRIGHT

© 2022 Wang, Wang, Ding, Zhao,  
Zhang, Wang, Yang and Liu. This is an  
open-access article distributed under  
the terms of the [Creative Commons  
Attribution License \(CC BY\)](https://creativecommons.org/licenses/by/4.0/). The use,  
distribution or reproduction in other  
forums is permitted, provided the  
original author(s) and the copyright  
owner(s) are credited and that the  
original publication in this journal is  
cited, in accordance with accepted  
academic practice. No use, distribution  
or reproduction is permitted which does  
not comply with these terms.

# Alleviating effect of quercetin on cadmium-induced oxidative damage and apoptosis by activating the Nrf2-keap1 pathway in BRL-3A cells

Jicang Wang<sup>1\*†</sup>, Ke Wang<sup>1†</sup>, Lulu Ding<sup>1</sup>, Pengli Zhao<sup>1</sup>,  
Cai Zhang<sup>1</sup>, Hongwei Wang<sup>1</sup>, Zijun Yang<sup>1</sup> and Zongping Liu<sup>2</sup>

<sup>1</sup>College of Animal Science and Technology, Henan University of Science and Technology, Luoyang, China, <sup>2</sup>College of Veterinary Medicine, Yangzhou University, Yangzhou, China

Cadmium (Cd) is a toxic heavy metal extensively used in industrial and agricultural production. Among the main mechanisms of Cd-induced liver damage is oxidative stress. Quercetin (QE) is a natural antioxidant. Herein, the protective effect of QE on Cd-induced hepatocyte injury was investigated. BRL-3A cells were treated with 12.5  $\mu\text{mol/L}$  CdCl<sub>2</sub> and/or 5  $\mu\text{mol/L}$  QE for 24 h. The cells and medium supernatant were collected, and the ALT, AST, and LDH contents of the medium supernatant were detected. The activities or contents of SOD, CAT, GSH, and MDA in cells were determined. Intracellular ROS levels were examined by flow cytometry. Apoptosis rate and mitochondrial-membrane potential ( $\Delta\Psi\text{m}$ ) were detected by Hoechst 33,258 and JC-1 methods, respectively. The mRNA and protein expression levels of Nrf2, NQO1, Keap1, CytC, caspase-9, caspase-3, Bax, and Bcl-2 were determined by real-time PCR (RT-PCR) and Western blot methods. Results showed that Cd exposure injured BRL-3A cells, the activity of antioxidant enzymes decreased and the cell ROS level increased, whereas the  $\Delta\Psi\text{m}$  decreased, and the expression of apoptotic genes increased. Cd inhibited the Nrf2-Keap1 pathway, decreased Nrf2 and NQO1, or increased Keap1 mRNA and protein expression. Through the combined action of Cd and QE, QE activated the Nrf2-Keap1 pathway. Consequently, antioxidant-enzyme activity decreased, cellular ROS level decreased,  $\Delta\Psi\text{m}$  increased, Cd-induced BRL-3A cell damage was alleviated, and cell apoptosis was inhibited. After the combined action of QE and Cd, Nrf2 and NQO1 mRNA and protein expression increased, Keap1 mRNA and protein expression decreased. Therefore, QE exerted an antioxidant effect by activating the Nrf2-Keap1 pathway in BRL-3A cells.

## KEYWORDS

cadmium, quercetin, BRL-3A cells, apoptosis, oxidative damage, Nrf2-Keap1 pathway

## Introduction

Cadmium (Cd) is one of the most toxic pollutants in natural and occupational environments. Industrial heavy-metal pollution, fossil-fuel use, and other human activities affect the existence of Cd (Liu et al., 2014). Cd is also extensively used in electroplating, painting, anticorrosion agents, plastic stabilizers, and electrical contact materials. Once absorbed by the body, Cd persists in humans and animals for a long time, affecting various organs, including kidney, heart, liver, and brain (Winiarska-Mieczan et al., 2013; Amamou et al., 2015; Wen et al., 2021; Gong et al., 2022). The liver is the primary target organ for Cd to accumulate and exert its harmful effects. Most studies have shown that Cd is preferentially localized to hepatocytes *in vivo* and *in vitro* (Li et al., 2013; Horiguchi and Oguma, 2016).

Cd exposure induces oxidative stress in cells, leading to the accumulation of reactive oxygen species (ROS) and malondialdehyde (MDA), resulting in lipid peroxidation and oxidative damage (Vicente-Sánchez et al., 2008; Khan et al., 2019). Cd further causes changes in mitochondrial membrane permeability, releases CytC, and induces mitochondrial caspase-dependent apoptotic protein expression through a cascade reaction, leading to apoptosis (Banik et al., 2019).

Quercetin (QE), a natural flavonoid widely distributed and abundant in vegetables and fruits (Donmez et al., 2019), has strong antioxidant activity. It can directly scavenge reactive oxygen species, chelate metal ions, and inhibit oxidative damage. It also has anti-inflammatory, antitumor, antiviral, and liver- and cardiovascular-protective effects (Boots et al., 2008; Zhao et al., 2021).

The present study aimed to examine the impact of QE on Cd-induced apoptosis and oxidative damage in rat liver cells, as well as the role of the caspase-dependent and Nrf2 signaling pathways in these processes.

## Materials and methods

### Chemicals

Cadmium chloride (CdCl<sub>2</sub>; purity >99.99%) was purchased from Sigma-Aldrich Industrial Corporation. QE (purity >97%) was purchased from Shanghai Yien Chemical Technology (Shanghai, China). ALT, AST, and LDH kits were purchased from Nanjing Jiancheng Bioengineering Institute (Nanjing, China). Rat SOD, CAT, GSH, and MDA ELISA kits were purchased from Shanghai Yubo Biotechnology (Shanghai, China). Fetal bovine serum (FBS) was purchased from Thermo Fisher Scientific CN, Benzyl penicillin and streptomycin were purchased from Beyotime Biotechnology (Shanghai, China). β-Actin, CytC, caspase-9, caspase-3, Bcl-2, Bax, Nrf2, NQO1, and Keap1 were purchased from Proteintech

TABLE 1 Treatment of cells.

Group	Treatment
Control group	normal medium
Cd group	12.5 μmol/L CdCl <sub>2</sub>
Cd + QE group	12.5 μmol/L CdCl <sub>2</sub> +5 μmol/L QE
QE group	5 μmol/L QE

Group (Wuhan, China). Detection kits of ROS, Hoechst 33,258, and Annexin V-FITC apoptosis were purchased from Beyotime Biotechnology (Shanghai, China). RNA-Isolation Total RNA Extraction Reagent, HiScript III RT SuperMix for qPCR (+gDNA wiper), and ChamQ universal SYBR qPCR Master Mix were purchased from novozan Biotechnology (Nanjing, China). All other routine chemicals and solvents were of pure analytical grade.

### Cell culture

BRL-3A cells were obtained from Yangzhou University. They were cultivated in high-glucose DMSO containing 10% FBS, 2% streptomycin, and penicillin. They were then cultured in an incubator at 37°C with 5% CO<sub>2</sub>. The cells were divided into four groups and treated in medium supplemented with CdCl<sub>2</sub> and/or QE for 24 h. The treatment results are shown in Table 1.

### Cell viability detected by MTT

The BRL-3A cells were inoculated on 96-well plates with a cell density of  $1 \times 10^4/L$ , and 200 μl culture medium was added to each well until the cell-coverage area reached 60–70%. Each well was exposed to 10 μl of MTT (5 mg/ml) after various treatments were conducted according to the experimental requirements. After gentle mixing and culturing at 37°C with 5% CO<sub>2</sub> for 4 h, we carefully sucked and discarded the culture medium in the hole with a syringe. Then, 100 μl of formazan solubilization solution was added to each well. The 96-well plate was placed on a horizontal shaking table and shook slowly for 10 min. Absorbance was measured at 570 nm by enzyme immunoassay.

### Determination of liver-marker enzymes and antioxidants

ALT, AST, and LDH were measured using diagnostic kits. SOD, CAT, GSH, and MDA activities or content were measured using diagnostic ELISA kits following the manufacturer's protocol.

TABLE 2 Gene primers sequence and their GenBank accession number used for qPCR.

Gene name	Accession number	Primer sequences (5'-3')
Nrf2	NM_001399173.1	Forward: AGCACATCCAGACAGACACCA Reverse: TATCCAGGCAAGCGACTC
Keap1	NM_057152.2	Forward: AGCAGGCTTTGGCATCAT Reverse: CCGTGTAGGCGAACTCAATTAG
NQO1	NM_017000.3	Forward: GGTGAGAAGAGCCCTGATTGT Reverse: CTCCTGTGATGTCGTTTC
Bcl-2	NM_016993.2	Forward: CAAGCCGGGAGAACAGGGTA Reverse: CCCACCGAACTCAAAGAAGGC
Bax	NM_017059.2	Forward: CCGAGAGGTCTTCTCCGTGTG Reverse: GCCTCAGCCCATCTTCTTCCA
Caspase-3	NM_012922.2	Forward: GCAGCAGCCTCAAATTGTTGACTA Reverse: TGCTCCGGCTCAAACCATC
Caspase-9	NM_031632.2	Forward: CTGAGCCAGATGCTGTCCCAT Reverse: CCAAGGTCTCGATGTACCAGAA
CytC	NM_012839.2	Forward: GGAGAGGATACCCTGATGGA Reverse: GTCTGCCCTTTCTCCCTTCT
$\beta$ -actin	NM_031144.3	Forward: AGGAAATCGTGCGTGACAT Reverse: CCTCGGGGCATCGGAA

## Intracellular ROS determination

The BRL-3A cells were inoculated in a six-well culture dish until the cell-coverage area reached 60–70%. Cells were then treated according to the experimental groups. After 24 h, the cells were incubated with the ROS detection kit. The cells were incubated in a 37°C cell incubator for 20 min. ROS level was measured by flow cytometry.

## Mitochondrial membrane potential ( $\Delta\Psi_m$ ) detection

The BRL-3A cells were inoculated in six-well plates, and cells were treated according to experimental groups. The cells were incubated with the  $\Delta\Psi_m$  detection kit (JC-1) and then incubated again in a 37°C cell incubator for 20 min. According to the manufacturer's protocol, changes in  $\Delta\Psi_m$  were detected.

## Hoechst 33258

Apoptosis was detected with a Hoechst 33258 kit. The BRL-3A cells were inoculated into six-well plates for 12 h and then treated with Cd (12.5  $\mu\text{mol/L}$ ) and QE (5  $\mu\text{mol/L}$ ) for 24 h. Following a PBS wash, cells were incubated for 30 min with Hoechst 33,258 staining solution in a cell incubator. The staining solution was discarded, and the cells were washed twice with PBS.

An inverted fluorescence microscope was used to observe and photograph the cells.

## mRNA expression

Total RNA was extracted from rat liver tissue by using an RNA-isolater Total RNA Extraction Reagent. Then, using HiScript III RT SuperMix for qPCR (+gDNA wiper), total RNA was reverse transcribed to synthesize cDNA. We identified the mRNA sequence of rat caspase-9, caspase-3, and other genes from GenBank. The primers were designed using Primer Premier six and tested specifically in NCBI-Primer. Following the kit, ChamQ universal SYBR qPCR Master Mix was used for qRT-PCR. Three technical repetitions were performed for each sample, and the mean was considered to represent mRNA levels.  $\beta$ -Actin served as the endogenous control. The relative mRNA levels were analyzed by  $2^{-\Delta\Delta C_t}$  method. The primers for Nrf2, Keap1, NQO1, Bcl-2, Bax, CytC, caspase-9, caspase-3, and  $\beta$ -actin are listed in Table 2.

## Western blot

Following gentle washing with PBS, the cells were lysed with RIPA to extract total protein, and the cells were lysed with nuclear protein extract to extract nuclear protein. A BCA kit was used to extract and detect the protein concentration of each group. After adding loading buffer to the protein and boiling it for storage, SDS-PAGE electrophoresis (10% separation gel and 5% concentrated gel for protein electrophoresis) was performed. After transferring the protein onto PVDF membranes, they were sealed with 5% skimmed milk for 1 h. The primary antibody was cultured in a shaking table at 4°C for 12 h and washed with TBST. The secondary antibody was incubated for 1 h at room temperature and subjected to ECL chemiluminescence analysis with photos taken.

## Statistical analysis

SPSS (version 17) was used to analyze the data obtained under different experimental conditions. One-way ANOVA was used to compare results between the control and test groups.

## Results

### Effects of Cd and QE on cell viability in BRL-3A cells

BRL-3A cell viability was detected at six CdCl<sub>2</sub> concentrations by MTT assay. As shown in Figure 1A, the IC<sub>50</sub> of CdCl<sub>2</sub> was about

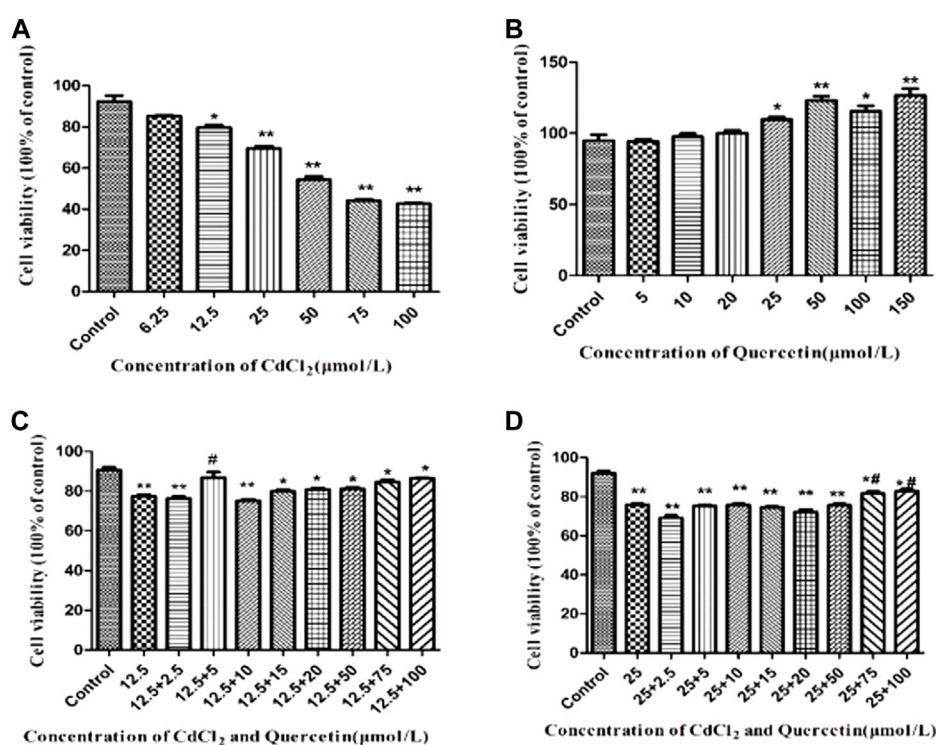


FIGURE 1

Detection of cell viability by MTT assay. The data are expressed in the form of (mean  $\pm$  SEM), “\*” indicates significant difference compared with the control group ( $p < 0.05$ ), “\*\*\*” indicates extremely significant difference compared with the control group ( $p < 0.01$ ), “#” indicates significant difference compared with the 12.5  $\mu\text{mol/L}$  CdCl<sub>2</sub> group or the 25  $\mu\text{mol/L}$  CdCl<sub>2</sub> group ( $p < 0.05$ ), “##” indicates extremely significant difference compared with the 12.5  $\mu\text{mol/L}$  CdCl<sub>2</sub> group or the 25  $\mu\text{mol/L}$  CdCl<sub>2</sub> group ( $p < 0.01$ ).

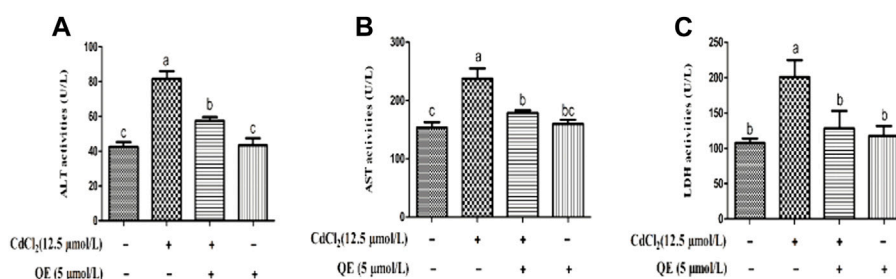


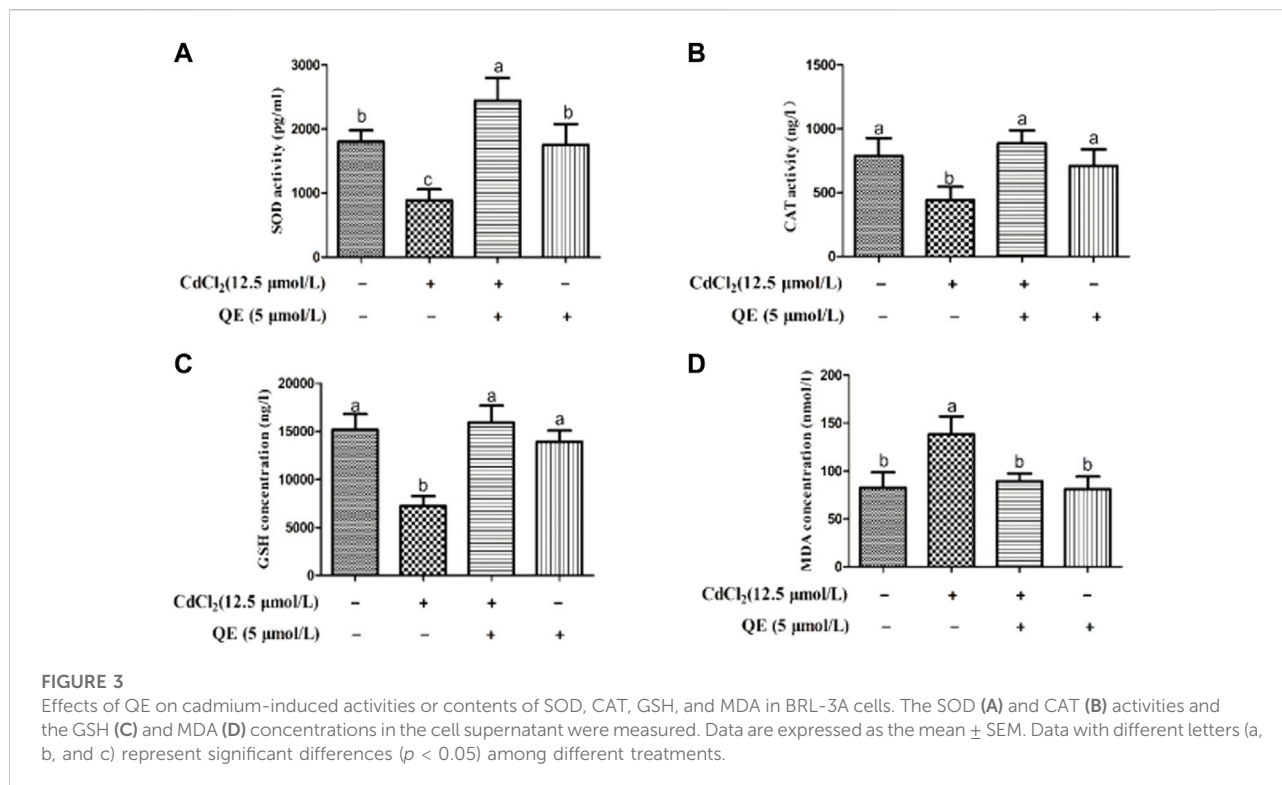
FIGURE 2

Effects of QE on Cd-induced changes in the levels of AST, ALT, and LDH in BRL-3A cells. The activities of ALT (A), AST (B), and LDH (C) in the medium supernatant were measured. Data are expressed as the mean  $\pm$  SEM, and data with different letters (a, b, and c) represent significant differences ( $p < 0.05$ ) among different treatments.

50  $\mu\text{mol/L}$ . Figure 1B shows that compared with the control group, when the QE concentration was 5–150  $\mu\text{mol/L}$ , QE had no inhibitory effect on cell activity. According to the results in Figures 1A–D and referring to the findings of Yang et al. (2019), the CdCl<sub>2</sub> and QE concentrations were finally determined to be 12.5 and 5  $\mu\text{mol/L}$ , respectively, *in vitro*.

## Medium supernatant liver-marker enzyme status

Figure 2 shows that after the CdCl<sub>2</sub> treatment of BRL-3A cells for 24 h, the AST, ALT, and LDH contents in the medium of the Cd group significantly increased ( $p < 0.05$ ). This finding indicated



that the cell membrane was ruptured and liver enzymes were released. However, after cotreatment with QE, compared with the Cd group, the AST, ALT, and LDH contents in the medium decreased significantly ( $p < 0.05$ ). This finding indicated that QE significantly improved the damage inflicted by CdCl<sub>2</sub> to cells.

## Antioxidant-enzyme activity and oxidative injuries

Figure 3 shows that compared with the control group, the activities of SOD and CAT in the Cd group decreased significantly, the GSH content decreased significantly, and the MDA content increased significantly ( $p < 0.05$ ). After cotreatment with QE, compared with those in the Cd group, the SOD and CAT activities increased, the GSH content increased, and the MDA content decreased in the Cd + QE group, with significant differences ( $p < 0.05$ ). Compared with those in the control group, the SOD and CAT activities and the GSH and MDA contents did not significantly differ ( $p > 0.05$ ), and the levels returned to normal.

## Effects of QE on the mRNA Expression Levels of Cd-induced the Nrf2 Signaling Pathway in BRL-3A Cells

Figure 4 shows that compared with the control group, the mRNA expression levels of Nrf2 and NQO1 in the Cd group

decreased significantly ( $p < 0.05$ ). The mRNA expression level of Keap1 increased significantly ( $p < 0.05$ ). After cotreatment with QE, compared with the Cd group, the mRNA expression levels of Nrf2 and NQO1 in the Cd + QE group increased significantly ( $p < 0.05$ ), whereas the mRNA expression level of Keap1 decreased significantly ( $p < 0.05$ ), and the expression level tended to the control group.

Figure 5A shows the protein-band diagram and the protein expression levels of Nrf2 signal pathway in BRL-3A cells. Compared with the control group, the expression level of Nrf2 protein in the Cd group decreased significantly ( $p < 0.05$ ), whereas those of NQO1 protein decreased and Keap1 protein increased significantly. After QE treatment, compared with the Cd group, the protein expression levels of Nrf2 and NQO1 in the Cd + QE group increased significantly ( $p < 0.05$ ), and the mRNA expression level of Keap1 decreased significantly ( $p < 0.05$ ).

## Effects of QE on ROS level in Cd-induced BRL-3A cells

DCFH-DA is a fluorescent dye that can measure the activity of intracellular ROS, which can oxidize DCFH to generate fluorescent DCF. Figure 6 shows that when BRL-3A cells were treated with CdCl<sub>2</sub>, the fluorescence peak of the Cd group shifted to the right compared with the control group, indicating increased ROS generation. After QE intervention, compared

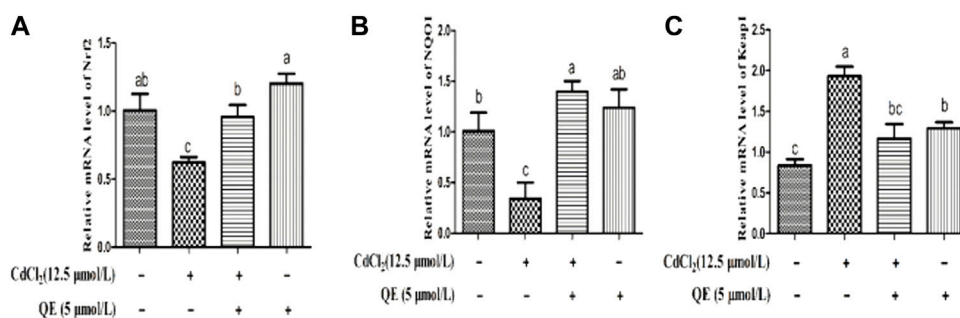


**FIGURE 4** Effects of QE on the mRNA expression of Cd-induced the Nrf2 signal pathway related genes in BRL-3A cells. Relative mRNA levels of Nrf2 (A), NQO1 (B), and Keap1 (C) in BRL-3A cells. Data are expressed as the mean ± SEM, and data with different letters (a, b, and c) represent significant differences ( $p < 0.05$ ) among different treatments.

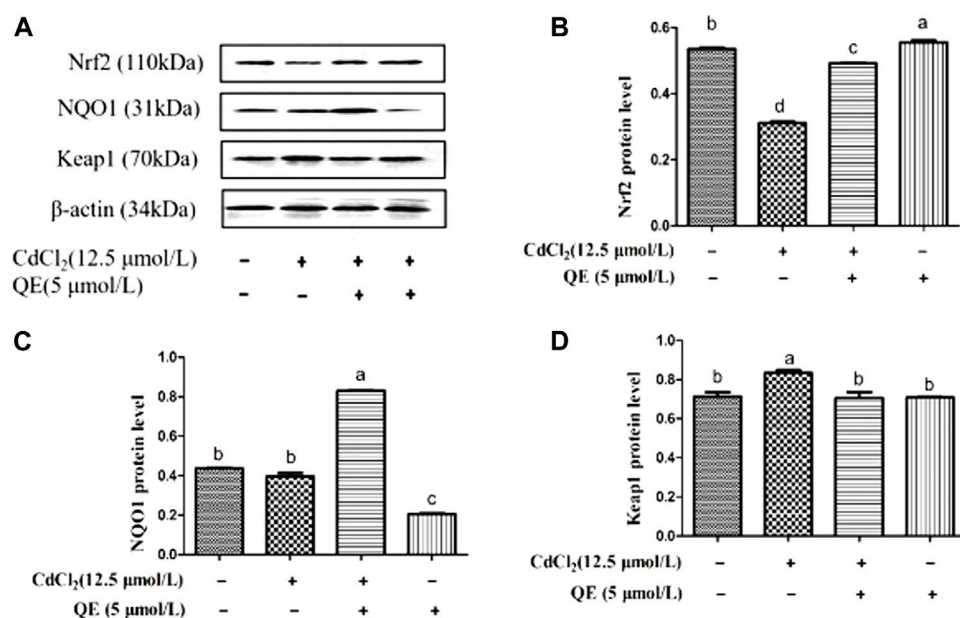


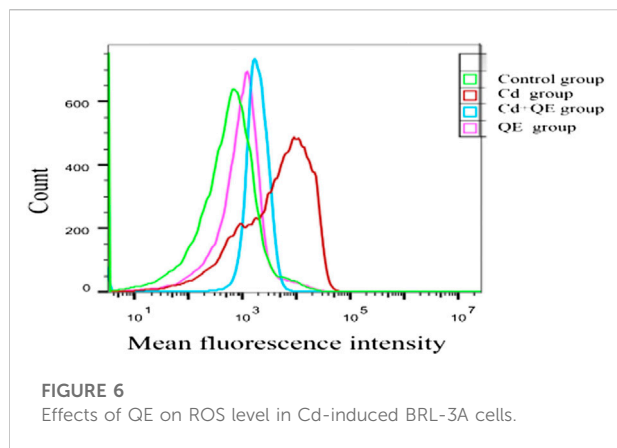
**FIGURE 5** Effects of QE on protein expression of Cd-induced the Nrf2 signal pathway related genes in BRL-3A cells. The levels of Nrf2, NQO1 and Keap1 proteins (A) were measured by Western blot. The protein levels of Nrf2 (B) NQO1 (C) and Keap1 (D) in BRL-3A cells. β-actin was used as a control. The data are expressed in the form of mean ± SEM, and data with different letters (a, b, and c) represent significantly different ( $p < 0.05$ ) among different treatments.

with the Cd group, the fluorescence peak shifted to the left, indicating that QE reduced the ROS generation.

### Effects of QE on ΔΨm in Cd-induced BRL-3A cells

JC-1 (C<sub>25</sub>H<sub>27</sub>Cl<sub>4</sub>IN<sub>4</sub>) is a fluorescent probe used to detect ΔΨm. Red fluorescence indicates that the ΔΨm is relatively normal, and green fluorescence indicates decreased ΔΨm and possibly early-stage

cell apoptosis. Figure 7 shows that cells in the control group were closely arranged under a microscope, grew well, and were oval and full. Under fluorescent conditions, the red fluorescence was strong, the green fluorescence was weak, and the ΔΨm is normal. Compared with the control group, cells in the QE group showed no difference in cell state and fluorescence intensity. Cells in the Cd group were long spindle shaped with sparse cells, and some cells died and fell off the bottom of the culture dish. The red fluorescence was weak and the green fluorescence was strong, and the ΔΨm decreased. Compared with the Cd group, cells were in good condition, the



red fluorescence was enhanced, and the green fluorescence was weakened in the Cd + QE group. This finding indicated that QE could significantly improve the effect of Cd-induced BRL-3A cells on  $\Delta\Psi_m$ .

## Effects of QE on the mRNA Expression Levels of Cd-induced Apoptosis Genes in BRL-3A cells

Figure 8 shows that compared with the control group, the mRNA expression levels of CytC, caspase-9, caspase-3 and Bax in the Cd group increased significantly ( $p < 0.05$ ), and the mRNA

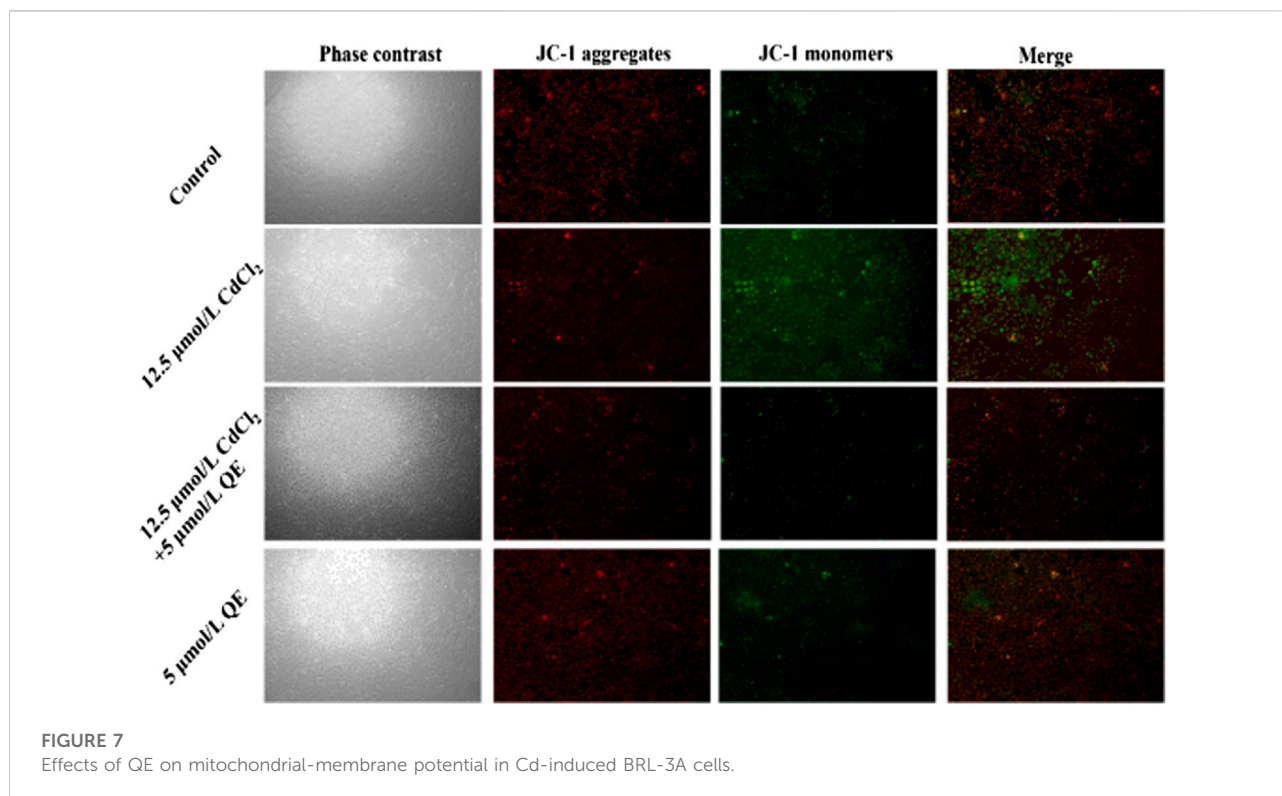
expression level of Bcl-2 in the Cd group decreased significantly ( $p < 0.05$ ). After adding QE, the mRNA expression levels of CytC, caspase-9, caspase-3, and Bax in the Cd + QE group decreased significantly ( $p < 0.05$ ), whereas the mRNA expression level of Bcl-2 increased significantly ( $p < 0.05$ ) compared with the Cd group.

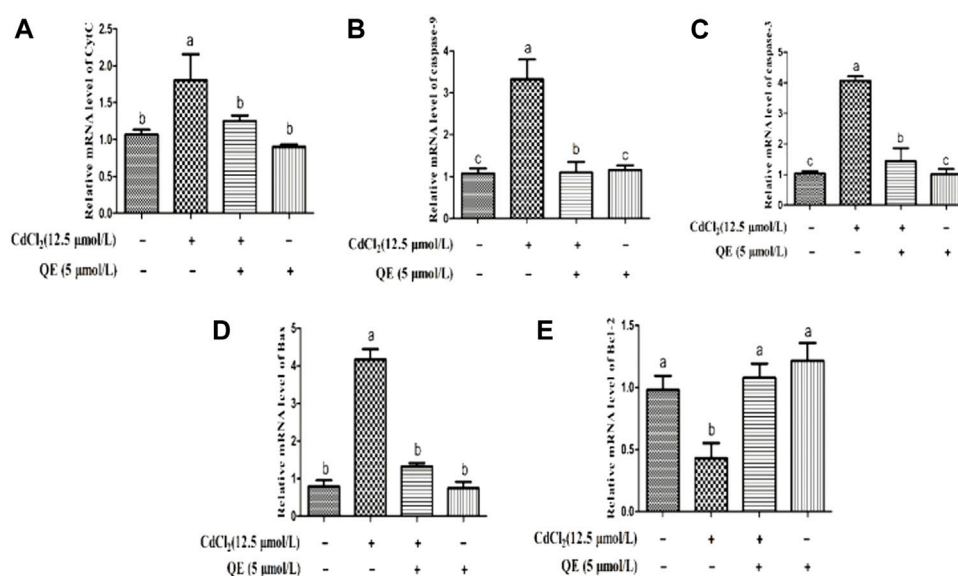
## Effects of QE on the Protein Expression Levels of Cd-induced Apoptosis Genes in BRL-3A Cells

Figure 9 shows the protein bands and protein expression levels of caspase-pathway-related genes. Compared with the control group, the protein expression levels of CytC, caspase-9, caspase-3, and Bax in the Cd group increased significantly ( $p < 0.05$ ). The protein expression level of Bcl-2 in the Cd group decreased significantly ( $p < 0.05$ ). After adding QE, compared with the Cd group, the protein expression levels of CytC, caspase-9, caspase-3, and Bax in the Cd + QE group decreased significantly ( $p < 0.05$ ), and whereas protein expression level of Bcl-2 increased significantly ( $p < 0.05$ ).

## Discussion

Cd is a toxic heavy metal widely used in industrial and agricultural production. The applications of Cd cause environmental pollution that is becoming increasingly serious. Cd can inflict serious toxic damage to the liver, kidney, and





**FIGURE 8**

Effects of QE on Cd-induced BRL-3A cell apoptosis-related gene mRNA expression. The relative mRNA level of CytC (A), caspase-9 (B), caspase-3 (C), Bax (D) and Bcl-2 (E) in BRL-3A cells. The data are expressed in the form of mean  $\pm$  SEM, and data with different letters (a, b, and c) represent significantly different ( $p < 0.05$ ) among different treatments.

reproductive system of humans and animals. The liver is the main target organ of Cd poisoning, and its damage is serious (Gong et al., 2019). Increasing evidence indicates that Cd accumulates in the liver, induces oxidative stress and apoptosis, and leads to liver damage (Cao et al., 2017). Oxidative stress and apoptosis can be inhibited by regulating the corresponding signaling pathways, which can be effective interventions for the treatment of Cd-induced hepatotoxicity (Yang et al., 2019). QE is a flavonoid rich in antioxidant, antiapoptotic, and anti-inflammatory properties (Anand David et al., 2016). It protects the liver from damage and inhibits its oxidation (Fang et al., 2021). It exerts a protective effect on the toxic damage inflicted by Cd (Prabu et al., 2010), although the mechanisms of protection are not well understood. This study explored the protective effect of QE on Cd-induced BRL-3A cells through the Nrf2 signaling pathway and mitochondrial caspase-dependent apoptosis pathway.

The safe concentrations for CdCl<sub>2</sub> and QE were determined by measuring the relative survival rate of BRL-3A cells. The IC<sub>50</sub> of CdCl<sub>2</sub> was about 50 μmol/L and QE had no inhibitory effect on cell activity. BRL-3A cells were cultured in Cd (12.5 μmol/L) and QE (5 μmol/L). It was found that QE improved the cytotoxicity induced by Cd, and the survival rate was significantly higher than that of Cd group. According to reference of Yang et al. (2019), the CdCl<sub>2</sub> and QE concentrations were finally determined to be 12.5 and 5 μmol/L, respectively.

Elevated levels of liver enzymes represent severe damage to the liver cell membrane, so liver enzymes can be used as markers to assess liver integrity and function (Gong et al., 2019). When the body

is healthy, transaminase exists in cells and has little content in serum, when liver cells have pathological changes, the permeability of cell membrane increases, and the transaminase in the cell is released into the blood, resulting in increased transaminase content in the blood (Zhang et al., 2017). LDH is abundant in animal tissues and organs and is released from cells only when the cell membrane is damaged (Jurisic et al., 2015). In the present study, Cd exposure resulted in increased contents of ALT, AST, and LDH medium supernatants, indicating that Cd damaged the hepatocyte membrane.

The main mechanism of Cd-induced liver injury is oxidative stress. Oxidative stress is essentially due to the depletion of antioxidants or the accumulation of ROS, resulting in imbalanced oxidative and antioxidant levels in the body. Cd exposure can directly or indirectly generate excess ROS. Antioxidants in the body such as SOD, CAT, GSH, etc. constitute the antioxidant system of tissue cells and play antioxidant roles. The existence of oxidase inhibits the oxidative reaction in the body, has the ability to remove ROS and resist oxidative damage, and plays an important role in resisting oxidative damage in animals (Chen et al., 2018). SOD has the function of scavenging oxygen free radicals in the body and SOD levels in organs, which can assess the degree of oxidative damage to organs. CAT breaks down H<sub>2</sub>O<sub>2</sub> into water and oxygen to reduce oxidative damage to the body. GSH is a potent free-radical scavenger that inhibits ROS generation and is the first line of defense for non-enzymatic antioxidants (NicoleCnubben et al., 2001). The production of MDA indicates the level of cellular damage because MDA is an intermediate product of lipid

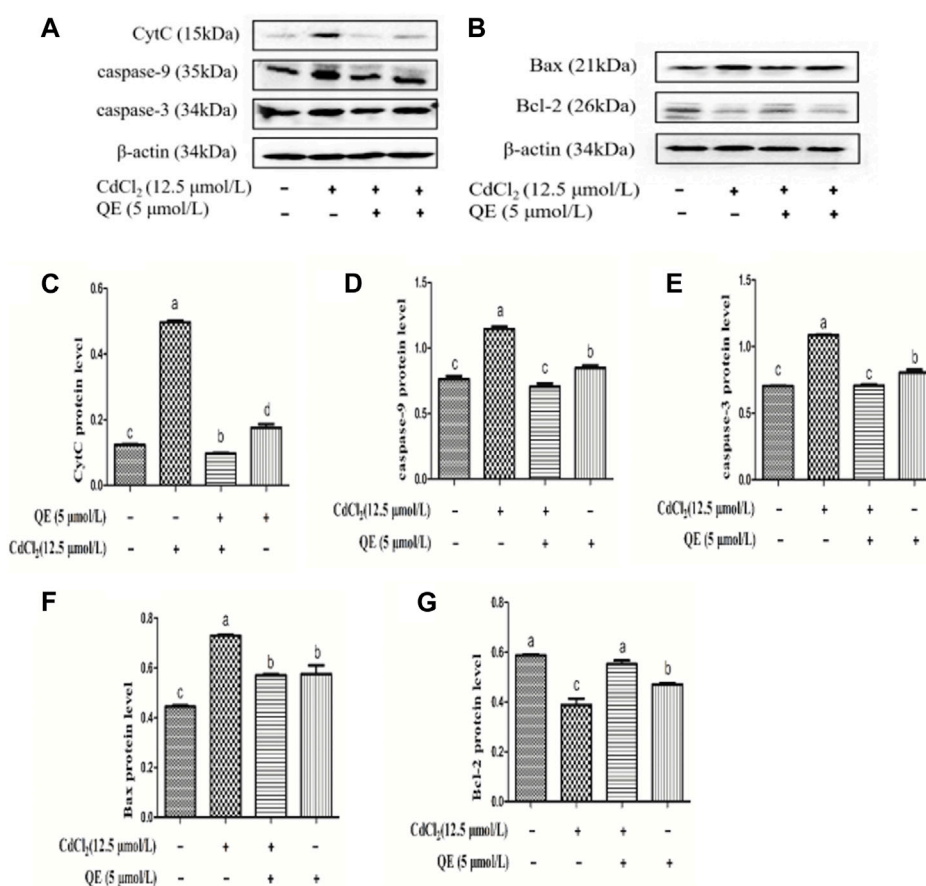


FIGURE 9

Effects of QE on Cd-induced BRL-3A cell apoptosis-related gene and protein expression. The levels of CytC, caspase-9, caspase-3, Bax and Bcl-2 proteins (A-B) were measured by Western blot. The protein levels of CytC (C), caspase-9 (D), caspase-3 (E), Bax (F) and Bcl-2 (G) in BRL-3A cells. The data are expressed in the form of mean  $\pm$  SEM, and data with different letters (a, b, and c) represent significantly different ( $p < 0.05$ ) among different treatments.

peroxidation (Luo et al., 2017). In the present study, Cd exposure significantly decreased the SOD and CAT activities and GSH content and significantly increased the MDA content. This finding indicated that Cd exposure led to lipid peroxidation in cells, consumption of antioxidant substances SOD, CAT, and GSH, and oxidative stress in cells.

ROS are highly reactive and can oxidize various biomolecules such as DNA, lipids, and proteins (Cao et al., 2017). ROS can also induce lipid peroxidation, destroy the balance of oxidative and antioxidant systems (Katwal et al., 2018), and disturb the homeostasis of cells and tissues, eventually causing cell damage. Mitochondria are the main targets of Cd-induced apoptosis (Nair et al., 2015; Zhang and Reynolds, 2019), which primarily occurs by activating the mitochondrial apoptosis pathway (Pi et al., 2013; Yin et al., 2018). Cd can directly or indirectly generate excess ROS (Savaugeau and Jumarie, 2013). Sustained and massive ROS production leads to the swelling of mitochondria, rupture of the outer membrane,

and decreased  $\Delta\Psi_m$  (Wang et al., 2020). Moreover, Cd exposure activates the proapoptotic protein Bax (Wang et al., 2020), thereby increasing mitochondrial-membrane permeability, promoting CytC release, triggering a caspase cascade, and leading to apoptosis (Pi et al., 2013; Sandoval-Acuña et al., 2014). In the present study, Cd exposure produced a large amount of ROS, resulting in decreased  $\Delta\Psi_m$  of BRL-3A cells. The expression levels of Bax mRNA and protein, CytC as well as mRNA and protein, increased. They were released from mitochondria, and the mitochondrial caspase-dependent apoptosis pathway was activated. The expression levels of caspase-9 and caspase-3 mRNA and protein increased, leading to apoptosis. These results were consistent with those of Paria A et al. (Amanpour et al., 2020).

Several studies have shown that chronic or acute exposure to Cd can produce large amounts of free radicals, which can lead to oxidative stress in various organs (Patra et al., 2011; Nna et al., 2017). Our findings suggested that Cd induced hepatocyte

apoptosis through oxidative stress, so an antioxidant was urgently needed to alleviate the oxidative damage caused by Cd exposure. QE is a natural organic antioxidant (Bahar et al., 2019). It can reportedly counteract Cd-induced neurotoxicity in rat brain, significantly improve Cd-induced abnormalities in biochemical and histological indicators (Prabu et al., 2010), and inhibit Cd-induced autophagy in mouse kidneys (Yuan et al., 2016). In the current work, after QE intervention, the contents of ALT, AST, and LDH in the supernatant of culture medium were reduced, and the damage inflicted by Cd to hepatocytes decreased. We found that QE activated the Cd-inhibited Nrf2 signaling pathway, significantly increased the SOD and CAT activities and the GSH content, significantly decreased the MDA content, reduced ROS generation, and inhibited the expression of the pro-apoptotic proteins Bax, CytC, caspase-9, and caspase-3 mRNA and protein expression. QE also increased the  $\Delta\Psi_m$  and reduced apoptosis. These results indicated that QE can reduce Cd-induced oxidative stress and apoptosis. The results of Morales et al. (2006) and Bu et al. (2011) supported this conclusion.

The Nrf2 signaling pathway and heavy-metal-induced oxidative stress are closely related (Chen et al., 2018; Caiyu Lian et al., 2022). Therefore, the Nrf2 pathway is an important target for preventing Cd-induced liver injury and is a mechanism by which the body resists environmental oxidants (Almeer et al., 2018). Nrf2 is an essential transcription factor whose function is to translocate into the nucleus and interact with the antioxidant response element to promote the transcription of target genes (Yang et al., 2018). Our results showed that Cd exposure inhibited the expression of the Nrf2 signal pathway-related genes and promoted ROS accumulation in cells. After QE intervention, Nrf2 was activated and its entry into the nucleus was promoted, and the expression of Nrf2 nuclear protein increased. Therefore, QE was an effective antioxidant that increased the activity of antioxidant enzymes by activating the Nrf2 signaling pathway, eliminating Cd-induced ROS, alleviating mitochondrial membrane damage, and maintaining the  $\Delta\Psi_m$ . Consequently, the mitochondrial caspase-dependent apoptosis pathway was inhibited, cell apoptosis was reduced, and the Cd-induced oxidative stress and apoptosis of hepatocytes were alleviated.

## Conclusion

QE exerted an antioxidant effect by activating the Nrf2 signaling pathway in BRL-3A cells, eliminating ROS, and

maintaining the integrity of mitochondrial membrane, thereby inhibiting the occurrence of mitochondrial caspase-dependent apoptosis pathway. QE playing a protective role in Cd-induced hepatocyte damage.

## Data availability statement

The original contributions presented in the study are included in the article/Supplementary Material, further inquiries can be directed to the corresponding author.

## Author contributions

JW: Conceptualization, Project administration, Software, Writing—Original Draft, Review, Editing, Funding acquisition. KW: Conceptualization, Formal analysis, Data Curation, Writing—Original Draft. LD: Methodology, Resources. PZ: Data Curation, Formal analysis. CZ: Methodology, Formal analysis. HW: Methodology, Visualization. ZY: Visualization, Formal analysis. ZL: Resources, Validation, Formal analysis.

## Funding

This study was supported by grants from National Natural Science Foundation of China (No. 31972753), Henan science and technology research project (222102110340).

## Conflict of interest

The authors declare that the research was conducted in the absence of any commercial or financial relationships that could be construed as a potential conflict of interest.

## Publisher's note

All claims expressed in this article are solely those of the authors and do not necessarily represent those of their affiliated organizations, or those of the publisher, the editors and the reviewers. Any product that may be evaluated in this article, or claim that may be made by its manufacturer, is not guaranteed or endorsed by the publisher.

## References

Almeer, R. S., Alarifi, S., Alkahtani, S., Ibrahim, S. R., Ali, D., Moneim, A., et al. (2018). The potential hepatoprotective effect of royal jelly against cadmium chloride-induced hepatotoxicity in mice is mediated

by suppression of oxidative stress and upregulation of Nrf2 expression. *Biomed. Pharmacother.* 106, 1490–1498. doi:10.1016/j.biopha.2018.07.089

- Amamou, F., Nemmiche, S., Meziane, R., Didi, A., Yazit, S., Chabane-Sari, D., et al. (2015). Protective effect of olive oil and colocynth oil against cadmium-induced oxidative stress in the liver of Wistar rats. *Food Chem. Toxicol.* 78, 177–184. doi:10.1016/j.fct.2015.01.001
- Amanpour, P., Khodarahmi, P., and Salehipour, M. (2020). Protective effects of vitamin E on cadmium-induced apoptosis in rat testes. *Naunyn-Schmiedeb. Arch. Pharmacol.* 393 (3), 349–358. doi:10.1007/s00210-019-01736-w
- Anand David, A. V., Arulmoli, R., and Parasuraman, S. (2016). Overviews of biological importance of quercetin: A bioactive flavonoid. *Pharmacogn. Rev.* 10 (20), 84–89. doi:10.4103/0973-7847.194044
- Bahar, E., Lee, G.-H., Bhattarai, K. R., Lee, H.-Y., Kim, H.-K., Handigund, M., et al. (2019). Protective role of quercetin against manganese-induced injury in the liver, kidney, and lung; and hematological parameters in acute and subchronic rat models [Retraction]. *Drug Des. devel. Ther.* 13, 907–908. doi:10.2147/DDDT.S207534
- Banik, S., Akter, M., Corpus Bondad, S. E., Saito, T., Hosokawa, T., Kurasaki, M., et al. (2019). Carvacrol inhibits cadmium toxicity through combating against caspase dependent/independent apoptosis in PC12 cells. *Food Chem. Toxicol.* 134, 110835. doi:10.1016/j.fct.2019.110835
- Boots, A., Haenen, G., and Bast, A. (2008). Health effects of quercetin: From antioxidant to nutraceutical. *Eur. J. Pharmacol.* 585 (2–3), 325–337. doi:10.1016/j.ejphar.2008.03.008
- Bu, T., Mi, Y., Zeng, W., and Zhang, C. (2011). Protective effect of quercetin on cadmium-induced oxidative toxicity on germ cells in male mice. *Anat. Rec. Hob.* 294 (3), 520–526. doi:10.1002/ar.21317
- Caiyu Lian, B. C., Xia, W., Wang, Z., Fan, R., and Wang, L. (2022). Persistent activation of Nrf2 in a p62-dependent non-canonical manner aggravates lead-induced kidney injury by promoting apoptosis and inhibiting autophagy. *J. Adv. Res.* doi:10.1016/j.jare.2022.04.016
- Cao, Z., Fang, Y., Lu, Y., Tan, D., Du, C., Li, Y., et al. (2017). Melatonin alleviates cadmium-induced liver injury by inhibiting the TXNIP-NLRP3 inflammasome. *J. Pineal Res.* 62 (3), e12389. doi:10.1111/jpi.12389
- Chen, L., Zhang, J., Zhu, Y., and Zhang, Y. (2018). Interaction of chromium(III) or chromium(VI) with catalase and its effect on the structure and function of catalase: An *in vitro* study. *Food Chem.* 244, 378–385. doi:10.1016/j.foodchem.2017.10.062
- Donmez, H. H., Donmez, N., Kisadere, I., and Undag, I. (2019). Protective effect of quercetin on some hematological parameters in rats exposed to cadmium. *Biotech. Histochem.* 94 (5), 381–386. doi:10.1080/10520295.2019.1574027
- Fang, P., Dou, B., Liang, J., Hou, W., Ma, C., Zhang, Q., et al. (2021). Quercetin reduces oxidative stress and apoptosis by inhibiting HMGB1 and its translocation, thereby alleviating liver injury in ACLF rats. *Evid. Based. Complement. Altern. Med.* 2021, 2898995. doi:10.1155/2021/2898995
- Gong, Z. G., Wang, X. Y., Wang, J. H., Fan, R. F., and Wang, L. (2019). Trehalose prevents cadmium-induced hepatotoxicity by blocking Nrf2 pathway, restoring autophagy and inhibiting apoptosis. *J. Inorg. Biochem.* 192, 62–71. doi:10.1016/j.jinorgbio.2018.12.008
- Gong, Z. G., Zhao, Y., Wang, Z. Y., Fan, R. F., Liu, Z. P., Wang, L., et al. (2022). Epigenetic regulator BRD4 is involved in cadmium-induced acute kidney injury via contributing to lysosomal dysfunction, autophagy blockade and oxidative stress. *J. Hazard. Mat.* 423, 127110. doi:10.1016/j.jhazmat.2021.127110
- Horiguchi, H., and Oguma, E. (2016). Acute exposure to cadmium induces prolonged neutrophilia along with delayed induction of granulocyte colony-stimulating factor in the livers of mice. *Arch. Toxicol.* 90 (12), 3005–3015. doi:10.1007/s00204-016-1661-7
- Juriscic, V., Radenkovic, S., and Konjevic, G. (2015). The actual role of LDH as tumor marker, biochemical and clinical aspects. *Adv. Exp. Med. Biol.* 867, 115–124. doi:10.1007/978-94-017-7215-0\_8
- Katwal, G., Baral, D., Fan, X., Weiyang, H., Zhang, X., Ling, L., et al. (2018). SIRT3 a major player in attenuation of hepatic ischemia-reperfusion injury by reducing ROS via its downstream mediators: SOD2, CYP-D, and HIF-1 $\alpha$ . *Oxid. Med. Cell. Longev.* 2018, 2976957. doi:10.1155/2018/2976957
- Khan, A., Ikram, M., Muhammad, T., Park, J., and Kim, M. O. (2019). Caffeine modulates cadmium-induced oxidative stress, neuroinflammation, and cognitive impairments by regulating nrf-2/HO-1 *in vivo* and *in vitro*. *J. Clin. Med.* 14, 680. doi:10.3390/jcm8050680
- Li, J., Jiang, C., Li, S., and Xu, S. (2013). Cadmium induced hepatotoxicity in chickens (*Gallus domesticus*) and ameliorative effect by selenium. *Ecotoxicol. Environ. Saf.* 96, 103–109. doi:10.1016/j.ecoenv.2013.07.007
- Liu, Y., Su, C., Zhang, H., Li, X., and Pei, J. (2014). Interaction of soil heavy metal pollution with industrialisation and the landscape pattern in Taiyuan city, China. *PLoS one* 9 (9), e105798. doi:10.1371/journal.pone.0105798
- Luo, T., Liu, G., Long, M., Yang, J., Song, R., Wang, Y., et al. (2017). Treatment of cadmium-induced renal oxidative damage in rats by administration of alpha-lipoic acid. *Environ. Sci. Pollut. Res. Int.* 24 (2), 1832–1844. doi:10.1007/s11356-016-7953-x
- Morales A. I., C. V.-S., Santiago Sandoval, J. M., Egido, J., Mayoral, P., Arévalo, M. A., et al. (2006). Protective Effect of quercetin on experimental chronic cadmium nephrotoxicity in rats is based on its antioxidant properties. *Food Chem. Toxicol.* 44 (12), 2092–2100. doi:10.1016/j.fct.2006.07.012
- Nair, A. R., Lee, W. K., Smeets, K., Swennen, Q., Sanchez, A., Thévenod, F., et al. (2015). Glutathione and mitochondria determine acute defense responses and adaptive processes in cadmium-induced oxidative stress and toxicity of the kidney. *Arch. Toxicol.* 89 (12), 2273–2289. doi:10.1007/s00204-014-1401-9
- Nicole, H. P., Cnubben, I. M., Wortelboer, H., van Zanden, J., and van Bladeren, P. J. (2001). The interplay of glutathione-related processes in antioxidant defense. *Environmental Toxicology and Pharmacology* (No.4), 141–152. *Environ. Toxicol. Pharmacol.* 10 (4), 141–152. doi:10.1016/s1382-6689(01)00077-1
- Nna, V. U., Ujah, G. A., Mohamed, M., Etim, K. B., Igba, B. O., Augustine, E. R., et al. (2017). Cadmium chloride-induced testicular toxicity in male wistar rats; prophylactic effect of quercetin, and assessment of testicular recovery following cadmium chloride withdrawal. *Biomed. Pharmacother.* 94, 109–123. doi:10.1016/j.biopha.2017.07.087
- Patra, R. C., Rautray, A. K., and Swarup, D. (2011). Oxidative stress in lead and cadmium toxicity and its amelioration. *Vet. Med. Int.* 2011, 457327. doi:10.4061/2011/457327
- Pi, H., Xu, S., Zhang, L., Guo, P., Li, Y., Xie, J., et al. (2013). Dynamin 1-like-dependent mitochondrial fission initiates overactive mitophagy in the hepatotoxicity of cadmium. *Autophagy* 9 (11), 1780–1800. doi:10.4161/aut.25665
- Prabu, S. M., Shagirtha, K., and Renugadevi, J. (2010). Quercetin in combination with vitamins (C and E) improve oxidative stress and hepatic injury in cadmium intoxicated rats. *Biomed. Prev. Nutr.* 14 (11), 1–7. doi:10.1016/j.bionut.2010.12.003
- Sandoval-Acuña, C., Ferreira, J., and Speisky, H. (2014). Polyphenols and mitochondria: An update on their increasingly emerging ROS-scavenging independent actions. *Arch. Biochem. Biophys.* 559, 75–90. doi:10.1016/j.abb.2014.05.017
- Sauvageau, J.-A., and Jumarie, C. (2013). Different mechanisms for metal-induced adaptation to cadmium in the human lung cell lines A549 and H441. *Cell Biology and Toxicology* (No.3), 159–173. *Cell. Biol. Toxicol.* 29 (3), 159–173. doi:10.1007/s10565-013-9243-4
- Vicente-Sánchez, C., Egido, J., Sánchez-González, P. D., Pérez-Barriocanal, F., López-Novoa, J. M., Morales, A. I., et al. (2008). Effect of the flavonoid quercetin on cadmium-induced hepatotoxicity. *Food Chem. Toxicol.* 46 (6), 2279–2287. doi:10.1016/j.fct.2008.03.009
- Wang, C., Nie, G., Yang, F., Chen, J., Zhuang, Y., Dai, X., et al. (2020). Molybdenum and cadmium co-induce oxidative stress and apoptosis through mitochondria-mediated pathway in duck renal tubular epithelial cells. *J. Hazard. Mat.* 383, 121157. doi:10.1016/j.jhazmat.2019.121157
- Wen, S., Wang, L., Zou, H., Gu, J., Song, R., Bian, J., et al. (2021). Puerarin attenuates cadmium-induced neuronal injury via stimulating cadmium excretion, inhibiting oxidative stress and apoptosis. *Biomolecules* 11 (7), 978. doi:10.3390/biom11070978
- Winiarska-Mieczan, A., Krusiński, R., and Kwiecień, M. (2013). Tannic Acid influence on lead and cadmium accumulation in the hearts and lungs of rats. *Adv. Clin. Exp. Med.* 22 (5), 615–620.
- Yang, B., Bai, Y., Yin, C., Qian, H., Xing, G., Wang, S., et al. (2018). Activation of autophagic flux and the Nrf2/ARE signaling pathway by hydrogen sulfide protects against acrylonitrile-induced neurotoxicity in primary rat astrocytes. *Arch. Toxicol.* 92 (6), 2093–2108. doi:10.1007/s00204-018-2208-x
- Yang, S. H., Li, P., Yu, L. H., Li, L., Long, M., Liu, M. D., et al. (2019). Sulforaphane protect against cadmium-induced oxidative damage in mouse leydigs cells by activating Nrf2/ARE signaling pathway. *Int. J. Mol. Sci.* 20 (3), 630. doi:10.3390/ijms20030630
- Yin, J., Wang, A., Li, W., Shi, R., Jin, H., Wei, J., et al. (2018). Time-response characteristic and potential biomarker identification of heavy metal induced toxicity in zebrafish. *Fish. Shellfish Immunol.* 72, 309–317. doi:10.1016/j.fsi.2017.10.047

Yuan, Y., Ma, S., Qi, Y., Wei, X., Cai, H., Dong, L., et al. (2016). Quercetin inhibited cadmium-induced autophagy in the mouse kidney via inhibition of oxidative stress. *J. Toxicol. Pathol.* 29 (4), 247–252. doi:10.1293/tox.2016-0026

Zhang, C., Lin, J., Ge, J., Wang, L. L., Li, N., Sun, X. T., et al. (2017). Selenium triggers Nrf2-mediated protection against cadmium-induced chicken hepatocyte autophagy and apoptosis. *Toxicol. Vitro* 44, 349–356. doi:10.1016/j.tiv.2017.07.027

Zhang, H., and Reynolds, M. (2019). Cadmium exposure in living organisms: A short review. *Sci. Total Environ.* 678, 761–767. doi:10.1016/j.scitotenv.2019.04.395

Zhao, Y., Li, Z. F., Zhang, D., Wang, Z. Y., and Wang, L. (2021). Quercetin alleviates Cadmium-induced autophagy inhibition via TFEB-dependent lysosomal restoration in primary proximal tubular cells. *Ecotoxicol. Environ. Saf.* 208, 111743. doi:10.1016/j.ecoenv.2020.111743



## OPEN ACCESS

## EDITED BY

Xu Yang,  
Henan Agricultural University, China

## REVIEWED BY

Zhang Caiying,  
Jiangxi Agricultural University, China  
Wenda Wu,  
Nanjing Agricultural University, China  
Jin-Long Li,  
Northeast Agricultural University, China

## \*CORRESPONDENCE

Jicang Wang,  
wangjicang@126.com

## SPECIALTY SECTION

This article was submitted to Predictive Toxicology, a section of the journal Frontiers in Pharmacology

RECEIVED 11 July 2022

ACCEPTED 25 July 2022

PUBLISHED 16 August 2022

## CITATION

Huang R, Ding L, Ye Y, Wang K, Yu W, Yan B, Liu Z and Wang J (2022), Protective effect of quercetin on cadmium-induced renal apoptosis through cyt-c/caspase-9/caspase-3 signaling pathway. *Front. Pharmacol.* 13:990993. doi: 10.3389/fphar.2022.990993

## COPYRIGHT

© 2022 Huang, Ding, Ye, Wang, Yu, Yan, Liu and Wang. This is an open-access article distributed under the terms of the [Creative Commons Attribution License \(CC BY\)](https://creativecommons.org/licenses/by/4.0/). The use, distribution or reproduction in other forums is permitted, provided the original author(s) and the copyright owner(s) are credited and that the original publication in this journal is cited, in accordance with accepted academic practice. No use, distribution or reproduction is permitted which does not comply with these terms.

# Protective effect of quercetin on cadmium-induced renal apoptosis through cyt-c/caspase-9/caspase-3 signaling pathway

Ruxue Huang<sup>1</sup>, Lulu Ding<sup>1</sup>, Ying Ye<sup>1</sup>, Ke Wang<sup>1</sup>, Wenjing Yu<sup>1</sup>, Bingzhao Yan<sup>1</sup>, Zongping Liu<sup>2</sup> and Jicang Wang<sup>1\*</sup>

<sup>1</sup>College of Animal Science and Technology, Henan University of Science and Technology, Luoyang, China, <sup>2</sup>College of Veterinary Medicine, Yangzhou University, Yangzhou, China

Cadmium (Cd), a heavy metal, has harmful effects on animal and human health, and it can also obviously induce cell apoptosis. Quercetin (Que) is a flavonoid compound with antioxidant and other biological activities. To investigate the protective effect of Que on Cd-induced renal apoptosis in rats. 24 male SD rats were randomly divided into four groups. They were treated as follows: control group was administered orally with normal saline (10 ml/kg); Cd group was injected with 2 mg/kg CdCl<sub>2</sub> intraperitoneally; Cd + Que group was injected with 2 mg/kg CdCl<sub>2</sub> and intragastric administration of Que (100 mg/kg); Que group was administered orally with Que (100 mg/kg). The experimental results showed that the body weight of Cd-exposed rats significantly decreased and the kidney coefficient increased. In addition, Cd significantly increased the contents of Blood Urea Nitrogen, Creatinine and Uric acid. Cd also increased the glutathione and malondialdehyde contents in renal tissues. The pathological section showed that Cd can cause pathological damages such as narrow lumen and renal interstitial congestion. Cd-induced apoptosis of kidney, which could activate the mRNA and protein expression levels of Cyt-c, Caspase-9 and Caspase-3 were significantly increased. Conversely, Que significantly reduces kidney damage caused by Cd. Kidney pathological damage was alleviated by Que. Que inhibited Cd-induced apoptosis and decreased Cyt-c, Caspase-9 and Caspase-3 proteins and mRNA expression levels. To sum up, Cd can induce kidney injury and apoptosis of renal cells, while Que can reduce Cd-induced kidney damage by reducing oxidative stress and inhibiting apoptosis. These results provide a theoretical basis for the clinical application of Que in the prevention and treatment of cadmium poisoning.

## KEYWORDS

cadmium, kidney injury, apoptosis, quercetin, oxidative stress

## Introduction

Cadmium (Cd) is a silver-white heavy metal that is widespread in the environment. Cd pollution has the characteristics of a long half-life and long-lasting toxicity (Wang J. et al., 2020). Food and drinking water can cause the accumulation of Cd in the body. Cd has serious toxic effects on various tissues and organs of the body. For example, Cd has a toxic effect on the liver, kidney, bone, cardiovascular and reproductive system of mammals through bioaccumulation (Kazantzis, 2004; Varoni et al., 2017; Kim et al., 2018; Pérez Díaz et al., 2019; Zhu et al., 2019). The kidney is the primary organ in the body where Cd accumulates. In 1948, FRIBERG first reported the damage of Cd to the kidneys (Friberg, 1948). Cd exposure causes renal tubular reabsorption disorder (Gu et al., 2020). Cd leads to reactive oxygen species (ROS) to be accumulated in cells and damages the mitochondrial membrane potential (MMP) (Umar Ijaz et al., 2021). Cd exposure causes damage to mitochondria and ultimately induces apoptosis (Dong F. et al., 2021).

Quercetin (Que) is a flavonoid compound, found in a variety of plants, fruits, Chinese medicine and vegetables. A wide number of research have demonstrated that the most important biological function of Que is antioxidant. Que has a strong anti-tumor effect, which exerts anti-cancer functions through cell signal transduction pathways such as anti-oxidation, anti-proliferation and promotion of apoptosis (Zhou et al., 2016; Carrasco-Torres et al., 2017; Chen et al., 2018). The effects of carcinogens and mutagenic agents are inhibited, and the reproduction of malignant tumor cells is hindered. Que can eliminate DPPH, ·OH and ABTS<sup>+</sup> *in vitro*, and inhibit lipid peroxidation in organs. Que can improve the body's immunity and maintain the normal progress of various functions. Que has a protective effect on apoptosis (Feng et al., 2019).

Apoptosis is a self-destructive mechanism that exists in cells. However, excessive apoptosis can have detrimental effects on the body. Cd-induced apoptosis is mediated by mitochondria, apoptotic molecules will be released due to the increased permeability of the outer mitochondrial membrane, leading to apoptosis (Bauer and Murphy, 2020). Caspase-9 protein complex activates caspase-9, caspase-9 activates downstream caspase, such as caspase-3, which induces apoptosis (Choe et al., 2015). Previous studies have suggested that apoptosis pathways may be functionally involved in kidney injury. However, the specific signaling mechanism of apoptosis in Cd-induced nephrotoxicity is still unclear and needs further study.

In this work, we investigated the role of apoptosis in Cd-induced kidney damage in rats. Additionally, we addressed the protected effect of Que against Cd-induced kidney injury.

## Materials and methods

### Reagents

Uric acid (UA, C012-2-1), Creatinine (CRE, C011-2-1), Blood Urea Nitrogen (BUN, C013-2-1), Reduced glutathione (GSH, A006-2-1) and Malondialdehyde (MDA, A003-1-2) assay kits were from Jiancheng Bioengineering Institute (Nanjing, China). Anhydrous CdCl<sub>2</sub> (purity: >99.95%) was from Aladdin Industrial Corporation. Que (purity: > 97%) was from RHAWN (Shanghai, China). RNA isolater Total RNA Extraction Reagent (R401-01), HiScript III RT SuperMix for qPCR (+gDNA wiper, R323-01), and ChamQ universal SYBR qPCR Master Mix (Q711-02) were from novozan Biotechnology (Nanjing, China). β-Actin and antibodies against Caspase-3, Caspase-9 and Cyt-c were from Servicebio (Wuhan, China). BeyoECL Star was from Beyotime Biotechnology (P0018AM, Shanghai, China). All other routine chemicals and solvents were of pure analytical grade.

### Animal experiments

Twenty-four 5-week-old male SD rats were adaptively reared for 1 week with adequate feed and drinking water. They were put into four groups at random, each with six rats weighing around 150 ± 5 g. A 12-h light/dark cycle was set. All animal experimental processes were approved by the Institute of Zoology and Medical Ethics Committee of Henan University of Science and Technology and they were strictly designed under the consideration of animal welfare (approval number HAUST 20015).

The experiment was carried out for 3 weeks. The body weight of rats was recorded every week, and they were treated as follows. The control group was given normal saline (10 ml/kg) every day. The Cd-treated group was injected with 2 mg/kg CdCl<sub>2</sub> intraperitoneally. The Cd + Que group received 2 mg/kg CdCl<sub>2</sub> by intraperitoneal injection and 100 mg/kg Que intragastrically. Que treatment group was administered orally with Que (100 mg/kg). The doses of Cd and Que were chosen based on previous studies (Yang S. H. et al., 2019; Liang et al., 2020). After 3 weeks, the rats were anaesthetized with ether and sacrificed. Kidneys were collected for further investigation.

### Weight and kidney coefficient determination

The rats' body weight was measured every weekend. The effects of Cd and Que on the rat's body weight were analyzed. The kidney of the rat was removed. The blood on the kidney surface was washed with saline. The excess water on the kidney was

wiped clean, and the weight was weighed. The organ coefficient was calculated.

## Measure kidney function

Collected rat venous blood and left for a period of time, centrifuged 3000 r/min for 10 min, the serum was aspirated. The manufacturer's guidelines were followed while measuring UA, CRE and BUN in rat serum using diagnostic kits. These results were measured spectrophotometrically.

## Measure antioxidant index

0.4 g kidney tissues were cut, grind on the ice at a ratio of kidney tissue (g): saline (ml) = 1:9, and centrifuged (3,000 rpm for 10 min) the supernatant was obtained. The contents of MDA and GSH in rat kidney tissues were assessed using diagnostic kits according to the manufacturer's instructions. These results were measured spectrophotometrically.

## Histopathological studies

The fresh, morphological and structurally intact kidney tissues were fixed in 10% formalin for 48 h. Then rinsed with running water overnight and dehydrated with different concentrations of ethanol, transparent in xylene and embedded in paraffin. The paraffin blocks were cut with a microtome to a thickness of 5  $\mu\text{m}$ . The kidney sections were stained with hematoxylin-eosin and mounted for microscope observation.

## TdT-UTP nick end labeling (TUNEL)

The prepared paraffin sections were washed twice with xylene and then dipped in graded ethanol. After washing with PBS, proteinase K solution was added to hydrolyze for 15 min at room temperature to remove tissue proteins. Wash with distilled water, add 0.1% triton dropwise to cover the tissue. Washed with PBS, incubated with buffer. TDT enzyme, dUTP, and buffer were mixed according to the instructions of the TUNEL kit, the tissue was then covered and incubated at 37 °C for 2 h. Drop by drop, DAPI staining solution was applied and incubated in the dark for 10 min. The sections were washed in PBS and mounted with anti-fluorescence quenching mounting media. A fluorescent microscope was used to examine the sections, and photographs were taken.

## Real-time PCR (RT-PCR)

Total RNA Extraction reagent was used to extract total RNA from rat kidney tissue and the total RNA concentration and purity were measured by a nucleic acid protein analyzer. The mRNA was reverse transcribed to synthesize cDNA. The primers were designed using Primer Premier 6 (Table 1). The instructions in the ChamQ universal SYBR qPCR Master Mix Kit for RT-PCR were followed.  $\beta$ -Actin was used as a control. The expression level of mRNA was analyzed using the  $2^{-\Delta\Delta\text{CT}}$ .

## Western blotting

Prepare suitable concentration of separating gel and 5% stacking gel. Electrophoresis after adding protein samples, and transferred onto PVDF membranes. Skim milk was used to seal the membranes for 2 h. The membranes were incubated with proportionally diluted caspase-9 (1:3000), caspase-3 (1:3000) and Cyt-c (1:2000) antibodies for 12 h at 4°C. As a loading control,  $\beta$ -Actin was used. After washing thrice with TBST, the membranes were incubated with secondary antibody for 2 h. The ECL chromogenic solution was uniformly put over the membrane after three TBST washes and incubated for 60 s. The membranes detected signals by the gel imaging equipment. Photos were taken for subsequent analysis.

## Statistical analysis

The result was expressed in the form of mean  $\pm$  SEM. SPSS22.0 was used for statistical analysis. ANOVA was used to analyze the differences between multiple groups. LSD or Tamhane's T2 method was used following the homogeneity test of variance. When  $p < 0.05$  or  $p < 0.01$ , the difference is statistically significant.

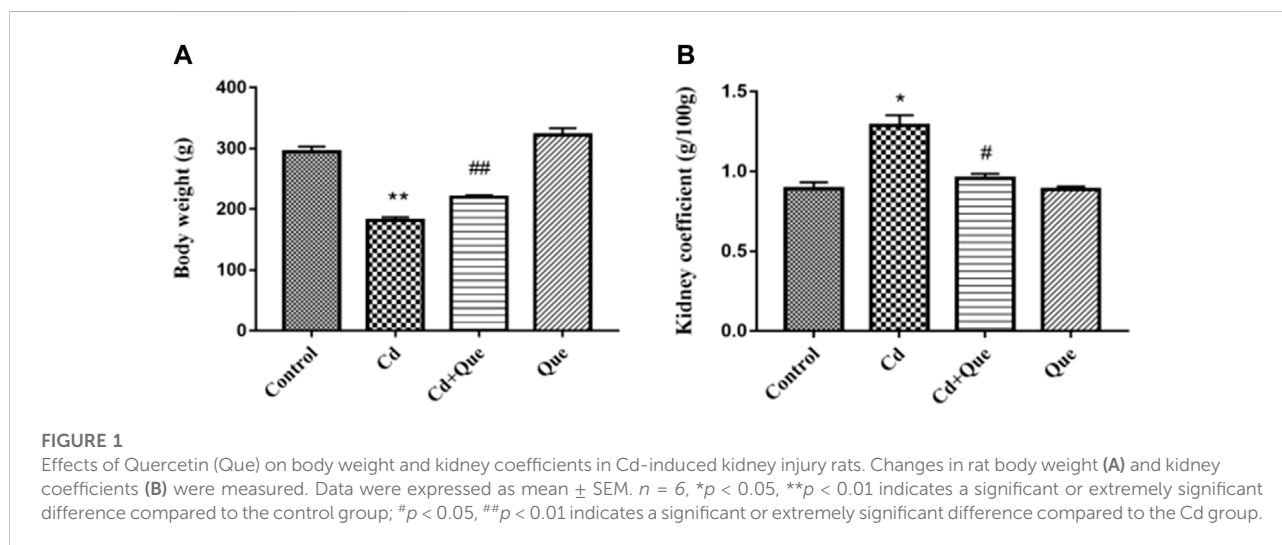
## Result

### Effect of Que on Cd-induced changes in body weight and kidney coefficient

The body weight and kidney coefficient of rats in each group were compared. Results showed that Cd decreased the rat body weight and increased the renal coefficient. As presented in Figures 1A,B, compared with the control group, the body weight of the rats in the Cd group decreased by 61.5% ( $p < 0.01$ ). The kidney coefficient in Cd-treated was 144% higher than that of the control ( $p < 0.05$ ). Compared with the Cd group, the body weight of the rats in Cd + Que-treated group increased by 121% ( $p < 0.01$ ) and the kidney coefficient decreased by 73.8% ( $p < 0.05$ ).

TABLE 1 Primer sequences of real-time PCR target genes.

Target gene	Primers sequences (5' → 3')	Products	Genbank no.
<i>Caspase-9</i>	F:CTGAGCCAGATGCTGTCCCATA R:CCAAGGTCTCGATGTACCAGGAA	106bp	NM_031632.2
<i>Caspase-3</i>	F:GCAGCAGCCTCAAATTGTTGACTA R:TGCTCCGGCTCAAACCATC	156bp	NM_012922.2
<i>Cyt-c</i>	F:GGAGAGGATACCCTGATGGA R:GTCTGCCCTTTCTCCCTTCT	130bp	NM_012839.2
<i>β-Actin</i>	F:AGGAAATCGTGCGTGACAT R:CCTCGGGGCATCGGAA	168bp	NM_031144.3



## Cd causes kidney damage and Que reduces kidney damage

Renal function related indicators were measured. As shown in Figures 2A,C, compared with the control group, the contents of BUN, CRE and UA in the serum of the rats in the Cd group were significantly increased ( $p < 0.01$ ). BUN, CRE and UA content increased by 149%, 265% and 137%, respectively. However, the contents of BUN and UA in the Cd + Que-treated were lower than those of the Cd-treated group by 78.9% and 84.7% ( $p < 0.05$ ). Also, the CRE content decreased by 63.7% ( $p < 0.01$ ). The difference between the control and Que groups was not significant.

## Effects of Cd and Que on the contents of GSH and MDA in rat kidney tissues

Cd induces oxidative damage to the kidney and lipid peroxidation. Que can weaken the kidney damage. As

presented in Figures 3A,B, the contents of GSH and MDA in the renal tissues increased by 170% and 162% in Cd-treated group compared with the control group. The contents of GSH and MDA in the Cd + Que-treated group decreased by 86.9% and 57.4% compared with the Cd-treated group ( $p < 0.05$ ).

## Observation of renal tissue pathological section

The size and shape of the glomeruli in the control group were normal with clear borders (Figures 4A,B). In the Cd group (Figures 4C,D), the renal tubular lumen was blocked, the renal tubules were dilated, the renal tubular epithelial cells were necrotic and fell into the lumen, the renal interstitium was congested, and the glomerular cyst cavity became obvious pathological changes. In the Cd and Que co-treatment group (Figure 4E and F), the size and shape of the

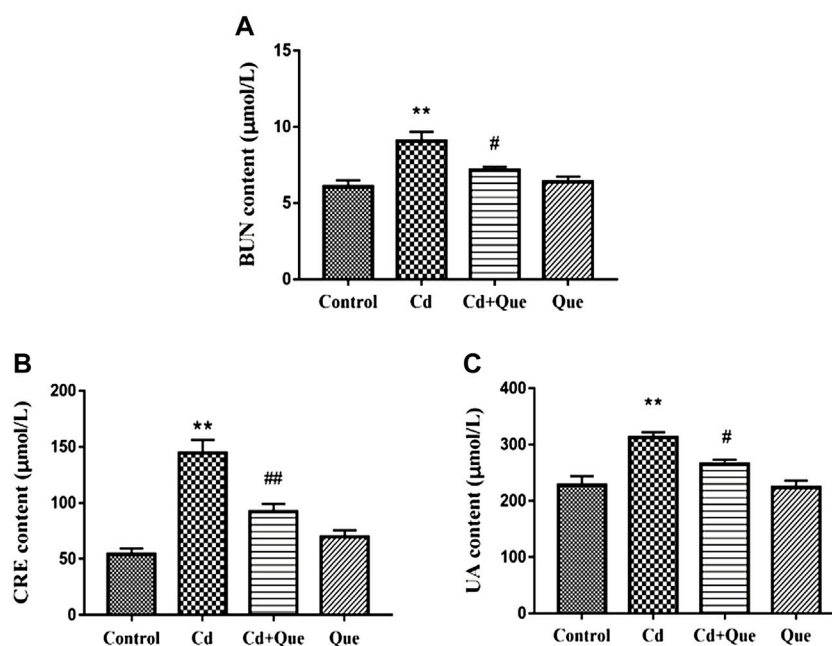


FIGURE 2

Effects of Quercetin (Que) on renal function in Cd-induced kidney injury rats. The content of BUN in serum (A), the content of CRE in serum (B) and the content of UA in serum (C) were measured. Data were expressed as mean  $\pm$  SEM.  $n = 6$ , \* $p = 0.05$ , \*\* $p = 0.01$  indicates a significant or extremely significant difference compared to the control group; # $p = 0.05$ , ## $p = 0.01$  indicates a significant or extremely significant difference compared to the Cd group.

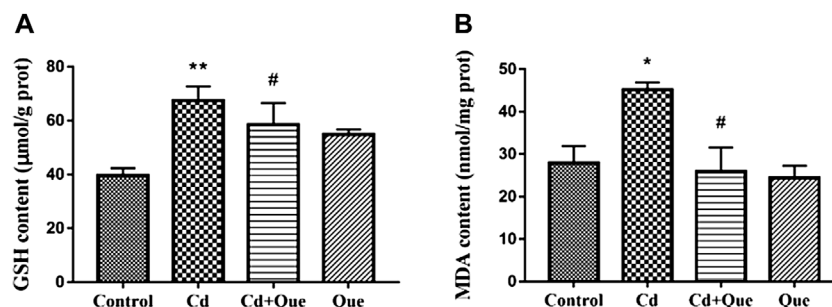


FIGURE 3

Effects of Quercetin (Que) on oxidative stress in Cd-induced kidney injury rats. The activity of GSH (A) and the content of MDA (B) in rats' kidney tissues were measured. Data were expressed as mean  $\pm$  SEM.  $n = 6$ , \* $p < 0.05$ , \*\* $p < 0.01$  indicates a significant or extremely significant difference compared to the control group; # $p < 0.05$ , ## $p < 0.01$  indicates a significant or extremely significant difference compared to the Cd group.

glomerulus return to normal, some of the cysts became smaller and adhered to the glomerulus, the tubular lumen was narrowed, and some tubular epithelial cells swelled and fell off into the lumen. The degree of damage was relieved compared with the Cd group. In the Que group (Figure 4G and H), the morphology and structure of the glomeruli were normal, with clear borders and no pathological changes.

## Effects of Cd and Que on apoptosis of rat kidney cells

The number of TUNEL apoptotic cells in Cd-treated kidney tissue (Figure 5B) was considerably higher than in the control group (Figure 5A), an increased of 267%. The ratio of TUNEL apoptotic cells in kidney tissue co-treated

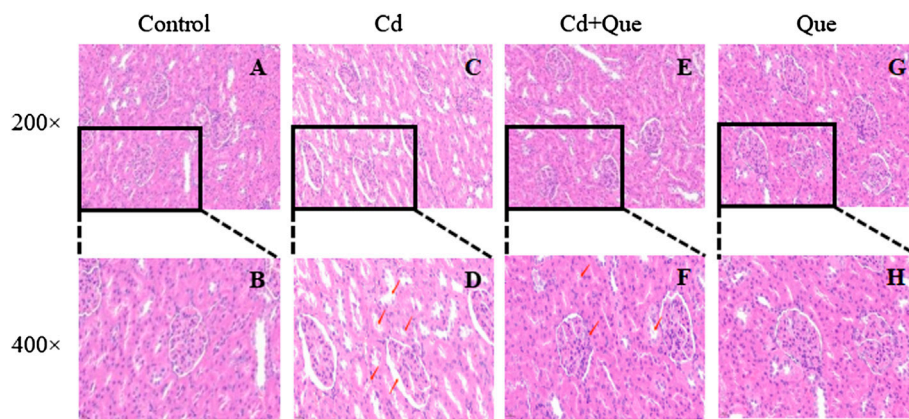


**FIGURE 4** Effects of Quercetin (Que) on histopathological changes in kidney tissues in Cd-induced kidney injury rats. Representative H&E sections of the kidney. **(A)** control 200x **(B)** control 400x **(C)** Cd, 2 mg/kg b.w. 200x **(D)** Cd, 2 mg/kg b.w. 400x **(E)** Cd, 2 mg/kg b.w. + Que, 100 mg/kg, 200x **(F)** Cd, 2 mg/kg b.w. + Que, 100 mg/kg, 400x **(G)** Que, 100 mg/kg, 200x **(H)** Que, 100 mg/kg, 400x.

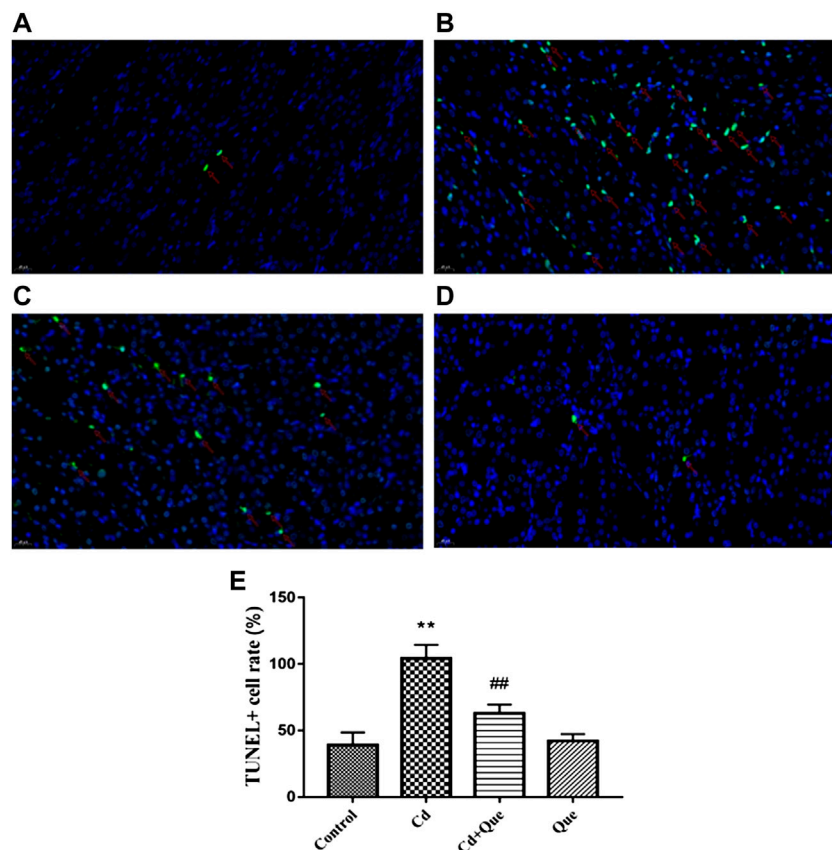


**FIGURE 5** Effects of Quercetin (Que) on the rate of TUNEL-positive apoptosis in Cd-induced kidney injury rats. **(A)** TUNEL-positive cells in the control group 400x. **(B)** TUNEL-positive cells in the Cd-treated group 400x. **(C)** TUNEL-positive cells in the Cd + Que-treated group 400x. **(D)** TUNEL-positive cells in the Que-treated group 400x. The green particles are apoptotic cells, and the blue particles are normal or proliferating cells. **(E)** The percentage of TUNEL-positive cells in control and Cd groups within or without Que using TUNEL staining. Data were expressed as mean  $\pm$  SEM.  $n = 3$ , \*\* $p < 0.01$  indicates extremely significant difference compared to the control group; ## $p < 0.01$  indicates extremely significant difference compared to the Cd group.

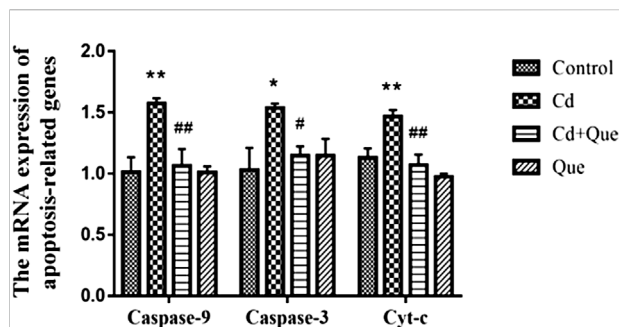


**FIGURE 6**  
Effects of Quercetin (Que) on mRNA expression of apoptosis-related genes in Cd-induced kidney injury rats. The mRNA expression of Caspase-9, Caspase-3 and Cyt-c in kidney tissue was reduced by Que. Data were expressed as mean ± SEM. *n* = 3, \**p* < 0.05, \*\**p* < 0.01 indicates a significant or extremely significant difference compared to the control group; #*p* < 0.05, ##*p* < 0.01 indicates a significant or extremely significant difference compared to the Cd group.

significantly between the control and Que groups (Figure 5A and D).

### Effects of Cd and Que on mRNA expression of apoptosis-related gene

The RT-PCR results showed that Cd exposure led to 130%, 155% and 149% increases in Cyt-c, Caspase-9 and Caspase-3 mRNA expression in kidney tissue, respectively. However, the intervention of Que significantly (*p* < 0.05) or extremely significantly (*p* < 0.01) decreased Cd-induced Cyt-c, Caspase-9 and Caspase-3 mRNA expression levels (Figure 6) by 73%, 67.6% and 74.6%.

### Cd induces apoptosis of kidney tissues and Que inhibits Cd-triggered apoptosis

The research showed that Cd exposure obviously enhanced the level of Cyt-c, Caspase-9 and -3 proteins in rats' kidney tissue (Figure 7). Compared with the control group, the increase was 413%, 162% and 185%. Compared with Cd-treated group, the

with Que and Cd (Figure 5C) was lower than that in Cd-treated kidney cells, an decreased 60.4%. The number of TUNEL apoptotic cells in renal tissue did not differ

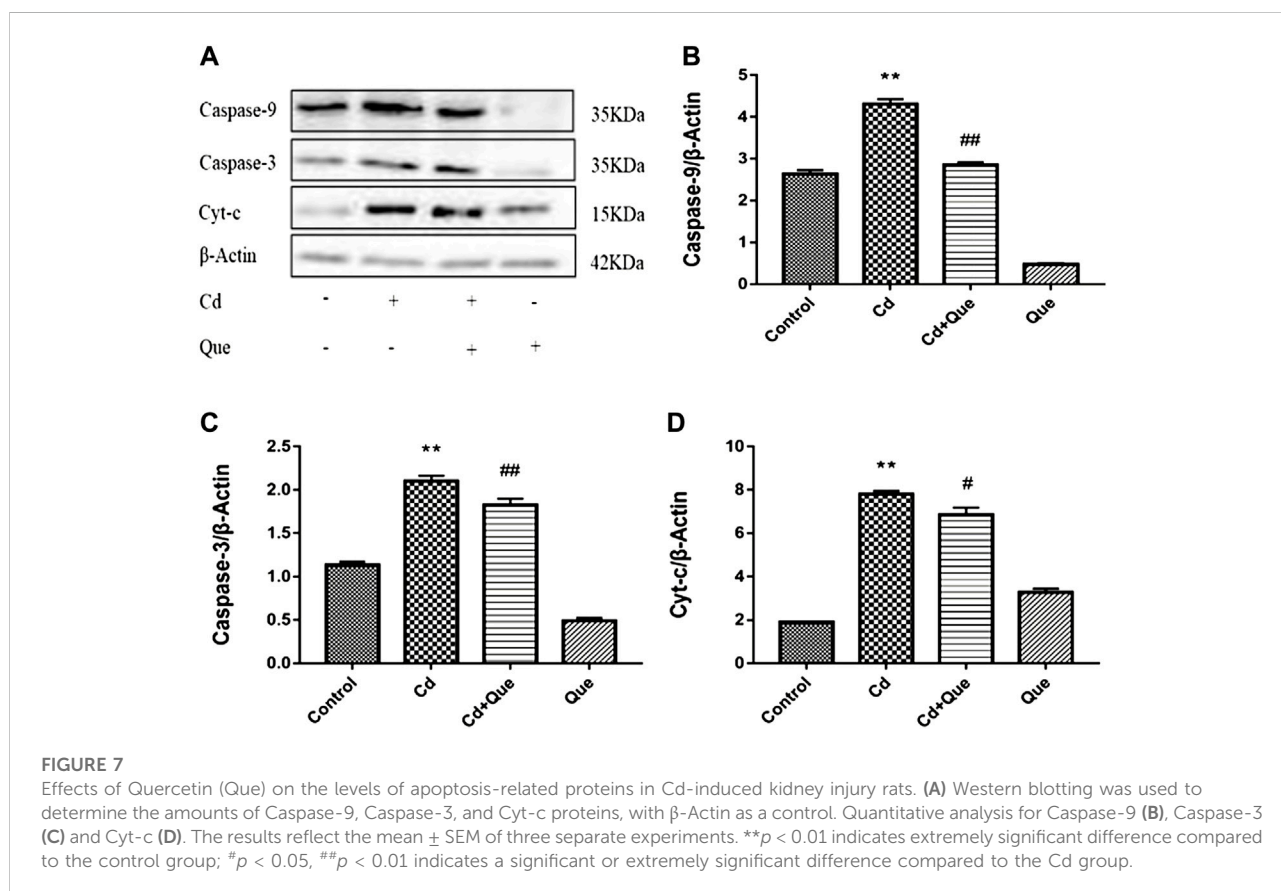


**FIGURE 7**  
Effects of Quercetin (Que) on the levels of apoptosis-related proteins in Cd-induced kidney injury rats. (A) Western blotting was used to determine the amounts of Caspase-9, Caspase-3, and Cyt-c proteins, with β-Actin as a control. Quantitative analysis for Caspase-9 (B), Caspase-3 (C) and Cyt-c (D). The results reflect the mean ± SEM of three separate experiments. \*\**p* < 0.01 indicates extremely significant difference compared to the control group; #*p* < 0.05, ##*p* < 0.01 indicates a significant or extremely significant difference compared to the Cd group.

expression levels of Caspase-9 and -3 proteins reduced by 66.3 and 87% in Cd + Que-treated group ( $p < 0.01$ ). The protein expression of Cyt-c decreased by 88% ( $p < 0.05$ ).

## Discussion

In this study, we explored the role of apoptosis in kidney injury induced by Cd and the protective effect of quercetin. The damage mechanism of Cd to tissues is very complicated. Numerous studies have shown that Cd leads to kidney cell apoptosis, which mainly occurs through mitochondria-mediated signaling pathways (Indran et al., 2011). However, the detailed apoptotic signal of Cd-induced apoptosis in rat kidney cells is still unclear. Que has biological functions, such as anti-cancer, anti-inflammatory and anti-oxidant (Li et al., 2016), but the protective mechanism against Cd nephrotoxicity is still unclear.

Body weight reflects animal's health status and absorption of nutrients, the decline in the rat's health status is reflected by weight loss (Bhattacharya and Haldar, 2012). Consistent with the results of previous studies (Wang et al., 2021), the changes in rat body weight in this experiment showed that the heavy metal Cd hindered the growth of rats, while Que alleviates the toxicity of Cd in rats. The growth inhibition of rats may be due to the insufficient digestion and absorption of nutrients in intestinal mucosa caused by Cd (Eriyamremu et al., 2005). The kidney coefficient is used as a necessary test item for toxicology research. Increased organ coefficients indicate organ congestion and edema, and decreased organ coefficients indicate organ atrophy and other degenerative changes. Studies have shown that long-term exposure to 10 mg/kg of Cd increased liver and spleen weight (Tu et al., 2007). Here, we observed that kidney coefficients were increased by Cd, and Que antagonized the increase in kidney weight caused by Cd.

UA is the metabolic end product formed by the decomposition of nucleic acid into purine and then oxidized in the liver. Hypertension, obesity and renal disease can manifest as elevated UA (So and Thorens, 2010). UA can cause hippocampal inflammation, leading to cognitive dysfunction (Shao et al., 2016). CRE is the metabolite of muscle. Elevated serum CRE was found only in severely damaged kidneys (Stark, 1980). The end product of protein metabolism is BUN. Once the kidney is damaged, the glomerular filtration rate will decrease, resulting in increased BUN levels (Lee et al., 2006). Elevated serum levels of UA, CRE and BUN were associated with Cd-induced kidney damage. The amount they excrete is closely related to glomerular filtration and renal tubular reabsorption (Macedo, 2011). Luo et al. found that Cd exposure raised the serum CRE and BUN at 1 mg/kg, suggesting kidney filtration failure (Luo et al., 2016). The study by Iserhienrhien et al. also confirmed the damage of Cd exposure on rat renal function (Iserhienrhien and Okolie, 2022). Consistent with the research

results of the above scholars, Cd increases the content of kidney function-related indicators, leading to renal function damage. The index of the co-treatment group decreased, which proved that Que can reduce the renal function damage caused by Cd.

Cd causes increased levels of free radicals in cells, which ultimately cause tissue damage (Skipper et al., 2016). Cd induces a large number of reactive oxygen species (ROS) in mitochondria by inhibiting cellular respiration (Wang et al., 2004). ROS causes cellular oxidative damage (Zhu et al., 2016; Vodošek Hojs et al., 2020). GSH has the capability to remove heavy metal Cd or ROS. Loss of reducibility by GSH after binding to Cd cannot scavenge ROS, which accumulates in large amounts *in vivo* and leads to oxidative damage (Hart et al., 2001). Some studies have shown that Cd pollution increased GSH levels (Maity et al., 2018; Dong A. et al., 2021). GSH levels in Cd-treated rats were greater than in control rats in the current study. However, some reports indicated that Cd exposure significantly reduced GSH levels, which is inconsistent with some research findings (Jihen el et al., 2010; Renugadevi and Prabu, 2010; Owumi et al., 2019). The reason may be that after Cd enters the body, in order to resist the oxidative damage caused by stress, a large amount of GSH is produced in the body through chelation to remove free Cd<sup>2+</sup>. In addition, the difference may also be related to factors such as dosage, duration of exposure, and age of animals. Oxidative stress causes lipid peroxidation in animal and plant cells. MDA is a natural product of lipid oxidation and is considered to be one of the biomarkers of oxidative stress (Zhang et al., 2014). Zhang et al. demonstrated that Cd increased MDA content by disrupting the antioxidant system of shrimp (Zhang et al., 2021). The results of Messaoudi et al. showed that the MDA concentration increased in rat kidney tissue of Cd-treated (Messaoudi et al., 2009). The current investigation found that the content of MDA in the kidney tissue of the Cd group was higher than that of the control group. Further results showed that Cd promoted lipid oxidation in kidney cells. This is consistent with the previous findings of our group (Wang et al., 2014). However, studies have shown that Que can alleviate cadmium-induced kidney damage by reducing cell membrane lipid peroxidation and enhancing total antioxidant capacity (Yuan et al., 2016). In the HepG2 cell model, Que eliminated lipid droplets and reduced total cholesterol and triglyceride levels, suggesting that Que can restore NAFLD by reducing oxidative stress and improving lipid metabolism (Yang H. et al., 2019). GSH and MDA levels in the Cd + Que-treated group were significantly lower than in the Cd-treated group. We found that Que reduced the oxidative damage and intracellular lipid oxidation induced by Cd, and exerted a protective effect on rat kidney tissue.

Histopathological changes could directly reflect the damage to kidney tissue. Cd caused significant histomorphological changes in the kidney, a similar phenomenon was also observed by Owumi et al. (Owumi et al., 2019). It is speculated that it may be related to the excessive

accumulation of free radicals in the body caused by Cd exposure (Jihen et al., 2009). Cd could regulate the body's enzymatic activity to induce the accumulation of ROS (Zhong et al., 2015), leading to oxidative damage (Zhu et al., 2020), which in turn leads to pathological changes in the morphological structure of kidney tissue. Que is an effective scavenger of ROS and RNS. It has been reported that Que can scavenge ROS directly *in vitro* when the concentration of Que is in the range of 5–50  $\mu\text{M}$  (Saw et al., 2014). In addition, Que can also downregulate ROS-induced oxidative stress by modulating signaling pathways (Veith et al., 2017). In this study, pathological sections showed that Cd caused severe damage to renal tissue, such as Enlarged glomerular cavity, tubular lumen obstruction and renal interstitial congestion. Nonetheless, Que attenuated Cd-induced renal lesions.

Cd causes apoptosis *in vivo* and *in vitro*, according to numerous studies (El-Baz et al., 2015; Dai et al., 2018; Wang C. et al., 2020). Consistent with previous studies, we also proved that Cd triggered caspase-dependent apoptosis in kidney cells. However, whether Que could inhibit Cd-induced apoptosis in renal tissue remains unclear. Mitochondria release cytochrome c (Cyt-c) via increased Bax levels (Song et al., 2016). Cyt-c is a sign of apoptosis (Zhang et al., 2017). And caspase-9 is activated. The current study found that activation of Caspase-9, an important indicator of apoptosis induced by the mitochondrial pathway, contributed to Cd-induced apoptosis in kidney cells (Choe et al., 2015). Caspase-9 is the initiator of the protease cascade. Activation of Caspase-3 is an important sign of apoptosis and Caspase-3 acts as the executor to induce apoptosis (Wasilewski and Scorrano, 2009). TUNEL-positive cells were found in larger numbers in the Cd-treated kidney than in the controls in this investigation. The rate of TUNEL-positive cells was significantly reduced under the intervention of Que. Cd exposure significantly increased the mRNA expressions of Cyt-c, Caspase-9 and Caspase-3 in kidney tissue, while those in the Que-treated group were significantly decreased compared with those in the Cd group. Consistent with the above results, Cd exposure obviously enhanced the level of Cyt-c, Caspase-9 and -3 proteins in rats' kidney tissue. However, Cd-induced apoptosis was inhibited by Que. Overall, Cd triggers apoptosis in kidney cells, at least through the caspase-9-dependent mitochondrial signaling pathway. Que interferes with renal cell apoptosis induced by Cd and has a protective effect on rats' kidney.

In summary, Cd decreases the body weight of rats, increases the renal coefficient, damages kidney function, causes oxidative stress, promotes cell lipid oxidation, and ultimately leads to apoptosis in kidney cells. Reversely, Que alleviated these changes, which has a protective effect against Cd-induced damage on rats' kidney and inhibited apoptosis. To offer a theoretical foundation for the use of quercetin in the treatment of cadmium poisoning.

## Data availability statement

The original contributions presented in the study are included in the article/Supplementary Material, further inquiries can be directed to the corresponding author.

## Ethics statement

All animal experimental processes were approved by the Institute of Zoology and Medical Ethics Committee of Henan University of Science and Technology.

## Author contributions

RH: Conceptualization, Writing-Original Draft, Formal analysis, Data Curation. LD: Methodology, Resources. YY: Data Curation, Formal analysis. KW: Conceptualization, Formal analysis. WY: Data Curation, Formal analysis. BY: Data Curation. ZL: Resources, Validation, Formal analysis. JW: Conceptualization, Project administration, Review, Editing, Funding acquisition.

## Funding

This study was supported by funds from the National Natural Science Foundation of China (No. 31972753), Henan science and technology research project (222102110340).

## Conflict of interest

The authors declare that the research was conducted in the absence of any commercial or financial relationships that could be construed as a potential conflict of interest.

## Publisher's note

All claims expressed in this article are solely those of the authors and do not necessarily represent those of their affiliated organizations, or those of the publisher, the editors and the reviewers. Any product that may be evaluated in this article, or claim that may be made by its manufacturer, is not guaranteed or endorsed by the publisher.

## Supplementary material

The Supplementary Material for this article can be found online at: <https://www.frontiersin.org/articles/10.3389/fphar.2022.990993/full#supplementary-material>

## References

- Bauer, T. M., and Murphy, E. (2020). Role of mitochondrial calcium and the permeability transition pore in regulating cell death. *Circ. Res.* 126 (2), 280–293. doi:10.1161/CIRCRESAHA.119.316306
- Bhattacharya, S., and Haldar, P. K. (2012). Trichosanthes dioica fruit ameliorates experimentally induced arsenic toxicity in male albino rats through the alleviation of oxidative stress. *Biol. Trace Elem. Res.* 148 (2), 232–241. doi:10.1007/s12011-012-9363-3
- Carrasco-Torres, G., Monroy-Ramírez, H. C., Martínez-Guerra, A. A., Baltiérrez-Hoyos, R., Romero-Tlalolini, M., Villa-Treviño, S., et al. (2017). Quercetin reverses rat liver preneoplastic lesions induced by chemical carcinogenesis. *Oxid. Med. Cell. Longev.* 2017, 4674918. doi:10.1155/2017/4674918
- Chen, H. H., Chen, S. P., Zheng, Q. L., Nie, S. P., Li, W. J., Hu, X. J., et al. (2018). Genistein promotes proliferation of human cervical cancer cells through estrogen receptor-mediated PI3K/Akt-NF- $\kappa$ B pathway. *J. Cancer* 9 (2), 288–295. doi:10.7150/jca.20499
- Choe, J. Y., Park, K. Y., and Kim, S. K. (2015). Oxidative stress by monosodium urate crystals promotes renal cell apoptosis through mitochondrial caspase-dependent pathway in human embryonic kidney 293 cells: Mechanism for urate-induced nephropathy. *Apoptosis* 20 (1), 38–49. doi:10.1007/s10495-014-1057-1
- Dai, X., Xing, C., Cao, H., Luo, J., Wang, T., Liu, P., et al. (2018). Alterations of mitochondrial antioxidant indexes and apoptosis in duck livers caused by Molybdenum or/and cadmium. *Chemosphere* 193, 574–580. doi:10.1016/j.chemosphere.2017.11.063
- Dong, A., Huo, J., Yan, J., and Dong, A. (2021a). Oxidative stress in liver of turtle *Mauremys reevesii* caused by cadmium. *Environ. Sci. Pollut. Res. Int.* 28 (6), 6405–6410. doi:10.1007/s11356-020-11017-2
- Dong, F., Xiao, P., Li, X., Chang, P., Zhang, W., and Wang, L. (2021b). Cadmium triggers oxidative stress and mitochondrial injury mediated apoptosis in human extravillous trophoblast HTR-8/SVneo cells. *Reprod. Toxicol.* 101, 18–27. doi:10.1016/j.reprotox.2021.02.003
- El-Baz, M. A., El-Deeb, T. S., El-Nowehi, A. M., Mohany, K. M., Shaaban, O. M., and Abbas, A. M. (2015). Environmental factors and apoptotic indices in patients with intrauterine growth retardation: A nested case-control study. *Environ. Toxicol. Pharmacol.* 39 (2), 589–596. doi:10.1016/j.etap.2015.01.009
- Eriyamremu, G. E., Asagba, S. O., Onyeneke, E. C., and Adaikpoh, M. A. (2005). Changes in carboxypeptidase A, dipeptidase and Na<sup>+</sup>/K<sup>+</sup> ATPase activities in the intestine of rats orally exposed to different doses of cadmium. *Biometals* 18 (1), 1–6. doi:10.1007/s10534-004-1202-3
- Feng, K., Chen, Z., Pengcheng, L., Zhang, S., and Wang, X. (2019). Quercetin attenuates oxidative stress-induced apoptosis via SIRT1/AMPK-mediated inhibition of ER stress in rat chondrocytes and prevents the progression of osteoarthritis in a rat model. *J. Cell. Physiol.* 234 (10), 18192–18205. doi:10.1002/jcp.28452
- Friberg, L. (1948). Proteinuria and kidney injury among workmen exposed to cadmium and nickel dust; preliminary report. *J. Ind. Hyg. Toxicol.* 30 (1), 32–36.
- Gu, J., Ren, Z., Zhao, J., Peprah, F. A., Xie, Y., Cheng, D., et al. (2020). Calcimimetic compound NPS R-467 protects against chronic cadmium-induced mouse kidney injury by restoring autophagy process. *Ecotoxicol. Environ. Saf.* 189, 110052. doi:10.1016/j.ecoenv.2019.110052
- Hart, B., Potts, R., and Watkin, R. (2001). Cadmium adaptation in the lung - a double-edged sword? *Toxicology* 160, 65–70. doi:10.1016/s0300-483x(00)00436-4
- Indran, I. R., Tufo, G., Pervaiz, S., and Brenner, C. (2011). Recent advances in apoptosis, mitochondria and drug resistance in cancer cells. *Biochim. Biophys. Acta* 1807 (6), 735–745. doi:10.1016/j.bbabi.2011.03.010
- Iserhienrhien, L. O., and Okolie, N. P. (2022). Protective effect of *Geophila obvallata* (Shumach) Didr leaf extract and its fractions against cadmium-induced nephrotoxicity in male Wistar rats. *Toxicol. Rep.* 9, 87–93. doi:10.1016/j.toxrep.2021.12.008
- Jihen, H., Fatima, H., Nouha, A., Baati, T., Imed, M., and Abdelhamid, K. (2010). Cadmium retention increase: A probable key mechanism of the protective effect of zinc on cadmium-induced toxicity in the kidney. *Toxicol. Lett.* 196 (2), 104–109. doi:10.1016/j.toxlet.2010.04.006
- Jihen, H., Imed, M., Fatima, H., and Abdelhamid, K. (2009). Protective effects of selenium (Se) and zinc (Zn) on cadmium (Cd) toxicity in the liver of the rat: Effects on the oxidative stress. *Ecotoxicol. Environ. Saf.* 72 (5), 1559–1564. doi:10.1016/j.ecoenv.2008.12.006
- Kazantzis, G. (2004). Cadmium, osteoporosis and calcium metabolism. *Biometals* 17 (5), 493–498. doi:10.1023/b:biom.0000045727.76054.f3
- Kim, K. S., Lim, H. J., Lim, J. S., Son, J. Y., Lee, J., Lee, B. M., et al. (2018). Curcumin ameliorates cadmium-induced nephrotoxicity in Sprague-Dawley rats. *Food Chem. Toxicol.* 114, 34–40. doi:10.1016/j.fct.2018.02.007
- Lee, J. I., Kim, M. J., Park, C. S., and Kim, M. C. (2006). Influence of ascorbic acid on BUN, creatinine, resistive index in canine renal ischemia-reperfusion injury. *J. Vet. Sci.* 7 (1), 79–81. doi:10.4142/jvs.2006.7.1.79
- Li, Y., Yao, J., Han, C., Yang, J., Chaudhry, M. T., Wang, S., et al. (2016). Quercetin, inflammation and immunity. *Nutrients* 8 (3), 167. doi:10.3390/nu8030167
- Liang, Y., Xu, K., Zhang, P., Zhang, J., Chen, P., He, J., et al. (2020). Quercetin reduces tendon adhesion in rat through suppression of oxidative stress. *BMC Musculoskelet. Disord.* 21 (1), 608. doi:10.1186/s12891-020-03618-2
- Luo, B., Lin, Y., Jiang, S., Huang, L., Yao, H., Zhuang, Q., et al. (2016). Endoplasmic reticulum stress eIF2 $\alpha$ -ATF4 pathway-mediated cyclooxygenase-2 induction regulates cadmium-induced autophagy in kidney. *Cell Death Dis.* 7 (6), e2251. doi:10.1038/cddis.2016.78
- Macedo, E. (2011). Blood urea nitrogen beyond estimation of renal function. *Crit. Care Med.* 39 (2), 405–406. doi:10.1097/CCM.0b013e318205c33a
- Maity, S., Banerjee, R., Goswami, P., Chakrabarti, M., and Mukherjee, A. (2018). Oxidative stress responses of two different ecophysiological species of earthworms (*Eutyphoeus waltoni* and *Eisenia fetida*) exposed to Cd-contaminated soil. *Chemosphere* 203, 307–317. doi:10.1016/j.chemosphere.2018.03.189
- Messaoudi, I., El Heni, J., Hammouda, F., Saïd, K., and Kerkeni, A. (2009). Protective effects of selenium, zinc, or their combination on cadmium-induced oxidative stress in rat kidney. *Biol. Trace Elem. Res.* 130 (2), 152–161. doi:10.1007/s12011-009-8324-y
- Owumi, S. E., Dim, U. J., and Najoppe, E. S. (2019). Diethylnitrosamine aggravates cadmium-induced hepatorenal oxidative damage in prepubertal rats. *Toxicol. Ind. Health* 35 (8), 537–547. doi:10.1177/0748233719863287
- Pérez Díaz, M. F. F., Plateo Pignatari, M. G., Filippa, V. P., Mohamed, F. H., Marchevsky, E. J., Gimenez, M. S., et al. (2019). A soybean-based diet modulates cadmium-induced vascular apoptosis. *J. Trace Elem. Med. Biol.* 52, 239–246. doi:10.1016/j.jtemb.2019.01.007
- Renugadevi, J., and Prabhu, S. M. (2010). Cadmium-induced hepatotoxicity in rats and the protective effect of naringenin. *Exp. Toxicol. Pathol.* 62 (2), 171–181. doi:10.1016/j.etp.2009.03.010
- Saw, C. L., Guo, Y., Yang, A. Y., Paredes-Gonzalez, X., Ramirez, C., Pung, D., et al. (2014). The berry constituents quercetin, kaempferol, and pterostilbene synergistically attenuate reactive oxygen species: Involvement of the nrf2-ARE signaling pathway. *Food Chem. Toxicol.* 72, 303–311. doi:10.1016/j.fct.2014.07.038
- Shao, X., Lu, W., Gao, F., Li, D., Hu, J., Li, Y., et al. (2016). Uric acid induces cognitive dysfunction through hippocampal inflammation in rodents and humans. *J. Neurosci.* 36 (43), 10990–11005. doi:10.1523/JNEUROSCI.1480-16.2016
- Skipper, A., Sims, J. N., Yedjou, C. G., and Tchounwou, P. B. (2016). Cadmium chloride induces DNA damage and apoptosis of human liver carcinoma cells via oxidative stress. *Int. J. Environ. Res. Public Health* 13 (1), E88. doi:10.3390/ijerph13010088
- So, A., and Thorens, B. (2010). Uric acid transport and disease. *J. Clin. Invest.* 120 (6), 1791–1799. doi:10.1172/jci42344
- Song, X. B., Liu, G., Wang, Z. Y., and Wang, L. (2016). Puerarin protects against cadmium-induced proximal tubular cell apoptosis by restoring mitochondrial function. *Chem. Biol. Interact.* 260, 219–231. doi:10.1016/j.cbi.2016.10.006
- Stark, J. L. (1980). BUN/creatinine: Your keys to kidney function. *Nursing* 10 (5), 33–38. doi:10.1097/00152193-198005000-00007
- Tu, Y. J., Han, X. Y., Xu, Z. R., Wang, Y. Z., and Li, W. F. (2007). Effect of cadmium in feed on organs and meat colour of growing pigs. *Vet. Res. Commun.* 31 (5), 621–630. doi:10.1007/s11259-007-3468-8
- Umar Ijaz, M., Batool, M., Batool, A., Al-Ghanimd, K. A., Zafar, S., Ashraf, A., et al. (2021). Protective effects of vitexin on cadmium-induced renal toxicity in rats. *Saudi J. Biol. Sci.* 28 (10), 5860–5864. doi:10.1016/j.sjbs.2021.06.040
- Varoni, M. V., Pasciu, V., Gadau, S. D., Baralla, E., Serra, E., Palomba, D., et al. (2017). Possible antioxidant effect of Lycium barbarum polysaccharides on hepatic cadmium-induced oxidative stress in rats. *Environ. Sci. Pollut. Res. Int.* 24 (3), 2946–2955. doi:10.1007/s11356-016-8050-x
- Veith, C., Drent, M., Bast, A., van Schooten, F. J., and Boots, A. W. (2017). The disturbed redox-balance in pulmonary fibrosis is modulated by the plant flavonoid quercetin. *Toxicol. Appl. Pharmacol.* 336, 40–48. doi:10.1016/j.taap.2017.10.001

- Vodošek Hojs, N., Bevc, S., Ekart, R., and Hojs, R. (2020). Oxidative stress markers in chronic kidney disease with emphasis on diabetic nephropathy. *Antioxidants (Basel)* 9 (10), E925. doi:10.3390/antiox9100925
- Wang, C., Nie, G., Zhuang, Y., Hu, R., Wu, H., Xing, C., et al. (2020a). Inhibition of autophagy enhances cadmium-induced apoptosis in duck renal tubular epithelial cells. *Ecotoxicol. Environ. Saf.* 205, 111188. doi:10.1016/j.ecoenv.2020.111188
- Wang, J., Zhu, H., Lin, S., Wang, K., Wang, H., and Liu, Z. (2021). Protective effect of naringenin against cadmium-induced testicular toxicity in male SD rats. *J. Inorg. Biochem.* 214, 111310. doi:10.1016/j.jinorgbio.2020.111310
- Wang, J., Zhu, H., Liu, X., and Liu, Z. (2014). N-acetylcysteine protects against cadmium-induced oxidative stress in rat hepatocytes. *J. Vet. Sci.* 15 (4), 485–493. doi:10.4142/jvs.2014.15.4.485
- Wang, J., Zhu, H., Wang, K., Yang, Z., and Liu, Z. (2020b). Protective effect of quercetin on rat testes against cadmium toxicity by alleviating oxidative stress and autophagy. *Environ. Sci. Pollut. Res. Int.* 27 (20), 25278–25286. doi:10.1007/s11356-020-08947-2
- Wang, Y., Fang, J., Leonard, S. S., and Rao, K. M. (2004). Cadmium inhibits the electron transfer chain and induces reactive oxygen species. *Free Radic. Biol. Med.* 36 (11), 1434–1443. doi:10.1016/j.freeradbiomed.2004.03.010
- Wasilewski, M., and Scorrano, L. (2009). The changing shape of mitochondrial apoptosis. *Trends Endocrinol. Metab.* 20 (6), 287–294. doi:10.1016/j.tem.2009.03.007
- Yang, H., Yang, T., Heng, C., Zhou, Y., Jiang, Z., Qian, X., et al. (2019a). Quercetin improves nonalcoholic fatty liver by ameliorating inflammation, oxidative stress, and lipid metabolism in db/db mice. *Phytother. Res.* 33 (12), 3140–3152. doi:10.1002/ptr.6486
- Yang, S. H., He, J. B., Yu, L. H., Li, L., Long, M., Liu, M. D., et al. (2019b). Protective role of curcumin in cadmium-induced testicular injury in mice by attenuating oxidative stress via Nrf2/ARE pathway. *Environ. Sci. Pollut. Res. Int.* 26 (33), 34575–34583. doi:10.1007/s11356-019-06587-9
- Yuan, Y., Ma, S., Qi, Y., Wei, X., Cai, H., Dong, L., et al. (2016). Quercetin inhibited cadmium-induced autophagy in the mouse kidney via inhibition of oxidative stress. *J. Toxicol. Pathol.* 29 (4), 247–252. doi:10.1293/tox.2016-0026
- Zhang, C., Jin, Y., Yu, Y., Xiang, J., and Li, F. (2021). Cadmium-induced oxidative stress, metabolic dysfunction and metal bioaccumulation in adult palaemonid shrimp *Palaemon macrodactylus* (Rathbun, 1902). *Ecotoxicol. Environ. Saf.* 208, 111591. doi:10.1016/j.ecoenv.2020.111591
- Zhang, H., Pan, L., and Tao, Y. (2014). Antioxidant responses in clam *Venerupis philippinarum* exposed to environmental pollutant hexabromocyclododecane. *Environ. Sci. Pollut. Res. Int.* 21 (13), 8206–8215. doi:10.1007/s11356-014-2801-3
- Zhang, R., Yi, R., Bi, Y., Xing, L., Bao, J., and Li, J. (2017). The effect of selenium on the Cd-induced apoptosis via NO-mediated mitochondrial apoptosis pathway in chicken liver. *Biol. Trace Elem. Res.* 178 (2), 310–319. doi:10.1007/s12011-016-0925-7
- Zhong, L., Wang, L., Xu, L., Liu, Q., Jiang, L., Zhi, Y., et al. (2015). The role of nitric oxide synthase in an early phase Cd-induced acute cytotoxicity in MCF-7 cells. *Biol. Trace Elem. Res.* 164 (1), 130–138. doi:10.1007/s12011-014-0187-1
- Zhou, J., Li, L. U., Fang, L. I., Xie, H., Yao, W., Zhou, X., et al. (2016). Quercetin reduces cyclin D1 activity and induces G1 phase arrest in HepG2 cells. *Oncol. Lett.* 12 (1), 516–522. doi:10.3892/ol.2016.4639
- Zhu, H. L., Xu, X. F., Shi, X. T., Feng, Y. J., Xiong, Y. W., Nan, Y., et al. (2019). Activation of autophagy inhibits cadmium-triggered apoptosis in human placental trophoblasts and mouse placenta. *Environ. Pollut.* 254, 112991. doi:10.1016/j.envpol.2019.112991
- Zhu, M. K., Li, H. Y., Bai, L. H., Wang, L. S., and Zou, X. T. (2020). Histological changes, lipid metabolism, and oxidative and endoplasmic reticulum stress in the liver of laying hens exposed to cadmium concentrations. *Poult. Sci.* 99 (6), 3215–3228. doi:10.1016/j.psj.2019.12.073
- Zhu, Y., Hu, C., Zheng, P., Miao, L., Yan, X., Li, H., et al. (2016). Ginsenoside Rb1 alleviates aluminum chloride-induced rat osteoblasts dysfunction. *Toxicology* 368–369, 183–188. doi:10.1016/j.tox.2016.07.014



## OPEN ACCESS

## EDITED BY

Xu Yang,  
Henan Agricultural University, China

## REVIEWED BY

Jin Hongtao,  
Chinese Academy of Medical Sciences  
and Peking Union Medical College,  
China  
Fen Pei,  
Roivant Sciences, United States

## \*CORRESPONDENCE

Yongbiao Guan,  
guanyb@hotmail.com  
Quanjun Wang,  
wangquanjunbeijing@163.com

## SPECIALTY SECTION

This article was submitted to Predictive  
Toxicology,  
a section of the journal  
Frontiers in Pharmacology

RECEIVED 03 August 2022

ACCEPTED 22 August 2022

PUBLISHED 12 September 2022

## CITATION

Han J, Tian Y, Wang M, Li Y, Yin J, Qu W,  
Yan C, Ding R, Guan Y and Wang Q  
(2022), Proteomics unite traditional  
toxicological assessment methods to  
evaluate the toxicity of iron  
oxide nanoparticles.  
*Front. Pharmacol.* 13:1011065.  
doi: 10.3389/fphar.2022.1011065

## COPYRIGHT

© 2022 Han, Tian, Wang, Li, Yin, Qu, Yan,  
Ding, Guan and Wang. This is an open-  
access article distributed under the  
terms of the [Creative Commons  
Attribution License \(CC BY\)](https://creativecommons.org/licenses/by/4.0/). The use,  
distribution or reproduction in other  
forums is permitted, provided the  
original author(s) and the copyright  
owner(s) are credited and that the  
original publication in this journal is  
cited, in accordance with accepted  
academic practice. No use, distribution  
or reproduction is permitted which does  
not comply with these terms.

# Proteomics unite traditional toxicological assessment methods to evaluate the toxicity of iron oxide nanoparticles

Junyuan Han, Yongzhang Tian, Minghan Wang, Yajuan Li,  
Jiye Yin, Wensheng Qu, Changhui Yan, Rigao Ding,  
Yongbiao Guan\* and Quanjun Wang\*

State Key Laboratory of Toxicology and Medical Countermeasures, Institute of Pharmacology and Toxicology, Beijing, China

Iron oxide nanoparticles (IONPs) are the first generation of nanomaterials approved by the Food and Drug Administration for use as imaging agents and for the treatment of iron deficiency in chronic kidney disease. However, several IONPs-based imaging agents have been withdrawn because of toxic effects and the poor understanding of the underlying mechanisms. This study aimed to evaluate IONPs toxicity and to elucidate the underlying mechanism after intravenous administration in rats. Seven-week-old rats were intravenously administered IONPs at doses of 0, 10, 30, and 90 mg/kg body weight for 14 consecutive days. Toxicity and molecular perturbations were evaluated using traditional toxicological assessment methods and proteomics approaches, respectively. The administration of 90 mg/kg IONPs induced mild toxic effects, including abnormal clinical signs, lower body weight gain, changes in serum biochemical and hematological parameters, and increased organ coefficients in the spleen, liver, heart, and kidneys. Toxicokinetics, tissue distribution, histopathological, and transmission electron microscopy analyses revealed that the spleen was the primary organ for IONPs elimination from the systemic circulation and that the macrophage lysosomes were the main organelles of IONPs accumulation after intravenous administration. We identified 197 upregulated and 75 downregulated proteins in the spleen following IONPs administration by proteomics. Mechanically, the AKT/mTOR/TFEB signaling pathway facilitated autophagy and lysosomal activation in splenic macrophages. This is the first study to elucidate the mechanism of IONPs toxicity by combining proteomics with traditional methods for toxicity assessment.

## KEYWORDS

iron oxide nanoparticles, toxicity, lysosome, proteomics, autophagy, AKT/mTOR/TFEB signaling pathway

## 1 Introduction

Iron oxide nanoparticles (IONPs) are used for a wide variety of biomedical and bioengineering applications, such as magnetic resonance imaging, drug delivery, cancer therapy, hyperthermia, and tissue repair, because of their unique physical and chemical properties (Anderson et al., 2019; Soetaert et al., 2020). Some of the IONPs evaluated in preclinical and clinical trials have been approved by the European Medicines Agency and United States Food and Drug Administration for the treatment of iron deficiency in chronic kidney disease and imaging of liver lesions and lymph node metastasis (Bobo et al., 2016). However, several approved IONPs-based imaging agents were later withdrawn because of severe toxic effects (Frtus et al., 2020). Emerging evidence indicates that traditional preclinical safety models might neglect secondary toxic effects, leading to inadequate comprehension of the mechanisms by which IONPs act at the cellular and subcellular levels (Frtus et al., 2020; Chrishtop et al., 2021). Although numerous *in vitro* and *in vivo* studies have explored the mechanisms of IONPs-mediated toxicities such as neurotoxicity, immunotoxicity, and cardiovascular toxicity (Mahmoudi et al., 2012; Chrishtop et al., 2021), the results have been inconsistent or even contradictory. Indeed, IONPs are known to affect multiple organelles and signaling pathways to mediate different biological responses (Zhang et al., 2016). Therefore, the mechanisms underlying IONPs-mediated toxicity should be investigated using an integrative and systematic approach.

As an emerging branch of life science research, proteomics is a high-throughput technology with high sensitivity. Several proteomics studies have revealed the toxic effects of nanomaterials and the underlying mechanisms (Frohlich, 2017; Zhang et al., 2018). New toxicological mechanisms of nanomaterials at the protein level can be revealed based on the analysis of the whole proteome using this approach (Matysiak et al., 2016). In recent years, proteomics studies have revealed several novel toxicological mechanisms of IONPs. For example, Askri et al. (2019a) used proteomics techniques to show that IONPs affected signaling pathways regulating cytoskeleton, apoptosis, and carcinogenesis in SH-SY5Y cells. However, compared to various *in vitro* proteomics studies investigating nanoparticles (Nath Roy et al., 2016), to our knowledge, only one *in vivo* proteomics study examined the effects of IONPs in the liver, brain, and lungs after intranasal exposure (Askri et al., 2019b). In fact, proteomics techniques should be considered a powerful tool to identify potential biomarkers and to evaluate toxicity following IONPs exposure. Furthermore, the identification of differentially expressed proteins (DEPs) after IONPs exposure can aid in gaining a deep insight into the mechanisms of toxicity. However, no study to date has examined the changes in the proteome following the administration of IONPs through clinically used routes, especially intravenous injection.

Furthermore, no study has investigated the effects of IONPs using proteomics in combination with traditional preclinical safety assessment methods.

In the present study, we aimed to evaluate IONPs toxicity following intravenous administration for 14 days in rats using emerging proteomics methods in combination with traditional toxicological assessment methods, including hematology, serum biochemistry, histopathology, and toxicokinetics. Furthermore, we aimed to reveal the molecular mechanisms of IONPs toxicity by comparing traditional toxicological and proteomics parameters in this animal model.

## 2 Material and methods

### 2.1 Physicochemical characteristics of injected iron oxide nanoparticles

Injected IONPs in the form of polyethylene glycol-coated Fe<sub>3</sub>O<sub>4</sub> nanoparticles in water, which contained a concentration of Fe 10 mg/ml, were kindly provided by Mingyuan Gao and Jianfeng Zeng from Soochow University, China. The IONPs were prepared using the flow synthesis method as previously reported (Jiao et al., 2015). The characteristic morphology of injected IONPs was determined using transmission electron microscopy (TEM, Tecnai G20, FEI, United States) operating at an acceleration voltage of 200 kV. The zeta potential and hydrodynamic particle size of injected IONPs were measured at 25°C using dynamic light scattering with a particle size analyzer (Zetasizer Nano ZS90, Malvern Instruments, United Kingdom).

### 2.2 Animal care

In total, 62 male and 62 female specific pathogen-free Sprague-Dawley rats aged 7 weeks were purchased from Vital River Laboratory Animal Technology (Beijing, China). The animals were dosed after one week of acclimation. During the study, all procedures for the care and use of animals were reviewed and approved by the Institutional Animal Care and Use Committee of National Beijing Center for Drug Safety Evaluation and Research (IACUC-2021-009). The laboratory animal program is fully accredited by the Association for Assessment and Accreditation of Laboratory Animal Care.

### 2.3 Study design

IONPs were intravenously administered through the tail vein. IONPs were diluted to desired concentrations in 5% glucose solution (dissolved by sterile water) under sterile conditions. Animals were randomly assigned to four groups with 11 rats per sex (rats/sex) for vehicle group and 17 rats/sex which six rats/sex

served as toxicokinetic animals in IONPs treated groups. IONPs at doses of 10, 30, and 90 mg/kg or the vehicle (5% glucose solution) were administered once daily for 14 days. The parameters evaluated during the in-life phase included clinical observations such as mortality, moribundity, general health, and signs of toxicity (once daily); food consumption (twice weekly); and body weight (twice weekly).

## 2.4 Clinical chemistry, hematology, and coagulation

Clinicopathological evaluations, including clinical chemistry, hematology, and coagulation parameters, were conducted on 5 rats per sex per group after intravenous IONPs administration for 14 days. In all animals, blood samples were collected from the inferior vena cava with the animal anesthetized using pentobarbital at the time of sacrifice. Serum chemistry parameters were analyzed using an auto analyzer (Hitachi 7,180, Hitachi). Hematological parameters were analyzed using an automatic hematology analyzer (Sysmex XN-1000v, Sysmex). Coagulation parameters were analyzed using an automated coagulation analyzer (Sysmex CS-5100, Sysmex).

## 2.5 Determination of organ coefficients

In all animals, body weight was measured immediately before sacrifice. A full necropsy was conducted in all animals, and the brain, heart, liver, spleen, and kidney were removed and immediately weighed in 5 rats/sex/group. Organ coefficients were calculated as the ratio of tissue wet weight (mg) to body weight (g).

## 2.6 Histopathological examination

The following organs were collected from 5 rats/sex/group and fixed in 10% neutral-buffered saline: brain, heart, liver, spleen, kidneys, lungs, thymus, adrenal glands, trachea, esophagus, aorta, thyroid, and parathyroid glands, pancreas, stomach, small and large intestines, mesenteric lymph nodes, uterus, vagina, ovaries, prostate gland, epididymis, seminal vesicles, urinary bladder, biceps femoris muscle, femur and sternum with bone marrow, sciatic nerve, mammary glands, and skin. Eyes with Harderian glands and testes were fixed in modified Davidson's fixative and transferred to 10% neutral-buffered formalin within 24–48 h. Paraffin-embedded sections (3–4  $\mu$ m) were prepared from all tissues and stained with hematoxylin and eosin. Microscopic examination was conducted for all tissues in all groups. Additionally, spleen sections were stained with Perls' Prussian blue for iron detection.

## 2.7 Immunohistochemistry and immunofluorescence

For immunofluorescent staining for light chain 3 (LC3) in spleen sections, nonspecific binding was blocked with 5% goat serum (cat. No: SL038, Solarbio Life Sciences), followed by immunolabeling using a primary antibody against LC3 (cat. No: 4,108; Cell Signaling Technology) and a secondary antibody conjugated to fluorescein isothiocyanate (cat. No: ZF-0311, ZSGB-BIO). Immunofluorescence images were acquired using a 3DHISTECH P250 FLASH confocal microscope with a  $\times 63$  objective. For immunohistochemistry, tissue sections were incubated with a primary antibody against lysosome-associated membrane protein (LAMP) 2 (cat. No: 125,068, Abcam) or ferritin heavy chain 1 (FTH1, cat. No: 4,393, Cell Signaling Technology) and visualized using a streptavidin–biotin immunoenzymatic antigen detection system (cat. No: PV-9000, ZSGB-BIO).

## 2.8 TEM and TEM-energy-dispersive spectrometer analysis

Spleens collected at sacrifice were cut into approximately 1-mm<sup>3</sup> pieces, fixed in 2.5% glutaraldehyde in 0.1 M phosphate buffer, and postfixed with 1% osmium tetroxide. After washing in double distilled H<sub>2</sub>O, the samples were gradually dehydrated in ethanol, embedded in epoxy resin, and sliced into 70-nm-thick sections. The sections were observed under bright field using an electron microscope (JEM-7610EX, JEOL, Japan) operated at 80 kV.

The samples prepared from the animals in the vehicle and 90 mg/kg IONPs groups were also analyzed to determine the element distribution of iron using TEM (JEM-2100, JEOL, Japan) equipped with an energy-dispersive spectrometry (EDS) device. The TEM images were captured at 200 kV and used for qualitative elemental analysis of the energy-dispersive spectra of the whole area.

## 2.9 Toxicokinetic and tissue distribution analyses

In animals used for toxicokinetic analysis (three rats per sex in IONPs treated groups), approximately 0.25 ml of whole blood was collected via jugular vein puncture prior to; 5, 15, and 30 min; and 1, 3, 6, and 24 h after the first (day 1) and last (day 14) doses. The collected blood samples were maintained at room temperature (18–26°C) for 30–60 min, followed by centrifugation at 1800 g for 10 min at 4°C to obtain serum samples, which were stored at –80°C. Following sacrifice, the spleen, liver, lungs, mesenteric lymph nodes, kidneys, heart, and brain (cerebellum and cerebrum) from three rats/sex/group were

dissected and stored at  $-80^{\circ}\text{C}$ . Concentrations of IONPs (expressed as total iron, ng/mL) of three rats/sex/group were determined using an inductively coupled plasma (ICP)-mass spectrometry (MS) method. The lower limits of quantitation were 25 and 75 ng/ml for serum and tissue samples, respectively. The WinNonlin software package was used for the calculation of serum toxicokinetic parameters, and the predose value was subtracted prior to the calculation.

## 2.10 Tandem mass tag-labeled quantitative proteomics

Proteomics analysis of the spleen tissue samples of the vehicle and 90 mg/kg IONPs groups was performed using the tandem mass tag (TMT)-labeled quantitative proteomic approach. The procedures included protein sample preparation, proteolysis and TMT labeling, liquid chromatography-tandem MS and high-performance liquid chromatograph analysis, and proteomics data analysis. Briefly, the spleen tissues of 12 animals (6 animals/group) were collected and ground into powder with liquid nitrogen. Lysis buffer supplemented with 1 mM phenylmethylsulfonyl fluoride (cat. No: A610425-0005, Sangon Biotech) was added to the samples, which were sonicated on ice for 3 min, followed by centrifugation twice at 12,000  $g$  for 10 min at room temperature to collect the supernatants. The protein concentrations were confirmed using a bicinchoninic acid protein assay kit (cat. No: 23,225, Thermo Fisher Scientific) per the manufacturer's descriptions. Sodium dodecyl sulfate-polyacrylamide gel electrophoresis was performed for protein quality control prior to proteomic experiments. The protein solutions were digested with trypsin, reduced/alkylated, precipitated with acetone, and enzymatically hydrolyzed at  $37^{\circ}\text{C}$ . The obtained peptides were reconstituted and labeled using a TMT kit (cat. No: A44520, Thermo Fisher Scientific). The labeled peptides were fractionated using a high-performance liquid chromatograph (Agilent 1,100 series, Agilent) with an Agilent Zorbax Extend C18 column ( $5\ \mu\text{m}$ ,  $150\ \text{mm} \times 2.1\ \text{mm}$ ). The tryptic peptides were dissolved in mobile phase A (aqueous solution containing 0.1% formic acid) and injected into Q Exactive MS (Thermo Fisher Scientific) for separation using liquid chromatography-tandem MS. The liquid phase gradient was set as follows: 0–1 min, 2%–6% mobile phase B (acetonitrile solution containing 0.1% formic acid); 1–49 min, 6%–25% mobile phase B; 49–54 min, 25%–35% mobile phase B; 54–56 min, 35%–90% mobile phase B; and 56–60 min, 90% mobile phase B. The flow rate was maintained at 350 nL/min. Full MS scanning was acquired in a mass resolution of 120,000 with a mass range of 350–1,650  $m/z$ , and the target automatic gain control was set at  $3 \times 10^6$ . Fifteen most intense peaks in MS were fragmented using higher energy collisional dissociation with a collision energy of 32. The MS/

MS spectra were obtained with a resolution of 60,000, target automatic gain control of  $1 \times 10^5$ , and max injection time of 55 ms. The Q Exactive dynamic exclusion time was set to 40 s and run in positive mode.

## 2.11 Database search and bioinformatics analysis

Proteome Discoverer v2.4 (Thermo Fisher Scientific) was used to thoroughly search the experimental data against the UniProt database for *Rattus norvegicus* (<https://www.uniprot.org>, database released in July 2021, uniprot-proteome\_UP000002494) with trypsin digestion specificity. The search settings were as follows: tolerance of first-stage precursor iron mass error, 10 ppm; number of missed cleavages, 2; and mass error tolerance of the secondary fragment ion, 0.02 Da. Cysteine alkylation was set as a fixed modification. False discovery rate (FDR) was adjusted to  $<1\%$ , and the quantification of protein groups required  $\geq 2$  peptides. The screening criteria for DEPs with significance were a  $p$  value of  $<0.05$  and a fold change of  $>2$  (90 mg/kg IONPs group vs. vehicle group). The Gene Ontology (GO) database (<http://www.geneontology.org/>, released in July 2021) was used for GO analysis. The DEPs were annotated into three ontological categories (biological process, molecular function, and cellular component) using GO terms. Gene-related metabolic pathways were identified using the Kyoto Encyclopedia of Genes and Genomes (KEGG) database (<http://www.genome.jp.kegg/>, released in July 2021). GO and KEGG pathway enrichment analysis based on hypergeometric distribution  $R$ . For each category, a two-tailed Fisher's exact test was used to test the enrichment of DEPs. The GO terms or the KEGG pathways with corrected  $p$  values of  $<0.05$  were considered significant. An enrichment score was calculated based on the formula of  $(\frac{m}{n})/(\frac{M}{N})$  to indicate the number of DEPs enriched to this GO term or KEGG pathway. In this formula, "N" is the number of GO/KEGG annotations in rat proteins; "n" is the number of GO/KEGG annotations in differential proteins; "M" is the number of a specific GO terms or KEGG pathways annotated in the protein of rats; "m" is the number of DEPs annotated as a specific GO term or KEGG pathway.

## 2.12 Parallel reaction monitoring for protein expression verification

The abundances of LAMP1 and Niemann–Pick C1 (NPC1), two of the DEPs identified in the 90 mg/kg IONPs group, were validated using parallel reaction monitoring of all groups administered IONPs as well as the vehicle group. The experimental and data analysis methods were previously described by Chen et al. (2021).

## 2.13 Western blot analysis

Western blotting was performed in the spleen of 10, 30, and 90 mg/kg IONPs treated and vehicle groups. The expression levels of LAMP2, FTH1, LC3, AKT, phosphorylated (p)-AKT, mammalian target of rapamycin (mTOR), p-mTOR, transcription factor EB (TFEB), and p-TFEB were detected. The rabbit anti-LAMP2 antibody (ab125068, 1:2000) was purchased from Abcam. The rabbit antibodies against LC3 (cat. No: 4,108; 1:1,000), FTH1 (cat. No: 4,393; 1:1,000), AKT (cat. No: 4,691; 1:1,000), p-AKT (cat. No: 4,060; 1:1,000), mTOR (cat. No: 2,983; 1:1,000), p-mTOR (cat. No: 5,536; 1:1,000), TFEB (cat. No: 83,010; 1:1,000), glyceraldehyde-3-phosphate dehydrogenase (cat. No: 5,174; 1:1,000), and  $\beta$ -actin (cat. No: 8,457; 1:3,000) were purchased from Cell Signaling Technology. The rabbit polyclonal p-TFEB antibody (cat. No: PA5-114662; 1:1,000) was purchased from Thermo Fisher Scientific. Briefly, the spleens of three rats/sex/group were homogenized and lysed in radioimmunoprecipitation assay buffer containing phosphatase and protease inhibitors. The lysates were centrifugated at 12,000 g for 10 min at 4°C, and protein concentrations were determined using the bicinchoninic acid protein assay kit (cat. No: 23,225, Thermo Fisher Scientific). Equal amounts of protein lysates were separated on sodium dodecyl sulfate-polyacrylamide gels and transferred to polyvinylidene difluoride membranes, which were blocked with 5% nonfat dry milk in Tris-buffered saline containing 0.05% Tween 20 for 1 h at room temperature. Next, the membranes were incubated with primary antibodies in primary antibody dilution buffer (cat. No: P0023A; Beyotime) overnight at 4°C. After washing three times with Tris-buffered saline containing 0.05% Tween 20, 5 min each, the membranes were incubated with anti-rabbit immunoglobulin G antibody (cat. No: 7,074; 1:10,000; Cell Signaling Technology) for 1 h at room temperature. The signals were detected by incubating the membranes with an enhanced chemiluminescence reagent (cat. No: 34,577; Thermo Fisher Scientific), and band intensities were analyzed using ImageJ.

## 2.14 Statistical analysis

Data were expressed as means  $\pm$  standard deviation and analyzed using GraphPad Prism 5.0 (GraphPad, San Diego, CA, United States). One-way analysis of variance, followed by Dunnett's test, was used for all statistical analysis. A *p* value of <0.05 was considered to indicate statistical significance.

## 3 Results

### 3.1 Characterization of the injected iron oxide nanoparticles

The TEM images of the injected IONPs and the corresponding particle size distribution are shown in

Supplementary Figures S1A,B, respectively. The average particle size was  $3.6 \pm 0.3$  nm (Supplementary Figure S1C). The zeta potential of IONPs was  $-7$  mV.

### 3.2 General physiological findings

The careful monitoring of the clinical signs and symptoms throughout the 14-days consecutive dosing period revealed slight piloerection and red perirhinal discharge in the 90 mg/kg IONPs group. No abnormal clinical signs were observed in the vehicle group and the 10 and 30 mg/kg IONPs groups.

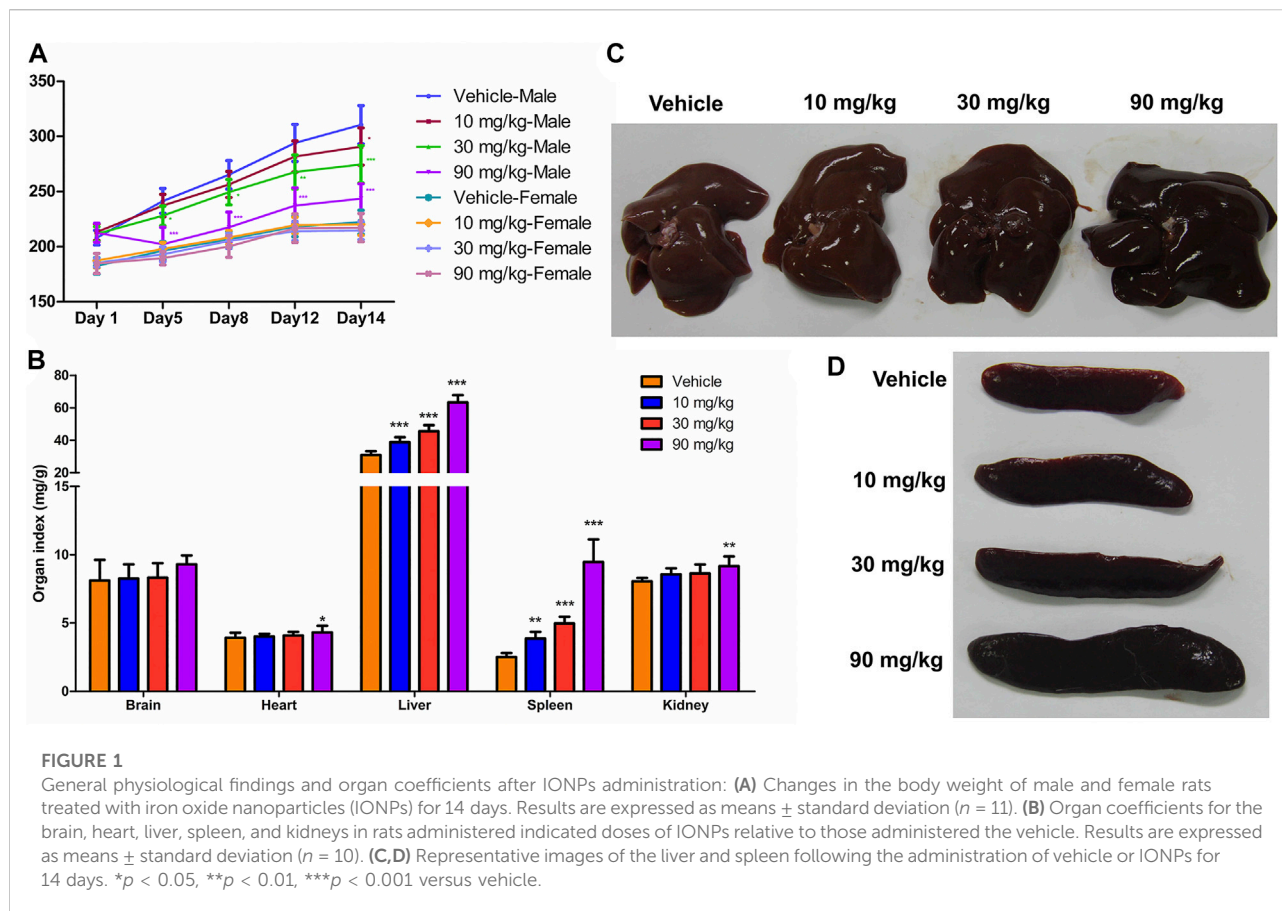
The body weights continually increased during the experimental period, and the body weight gain was lower in the IONPs-administered male rats than in the vehicle-administered male rats (Figure 1A). At the end of the experimental period, the average body weights of the male rats in the 10, 30, and 90 mg/kg IONPs groups were significantly decreased than in the vehicle group with 0.94-, 0.88-, and 0.78-fold of the average body weight, respectively, especially in later two IONPs groups ( $p < 0.001$ ). Significantly decreased food intake was noted in the 90 mg/kg IONPs group, which was correlated with lower body weight gain (data not shown).

### 3.3 Organ coefficients

The organ coefficients, which were determined based on the terminal organ and body weights following an overnight fasting period prior to necropsy, were used as a highly sensitive measurement of toxicity reflecting significant changes even before the observation of histological changes. The organ coefficients of the heart and kidneys were higher in the 90 mg/kg IONPs group than in the vehicle group ( $p < 0.05$ ), and the organ coefficients of the liver and spleen were significantly higher in all IONPs groups than in the vehicle group ( $p < 0.01$ ) in a dose-dependent manner (Figures 1B–D).

### 3.4 Clinical chemistry

The clinical chemistry data of the male and female rats are summarized in Table 1. Briefly, the levels of total bile acids, cholesterol, triglycerides, and lipase were significantly increased in both the male and female rats administered 90 mg/kg IONPs compared to the vehicle group, which suggested the effect of IONPs on lipid metabolism. All other alterations in clinical chemistry parameters, including those exhibiting statistically significant differences, were not considered to be IONPs toxicity because the changes were negligible in magnitude, lacked dose dependency, were within normal biological variation, or were without toxicological significance.



### 3.5 Hematology and coagulation

The total leucocyte number and the neutrophil percentage were significantly higher and the percentage of lymphocytes was significantly lower in the 90 mg/kg IONP group than in the vehicle group (Table 2). Aforementioned results suggested that the administration of 90 mg/kg IONPs induced a mild inflammatory response dominated by neutrophils. A significant decrease in mean corpuscular hemoglobin concentration was observed in the female rats in the 30 and 90 mg/kg IONPs groups, although the magnitude was small and within the range of the historical control data. The increase in fibrinogen noted in the 90 mg/kg IONPs group was not considered toxicologically meaningful because of the absence of differences in other coagulation parameters. The other changes noted in hematology and coagulation parameters were not considered to be related to IONPs administration because of the inconsistent direction of changes or the lack of any relationship to dose.

### 3.6 Histopathology

The histopathological findings are summarized in Supplementary Table S1. IONPs induced dose-dependent

pigmentation in multiple organs, especially in the spleen (Figures 2A–D, arrows), and no apparent cellular structural changes were noted at any dose level. The pigmentation of macrophages in the spleen was confirmed as ferric iron using Perls' Prussian blue staining (Figures 2E–H, arrows).

### 3.7 Subcellular iron oxide nanoparticles localization and ultrastructural alterations in the spleen

TEM was used to investigate the subcellular localization of the IONPs and the ultrastructural alterations in the spleen. Hypertrophied macrophages exhibited IONPs incorporated within the phagolysosomes. Dose-dependent accumulation of degradative autophagic vacuoles (AVDs) was noticeable in macrophages (Figures 2I–L, arrows). The corresponding EDS spectra of whole areas in the 90 mg/kg IONPs group indicated that the element iron was included in the AVDs with high electron density (Figures 2M–P). Iron was not detected in other areas without vesicles in the IONPs groups or the vehicle group. However, other ultrastructural features were normal,

TABLE 1 Clinical chemistry parameters of rats treated with/without IONPs for 14 days.

Parameters	Vehicle		10 mg/kg		30 mg/kg		90 mg/kg	
	Male	Female	Male	Female	Male	Female	Male	Female
Liver profile								
Total protein (g/L)	50.2 ± 0.6	54.9 ± 1.9	50.1 ± 2.6	53.1 ± 6.3	49.0 ± 4.5	51.1 ± 2.9	58.1 ± 1.6**	56.2 ± 2.9
Albumin (g/L)	28.1 ± 0.4	31.2 ± 0.7	27.0 ± 0.6	28.3 ± 3.1	26.2 ± 2.3	26.5 ± 1.0**	27.4 ± 1.3	26.8 ± 1.0**
Globulin (g/L)	22.1 ± 0.6	23.7 ± 1.2	23.1 ± 2.0	24.8 ± 4.2	22.7 ± 2.3	24.6 ± 2.5	30.6 ± 1.1***	29.3 ± 2.1*
ALP (U/L)	181 ± 31	94 ± 31	144 ± 27	96 ± 16	126 ± 31*	87 ± 53	201 ± 25	191 ± 43**
ALT (U/L)	36 ± 5	25 ± 4	33 ± 8	23 ± 2	30 ± 9	23 ± 3	52 ± 35	25 ± 5
AST (U/L)	166 ± 63	129 ± 30	106 ± 13	127 ± 20	93 ± 19	111 ± 21	172 ± 94	129 ± 30
Total bilirubin (μmol/L)	0.62 ± 0.14	0.47 ± 0.18	0.95 ± 0.30	0.52 ± 0.16	0.83 ± 0.25	0.63 ± 0.19	1.64 ± 0.19	1.46 ± 0.74**
Total bile acid (μmol/L)	5.6 ± 1.4	55.3 ± 6.5	6.2 ± 2.5	68.1 ± 9.7	6.0 ± 4.0	70.8 ± 7.8	24.3 ± 9.3***	79.5 ± 16.0*
Renal profile								
Creatinine (μmol/L)	37.8 ± 2.4	47.5 ± 2.2	39.0 ± 2.7	41.4 ± 3.3	38.8 ± 4.2	41.8 ± 4.8	45.9 ± 2.2**	37.0 ± 4.2**
Blood urea (mmol/L)	5.12 ± 0.73	4.87 ± 0.69	5.04 ± 0.51	4.16 ± 0.41	5.15 ± 1.08	3.95 ± 0.48	6.05 ± 0.74	4.91 ± 0.96
Cardiac profile								
Creatine kinase (U/L)	820 ± 393	762 ± 273	474 ± 61*	810 ± 401	345 ± 127**	416 ± 118	334 ± 56**	404 ± 116
LDH (U/L)	1,600 ± 507	1,557 ± 506	1,017 ± 235	1,613 ± 382	649 ± 296	1,144 ± 248	582 ± 104	951 ± 232
Lipid profile								
Cholesterol (mmol/L)	1.20 ± 0.29	1.54 ± 0.21	1.64 ± 0.24	1.78 ± 0.32	2.22 ± 0.34***	2.11 ± 0.44	2.68 ± 0.26***	2.99 ± 0.52***
Triglyceride (mmol/L)	0.39 ± 0.11	0.27 ± 0.07	0.82 ± 0.47	0.29 ± 0.03	0.99 ± 0.08*	0.57 ± 0.19**	0.75 ± 0.22	0.63 ± 0.16**
Lipase (U/L)	26 ± 1	28 ± 2	28 ± 1	28 ± 1	30 ± 1**	31 ± 2	38 ± 3***	38 ± 2***
Serum electrolytes								
Na <sup>+</sup> (mmol/L)	144.1 ± 0.6	145.1 ± 2.0	143.8 ± 1.7	144.5 ± 2.6	143.3 ± 1.1	144.8 ± 0.5	142.3 ± 1.4	144.5 ± 2.3
K <sup>+</sup> (mmol/L)	4.66 ± 0.27	4.54 ± 0.36	4.19 ± 0.32	4.74 ± 0.43	4.11 ± 0.36*	4.76 ± 0.65	3.97 ± 0.26**	4.49 ± 0.52
Cl <sup>-</sup> (mmol/L)	109.0 ± 2.6	102.6 ± 0.4	106.8 ± 2.4	102.2 ± 1.7	107.6 ± 2.8	101.4 ± 2.7	103.2 ± 2.0**	101.0 ± 1.2
Ca (mmol/L)	2.44 ± 0.07	2.50 ± 0.05	2.34 ± 0.06	2.45 ± 0.11	2.38 ± 0.07	2.42 ± 0.12	2.47 ± 0.06	2.41 ± 0.05
P (mmol/L)	2.96 ± 0.19	2.54 ± 0.25	2.67 ± 0.15*	2.41 ± 0.09	2.54 ± 0.13***	2.50 ± 0.18	2.65 ± 0.09**	2.36 ± 0.13
Mg (mmol/L)	0.76 ± 0.03	0.79 ± 0.02	0.74 ± 0.01	0.79 ± 0.02	0.72 ± 0.02	0.78 ± 0.03	0.73 ± 0.02	0.77 ± 0.02
Glucose profile								
Glucose (mmol/L)	6.65 ± 1.24	6.42 ± 0.71	5.50 ± 1.05	7.61 ± 1.43	6.73 ± 0.24	6.94 ± 0.66	6.68 ± 0.40	6.65 ± 0.52

Notes: Values are means ± standard deviation ( $n = 5$ ).

\* $p < 0.05$ .

\*\* $p < 0.01$ .

\*\*\* $p < 0.001$  vs. vehicle.

Abbreviations: ALP, alkaline phosphatase; ALT, alanine aminotransferase; AST, aspartate aminotransferase; LDH, lactate dehydrogenase.

including mitochondria and normal nucleus with regular nuclear membranes and nucleopores.

### 3.8 Toxicokinetics and tissue distribution

Sex-related differences in toxicokinetics were not observed following systemic exposure to IONPs, and the male/female ratio for  $C_{max}$  and area under the curve (AUC) were less than two-fold. Therefore, the toxicokinetic parameters and the mean concentration–time curves shown in Figures 3A,B include the combined data of male and female animals. After intravenous administration of IONPs,  $T_{max}$  appeared

at 5 min postdose,  $T_{1/2}$  was at approximately 2–4 h, and the mean residence time was within the range of 2–4 h. Systemic exposure expressed as  $C_{max}$  and AUC increased with increasing IONPs doses from 10 to 90 mg/kg close to or greater than the dose-proportion manner on days 1 and 14. IONPs accumulation after administration for 14 consecutive days was not observed at any dose. Tissue distribution analysis suggested that iron translocated into a range of tissues throughout the body, including the brain (cerebellum and cerebrum), heart, liver, spleen, kidneys, lungs, and mesenteric lymph nodes (Figures 3C–J). A dose-dependent increase in iron levels was observed in the spleen, liver, lungs, lymph nodes, kidneys, and heart. The accumulation pattern in organs

TABLE 2 Hematological parameters of rats treated with/without IONPs for 14 days.

Parameters	Vehicle		10 mg/kg		30 mg/kg		90 mg/kg	
	Male	Female	Male	Female	Male	Female	Male	Female
WBC (10 <sup>9</sup> /L)	4.42 ± 1.81	3.81 ± 1.16	8.14 ± 1.43*	3.91 ± 1.30	6.48 ± 1.91	6.43 ± 1.63	13.33 ± 2.21***	10.65 ± 3.05***
Ne (%)	13.4 ± 5.7	11.2 ± 4.8	15.3 ± 3.0	13.8 ± 5.5	16.6 ± 5.4	18.7 ± 5.3	30.5 ± 7.2***	24.2 ± 5.3**
Mo (%)	9.7 ± 3.6	8.1 ± 2.1	9.0 ± 1.4	9.9 ± 2.8	10.2 ± 2.5	10.1 ± 1.3	14.5 ± 4.0	10.5 ± 2.7
Ly (%)	76.0 ± 9.5	79.2 ± 7.0	75.1 ± 4.2	75 ± 7.4	72.4 ± 6.7	70.1 ± 5.2	54.1 ± 9.4**	64.1 ± 6.3**
Eo (%)	0.7 ± 0.5	1.1 ± 0.2	0.5 ± 0.3	1.0 ± 0.4	0.7 ± 0.4	0.9 ± 0.2	0.6 ± 0.3	0.9 ± 0.4
RBC (10 <sup>12</sup> /L)	6.56 ± 0.51	6.76 ± 0.35	6.67 ± 0.21	6.03 ± 0.52*	7.07 ± 0.45	6.23 ± 0.39	6.35 ± 0.38	6.47 ± 0.18
HGB (g/L)	134 ± 7	138 ± 7	137 ± 5	124 ± 6**	146 ± 4*	130 ± 4	131 ± 7	136 ± 2
HCT (%)	38.9 ± 1.8	39.5 ± 1.6	39.6 ± 0.8	36.3 ± 2.0*	41.9 ± 1.2**	38.3 ± 1.1	37.4 ± 1.5	40.0 ± 1.0
MCV (fL)	59.4 ± 2.4	58.4 ± 1.9	59.4 ± 0.8	60.3 ± 1.9	59.3 ± 2.7	61.5 ± 3.1	59.0 ± 1.7	61.8 ± 2.3
MCHC (g/dl)	34.4 ± 0.7	34.9 ± 0.6	34.6 ± 0.7	34.1 ± 0.4	34.9 ± 0.2	34.0 ± 0.7*	34.9 ± 1.0	33.9 ± 0.3*
PLT (10 <sup>9</sup> /L)	1,068 ± 88	1,142 ± 75	1,470 ± 178***	1,085 ± 577	1,245 ± 135	1,404 ± 158	1,037 ± 93	1,440 ± 112
MPV (fL)	7.5 ± 0.4	7.1 ± 0.2	7.1 ± 0.1	7.2 ± 0.4	7.2 ± 0.1	6.9 ± 0.2	7.6 ± 0.4	7.1 ± 0.1
Coagulation								
Fbg (g/L)	2.19 ± 0.11	1.79 ± 0.21	2.56 ± 0.09	2.26 ± 0.51	2.53 ± 0.12	2.30 ± 0.63	3.68 ± 0.54***	2.78 ± 0.31**
PT (s)	9.5 ± 0.3	7.4 ± 0.2	9.4 ± 0.9	7.2 ± 0.2	11.1 ± 1.6	7.1 ± 0.1*	9.1 ± 0.7	7.2 ± 0.1
APTT (s)	18.9 ± 1.1	12.7 ± 1.6	16.6 ± 3.7	13.8 ± 1.9	21.3 ± 2.8	13.3 ± 3.4	16.1 ± 3.0	12.5 ± 1.2
TT (s)	34.8 ± 1.7	30.3 ± 2.5	31.7 ± 5.3	29.5 ± 0.5	35.4 ± 4.9	30.1 ± 2.8	33.9 ± 1.8	30.1 ± 2.0

Notes: Values are means ± standard deviation ( $n = 5$ ).

\* $p < 0.05$ .

\*\* $p < 0.01$ .

\*\*\* $p < 0.001$  vs. vehicle.

Abbreviations: WBC, white blood cell count; Ne, neutrophil; Mo, monocyte; Ly, lymphocyte; Eo, eosinophil RBC, red blood cell count; HGB, hemoglobin; HCT, hematocrit; MCV, mean corpuscular volume; MCHC, mean corpuscular hemoglobin concentration; PLT, platelet count; MPV, mean platelet volume; Fbg, fibrinogen; PT, prothrombin time; APTT, activated partial thromboplastin time; TT, thrombin time.

was as follows: spleen > liver > lungs > mesenteric lymph nodes > kidneys > heart > brain.

### 3.9 Proteomics analysis of differentially expressed proteins in the spleen after iron oxide nanoparticles administration

#### 3.9.1 Protein identification

Traditional toxicological analyses indicated that spleen was the primarily affected organ, which was also involved in elimination after the intravenous administration of IONPs. However, no study has studied proteins with differential abundance in the spleen after IONPs exposure *in vivo*. Therefore, we used the TMT-based proteomics to investigate the changes in protein abundance in the spleen between the 90 mg/kg IONPs administration and vehicle groups.

The proteomes of the different administration groups were compared using Principal Component Analysis (PCA). As shown in Figure 4A, the PCA scatter plot showed differences in the DEPs profile between the 90 mg/kg IONPs and vehicle groups.

A total of 5,269 proteins were identified, and 5,104 proteins were quantified in the vehicle and IONPs groups. Among these, 272 DEPs, including 197 upregulated and 75 downregulated proteins, were in the IONPs group based on the comparison with the vehicle group (Figure 4B).

#### 3.9.2 Gene Ontology functional enrichment analysis of differentially expressed proteins

To further analyze the functional characteristics, the DEPs were annotated and enriched using GO analysis and classified into three ontological categories of cellular component, biological process, and molecular function. The GO enrichment analysis graph in Figure 4C shows the top 10 items enriched by  $p$  values in each category.

Briefly, in the 90 mg/kg IONPs group, 268 DEPs were enriched in 1,571 terms in the biological process category, including 110 terms that were significantly enriched. The most abundant biological process terms were the complement activation classical pathway (GO: 0006958), negative regulation of endopeptidase activity (GO: 0010951), acute-phase response (GO: 0006953), cellular iron ion homeostasis (GO: 0006879), and vasodilation (GO: 0042311). In the cellular component category,

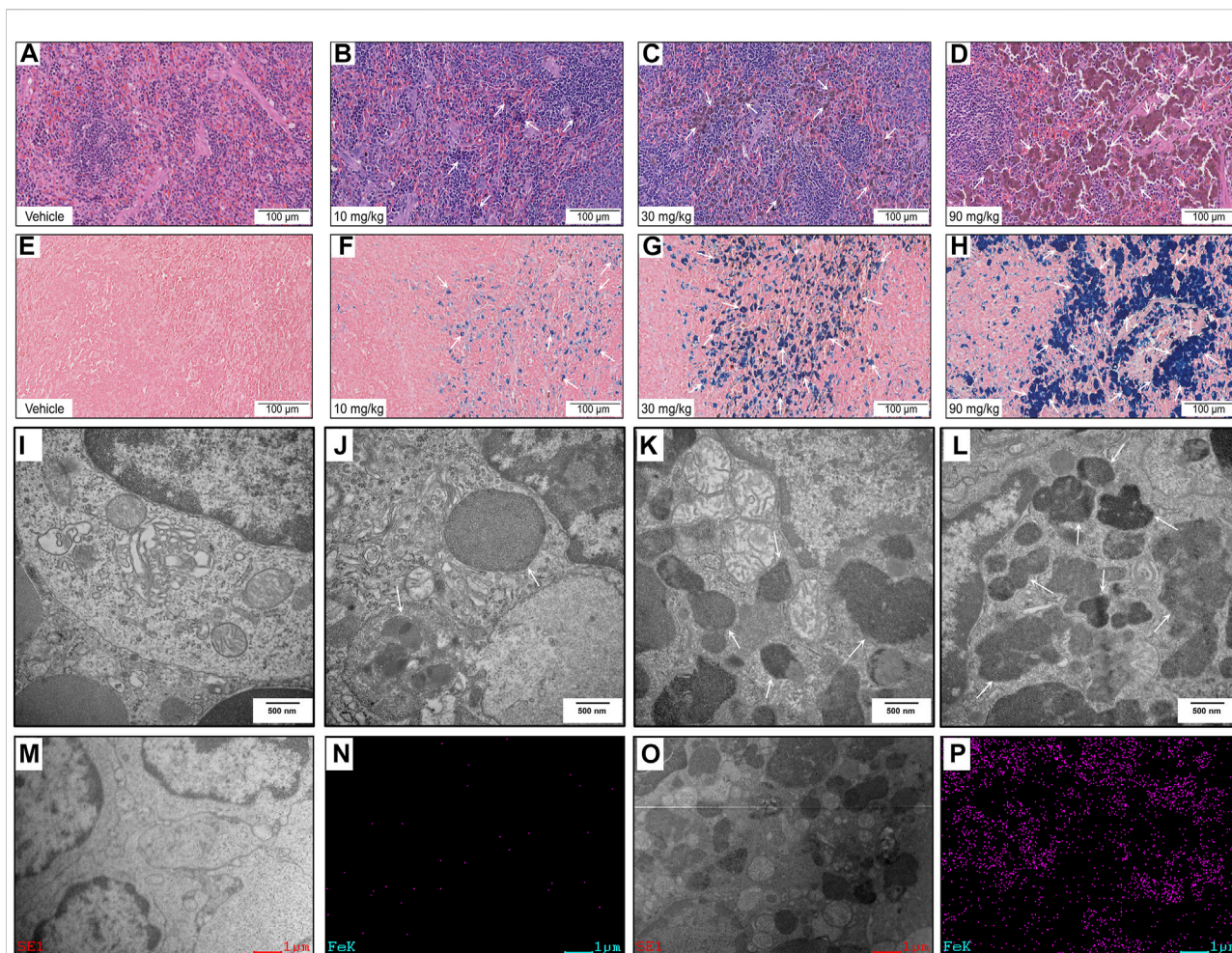


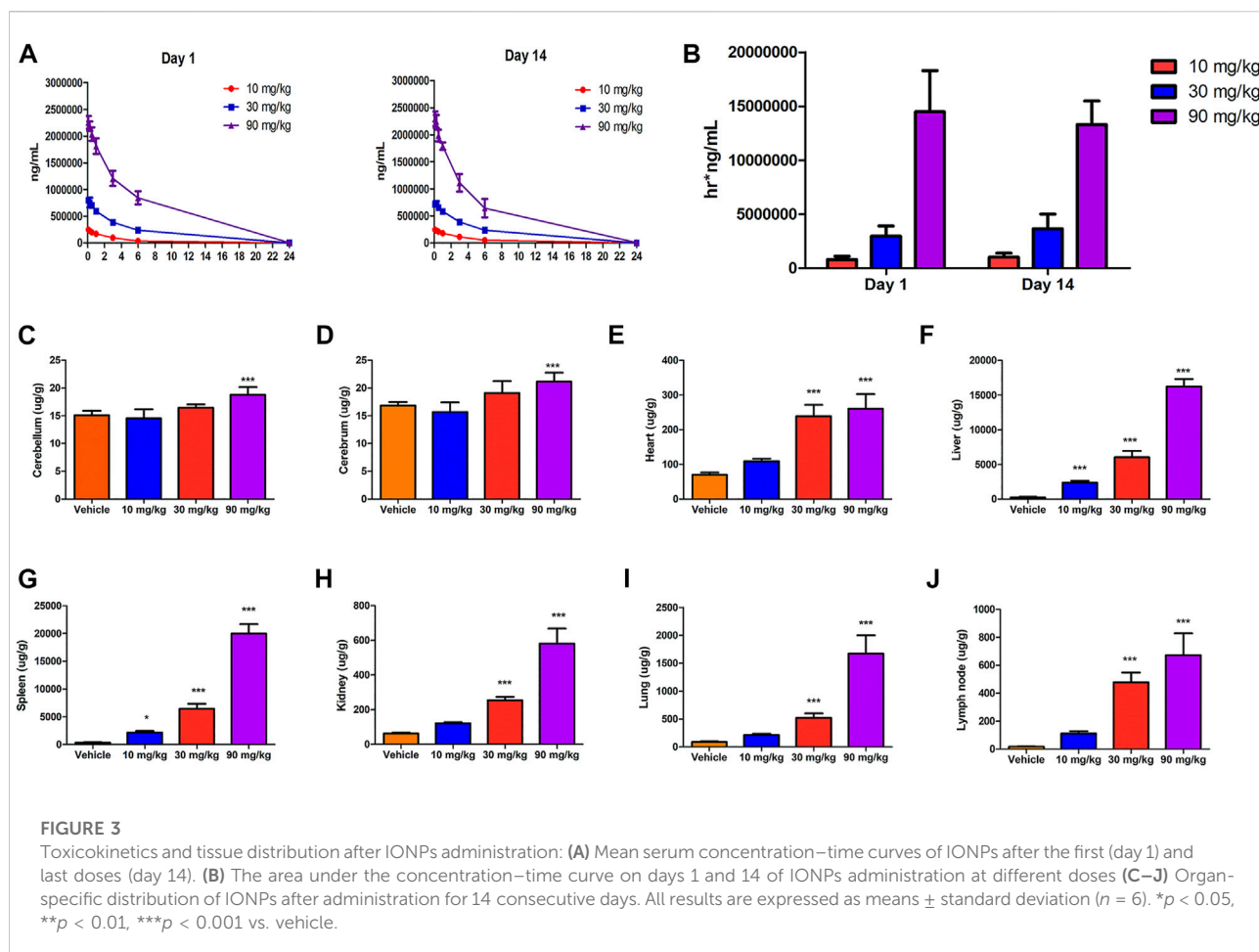
**FIGURE 2**

Histopathology and ultrastructural alterations in the spleen: (A–H) Representative images of specimens stained with hematoxylin and eosin (A–D) and Perls' Prussian blue (E–H) after treatment with vehicle or IONPs for 14 days. (I–L) Representative transmission electron microscopy (TEM) images of spleen specimens following treatment with vehicle or IONPs for 14 days. (M–P) TEM-energy-dispersive spectrometry (EDS) analysis of the spleen after treatment with vehicle or 90 mg/kg IONPs for 14 days; (M,O) and (N,P) show the TEM and corresponding iron element distribution in the EDS images of the spleens after treatment with vehicle and IONPs, respectively. The EDS images show the element distribution of iron in the entire TEM image.

32 out of the 287 terms were significantly enriched and the five terms with the highest enrichment degree were extracellular space (GO: 0005615), lysosome (GO: 0005764), lysosomal membrane (GO: 0005765), late endosome (GO: 0005770), and high-density lipoprotein particle (GO: 0034364). Of a total of 442 terms enriched in the molecular function category, 37 were significantly enriched. The five most enriched terms were identical protein binding (GO: 0042802), protein-containing complex binding (GO: 0044877), serine-type endopeptidase inhibitor activity (GO: 0004867), heparin binding (GO: 0008201), and proton-transporting ATPase activity, rotational mechanism (GO: 0046961) (Figure 4C).

### 3.1.3 Pathway enrichment analysis of differentially expressed proteins

We also analyzed the effect of IONPs 90 mg/kg administration on protein expression using KEGG pathway analysis. The analysis showed enrichment in 153 differentially abundant proteins in 226 pathways in the IONPs group, and 37 pathways were significantly enriched ( $p < 0.05$ ). We noted significant enrichment in the expression of proteins involved in the lysosome, phagosome, rheumatoid arthritis, mTOR signaling pathway, oxidative phosphorylation, complement and coagulation cascades, collecting duct acid secretion, neutrophil extracellular trap formation and cholesterol metabolism were significantly enriched compared with the vehicle group,



respectively. Overall, transport and catabolism, and the immune and excretory systems were significantly enriched by DEPs identified between the 90 mg/kg IONPs group and vehicle group (Figure 4D).

### 3.9.4 Iron oxide nanoparticles administration leads to lysosomal activation and autophagy in splenic macrophages

We analyzed proteomic data of 90 mg/kg spleen after IONPs administration using heatmaps and found significant differences in most proteins associated with lysosomal activation and autophagy (Figure 5A). The abundance of LAMP1, LAMP2, and NPC1 was significantly higher in the 30 and 90 mg/kg IONPs groups than in the vehicle group (Figures 5C–F). LAMP1 and LAMP2 play crucial roles in lysosomal enzyme targeting, autophagy, and lysosomal biogenesis (Fukuda, 1991; Eskelinen et al., 2003; Eskelinen et al., 2004; Huynh et al., 2007). NPC1 is a polytopic membrane protein located in the membranes of endosomes and lysosomes (Qian et al., 2020). TEM results showed dose-dependent increase of AVDs in

splenic macrophages after IONPs administration. Therefore, these results indicated the lysosomal activation of splenic macrophages after IONPs administration. Meanwhile, the increase in LC3-II expression and the turnover of LC3-I to LC3-II indicated the activation of autophagy in spleen (Figures 5B,C). The activation of the lysosome-dependent autophagy can lead to IONPs degradation and to the liberate of free iron ions, which may trigger the excessive production of reactive oxygen species, cellular damage, and inflammatory response. FTH1 is the major protein responsible for the intracellular storage of iron in a soluble and nontoxic state. In the present study, the increase in FTH1 protein levels indicated that the degraded iron released from the IONPs was sequestered and stored in a nontoxic and bioavailable state (Figures 5C,D).

### 3.9.5 The AKT/mTOR/TFEB signaling pathway facilitates in iron oxide nanoparticles-induced autophagy

We also found that the IONPs-induced autophagy by inhibiting the AKT/mTOR signaling pathway in a dose-

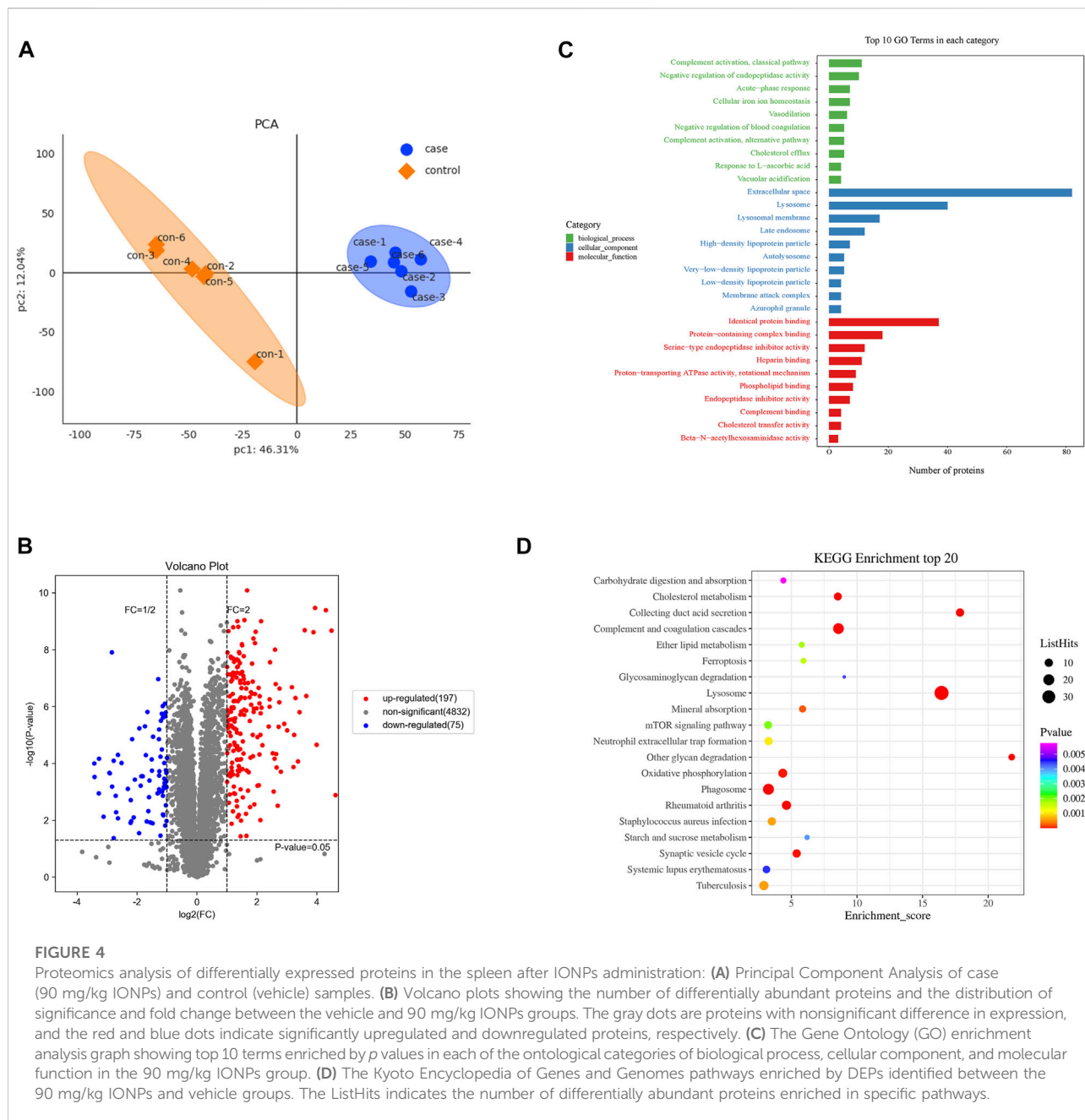


FIGURE 4

Proteomics analysis of differentially expressed proteins in the spleen after IONPs administration: **(A)** Principal Component Analysis of case (90 mg/kg IONPs) and control (vehicle) samples. **(B)** Volcano plots showing the number of differentially abundant proteins and the distribution of significance and fold change between the vehicle and 90 mg/kg IONPs groups. The gray dots are proteins with nonsignificant difference in expression, and the red and blue dots indicate significantly upregulated and downregulated proteins, respectively. **(C)** The Gene Ontology (GO) enrichment analysis graph showing top 10 terms enriched by  $p$  values in each of the ontological categories of biological process, cellular component, and molecular function in the 90 mg/kg IONPs group. **(D)** The Kyoto Encyclopedia of Genes and Genomes pathways enriched by DEPs identified between the 90 mg/kg IONPs and vehicle groups. The ListHits indicates the number of differentially abundant proteins enriched in specific pathways.

dependent fashion (Figures 6A,B). As an important transcription factor of autophagy downstream of the mTOR signaling pathway, TFEB in the spleen was significantly activated after IONPs administration. TFEB has been shown to be able to couple with autophagosomes to promote the maturation of LC3-driven autophagosomes and to regulate the fusion of autophagosomes with lysosomes. In the present study, we observed that the AKT/mTOR signaling pathway was inhibited and that the TFEB activity was significantly increased, which might be a primary mechanism by which IONPs induce autophagy in the spleen.

## 4 Discussion

IONPs have vast potential for utility in biomedical applications, especially magnetic resonance imaging (Liu et al., 2013; Dadfar et al., 2019). However, the toxicity profile of intravenously administered IONPs has not been fully elucidated. In the present study, we intravenously delivered IONPs in rats and evaluated toxicity and IONPs mechanisms using traditional toxicological assessment methods, such as physiological observations, clinical pathology, and histopathology, in combination with emerging proteomics analyses.

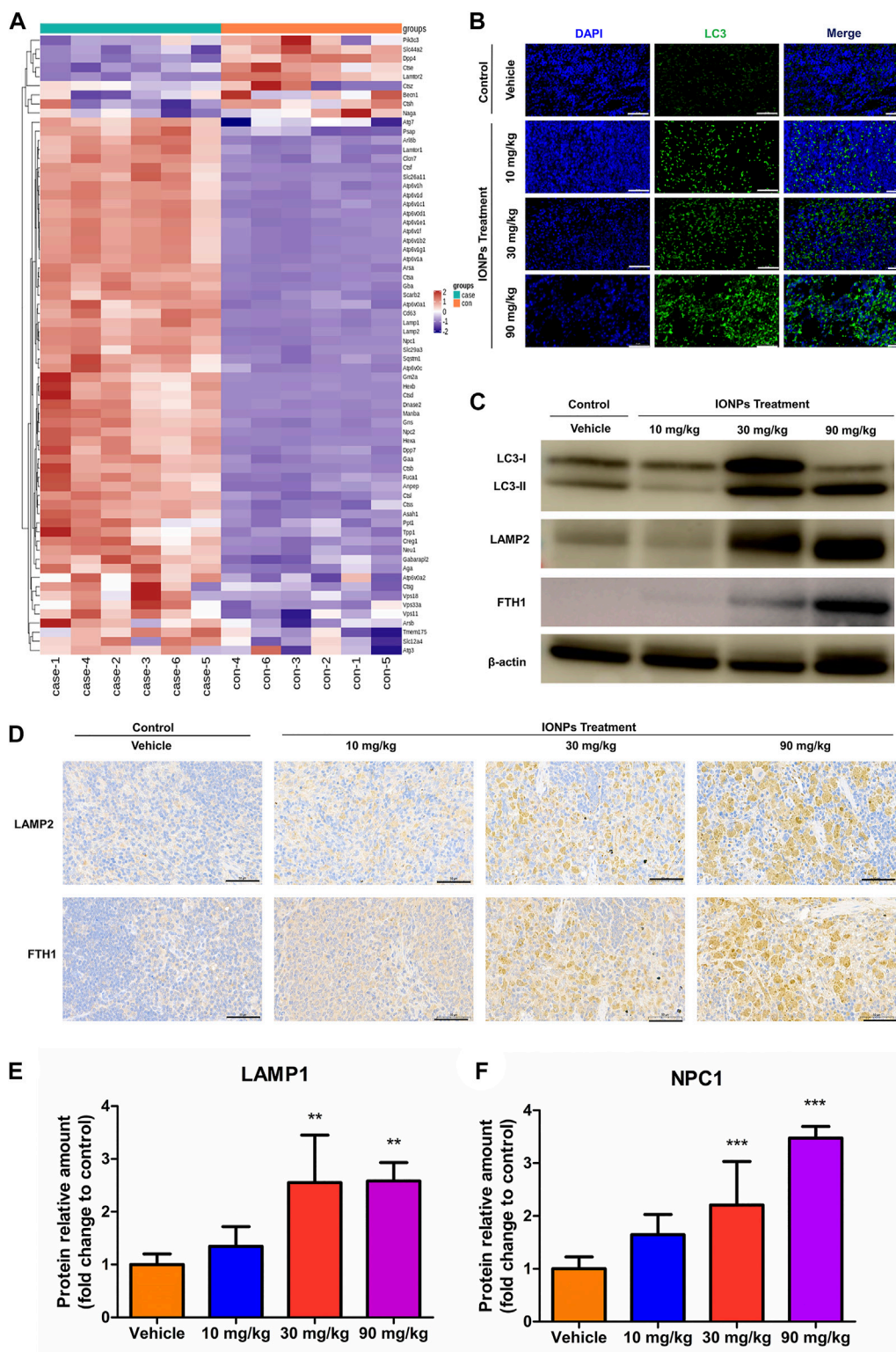
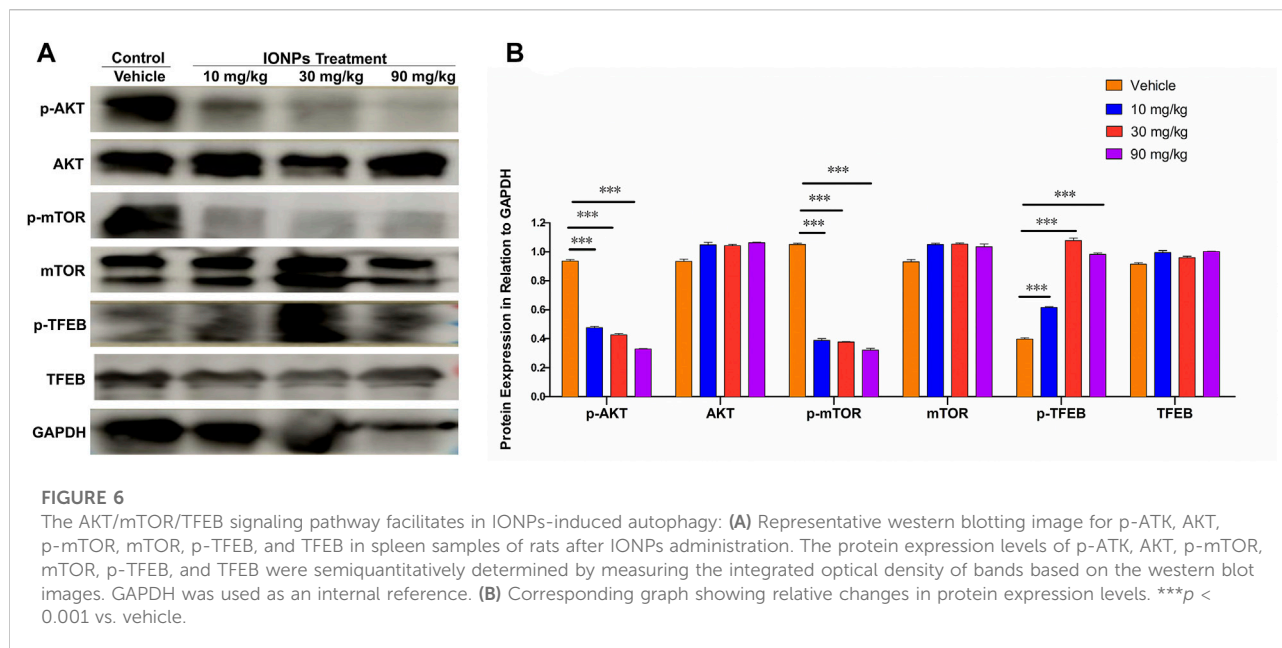


FIGURE 5

IONPs administration leads to lysosomal activation and autophagy in splenic macrophages: (A) Clustering heatmap of differentially expressed proteins associated with lysosomal activation (B) Immunofluorescence staining showing the expression of light chain 3 (LC3) in spleen specimens collected from rats treated with vehicle or different doses of IONPs. Nuclei are stained with DAPI. Scale bars: 50  $\mu$ m. (C) The protein levels of LC3, FTH1, and LAMP2 were analyzed using western blotting, and  $\beta$ -actin was used as internal reference (D) Immunohistochemical staining showing the expression of ferritin heavy chain 1 (FTH1) and lysosome-associated membrane protein (LAMP) 2 in spleen specimens of rats treated with vehicle or different doses of IONPs. (E) and (F) The verification of LAMP1 and NPC1 abundance using parallel reaction monitoring. Data are shown as means  $\pm$  standard deviation ( $n = 6$ ). \*\* $p < 0.01$ , \*\*\* $p < 0.001$  vs. vehicle.



The established toxicological tests revealed that the administration of 90 mg/kg IONPs led to mild clinical signs and lower body weight gains in male rats. Serum biochemical analyses indicated that IONPs did not exert an obvious adverse effect on hepatic, renal, and cardiac functions. However, the increases in total bile acids, cholesterol, triglycerides, and lipase suggested a lipid metabolism disorder. Similarly, persistent iron-enriched diet fed to rats led to the impairment in the plasma lipid transport and hepatic sterol metabolism (Brunet et al., 1999). Dietary iron overload induces lipid peroxidation and increases in cholesterol and triglycerides, indicating the risk of hyperlipidemia. Meanwhile, the increase in total bile acids is related to cholesterol metabolism. Overall, these findings indicated that the altered lipid transport and cholesterol metabolism were related to the iron overload following IONPs administration. Hematological assessment revealed increases in leucocyte count and neutrophil percentage in the 90 mg/kg IONPs group, although there were no findings of evident inflammation during histopathological examination in entire organs. Neutrophils drive effecting mechanisms through phagocytosis, degranulation, and neutrophil extracellular traps (NET) formation (Burn et al., 2021). Studies investigating nanomaterial clearance by the immune system indicate that NETs act as physical barriers for nanoparticles (Bartneck et al., 2009). Consistently, Kuzmicka et al. demonstrated that excess iron increased the release of NETs and reactive oxygen species (Kuzmicka et al., 2022). Therefore, the observed increases in the leucocyte count and neutrophil percentage indicate a primary immune response and a potential mechanism of clearance of the IONPs from the systemic circulation after intravenous administration.

Toxicokinetic analysis showed that IONPs exhibited an appropriate elimination rate and a favorable dose-response relationship in the blood after intravenous administration. The tissue distribution results indicated that IONPs were delivered to a range of organ systems after entering the systemic circulation, in accordance with the results from numerous studies (Yu et al., 2018; Gaharwar et al., 2019; Bolandparvaz et al., 2020). In the present study, the highest IONPs deposition in the spleen and liver indicated that these two organs played the most important role in IONPs elimination from the systemic circulation. The increases in the size and organ coefficient of the spleen and liver were consistent with the iron levels obtained through the tissue distribution analysis. Both the spleen and the liver contain a large number of macrophages, including Kupffer cells in the liver, and are highly vascular, which are considered to exhibit prominent ability to actively capture the IONPs (Allard-Vannier et al., 2012; Barrefelt et al., 2013; Vercoza et al., 2019).

Histopathology findings were limited to pigmentation in multiple organs, which was confirmed as iron deposits using Perls' Prussian blue staining, and cellular structural alterations were absent. These results demonstrated that IONPs administration had no adverse effect on microscopic morphology in any of the examined organs (Supplementary Table S1). Further ultrastructure examination of the spleen, which exhibited the highest iron accumulation, indicated that IONPs did not lead to subcellular structural changes, except for the dose-dependent increase in AVDs. TEM-EDS revealed the elemental enrichment of these AVDs as the subcellular distribution of the IONPs expressed as elemental iron. Our results are in accordance with previous *in vitro* studies in

macrophages demonstrating the internalization of IONPs in a membrane-bound manner (Gu et al., 2011).

Proteomics is a powerful method to examine the mechanism of IONPs toxicity in studies evaluating their safety. The identification of the DEPs and the GO enrichment analysis revealed that the DEPs induced by the IONPs, compared with the vehicle group, were mainly involved in the cellular component category. Extracellular space, the GO term with the highest enrichment in the cellular component category, is potentially related to the gross pathological finding of increased spleen size (Mo, 2017). Complement activation, which was enriched in both the GO and KEGG pathway analyses, was not considered toxicologically meaningful because of the possible development of pseudoallergy by the rapid injection of iron-containing products (Rampton et al., 2014; Hempel et al., 2017). The significant enrichment of the term cholesterol metabolism was consistent with the changes in total bile acids, cholesterol, triglycerides, and lipase noted in serum biochemical analysis. NPC1, a multimembrane-spanning protein, is the central protein for lysosomal transfer of cholesterol (Meng et al., 2020). The trend in the protein expression was fully consistent with the results of the serum biochemistry tests. Therefore, the proteomics analyses used in the present study revealed the mechanisms of IONPs toxicity.

Numerous studies investigating nanoparticle uptake mechanisms have exhibited that endocytosis is the main route for the cellular entry of the nanoparticles and that the endocytic entry can be subdivided into the categories of phagocytosis, clathrin/caveolin-independent endocytosis, clathrin-mediated endocytosis, caveolin-mediated endocytosis, and micropinocytosis (Mailänder and Landfester, 2009; Nel et al., 2009; Francia et al., 2020; Yao et al., 2020). Phagosome was a highly enriched term in the KEGG pathway analysis of the proteomics results, demonstrating phagocytosis as the main mechanism of IONPs entry into splenic macrophages. Notably, the increase in AVDs and the abundance of lysosome-related terms noted in the GO and KEGG analyses indicate that lysosome-mediated degradation plays a crucial role in responses to IONPs administration. In fact, macrophages were shown to engulf and accumulate IONPs in lysosomes (Lunov et al., 2011a; Lunov et al., 2011b; Beddoes et al., 2015). The process for the intracellular biodegradation of IONPs can be quite long, and IONPs may retain in the body from several days to several weeks after intravenous injection (Lunov et al., 2010; Feng et al., 2018; Van de Walle et al., 2020). Therefore, it is plausible that IONPs substantially modulate lysosome-related signaling pathways. Many processes involved in cell death and pathological conditions have been shown to be associated with lysosomal dysfunction (Boya and Kroemer, 2008). Overall, our results revealed that the lysosome-related signaling pathways are the primary mechanism of IONPs toxicity in the spleen after intravenous administration.

The upregulation of both LAMP1 and LAMP2 confirmed in the present study indicates increases in lysosomal biogenesis and autophagic activity after IONPs administration. Notably, IONPs

induce autophagy in numerous cultured cell types *in vitro* (Jin et al., 2019; Uzhychak et al., 2020), which has not been thoroughly confirmed in animal models *in vivo*. Interestingly, the degree of autophagy, expressed as the turnover of the microtubule-associated protein LC3 (Mizushima et al., 2010), was significantly increased in a dose-related manner after IONPs administration in the present study. The AKT/mTOR signaling pathway inhibition has been reported to induce autophagy in human fetal neural stem cells fNSCs (Liang et al., 2016) and human lung cancer cells H460 cells (Fu et al., 2009) as well as the mouse mammary epithelial cells HC11 (Hou et al., 2020). mTOR is generally located on the lysosomal membrane, and TFEB in the cytoplasm is phosphorylated by mTOR under normal conditions, inducing mTOR activation (Settembre et al., 2012). Conversely, under pathological conditions, TFEB translocates from the cytoplasm to the nucleus, leading to the upregulation of autophagic proteins while mTOR is released from the lysosomal membrane, and the ensuing inhibition of mTOR activity can promote autophagy (Sardiello et al., 2009; Rocznik-Ferguson et al., 2012). In the present study, the AKT and mTOR activities in the spleen were significantly decreased after IONPs administration. The mTOR/TFEB signaling pathway, which is crucial for lysosomal biogenesis and autophagy activation, was significantly activated. Interestingly, the p-TFEB increased in the IONPs treated groups, but it was not higher in the 90 mg/kg group than in the 30 mg/kg group. This may be because of the *in vivo* environment has been significantly altered by the administration of 90 mg/kg IONPs, which may reduce p-TFEB, consistent with in previous study (Ballabio, 2016). This is worth exploring more profound in future work. Autophagy is dependent on lysosomal degradation, which has been demonstrated to be an important regulator of various diseases and conditions (Mizushima and Levine, 2020; Jiang et al., 2021; Viret et al., 2021). Park et al. (2014) at Demonstrated that autophagy was an important protective mechanism of IONPs-induced apoptotic cell death and endoplasmic reticulum stress in RAW264.7 cells. Not surprisingly, rats treated with IONPs for 14 days did not exhibit severe inflammatory or toxic reactions based on the roles of autophagy in stress adaptation, immune, and inflammatory response (Cadwell, 2016). However, some studies showed that IONPs caused cell damage by inducing autophagy (Du et al., 2016; Zhang et al., 2020). Therefore, the role of autophagy in IONPs toxicity remains to be further elucidated.

Iron is an essential component of the human body, playing a crucial role in the activity of cytochromes, hemoproteins, and hemoglobin (Andrews, 2000). However, iron overload causes cell dysfunction and death, leading to tissue damage and organ dysfunction (Trinder et al., 2002). FTH1 is a universally expressed and highly conserved protein that plays a major role in iron balance by sequestering and storing ions in a nontoxic and bioavailable manner (Munro et al., 1988; Edison et al., 2008). In the present study, FTH1 expression was significantly upregulated, suggesting the sequestration of iron released from the lysosomal IONPs degradation. Therefore, no obvious toxicity due to iron overload was noted after the intravenous IONPs administration in rats.

## 5 Conclusion

This is the first study utilizing a combination of traditional and emerging proteomics methods to assess IONPs toxicity following intravenous administration in rats and to elucidate underlying mechanisms. We showed that the lysosome is the master regulator of IONPs-mediated toxicity in spleen, the target organ of intravenously administered IONPs, and that the lysosome-related signaling pathways are the primary mechanism of toxicity in splenic macrophages. We also showed that the AKT/mTOR/TFEB signaling pathway facilitates in the IONPs-induced autophagy of splenic macrophages.

## Data availability statement

The datasets presented in this study can be found in online repositories. The names of the repository/repositories and accession number(s) can be found below: ProteomeXchange Consortium (<http://proteomecentral.proteome.mexchange.org>) via the iProX partner repository with the dataset identifier PXD035970.

## Ethics statement

The animal study was reviewed and approved by Institutional Animal Care and Use Committee of National Beijing Center for Drug Safety Evaluation and Research.

## References

- Allard-Vannier, E., Cohen-Jonathan, S., Gautier, J., Herve-Aubert, K., Munnier, E., Souce, M., et al. (2012). Pegylated magnetic nanocarriers for doxorubicin delivery: A quantitative determination of stealthiness *in vitro* and *in vivo*. *Eur. J. Pharm. Biopharm.* 81 (3), 498–505. doi:10.1016/j.ejpb.2012.04.002
- Anderson, S. D., Gwenin, V. V., and Gwenin, C. D. (2019). Magnetic functionalized nanoparticles for biomedical, drug delivery and imaging applications. *Nanoscale Res. Lett.* 14 (1), 188. doi:10.1186/s11671-019-3019-6
- Andrews, N. C. (2000). Iron homeostasis: Insights from genetics and animal models. *Nat. Rev. Genet.* 1 (3), 208–217. doi:10.1038/35042073
- Askri, D., Cunin, V., Beal, D., Berthier, S., Chovelon, B., Arnaud, J., et al. (2019a). Investigating the toxic effects induced by iron oxide nanoparticles on neuroblastoma cell line: An integrative study combining cytotoxic, genotoxic and proteomic tools. *Nanotoxicology* 13 (8), 1021–1040. doi:10.1080/17435390.2019.1621399
- Askri, D., Cunin, V., Ouni, S., Beal, D., Rachidi, W., Sakly, M., et al. (2019b). Effects of iron oxide nanoparticles (gamma-Fe<sub>2</sub>O<sub>3</sub>) on liver, lung and brain proteomes following sub-acute intranasal exposure: A new toxicological assessment in rat model using iTRAQ-based quantitative proteomics. *Int. J. Mol. Sci.* 20 (20), E5186. doi:10.3390/ijms20205186
- Ballabio, A. (2016). The awesome lysosome. *EMBO Mol. Med.* 8 (2), 73–76. doi:10.15252/emmm.201505966
- Barrefelt, A., Saghafian, M., Kuiper, R., Ye, F., Egri, G., Klickermann, M., et al. (2013). Biodistribution, kinetics, and biological fate of SPION microbubbles in the rat. *Int. J. Nanomedicine* 8, 3241–3254. doi:10.2147/IJN.S49948
- Bartneck, M., Keul, H. A., Zwadlo-Klarwasser, G., and Groll, J. (2009). Phagocytosis independent extracellular nanoparticle clearance by human immune cells. *Nano Lett.* 10 (1), 59–63. doi:10.1021/nl902830x
- Beddoes, C. M., Case, C. P., and Briscoe, W. H. (2015). Understanding nanoparticle cellular entry: A physicochemical perspective. *Adv. Colloid Interface Sci.* 218, 48–68. doi:10.1016/j.cis.2015.01.007
- Bobo, D., Robinson, K. J., Islam, J., Thurecht, K. J., and Corrie, S. R. (2016). Nanoparticle-based Medicines: A review of FDA-approved materials and clinical trials to date. *Pharm. Res.* 33 (10), 2373–2387. doi:10.1007/s11095-016-1958-5
- Bolandparvaz, A., Vapniarsky, N., Harriman, R., Alvarez, K., Saini, J., Zang, Z., et al. (2020). Biodistribution and toxicity of epitope-functionalized dextran iron oxide nanoparticles in a pregnant murine model. *J. Biomed. Mat. Res. A* 108 (5), 1186–1202. doi:10.1002/jbm.a.36893
- Boya, P., and Kroemer, G. (2008). Lysosomal membrane permeabilization in cell death. *Oncogene* 27 (50), 6434–6451. doi:10.1038/onc.2008.310
- Brunet, S., Thibault, L., Delvin, E., Yotov, W., Bendayan, M., and Levy, E. (1999). Dietary iron overload and induced lipid peroxidation are associated with impaired plasma lipid transport and hepatic sterol metabolism in rats. *Hepatology* 29 (6), 1809–1817. doi:10.1002/hep.510290612
- Burn, G. L., Foti, A., Marsman, G., Patel, D. F., and Zychlinsky, A. (2021). The neutrophil. *Immunity* 54 (7), 1377–1391. doi:10.1016/j.immuni.2021.06.006
- Cadwell, K. (2016). Crosstalk between autophagy and inflammatory signalling pathways: Balancing defence and homeostasis. *Nat. Rev. Immunol.* 16 (11), 661–675. doi:10.1038/nri.2016.100
- Chen, S., Zhang, Y., and Zhan, Q. (2021). TMT-Based proteomics analysis of LPS-induced acute lung injury. *Exp. Lung Res.* 47 (8), 402–415. doi:10.1080/01902148.2021.1981494
- Christop, V. V., Mironov, V. A., Prilepskii, A. Y., Nikonorova, V. G., and Vinogradov, V. V. (2021). Organ-specific toxicity of magnetic iron oxide-based

## Author contributions

JH, YZ, and MW designed the experiments; JH wrote the manuscript; JH, YZ, MW, YL, JY, WQ, CY, and RD performed experiments and modified the procedures; YG and QW supervised the work and critically revised the manuscript. All authors read and approved the final manuscript.

## Funding

This work was supported by the National Key Research and Development Program of China (2018YFA0208802).

## Conflict of interest

The authors declare that the research was conducted in the absence of any commercial or financial relationships that could be construed as a potential conflict of interest.

## Supplementary material

The Supplementary Material for this article can be found online at: <https://www.frontiersin.org/articles/10.3389/fphar.2022.1011065/full#supplementary-material>

- nanoparticles. *Nanotoxicology* 15 (2), 167–204. doi:10.1080/17435390.2020.1842934
- Dadfar, S. M., Roemhild, K., Drude, N. L., von Stillfried, S., Knuchel, R., Kiessling, F., et al. (2019). Iron oxide nanoparticles: Diagnostic, therapeutic and theranostic applications. *Adv. Drug Deliv. Rev.* 138, 302–325. doi:10.1016/j.addr.2019.01.005
- Du, J., Zhu, W., Yang, L., Wu, C., Lin, B., Wu, J., et al. (2016). Reduction of polyethylenimine-coated iron oxide nanoparticles induced autophagy and cytotoxicity by lactosylation. *Regen. Biomater.* 3 (4), 223–229. doi:10.1093/rb/rbw023
- Edison, E. S., Bajel, A., and Chandy, M. (2008). Iron homeostasis: New players, newer insights. *Eur. J. Haematol.* 81 (6), 411–424. doi:10.1111/j.1600-0609.2008.01143.x
- Eskelinen, E.-L., Tanaka, Y., and Saftig, P. (2003). At the acidic edge: Emerging functions for lysosomal membrane proteins. *Trends Cell. Biol.* 13 (3), 137–145. doi:10.1016/s0962-8924(03)00005-9
- Eskelinen, E. L., Schmidt, C. K., Neu, S., Willenborg, M., Fuertes, G., Salvador, N., et al. (2004). Disturbed cholesterol traffic but normal proteolytic function in LAMP-1/LAMP-2 double-deficient fibroblasts. *Mol. Biol. Cell.* 15 (7), 3132–3145. doi:10.1091/mbc.e04-02-0103
- Feng, Q., Liu, Y., Huang, J., Chen, K., Huang, J., and Xiao, K. (2018). Uptake, distribution, clearance, and toxicity of iron oxide nanoparticles with different sizes and coatings. *Sci. Rep.* 8 (1), 2082. doi:10.1038/s41598-018-19628-z
- Francia, V., Montizaan, D., and Salvati, A. (2020). Interactions at the cell membrane and pathways of internalization of nano-sized materials for nanomedicine. *Beilstein J. Nanotechnol.* 11, 338–353. doi:10.3762/bjnano.11.25
- Frohlich, E. (2017). Role of omics techniques in the toxicity testing of nanoparticles. *J. Nanobiotechnology* 15 (1), 84. doi:10.1186/s12951-017-0320-3
- Frtus, A., Smolkova, B., Zhytychak, M., Lunova, M., Jirsa, M., Kubinova, S., et al. (2020). Analyzing the mechanisms of iron oxide nanoparticles interactions with cells: A road from failure to success in clinical applications. *J. Control. Release* 328, 59–77. doi:10.1016/j.jconrel.2020.08.036
- Fu, L., Kim, Y. A., Wang, X., Wu, X., Yue, P., Lonial, S., et al. (2009). Perifosine inhibits mammalian target of rapamycin signaling through facilitating degradation of major components in the mTOR axis and induces autophagy. *Cancer Res.* 69 (23), 8967–8976. doi:10.1158/0008-5472.CAN-09-2190
- Fukuda, M. (1991). Lysosomal membrane glycoproteins. Structure, biosynthesis, and intracellular trafficking. *J. Biol. Chem.* 266 (32), 21327–21330. doi:10.1016/s0021-9258(18)54636-6
- Gaharwar, U. S., Meena, R., and Rajamani, P. (2019). Biodistribution, clearance and morphological alterations of intravenously administered iron oxide nanoparticles in male wistar rats. *Int. J. Nanomedicine* 14, 9677–9692. doi:10.2147/IJN.S223142
- Gu, J., Xu, H., Han, Y., Dai, W., Hao, W., Wang, C., et al. (2011). The internalization pathway, metabolic fate and biological effect of superparamagnetic iron oxide nanoparticles in the macrophage-like RAW264.7 cell. *Sci. China. Life Sci.* 54 (9), 793–805. doi:10.1007/s11427-011-4215-5
- Hempel, J. C., Poppelars, F., Gaya da Costa, M., Franssen, C. F., de Vlaam, T. P., Daha, M. R., et al. (2017). Distinct *in vitro* complement activation by various intravenous iron preparations. *Am. J. Nephrol.* 45 (1), 49–59. doi:10.1159/000451060
- Hou, J., Zhao, L., Tang, H., He, X., Ye, G., Shi, F., et al. (2020). Silver nanoparticles induced oxidative stress and mitochondrial injuries mediated autophagy in HC11 cells through akt/AMPK/mTOR pathway. *Biol. Trace Elem. Res.* 199 (3), 1062–1073. doi:10.1007/s12011-020-02212-w
- Huynh, K. K., Eskelinen, E. L., Scott, C. C., Malevanets, A., Saftig, P., and Grinstein, S. (2007). LAMP proteins are required for fusion of lysosomes with phagosomes. *EMBO J.* 26 (2), 313–324. doi:10.1038/sj.emboj.7601511
- Jiang, T., Chen, X., Ren, X., Yang, J. M., and Cheng, Y. (2021). Emerging role of autophagy in anti-tumor immunity: Implications for the modulation of immunotherapy resistance. *Drug resist. updat.* 56, 100752. doi:10.1016/j.drug.2021.100752
- Jiao, M., Zeng, J., Jing, L., Liu, C., and Gao, M. (2015). Flow synthesis of biocompatible Fe<sub>3</sub>O<sub>4</sub> nanoparticles: Insight into the effects of residence time, fluid velocity, and tube reactor dimension on particle size distribution. *Chem. Mat.* 27 (4), 1299–1305. doi:10.1021/cm504313c
- Jin, R., Liu, L., Zhu, W., Li, D., Yang, L., Duan, J., et al. (2019). Iron oxide nanoparticles promote macrophage autophagy and inflammatory response through activation of toll-like Receptor-4 signaling. *Biomaterials* 203, 23–30. doi:10.1016/j.biomaterials.2019.02.026
- Kuzmicka, W., Manda-Handzlik, A., Mroczek, A., Cieloch, A., Moskalik, A., Demkow, U., et al. (2022). Iron excess affects release of neutrophil extracellular traps and reactive oxygen species but does not influence other functions of neutrophils. *Immunol. Cell. Biol.* 100 (2), 87–100. doi:10.1111/imcb.12509
- Liang, Q., Luo, Z., Zeng, J., Chen, W., Foo, S.-S., Lee, S.-A., et al. (2016). Zika virus NS4A and NS4B proteins deregulate akt-mTOR signaling in human fetal neural stem cells to inhibit neurogenesis and induce autophagy. *Cell. Stem Cell.* 19 (5), 663–671. doi:10.1016/j.stem.2016.07.019
- Liu, G., Gao, J., Ai, H., and Chen, X. (2013). Applications and potential toxicity of magnetic iron oxide nanoparticles. *Small* 9 (9–10), 1533–1545. doi:10.1002/smll.201201531
- Lunov, O., Syrovets, T., Loos, C., Beil, J., Delacher, M., Tron, K., et al. (2011a). Differential uptake of functionalized polystyrene nanoparticles by human macrophages and a monocytic cell line. *ACS Nano* 5 (3), 1657–1669. doi:10.1021/nn2000756
- Lunov, O., Syrovets, T., Rocker, C., Tron, K., Nienhaus, G. U., Rasche, V., et al. (2010). Lysosomal degradation of the carboxydextran shell of coated superparamagnetic iron oxide nanoparticles and the fate of professional phagocytes. *Biomaterials* 31 (34), 9015–9022. doi:10.1016/j.biomaterials.2010.08.003
- Lunov, O., Zablotskii, V., Syrovets, T., Rocker, C., Tron, K., Nienhaus, G. U., et al. (2011b). Modeling receptor-mediated endocytosis of polymer-functionalized iron oxide nanoparticles by human macrophages. *Biomaterials* 32 (2), 547–555. doi:10.1016/j.biomaterials.2010.08.111
- Mahmoudi, M., Hofmann, H., Rothen-Rutishauser, B., and Petri-Fink, A. (2012). Assessing the *in vitro* and *in vivo* toxicity of superparamagnetic iron oxide nanoparticles. *Chem. Rev.* 112 (4), 2323–2338. doi:10.1021/cr2002596
- Mailänder, V., and Landfester, K. (2009). Interaction of nanoparticles with cells. *Biomacromolecules* 10 (9), 2379–2400. doi:10.1021/bm900266r
- Matysiak, M., Kapka-Skrzypczak, L., Brzoska, K., Gutleb, A. C., and Kruszewski, M. (2016). Proteomic approach to nanotoxicity. *J. Proteomics* 137, 35–44. doi:10.1016/j.jprot.2015.10.025
- Meng, Y., Heybrock, S., Neculai, D., and Saftig, P. (2020). Cholesterol handling in lysosomes and beyond. *Trends Cell. Biol.* 30 (6), 452–466. doi:10.1016/j.tcb.2020.02.007
- Mizushima, N., and Levine, B. (2020). Autophagy in human diseases. *N. Engl. J. Med.* 383 (16), 1564–1576. doi:10.1056/NEJMra2022774
- Mizushima, N., Yoshimori, T., and Levine, B. (2010). Methods in mammalian autophagy research. *Cell.* 140 (3), 313–326. doi:10.1016/j.cell.2010.01.028
- Mo, J. S. (2017). The role of extracellular biophysical cues in modulating the Hippo-YAP pathway. *BMB Rep.* 50 (2), 71–78. doi:10.5483/bmbrep.2017.50.2.199
- Munro, H. N., Aziz, N., Leibold, E. A., Murray, M., Rogers, J., Vass, J. K., et al. (1988). The ferritin genes: Structure, expression, and regulation. *Ann. N. Y. Acad. Sci.* 526, 113–123. doi:10.1111/j.1749-6632.1988.tb55497.x
- Nath Roy, D., Goswami, R., and Pal, A. (2016). Nanomaterial and toxicity: What can proteomics tell us about the nanotoxicology? *Xenobiotica.* 47 (7), 632–643. doi:10.1080/00498254.2016.1205762
- Nel, A. E., Madler, L., Velegol, D., Xia, T., Hoek, E. M., Somasundaran, P., et al. (2009). Understanding biophysicochemical interactions at the nano-bio interface. *Nat. Mat.* 8 (7), 543–557. doi:10.1038/nmat2442
- Park, E. J., Choi, D. H., Kim, Y., Lee, E. W., Song, J., Cho, M. H., et al. (2014). Magnetic iron oxide nanoparticles induce autophagy preceding apoptosis through mitochondrial damage and ER stress in RAW264.7 cells. *Toxicol. Vitro* 28 (8), 1402–1412. doi:10.1016/j.tiv.2014.07.010
- Qian, H., Wu, X., Du, X., Yao, X., Zhao, X., Lee, J., et al. (2020). Structural basis of low-pH-dependent lysosomal cholesterol egress by NPC1 and NPC2. *Cell.* 182 (1), 98–111. doi:10.1016/j.cell.2020.05.020
- Rampton, D., Folkersen, J., Fishbane, S., Hedenus, M., Howaldt, S., Locatelli, F., et al. (2014). Hypersensitivity reactions to intravenous iron: Guidance for risk minimization and management. *Haematologica* 99 (11), 1671–1676. doi:10.3324/haematol.2014.111492
- Roczniak-Ferguson, A., Petit, C. S., Froehlich, F., Qian, S., Ky, J., Angarola, B., et al. (2012). The transcription factor TFEB links mTORC1 signaling to transcriptional control of lysosome homeostasis. *Sci. Signal.* 5 (228), ra42. doi:10.1126/scisignal.2002790
- Sardiello, M., Palmieri, M., di Ronza, A., Medina, D. L., Valenza, M., Gennarino, V. A., et al. (2009). A gene network regulating lysosomal biogenesis and function. *Science* 325 (5939), 473–477. doi:10.1126/science.1174447
- Settembre, C., Zoncu, R., Medina, D. L., Vetrini, F., Erdin, S., Erdin, S., et al. (2012). A lysosome-to-nucleus signalling mechanism senses and regulates the lysosome via mTOR and TFEB. *EMBO J.* 31 (5), 1095–1108. doi:10.1038/emboj.2012.32
- Soetaert, F., Korangath, P., Serantes, D., Fiering, S., and Ivkov, R. (2020). Cancer therapy with iron oxide nanoparticles: Agents of thermal and immune therapies. *Adv. Drug Deliv. Rev.* 163–164, 65–83. doi:10.1016/j.addr.2020.06.025

- Trinder, D., Fox, C., Vautier, G., and Olynyk, J. K. (2002). Molecular pathogenesis of iron overload. *Gut* 51 (2), 290–295. doi:10.1136/gut.51.2.290
- Uzhytchak, M., Smolková, B., Lunova, M., Jirsa, M., Frtús, A., Kubinová, Š., et al. (2020). Iron oxide nanoparticle-induced autophagic flux is regulated by interplay between p53-mTOR Axis and bcl-2 signaling in hepatic cells. *Cells* 9 (4), E1015. doi:10.3390/cells9041015
- Van de Walle, A., Kolosnjaj-Tabi, J., Lalatonne, Y., and Wilhelm, C. (2020). Ever-evolving identity of magnetic nanoparticles within human cells: The interplay of endosomal confinement, degradation, storage, and neocrystallization. *Acc. Chem. Res.* 53 (10), 2212–2224. doi:10.1021/acs.accounts.0c00355
- Vercoza, B. R., Bernardo, R. R., Penton-Madrigal, A., Sinnecker, J. P., Rodrigues, J. C., and Ia, S. d. O. (2019). Therapeutic potential of low-cost nanocarriers produced by green synthesis: Macrophage uptake of superparamagnetic iron oxide nanoparticles. *Nanomedicine (Lond)* 14 (17), 2293–2313. doi:10.2217/nmm-2018-0500
- Viret, C., Duclaux-Loras, R., Nancey, S., Rozieres, A., and Faure, M. (2021). Selective autophagy receptors in antiviral defense. *Trends Microbiol.* 29 (9), 798–810. doi:10.1016/j.tim.2021.02.006
- Yao, C., Akakuru, O. U., Stanciu, S. G., Hampp, N., Jin, Y., Zheng, J., et al. (2020). Effect of elasticity on the phagocytosis of micro/nanoparticles. *J. Mat. Chem. B* 8 (12), 2381–2392. doi:10.1039/c9tb02902h
- Yu, Q., Xiong, X. Q., Zhao, L., Xu, T. T., Bi, H., Fu, R., et al. (2018). Biodistribution and toxicity assessment of superparamagnetic iron oxide nanoparticles *in vitro* and *in vivo*. *Curr. Med. Sci.* 38 (6), 1096–1102. doi:10.1007/s11596-018-1989-8
- Zhang, T., Gaffrey, M. J., Thrall, B. D., and Qian, W. J. (2018). Mass spectrometry-based proteomics for system-level characterization of biological responses to engineered nanomaterials. *Anal. Bioanal. Chem.* 410 (24), 6067–6077. doi:10.1007/s00216-018-1168-6
- Zhang, T. G., Zhang, Y. L., Zhou, Q. Q., Wang, X. H., and Zhan, L. S. (2020). Impairment of mitochondrial dynamics involved in iron oxide nanoparticle-induced dysfunction of dendritic cells was alleviated by autophagy inhibitor 3-methyladenine. *J. Appl. Toxicol.* 40 (5), 631–642. doi:10.1002/jat.3933
- Zhang, X., Zhang, H., Liang, X., Zhang, J., Tao, W., Zhu, X., et al. (2016). Iron oxide nanoparticles induce autophagosome accumulation through multiple mechanisms: Lysosome impairment, mitochondrial damage, and ER stress. *Mol. Pharm.* 13 (7), 2578–2587. doi:10.1021/acs.molpharmaceut.6b00405



## OPEN ACCESS

## EDITED BY

Xu Yang,  
Henan Agricultural University, China

## REVIEWED BY

Pengli Liu,  
Northeast Agricultural University, China  
Yilong Cui,  
Inner Mongolia University for  
Nationalities, China

## \*CORRESPONDENCE

Yali Li,  
Yalilee@126.com

## SPECIALTY SECTION

This article was submitted to Predictive  
Toxicology,  
a section of the journal  
Frontiers in Pharmacology

RECEIVED 18 August 2022

ACCEPTED 05 September 2022

PUBLISHED 19 September 2022

## CITATION

Wang X, Wang R, Qiao Y and Li Y (2022),  
Progress on the efficacy and  
mechanism of action of panax ginseng  
monomer saponins treat toxicity.  
*Front. Pharmacol.* 13:1022266.  
doi: 10.3389/fphar.2022.1022266

## COPYRIGHT

© 2022 Wang, Wang, Qiao and Li. This is  
an open-access article distributed  
under the terms of the [Creative  
Commons Attribution License \(CC BY\)](#).  
The use, distribution or reproduction in  
other forums is permitted, provided the  
original author(s) and the copyright  
owner(s) are credited and that the  
original publication in this journal is  
cited, in accordance with accepted  
academic practice. No use, distribution  
or reproduction is permitted which does  
not comply with these terms.

# Progress on the efficacy and mechanism of action of panax ginseng monomer saponins treat toxicity

Xinyi Wang<sup>1</sup>, Rongcan Wang<sup>1</sup>, Yongfei Qiao<sup>1</sup> and Yali Li<sup>1,2\*</sup>

<sup>1</sup>Institute of Special Animal and Plant Sciences of Chinese Academy of Agricultural Sciences, Changchun, China, <sup>2</sup>Jilin Provincial Key Laboratory of Traditional Chinese Medicinal Materials Cultivation and Propagation, Changchun, China

As a traditional Chinese herbal medicine, *Panax ginseng* C. A. Meyer (PG) has preventive and therapeutic effects on various diseases. Ginsenosides are main active ingredients of PG and have good pharmacological effects. Due to the diversity of chemical structures and physicochemical properties of ginsenosides, Currently, related studies on PG monomer saponins are mainly focused on the cardiovascular system, nervous system, antidiabetic, and antitumor. There are few types of research on the toxin treatment, predominantly exogenous toxicity. PG and its monomer ginsenosides are undoubtedly a practical option for treating exogenous toxicity for drug-induced or metal-induced side effects such as nephrotoxicity, hepatotoxicity, cardiotoxicity, metal toxicity and other exogenous toxicity caused by drugs or metals. The mechanism focuses on antioxidant, anti-inflammatory, and anti-apoptotic, as well as modulation of signaling pathways. It summarized the therapeutic effects of ginseng monomer saponins on exogenous toxicity and demonstrated that ginsenosides could be used as potential drugs to treat exogenous toxicity and reduce drug toxicities.

## KEYWORDS

**ginsenosides, exogenous toxicity, Panax ginseng monomer saponins, treatment, mini-review**

## Introduction

*Panax ginseng* C. A. Meyer (PG) has been used worldwide as a traditional medicine for thousands of years; numerous studies have shown that ginsenosides are the main active ingredients of PG. Currently, more than 150 natural ginsenosides have been isolated and identified from various parts of ginseng herbs (Christensen, 2009). According to the different skeletons of ginsenoside glycosides, ginsenosides can be divided into three saponins, protopanaxdiol, protopanaxtriol and oleanolic acid (Wang et al., 2006). There are numerous reports on the biological effects of ginsenosides, such as immune enhancement (Bai et al., 2019), hepatoprotection (Fan et al., 2019), neuroprotection (Ying et al., 2019), anti-inflammatory (Chen et al., 2021), anti-tumour (Liu and Fan,

2019), and ginsenosides also reverse the drug resistance of tumour cells caused by other chemotherapy drugs (Meng et al., 2019). Different ginsenoside monomers have different functions. For example, ginsenoside Rh2 can inhibit the metastasis of cancer cells to other organs (Shi et al., 2014); ginsenoside Rg1 has the effect of excitation of the central nervous system and inhibition of platelet agglutination (Sun et al., 2016); ginsenoside Rg3 can inhibit the synthesis of proteins and adenine nucleoside triphosphate (ATP) in cancer cells during mitotic prophase and delay the proliferation and growth of cancer cells (Jiang et al., 2017).

Many western drugs are effective in the therapy treatment of diseases and play an essential role in the clinical management of tumors in particular, but their limitations are also evident; for example, the commonly used oncological drug Doxorubicin (DOX) causes cardiotoxicity. The items that contacted by us in our daily life may also contain toxic ingredients, for example, Trimethyltin in plastic stabilizers can cause neurotoxicity, and the presence of toxicity in metals such as iron and aluminum can also induce disease. Therefore, it is crucial to discover drugs from natural plants to mitigate drug toxicity and treat exogenous toxicity.

This paper reviewed the effects of ginsenosides on the treatment of exogenous toxins, and we hope that this review will lay the foundation for an in-depth study of biochemical mechanisms and pharmacological impact of ginsenosides and provide a reference for further development and utilization of ginsenosides in the treatment of exogenous toxicity.

## Effects of ginsenosides on cardiotoxicity

Tumours and cardiovascular diseases have become the top two causes of death in China's urban population (Ma et al., 2020). In addition, it has been reported in the literature that the two disciplines are cross-cutting and that some long-term surviving malignant tumour patients may eventually die from heart disease rather than tumour, and heart disease has become the leading cause of non-cancer-related death in tumour patients (Zaorsky et al., 2017). In clinical practice, some antitumor therapies can also cause cardiotoxicity. Anthracyclines, alkylating agents, 5-FU and paclitaxel, are common chemotherapeutic drugs with cardiotoxicity, which can cause cardiovascular diseases such as heart failure, coronary artery lesions, hypertension and thrombosis (Luis Zamorano et al., 2016). Although there are many drugs for clinical use in oncology, current information on the exogenous cardiotoxic effects of ginsenosides for the treatment of the heart is focused on the cardiotoxicity caused by DOX and Trastuzumab (TZM).

Although DOX is an anthracycline antibiotic with powerful anti-tumor effects, it causes cumulative and dose-dependent cardiotoxicity, which leads to an increased risk of death in cancer patients. Thus, its clinical application is limited (Zhao et al., 2018, 2; Rawat et al., 2021). Ginsenosides protect the heart from various cardiovascular diseases by regulating multiple cellular signaling pathways. Ginsenoside Rg1 ameliorates DOX-induced cardiac insufficiency by inhibiting endoplasmic reticulum stress and autophagy (Xu et al., 2018). Rg1 increases phosphorylation of Akt and Erk, increases the ratio of Bcl-2 and Bax, and reduces cytochrome c release in mitochondria, thereby protecting the heart from DOX-induced apoptosis (Zhu et al., 2017). Ginsenoside Rg2 attenuates DOX-induced apoptosis by upregulating Akt phosphorylation and inhibiting p53 expression through the PI3K/Akt pathway in cardiomyocytes (Qiu et al., 2021). In summary, Rh2 may become a new protective agent in the clinical application of DOX (Wang H. et al., 2012).

Similarly, ginsenosides can achieve cardioprotective effects by regulating autophagy. Rb1 attenuates DOX-induced reduction in cardiomyocyte viability and inhibits the increase in autophagy-related structures, the conversion of light chain 3-I to light chain 3-II, and the reduction in p62 protein expression (Li et al., 2017). In addition, endoplasmic reticulum stress is another cause of cardiac dysfunction, closely associated with autophagy activation (Rashid et al., 2015). Echocardiographic and pathological findings suggest that ginsenoside Rg1 can significantly reduce DOX-induced cardiotoxicity. Endoplasmic reticulum stress and inhibition of autophagy may be the mechanism by which Rg1 ameliorates DOX-induced cardiac dysfunction (Xu et al., 2018).

TZM is a standard clinical treatment for breast cancer, but it has significant cardiotoxicity (Koulaouzidis et al., 2021). Rg2 induces autophagy in human cardiomyocytes (HCMs) by upregulating the expression levels of (p)-Akt, p-mTOR, beclin 1, light chain 3 (LC3) and autophagy protein 5 (ATG5), thereby treating TZM-induced cardiotoxicity (Liu et al., 2021). Liu et al. (2022) suggested that Rg2 could inhibit TZM-induced cardiac cytotoxicity. The mechanism might be related to the downregulation of proapoptotic proteins caspase-3, caspase-9, and BAX expression, which inhibited TZM-induced apoptosis in cardiac myocytes.

## Effects of ginsenosides on neurotoxicity and brain toxicity

### Ginsenosides attenuate neurotoxicity

Trimethyltin (TMT) is a by-product of the production of plastic stabilizers. It has been found in domestic water

supplies, aquatic specimens, and marine environments (Gomez et al., 2007). TMT is a toxic organotin compound which selectively induces neurodegeneration in the limbic system, especially prominent in the hippocampus (Lee et al., 2016). Ginsenoside Re can against TMT-induced neurotoxicity through the PI3K/Akt signalling pathway of IL-6 (Tu et al., 2017). Another study discovered that Rg3 and Rh2 treat TMT-induced neurodegeneration by reducing oxidative stress and neuroinflammatory neurotoxicity (Hou et al., 2018). Hou et al. (2017) administered a single injection of 2 mg/kg body weight of TMT to ICR mice after pretreating them with ginsenoside Rd. Compared with saline-treated controls, Rd was found to act as a neuroprotective agent to prevent TMT-induced neurotoxicity. Cadmium (Cd) is a toxic and non-essential element for humans, which enters and accumulates in organisms through occupational exposure, contaminated air, water and food (Huang et al., 2017), Ren et al. (2021) reported that Rg1 eliminated Cd-induced toxicity and restored oxidative stress and inflammatory responses, and accordingly restored behavioural performance in animals, suggesting that Rg1 has an eliminating effect on Cd-induced neurotoxicity.

## Ginsenosides protect the brain from $\beta$ -amyloid-induced toxicity

$\beta$ -Amyloid ( $A\beta$ ) aggregates cause complex neurotoxicity and play a vital role in the progression of Alzheimer's disease (AD) (Ho et al., 2015). Prevention of  $A\beta$ -induced toxicity could lead to drug development for Alzheimer's disease. In a double-transgenic AD mouse experiment, Yun et al. (2022) found that ginsenoside F1 exerts its beneficial effects by increasing insulin-degrading enzyme (IDE) and neprilysin (NEP) expression, providing scientific evidence regarding the applicability of  $A\beta$  treatment in AD patients. It has been suggested that Rb1 is likely to protect neurons from  $A\beta$  toxicity through the antioxidant pathway (Qian et al., 2009). Xie et al. (Xie et al., 2010) pretreated cells with Rb1 for 24 h and then added  $A\beta_{25-35}$  to the medium for another 24 h. They found that Rb1 pretreatment inhibited  $A\beta$ -induced Reactive oxygen species (ROS) overproduction and lipid peroxidation, increased the Bcl-2/Bax ratio, and attenuated caspase-3 activation, thereby increasing cell survival and protecting against  $A\beta$ -induced cell damage.

## Effects of ginsenosides on metal-induced toxicity

Iron accumulation is thought to be involved in the pathogenesis of Parkinson's disease (PD) (Jiang et al., 2007).

Several studies have shown that selectively high iron levels and oxidative stress due to elevated iron levels in the substantia nigra pars compacta (SNpc), play a crucial role in developing PD (Youdim et al., 2004, 28; Zecca et al., 2008). Rg1 reduces cellular iron accumulation and attenuates the inappropriate upregulation of divalent metal transporter 1 with the iron-responsive element (DMT1 + IRE) through the IRE/Iron regulatory protein (IRP) system to achieve neuroprotective effects against iron toxicity (Xu et al., 2010a). In addition, it was found that Rg1 could reduce iron influx and iron-induced oxidative stress by inhibiting the upregulation of DMT1-IRE (Xu et al., 2010b). Wang et al. (Wang et al., 2009) suggested that the neuroprotective effect of Rg1 on dopaminergic neurons against 1-Methyl-4-phenyl-1,2,3,6-tetrahydropyridine (MPTP) is due to the ability to reduce nigrostriatal iron levels, which is achieved by regulating the expression of divalent metal transporter 1 (DMT1) and Ferroportin1 (FP1).

Aluminum (Al)-induced disorders of bone metabolism are a significant cause of osteoporosis. The research concluded that Rb1 significantly reverses osteoblast viability and osteoblast growth regulators, inhibits oxidative stress, and attenuates histological damage to osteoblasts by  $AlCl_3$  (Zhu et al., 2016), activating the TGF- $\beta$ 1/Smad signaling pathway is one of the mechanisms by which Rg3 alleviates Al-induced bone damage (Song et al., 2021). Song et al. (2020) reported that Rg3 effectively alleviated  $AlCl_3$ -induced osteoporosis by increasing the mRNA expression of transforming growth factor- $\beta$ 1, bone morphogenetic protein-2, insulin-like growth factor I, and core binding factor  $\alpha$ 1 to promote growth regulators and attenuate Al accumulation.

## Effects of ginsenosides on hepatotoxicity

Frequent overdose of acetaminophen (APAP) is one of the most common and essential triggers of acute hepatotoxicity (Xu et al., 2017). Ginsenoside Rg5 exerts hepatoprotective effects against APAP-induced acute hepatotoxicity. Wang et al. (2017) administered Rg5 to mice and found the protein expression of proliferating cell nuclear antigen (PCNA), Bax, cytochrome c, caspase-3, caspase-8, and caspase-9 was significantly inhibited in the Rg5 group compared with the control group. In contrast, the expression level of Bcl-2 protein was increased, indicating that Rg5 has anti-apoptotic ability in APAP-induced hepatotoxicity. Rk1 pretreatment significantly reduced serum alanine aminotransferase, aspartate aminotransferase, tumour necrosis factor, and interleukin-1 $\beta$  levels and significantly reversed APAP-induced liver tissue necrosis (Hu et al., 2019). Rb1 exhibits significant hepatoprotective effects against APAP-induced ALI by modulating MAPK and PI3K/Akt

TABLE 1 Therapeutic effect of ginsenosides on CP-induced nephrotoxicity.

Ginsenosides	Experimental model	Dosage and method	Mechanisms	Effects	References
Rb3	ICR mouse	10 and 20 mg/kg by oral gavage	(↓) p62, ATG3, ATG5, ATG7, p-mTOR, the ratio of LC3-I/LC3-II	Rb3 regulates AMPK-/mTOR-mediated autophagy and inhibits apoptosis <i>in vitro</i> and <i>in vivo</i> , thereby alleviating CP-induced nephrotoxicity	Xing et al. (2019)
Rh2	Male SPF grade ICR mice (22–25 g)	20 and 40 mg/kg by gavaged (P.O)	(↑) Bcl-2  (↓) p53, Bax, cytochrome c, caspase-8, caspase-9, and caspase-3	Rh2 protects against CP-induced nephrotoxicity by acting on caspase-mediated pathways	Qi et al. (2019)
Re	Male ICR mice	25 mg/kg by oral gavage	(↓) Renal dysfunction, inflammatory cytokines, apoptosis, malondialdehyde in the kidney	The renal protective potential of Re may be partly related to its antioxidant, anti-inflammatory and anti-apoptotic effects	Wang et al. (2018)
Rh3	pig kidney epithelium, CL-101		(↓) JNK, ERK, p38, caspase-3, Proportion of apoptotic cells in LLC-PK1	Inhibition of JNK and ERK mitogen-activated protein kinase signaling cascade plays an important role in the renoprotective effects of Rh3	Lee and Kang, (2017)
Rg5	Male ICR mice (6–8 weeks old)	10 and 20 mg/kg administered intragastrically	(↑) Bcl-2  (↓) NF-κB p65, COX-2, Bax	Rg5 attenuates CP-induced nephrotoxicity by reducing oxidative stress, inhibiting inflammation, and suppressing apoptosis in CP-treated mice	Li et al. (2016)

ATG3, autophagy related three; ATG5, autophagy related five; ATG7, autophagy related seven; LC3-I, light chain 3-I; LC3-II, light chain 3-II; JNK, c-Jun N-terminal kinase; ERK, extracellular signal-regulated kinase; LLC-PK1, porcine renal proximal epithelial tubular; NF-κB, nuclear factor-kappa B; COX-2, cyclooxygenase 2.

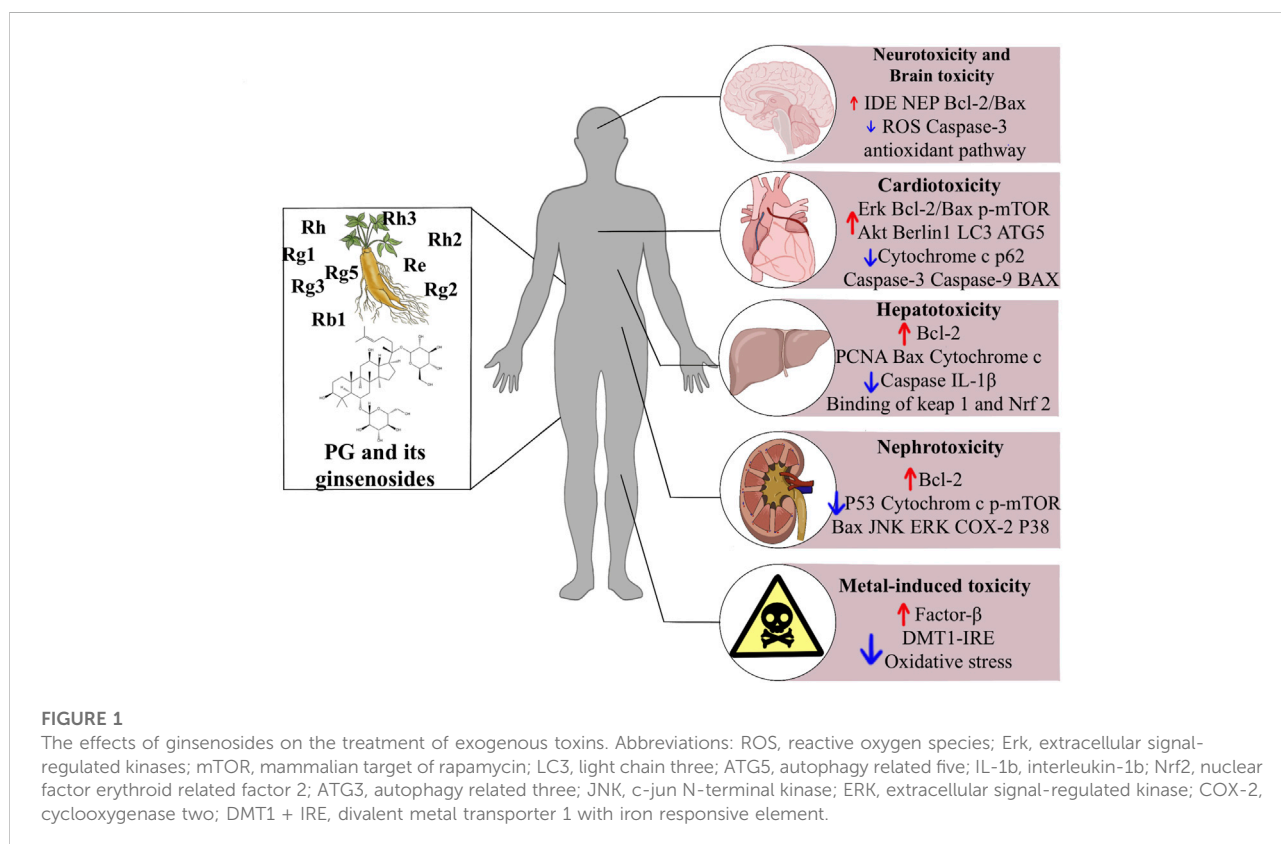


FIGURE 1

The effects of ginsenosides on the treatment of exogenous toxins. Abbreviations: ROS, reactive oxygen species; Erk, extracellular signal-regulated kinases; mTOR, mammalian target of rapamycin; LC3, light chain three; ATG5, autophagy related five; IL-1b, interleukin-1b; Nrf2, nuclear factor erythroid related factor 2; ATG3, autophagy related three; JNK, c-jun N-terminal kinase; ERK, extracellular signal-regulated kinase; COX-2, cyclooxygenase two; DMT1 + IRE, divalent metal transporter 1 with iron responsive element.

signalling pathway-mediated inflammatory responses (Ren et al., 2019). Rg3 exerts hepatoprotective effects on APAP-induced hepatotoxicity by inhibiting oxidative stress and inflammatory responses (Zhou et al., 2018).

Cisplatin (CP) is an effective antitumor drug widely used in cancer treatment, and hepatotoxicity is one of its side effects (Taghizadeh et al., 2021). Rg1 effectively prevents cisplatin-induced hepatotoxicity, mainly by inhibiting the binding of Keap1 and Nrf2, partly through the accumulation of p62 (Gao et al., 2017).

## Effects of ginsenosides on nephrotoxicity

Nephrotoxicity is a common side effect of chemotherapy and drugs. For example, the commonly used drug CP may cause severe nephrotoxicity, including tubular injury and renal failure (Miller et al., 2010; Manohar and Leung, 2017). Numerous studies have demonstrated that ginsenosides can promote the recovery of kidney function by regulating inflammation apoptosis and reducing kidney damage (Baek et al., 2006; Park et al., 2015; Wang et al., 2018). In CP mice, Rh2 treatment significantly increased the expression of Bcl-2. It decreased the expression of p53, Bax, cytochrome c, caspase-8, caspase-9, and caspase-3 in renal tissues, suggesting that Rh2 prevents CP-induced nephrotoxicity by acting on the cystein-mediated pathway (Qi et al., 2019). The increase in the percentage of apoptotic LLC-PK1 cells induced by CP treatment was also significantly reduced after Rh3 treatment (Lee and Kang, 2017). Thus, ginsenosides are potential agents for treating CP-induced nephrotoxicity (Table 1).

## Effects of ginsenosides on reproductive toxicity

The value of ginsenosides in reproductive function was demonstrated in several reports. Many studies have shown that bisphenol A (BPA) can cause reproductive toxicity. Wang et al. (Wang L. et al., 2012) showed that ginsenosides (75 µg/ml) significantly inhibited the decrease in cell viability and increase in apoptosis inhibited by BPA through *in vitro* cell culture model experiments. These effects are mediated by preventing ERK1/2 phosphorylation and enhancing cellular antioxidant capacity. Testicular toxicity is one of the side effects of chemotherapeutic drugs. Ji et al. (2007) reported the therapeutic and preventive effects of protopanaxatriol saponin (PT) on the testicular organs of male mice under toxicity induction of the chemotherapeutic drug busulfan, and the damage to spermatogenic tubules in mice injected with PT was less than that of busulfan treatment alone. These results suggest that PT is effective in recovering male reproductive organs and overcomes the toxicity of busulfan. PT may be indicated for recovering male infertility caused by

azoospermia and oligospermia. Endometriosis (EMS) is an estrogen-dependent gynaecological disorder, impaired NK cell cytotoxic activity is associated with clearance obstruction of ectopic endometrial tissue in the abdominal and pelvic cavity. Zhang et al. (2018) reported that PPD-pretreated ectopic endometrial stromal cells (eESCs) enhanced the cytotoxic activity of NK cells against eESCs, reduced the number of ectopic lesions and inhibited the growth of ectopic lesions in a mouse EMS model. They suggest that this effect may be through limiting estrogen-mediated autophagy regulation and enhancing NK cell cytotoxicity.

## Summary and observations

Due to the mutual influence and restriction of various saponin monomers, the unique medicinal and health-care properties of various monomeric saponins cannot be displayed, which significantly reduces the application value. In recent years, researchers at home and abroad have devoted themselves to the use of biological methods to produce ginsenoside products and have made corresponding progress and breakthroughs in biotechnology in various research fields such as tissue culture, transgenic plants, biosynthetic pathways and synthetic biology, which have laid an essential foundation for the preparation or production of ginsenoside products in large quantities. Most ginsenoside monomers on the market are relatively cheap, such as Rb1, Re, etc. The average price is about 0.289 USD/mg; individual monomeric saponins are rarer and more costly, with an average price of about 5.797 USD/mg.

This review briefly summarizes the therapeutic potential of ginsenosides in drug toxicities and exogenous toxins, and explains the mechanism of action (Figure 1). Ginsenosides play an essential role in treating drug toxicity, especially in treating cancer patients, and can reduce drug toxicity and improve the survival quality of cancer patients after the cure. The underlying mechanism may be related to an increase in antioxidant enzymes and anti-apoptotic, anti-inflammatory signalling and immunostimulatory factors, as well as a decrease in pro-apoptotic, pro-inflammatory, immunosuppressive and pro-oxidant indices. Further studies revealed that this mechanism involves several signalling pathways, such as the classical antioxidant pathway: P62/KEAP1/NRF2, the apoptosis-related pathway: JNK/P53/CASPASE3, and the AMPK/mTOR signalling pathway, which plays a crucial role in the development of autophagy. In addition, ginsenosides play an essential role in the treatment of metal toxicity and the accumulation of toxins that may be caused by chemicals added to household products. In conclusion, ginsenosides are potential drugs for preventing and treating exogenous toxins.

## Author contributions

XW contributed to the drafting of the manuscript and data collection. RW and YQ revised the manuscript and participated in the search. YL provided research directions and ideas. All authors read and approved the final manuscript.

## Acknowledgments

Authors sincerely thank the project of the Key R & D projects of Jilin Provincial Department of science and technology (No. 20210204178YY).

## References

- Baek, S. H., Piao, X. L., Lee, U. J., Kim, H. Y., and Park, J. H. (2006). Reduction of cisplatin-induced nephrotoxicity by ginsenosides isolated from processed ginseng in cultured renal tubular cells. *Biol. Pharm. Bull.* 29, 2051–2055. doi:10.1248/bpb.29.2051
- Bai, Y., Zheng, H., Wang, Y., and Zheng, S. (2019). Research progress on the immunomodulatory effect of ginseng. *Spec. Wild Econ. Anim. Plant Res.* 41, 99–103. doi:10.16720/j.cnki.tcyj.2019.01.022
- Chen, H., Yang, H., Deng, J., and Fan, D. (2021). Ginsenoside Rk3 ameliorates obesity-induced colitis by regulating of intestinal flora and the TLR4/NF-kappa B signaling pathway in C57bl/6 mice. *J. Agric. Food Chem.* 69, 3082–3093. doi:10.1021/acs.jafc.0c07805
- Christensen, L. P. (2009). "Ginsenosides: Chemistry, biosynthesis, analysis, and potential health effects," in *Advances in food and nutrition research*, vol 55. Editor S. L. Taylor (San Diego: Elsevier Academic Press Inc), 1–99. doi:10.1016/S1043-4526(08)00401-4
- Fan, J., Wang, Y.-S., You, Y., Ai, Z., Dai, W., Piao, C., et al. (2019). Fermented ginseng improved alcohol liver injury in association with changes in the gut microbiota of mice. *Food Funct.* 10, 5566–5573. doi:10.1039/c9fo01415b
- Gao, Y., Chu, S., Shao, Q., Zhang, M., Xia, C., Wang, Y., et al. (2017). Antioxidant activities of ginsenoside Rg1 against cisplatin-induced hepatic injury through Nrf2 signaling pathway in mice. *Free Radic. Res.* 51, 1–13. doi:10.1080/10715762.2016.1234710
- Gomez, F. D., Apodaca, P., Holloway, L. N., Pannell, K. H., and Whalen, M. M. (2007). Effect of a series of triorganotins on the immune function of human natural killer cells. *Environ. Toxicol. Pharmacol.* 23, 18–24. doi:10.1016/j.etap.2006.06.001
- Ho, S.-L., Poon, C.-Y., Lin, C.-Y., Yan, T., Kwong, D., Yung, K., et al. (2015). Inhibition of  $\beta$ -amyloid aggregation by albiflorin, aloemodin and neohesperidin and their neuroprotective effect on primary hippocampal cells against  $\beta$ -amyloid induced toxicity. *Curr. Alzheimer Res.* 12, 424–433. doi:10.2174/1567205012666150504144919
- Hou, J., Xue, J., Lee, M., and Sung, C. (2017). Ginsenoside Rd as a potential neuroprotective agent prevents trimethyltin injury. *Biomed. Rep.* 6, 435–440. doi:10.3892/br.2017.864
- Hou, J., Xue, J., Wang, Z., and Li, W. (2018). Ginsenoside Rg3 and Rh2 protect trimethyltin-induced neurotoxicity via prevention on neuronal apoptosis and neuroinflammation. *Phytother. Res.* 32, 2531–2540. doi:10.1002/ptr.6193
- Hu, J., Xu, X., Li, W., Wang, Y., Liu, Y., Wang, Z., et al. (2019). Ginsenoside Rk1 ameliorates paracetamol-induced hepatotoxicity in mice through inhibition of inflammation, oxidative stress, nitrate stress and apoptosis. *J. Ginseng Res.* 43, 10–19. doi:10.1016/j.jgr.2017.07.003
- Huang, Y., He, C., Shen, C., Guo, J., Mubeen, S., Yuan, J., et al. (2017). Toxicity of cadmium and its health risks from leafy vegetable consumption. *Food Funct.* 8, 1373–1401. doi:10.1039/c6fo01580h
- Ji, M., Minami, N., Yamada, M., and Imai, H. (2007). Effect of protopanaxatriol saponin on spermatogenic stem cell survival in busulfan-treated male mice. *Reprod. Med. Biol.* 6, 99–108. doi:10.1111/j.1447-0578.2007.00172.x

## Conflict of interest

The authors declare that the research was conducted in the absence of any commercial or financial relationships that could be construed as a potential conflict of interest.

## Publisher's note

All claims expressed in this article are solely those of the authors and do not necessarily represent those of their affiliated organizations, or those of the publisher, the editors and the reviewers. Any product that may be evaluated in this article, or claim that may be made by its manufacturer, is not guaranteed or endorsed by the publisher.

- Jiang, H., Song, N., Wang, J., Ren, L.-Y., and Xie, J.-X. (2007). Peripheral iron dextran induced degeneration of dopaminergic neurons in rat substantia nigra. *Neurochem. Int.* 51, 32–36. doi:10.1016/j.neuint.2007.03.006
- Jiang, J., Yuan, Z., Sun, Y., Bu, Y., Li, W., and Fei, Z. (2017). Ginsenoside Rg3 enhances the anti-proliferative activity of erlotinib in pancreatic cancer cell lines by downregulation of EGFR/PI3K/Akt signaling pathway. *Biomed. Pharmacother.* 96, 619–625. doi:10.1016/j.biopha.2017.10.043
- Koulaouzidis, G., Yung, A. E., Yung, D. E., Skonieczna-Zydecka, K., Marlicz, W., Koulaouzidis, A., et al. (2021). Conventional cardiac risk factors associated with trastuzumab-induced cardiotoxicity in breast cancer: Systematic review and meta-analysis. *Curr. Probl. Cancer* 45, 100723. doi:10.1016/j.cupr.2021.100723
- Lee, H., and Kang, K. (2017). Protective effect of ginsenoside Rh3 against anticancer drug-induced apoptosis in LLC-PK1 kidney cells. *J. Ginseng Res.* 41, 227–231. doi:10.1016/j.jgr.2017.01.011
- Lee, S., Yang, M., Kim, J., Kang, S., Kim, J., Kim, J.-C., et al. (2016). Trimethyltin-induced hippocampal neurodegeneration: A mechanism-based review. *Brain Res. Bull.* 125, 187–199. doi:10.1016/j.brainresbull.2016.07.010
- Li, L., Ma, Z., Wang, Y., Tang, X., Tan, H., Xiao, C., et al. (2017). Protective effect of ginsenoside Rb- on doxorubicin-induced myocardial autophagy. *Zhongguo Zhong Yao Za Zhi* 42, 1365–1369. doi:10.19540/j.cnki.cjcm.20170222.009
- Li, W., Yan, M., Liu, Y., Liu, Z., Wang, Z., Chen, C., et al. (2016). Ginsenoside Rg5 ameliorates cisplatin-induced nephrotoxicity in mice through inhibition of inflammation, oxidative stress, and apoptosis. *Nutrients* 8, E566. doi:10.3390/nu8090566
- Liu, G., Qi, X., Li, X., and Sun, F. (2021). Ginsenoside Rg2 protects cardiomyocytes against trastuzumab-induced toxicity by inducing autophagy. *Exp. Ther. Med.* 21, 473. doi:10.3892/etm.2021.9904
- Liu, G., Zhang, J., Sun, F., Ma, J., and Qi, X. (2022). Ginsenoside Rg2 attenuated trastuzumab-induced cardiotoxicity in rats. *Biomed. Res. Int.* 2022, 8866660. doi:10.1155/2022/8866660
- Liu, Y., and Fan, D. (2019). Ginsenoside Rg5 induces G2/M phase arrest, apoptosis and autophagy via regulating ROS-mediated MAPK pathways against human gastric cancer. *Biochem. Pharmacol.* 168, 285–304. doi:10.1016/j.bcp.2019.07.008
- Luis Zamorano, J., Lancellotti, P., Rodriguez Munoz, D., Aboyans, V., Asteggiano, R., Galderisi, M., et al. (2016). 2016 ESC Position Paper on cancer treatments and cardiovascular toxicity developed under the auspices of the ESC Committee for Practice Guidelines. *Kardiol. Pol.* 74, 1193–1233. doi:10.5603/KP.2016.0156
- Ma, L.-Y., Chen, W.-W., Gao, R.-L., Liu, L.-S., Zhu, M.-L., Wang, Y.-J., et al. (2020). China cardiovascular diseases report 2018: An updated summary. *J. Geriatr. Cardiol.* 17, 1–8. doi:10.11909/j.issn.1671-5411.2020.01.001
- Manohar, S., and Leung, N. (2017). Cisplatin nephrotoxicity: A review of the literature. *J. Nephrol.* 31, 15–25. doi:10.1007/s40620-017-0392-z
- Meng, L., Ji, R., Dong, X., Xu, X., Xin, Y., and Jiang, X. (2019). Antitumor activity of ginsenoside Rg3 in melanoma through downregulation of the ERK and Akt pathways. *Int. J. Oncol.* 54, 2069–2079. doi:10.3892/ijo.2019.4787

- Miller, R. P., Tadagavadi, R., Ramesh, G., and Reeves, W. B. (2010). Mechanisms of cisplatin nephrotoxicity. *Toxins* 2, 2490–2518. doi:10.3390/toxins2112490
- Park, J. Y., Choi, P., Kim, T., Ko, H., Kim, H., Kang, K., et al. (2015). Protective effects of processed ginseng and its active ginsenosides on cisplatin-induced nephrotoxicity: *In vitro* and *in vivo* studies. *J. Agric. Food Chem.* 63, 5964–5969. doi:10.1021/acs.jafc.5b00782
- Qi, Z., Li, W., Tan, J., Wang, C., Lin, H., Zhou, B., et al. (2019). Effect of ginsenoside Rh2 on renal apoptosis in cisplatin-induced nephrotoxicity *in vivo*. *Phytomedicine* 61, 152862. doi:10.1016/j.phymed.2019.152862
- Qian, Y.-H., Han, H., Hu, X.-D., and Shi, L.-L. (2009). Protective effect of ginsenoside Rb1 on beta-amyloid protein(1-42)-induced neurotoxicity in cortical neurons. *Neurol. Res.* 31, 663–667. doi:10.1179/174313209X385572
- Qiu, B., Mao, M., Zhang, S., Deng, B., Shen, L., Zhao, P., et al. (2021). Ginsenoside Rg2 attenuates doxorubicin-induced cardiomyocyte apoptosis via PI3K/Akt pathway. *Rev. Bras. Farmacogn.* 32, 433–439. doi:10.21203/rs.3.rs-191055/v1
- Rashid, H., Yadav, R., Kim, H.-R., and Chae, H. (2015). ER stress: Autophagy induction, inhibition and selection. *Autophagy* 11, 1956–1977. doi:10.1080/15548627.2015.1091141
- Rawat, P. S., Jaiswal, A., Khurana, A., Bhatti, J. S., and Navik, U. (2021). Doxorubicin-induced cardiotoxicity: An update on the molecular mechanism and novel therapeutic strategies for effective management. *Biomed. Pharmacother.* 139, 111708. doi:10.1016/j.biopha.2021.111708
- Ren, S., Leng, J., Xu, X., Jiang, S., Wang, Y., Yan, X., et al. (2019). Ginsenoside Rb1, A major saponin from Panax ginseng, exerts protective effects against acetaminophen-induced hepatotoxicity in mice. *Am. J. Chin. Med.* 47, 1815–1831. doi:10.1142/S0192415X19500927
- Ren, T.-T., Yang, J.-Y., Wang, J., Fan, S.-R., Lan, R., and Qin, X.-Y. (2021). Ginsenoside Rg1 attenuates cadmium-induced neurotoxicity *in vitro* and *in vivo* by attenuating oxidative stress and inflammation. *Inflamm. Res.* 70, 1151–1164. doi:10.1007/s00011-021-01513-7
- Shi, Q., Li, J., Feng, Z., Zhao, L., Luo, L., You, Z., et al. (2014). Effect of ginsenoside Rh2 on the migratory ability of HepG2 liver carcinoma cells: Recruiting histone deacetylase and inhibiting activator protein 1 transcription factors. *Mol. Med. Rep.* 10, 1779–1785. doi:10.3892/mmr.2014.2392
- Song, M., Cui, Y., Wang, Q., Zhang, X., Zhang, J., Liu, M., et al. (2021). Ginsenoside Rg3 alleviates aluminum chloride-induced bone impairment in rats by activating the TGF- $\beta$ 1/smad signaling pathway. *J. Agric. Food Chem.* 69, 12634–12644. doi:10.1021/acs.jafc.1c04695
- Song, M., Jia, F., Cao, Z., Zhang, H., Liu, M., and Gao, L. (2020). Ginsenoside Rg3 attenuates aluminum-induced osteoporosis through regulation of oxidative stress and bone metabolism in rats. *Biol. Trace Elem. Res.* 198, 557–566. doi:10.1007/s12011-020-02089-9
- Sun, X.-C., Ren, X.-F., Chen, L., Gao, X.-Q., Xie, J.-X., and Chen, W.-F. (2016). Glucocorticoid receptor is involved in the neuroprotective effect of ginsenoside Rg1 against inflammation-induced dopaminergic neuronal degeneration in substantia nigra. *J. Steroid Biochem. Mol. Biol.* 155, 94–103. doi:10.1016/j.jsmb.2015.09.040
- Taghizadeh, F., Hosseini-mehr, S., Zargari, M., Malekshah, A. K., Mirzaei, M., and Amiri, F. T. T. (2021). Alleviation of cisplatin-induced hepatotoxicity by gliclazide: Involvement of oxidative stress and caspase-3 activity. *Pharmacol. Res. Perspect.* 9, e00788. doi:10.1002/prp2.788
- Tu, T.-H. T., Sharma, N., Shin, E.-J., Tran, H.-Q., Lee, Y. J., Jeong, J. H., et al. (2017). Ginsenoside Re protects trimethyltin-induced neurotoxicity via activation of IL-6-mediated phosphoinositol 3-kinase/akt signaling in mice. *Neurochem. Res.* 42, 3125–3139. doi:10.1007/s11064-017-2349-y
- Wang, H., Yu, P., Gou, H., Zhang, J., Zhu, M., Wang, Z., et al. (2012a). Cardioprotective effects of 20(S)-Ginsenoside Rh2 against doxorubicin-induced cardiotoxicity *in vitro* and *in vivo*. *Evid. Based. Complement. Altern. Med.* 2012, 506214. doi:10.1155/2012/506214
- Wang, J., Xu, H.-M., Yang, H.-D., Du, X.-X., Jiang, H., and Xie, J.-X. (2009). Rg1 reduces nigral iron levels of MPTP-treated C57BL6 mice by regulating certain iron transport proteins. *Neurochem. Int.* 54, 43–48. doi:10.1016/j.neuint.2008.10.003
- Wang, L., Hao, J., Hu, J., Pu, J., Lu, Z., Zhao, L., et al. (2012b). Protective effects of ginsenosides against bisphenol A-induced cytotoxicity in 15P-1 sertoli cells via extracellular signal-regulated kinase 1/2 signalling and antioxidant mechanisms. *Basic Clin. Pharmacol. Toxicol.* 111, 42–49. doi:10.1111/j.1742-7843.2012.00857.x
- Wang, Y., Quan, X., Bai, L., Zhang, H., Chen, X., Ding, L., et al. (2006). Determination of Ginsenosides in the root of Radix Ginseng by high performance liquid chromatography/evaporative light Scattering detection. *Chin. J. Anal. Chem.* 83, 243–246.
- Wang, Z., Hu, J., Yan, M., Xing, J., Liu, W., and Li, W. (2017). Caspase-mediated anti-apoptotic effect of ginsenoside Rg5, a main rare ginsenoside, on acetaminophen-induced hepatotoxicity in mice. *J. Agric. Food Chem.* 65, 9226–9236. doi:10.1021/acs.jafc.7b03361
- Wang, Z., Li, Y., Han, X., Sun, Y., Zhang, L., Liu, W., et al. (2018). Kidney protection effect of ginsenoside Re and its underlying mechanisms on cisplatin-induced kidney injury. *Cell. Physiol. Biochem.* 48, 2219–2229. doi:10.1159/000492562
- Xie, X.-J., Wang, H.-T., Li, C., Gao, X., Ding, J., Zhao, H., et al. (2010). Ginsenoside Rb1 protects PC12 cells against  $\beta$ -amyloid-induced cell injury. *Mol. Med. Rep.* 3, 635–639. doi:10.3892/mmr.00000308
- Xing, J., Hou, J., Ma, Z.-N., Wang, Z., Ren, S., Wang, Y., et al. (2019). Ginsenoside Rb3 provides protective effects against cisplatin-induced nephrotoxicity via regulation of AMPK-/mTOR-mediated autophagy and inhibition of apoptosis *in vitro* and *in vivo*. *Cell Prolif.* 52, e12627. doi:10.1111/cpr.12627
- Xu, H., Jiang, H., Wang, J., and Xie, J. (2010a). Rg1 protects iron-induced neurotoxicity through antioxidant and iron regulatory proteins in 6-OHDA-treated MES23.5 cells. *J. Cell. Biochem.* 111, 1537–1545. doi:10.1002/jcb.22885
- Xu, H., Jiang, H., Wang, J., and Xie, J. (2010b). Rg1 protects the MPP<sup>+</sup>-treated MES23.5 cells via attenuating DMT1 up-regulation and cellular iron uptake. *Neuropharmacology* 58, 488–494. doi:10.1016/j.neuropharm.2009.09.002
- Xu, X., Hu, J., Liu, Z., Zhang, R., He, Y., Hou, W., et al. (2017). Saponins (ginsenosides) from the leaves of Panax quinquefolius ameliorated acetaminophen-induced hepatotoxicity in mice. *J. Agric. Food Chem.* 65, 3684–3692. doi:10.1021/acs.jafc.7b00610
- Xu, Z.-M., Li, C.-B., Liu, Q.-L., Li, P., and Yang, H. (2018). Ginsenoside Rg1 prevents doxorubicin-induced cardiotoxicity through the inhibition of autophagy and endoplasmic reticulum stress in mice. *Int. J. Mol. Sci.* 19, 3658. doi:10.3390/ijms19113658
- Ying, Y., Zhang, Y., Ma, C., Li, M., Tang, C., Yang, Y., et al. (2019). Neuroprotective effects of ginsenoside Rg1 against hyperphosphorylated tau-induced diabetic retinal neurodegeneration via activation of IRS-1/akt/GSK3 beta signaling. *J. Agric. Food Chem.* 67, 8348–8360. doi:10.1021/acs.jafc.9b02954
- Youdim, M. B. H., Stephenson, G., and Ben Shachar, D. (2004). “Ironing iron out in Parkinson’s disease and other neurodegenerative diseases with iron chelators - a lesson from 6-hydroxydopamine and iron chelators, desferal and VK-28,” in *Redox-active metals in neurological disorders*. Editors S. M. LeVine, J. R. Connor, and H. M. Schipper (New York: New York Acad Sciences), 306–325. doi:10.1196/annals.1306.025
- Yun, Y.-J., Park, B.-H., Hou, J., Oh, J.-P., Han, J.-H., and Kim, S.-C. (2022). Ginsenoside F1 protects the brain against amyloid beta-induced toxicity by regulating IDE and NEP. *Life* 12, 58. doi:10.3390/life12010058
- Zaorsky, N. G., Churilla, T. M., Egleston, B. L., Fisher, S. G., Ridge, J. A., Horwitz, E. M., et al. (2017). Causes of death among cancer patients. *Ann. Oncol.* 28, 400–407. doi:10.1093/annonc/mdw604
- Zecca, L., Casella, L., Albertini, A., Bellei, C., Zucca, F. A., Engelen, M., et al. (2008). Neuromelanin can protect against iron-mediated oxidative damage in system modeling iron overload of brain aging and Parkinson’s disease. *J. Neurochem.* 106, 1866–1875. doi:10.1111/j.1471-4159.2008.05541.x
- Zhang, B., Zhou, W.-J., Gu, C.-J., Wu, K., Yang, H.-L., Mei, J., et al. (2018). The ginsenoside PPD exerts anti-endometriosis effects by suppressing estrogen receptor-mediated inhibition of endometrial stromal cell autophagy and NK cell cytotoxicity. *Cell Death Dis.* 9, 1–13. doi:10.1038/s41419-018-0581-2
- Zhao, L., Qi, Y., Xu, L., Tao, X., Han, X., Yin, L., et al. (2018). MicroRNA-140-5p aggravates doxorubicin-induced cardiotoxicity by promoting myocardial oxidative stress via targeting Nrf2 and Sirt2. *Redox Biol.* 15, 284–296. doi:10.1016/j.redox.2017.12.013
- Zhou, Y., Hou, J., Liu, W., Ren, S., Wang, Y., Zhang, R., et al. (2018). 20(R)-ginsenoside Rg3, a rare saponin from red ginseng, ameliorates acetaminophen-induced hepatotoxicity by suppressing PI3K/AKT pathway-mediated inflammation and apoptosis. *Int. Immunopharmacol.* 59, 21–30. doi:10.1016/j.intimp.2018.03.030
- Zhu, C., Wang, Y., Liu, H., Mu, H., Lu, Y., Zhang, J., et al. (2017). Oral administration of Ginsenoside Rg1 prevents cardiac toxicity induced by doxorubicin in mice through anti-apoptosis. *Oncotarget* 8, 83792–83801. doi:10.18632/oncotarget.19698
- Zhu, Y., Hu, C., Zheng, P., Miao, L., Yan, X., Wang, Z., et al. (2016). Ginsenoside Rb1 alleviates aluminum chloride-induced rat osteoblasts dysfunction. *Toxicology* 368, 183–188. doi:10.1016/j.tox.2016.07.014



## OPEN ACCESS

## EDITED BY

Alex Boye,  
University of Cape Coast, Ghana

## REVIEWED BY

Ashutosh Kumar,  
Washington University in St. Louis,  
United States  
Ridha Oueslati,  
University Carthage -Sciences Faculty  
of Bizerte, Tunisia

## \*CORRESPONDENCE

Hamda A. Al-Naemi,  
halnaemi@qu.edu.qa

## SPECIALTY SECTION

This article was submitted to Predictive  
Toxicology,  
a section of the journal  
Frontiers in Pharmacology

RECEIVED 03 August 2022

ACCEPTED 20 September 2022

PUBLISHED 06 October 2022

## CITATION

Attia SM, Das SC, Varadharajan K and  
Al-Naemi HA (2022), White adipose  
tissue as a target for cadmium toxicity.  
*Front. Pharmacol.* 13:1010817.  
doi: 10.3389/fphar.2022.1010817

## COPYRIGHT

© 2022 Attia, Das, Varadharajan and Al-  
Naemi. This is an open-access article  
distributed under the terms of the  
[Creative Commons Attribution License  
\(CC BY\)](https://creativecommons.org/licenses/by/4.0/). The use, distribution or  
reproduction in other forums is  
permitted, provided the original  
author(s) and the copyright owner(s) are  
credited and that the original  
publication in this journal is cited, in  
accordance with accepted academic  
practice. No use, distribution or  
reproduction is permitted which does  
not comply with these terms.

# White adipose tissue as a target for cadmium toxicity

Sarra Mohammed Attia<sup>1,2</sup>, Sandra Concepcion Das<sup>1,2</sup>,  
Kavitha Varadharajan<sup>1</sup> and Hamda A. Al-Naemi<sup>1,2\*</sup>

<sup>1</sup>Laboratory Animal Research Center, Qatar University, Doha, Qatar, <sup>2</sup>Department of Biological and Environmental Science, Qatar University, Doha, Qatar

Cadmium (Cd) is a widespread heavy metal known as a toxic environmental pollutant. Cd exposure is threatening due to its bioaccumulation trait in living systems that exceeds 35 years without a beneficial biological role. Acute exposure to high Cd doses was reported to impact adipose tissue (AT) function adversely. The main aim of this study is to investigate the effect of low-dose chronic Cd exposure on the genes involved in adipose tissue (AT) functions. Adult male Sprague-Dawley rats were exposed to a low Cd dose (15 mg/kg B.W./day) for 10 weeks. Then, three AT depots-subcutaneous AT (SUB-AT), abdominal AT (AB-AT), and retroperitoneal AT (REtrop-AT) were excised for Cd accumulation measures and gene expression analysis. Adiponectin and leptin gene expression levels were investigated as markers for adipocytes function and homeostasis. Our results showed that Cd accumulated in all the tested adipose depots, but SUB-AT was found to be the depot to most accumulate Cd. Also, it was exhibited that chronic exposure to low Cd doses altered the gene expression of adipocytokines. The levels of adiponectin and leptin mRNA expression were downregulated in all tested AT-depots after Cd exposure. The significant adverse effect on SUB-AT compared to other depots indicates different responses based on AT depots location toward Cd exposure. Collectively, these results suggest a toxic effect of Cd that influenced adipocyte function.

## KEYWORDS

cadmium, heavy metals, environmental pollutant, adipose tissue, adipocytes dysfunction, adipokines

## Introduction

Environmental pollution is increasing due to the extensive urbanization and expanded industries. Cadmium (Cd) is classified as a toxic environmental pollutant that is listed among the top ten toxic substances by the Agency for Toxic Substances and Disease Registry (ATSDR, 2019). The recent global production of Cd reached 23,000 metric tons, highlighting the current challenge of Cd exposure worldwide (USGS, 2020). The main routes of Cd exposure are inhalation and ingestion of contaminated food and water (Andjelkovic et al., 2019; Fatima et al., 2019). Cadmium pose a toxic risk because of its prolonged biological half-life (10–30 years) with no known beneficial physiological function (Jacobo-Estrada et al., 2017; Rahimzadeh et al., 2017).

Cadmium accumulates in different tissues such as liver, kidney, skeletal muscle, pancreas, and also the adipose tissue (Ficková et al., 2003; Lee et al., 2012; Buha et al., 2018).

Adipose tissue (AT) is a key organ that regulates various physiological processes such as lipid metabolism and energy homeostasis. In addition, AT is responsible for releasing factors known as adipokines that regulate appetite, energy expenditure, and fat distribution. Adipokines are involved in metabolic regulation and play an essential role in maintaining systemic functions such as inflammatory and immunological responses, vascular events, reproductive functions, appetite regulation, and insulin sensitivity (Henriques et al., 2019). Additionally, some of these secreted adipokines exert both autocrine and paracrine actions, which mainly affect the processes of AT remodeling, angiogenesis, and adipogenesis (Ordovas and Corella, 2008; Henriques et al., 2019; Attia et al., 2022). The AT secretory status depends on the changes of cellular tissue composition, including alterations in the phenotypes, numbers, and site of adipose tissue depots (Ouchi et al., 2011). There are two types of adipokines- pro-inflammatory such as leptin, monocyte chemoattractant protein 1 (MCP-1), tumor necrosis factor- $\alpha$  (TNF- $\alpha$ ), interleukin 6 (IL-6) and anti-inflammatory such as adiponectin and interleukin 10 (IL-10) (Mancuso, 2016; Hui and Feng, 2018; Henriques et al., 2019).

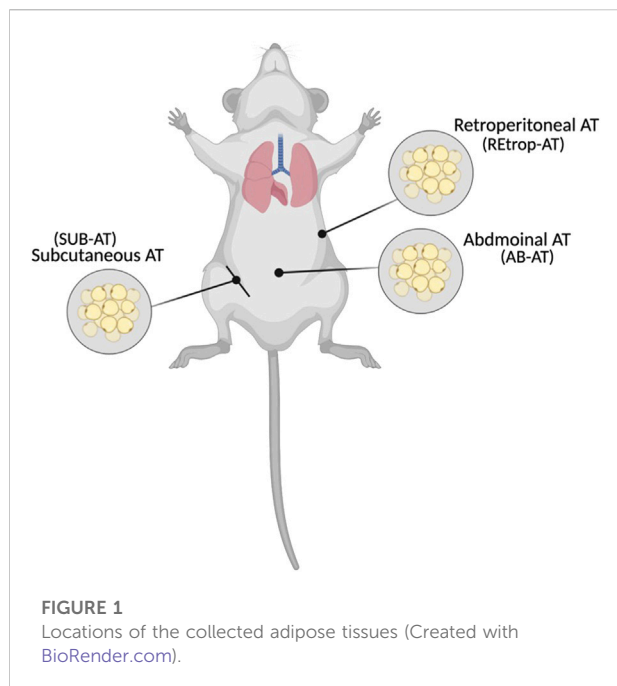
Regarding the adipokines, leptin is an adipokine secreted by AT and was the main reason for adipose tissue recognition as an endocrine organ when first discovered in 1994 (Zhang et al., 1994). Leptin signals have an essential contribution to regulating AT metabolism, appetite, satiety, puberty, fertility, and reproductive function (Fasshauer and Blüher, 2015; Stern et al., 2016). Moreover, leptin can directly increase pro-inflammatory cytokines such as TNF- $\alpha$  and IL-6 in monocytes and enhance the production of chemokines like MCP-1 and IL-8 in macrophages and the lipid mediators PGE2 cysteinyl leukotrienes (Ouchi et al., 2011; Mancuso, 2016). Adiponectin is an adipokine produced exclusively by adipocytes with a high level in the blood that ranges between 3 and 30  $\mu\text{g/ml}$ , and it targets different cell types (Fasshauer and Blüher, 2015; Mancuso, 2016). The metabolic properties of adiponectin are favorable since it is an anti-inflammatory adipokine that can inhibit the activation of nuclear factor kappa-light-chain-enhancer of activated B cells (NF- $\kappa\text{B}$ ). As a result, it inhibits inflammation, reduces the expression of TNF- $\alpha$  and IL-6, and regulates glucose metabolism and energy homeostasis (Chandrasekar et al., 2008; Novotny et al., 2012; Vasiliauskaitė-brooks et al., 2017). Studies showed that a dysregulation in the adipocyte secretion of adiponectin, leptin, resistin, and TNF- $\alpha$  is related to increased risk of type 2 diabetes and arteriosclerosis (Kawakami et al., 2010; Samaras et al., 2010). The crosstalk between the adipokines and cytokines under cadmium exposure were extensively reviewed by Attia et al. (2022).

White adipose tissue (WAT) is considered the main site of metabolic dysregulation in several metabolic diseases (Henriques et al., 2019). There are two main subtypes of WAT: the subcutaneous and the visceral. The latter also can be further subdivided into omental, mesenteric, perirenal, and peritoneal fat depots (Choe et al., 2016). Subcutaneous AT is located in the innermost layers of the skin and has a primary function of energy storage (Badimon and Cubedo, 2017; Henriques et al., 2019; Kahn et al., 2019). Moreover, subcutaneous AT is responsible for thermal insulation and providing a protective cushion against mechanical damage (Choe et al., 2016; Chait and den Hartigh, 2020). On the other hand, the visceral AT is located in the internal organs and is known for its high metabolic response (Badimon and Cubedo, 2017; Kahn et al., 2019). Both subcutaneous AT and visceral AT have different metabolic functions and different adipokine expression profiles.

Adipose tissue is a potential target for Cd accumulation. Recent study reported that Cd accumulates in AT of the human body with an average concentration of 12.6  $\mu\text{g/kg}$  (Egger et al., 2019). Moreover, results reported by Echeverría et al. (2019) showed that the mean Cd concentration in AT of breast and waist regions was 32 and 42  $\mu\text{g/kg}$ , respectively. The authors correlated this accumulation of Cd in AT with several parameters such as age, smoking, the types of food consumed, and body mass index. Data collected earlier from animal studies showed similar results. Kawakami et al. (2010) reported a correlation between Cd dose increments and elevation of Cd concentration in AT of male ICR: ICR mice. The risk of Cd accumulation in AT includes disrupting its capability to accommodate the surplus energy and produce the required adipokines for its endocrine function. Consequently, this may affect systemic homeostasis since AT occupies a large part of the whole body. Of note, few studies investigated the direct effect of Cd on AT function. Thus, this study aims to investigate the effect of chronic exposure to low dose of Cd on AT, where the pattern of adipocyte secretion will be evaluated to assess the white adipose tissue function.

## Materials and methods

The study design was established by Al-Naemi and Das (2020), and approved by the Institutional Animal Care and Use Committee (Approval# QU-IACUC 038/2017) Briefly, adult male Sprague-Dawley (SD) rats (8 weeks old) were divided into two groups, control (C) and cadmium-treated (Cd-T). The control group received standard chow and normal drinking water while cadmium treated group received standard chow and cadmium in drinking water with dose of 15 mg Cd/kg body weight as CdCl<sub>2</sub> (BDH Chemicals, England) for 10 weeks, *ad libitum*. During the study, the health status of the animals were observed and recorded. After 10 weeks, the animals were anesthetized, sacrificed and adipose tissue depots: subcutaneous and visceral (abdominal, and retroperitoneal) were collected as indicated in Figure 1,



frozen in liquid nitrogen and stored in the repository at  $-80^{\circ}\text{C}$ . The administered dose was chosen to represent the human equivalent dose (HED) of 2.4 mg/kg and similar to the reported intake in epidemiological studies (Reagan-Shaw et al., 2008; Bernhoft, 2013; Chunhabundit, 2016; Ghosh et al., 2018).

## Cadmium accumulation in adipose tissues

Sample preparation was adapted as previously published by Ishak et al. (2015). Harvested adipose tissue samples were weighed and digested in 69% of trace metal analysis grade nitric acid (VWR International) overnight at room temperature. Following digestion, samples were incubated at  $60^{\circ}\text{C}$  for 1 h, allowed to cool, and incubated in hydrogen peroxide at  $60^{\circ}\text{C}$  for 1 h. Then, samples were diluted to a final volume of 10 ml with deionized water and filtered using a  $0.2\ \mu\text{m}$  injection filter (GE Healthcare Life Sciences, United Kingdom) to remove any debris. Digested samples were analysed for cadmium quantification by Inductively Coupled Plasma Optical Emission Spectrometry (ICP-OES, Model: Optima 7300 DV) performed by Central Laboratories Unit, Qatar University. The limit of detection for the instrument is  $0.0001\ \mu\text{g/g}$ . Concentrations are represented as  $\mu\text{g/g}$  of tissue.

## Evaluation of Cd effect on white adipose tissues

The effect of Cd on WAT was evaluated by gene expression assay. Adipose tissue previously stored at  $-80^{\circ}\text{C}$  were

homogenized using both liquid nitrogen and probe sonicator (QSonica 500), then total RNA was extracted from adipose tissue using TRIzol™ LS Reagent (ThermoFisher Scientific, United States; 10296010). Slight modifications were followed at the washing step, where the RNA pellet was resuspended in ice cold 75% ethanol and kept at  $-20^{\circ}\text{C}$  overnight. Then, the sample was washed three times to enhance the RNA purity. Total RNA was quantified using nanophotometer (Implen; P330). A known amount of RNA (150 ng) was reverse transcribed into cDNA using the high capacity cDNA transcription kit (Applied Biosystems, Lithuania) following the manufacturer's instructions. Final volume of the reaction was  $20\ \mu\text{l}$  and stored at  $-20^{\circ}\text{C}$  until the performance of Real Time-PCR gene expression assays. RT-PCR was performed using diluted cDNA (1:3) and TaqMan® Fast Advanced Master Mix (Applied Biosystems, United States) for six targets as following: adiponectin (Rn00595250\_m1), leptin (Rn00565158\_m1), MCP-1 (Rn00580555\_m1), IL-6 (Rn01410330\_m1), IL-10 (Rn01483988\_g1), TNF- $\alpha$  (Rn01525859\_g1), GAPDH (Rn01775763\_g1). GAPDH was assigned as the endogenous control gene. The amplification was carried out in QuantStudio 6 flex system (Applied biosystem™). The relative quantity of gene expression was calculated using  $2^{-\Delta\Delta\text{Ct}}$  method. Results are presented as fold change ( $\log_2$ ) versus the mean values of the control samples normalized against the endogenous gene.

## Statistical analysis

Gene expression results were generated using  $2^{-\Delta\Delta\text{Ct}}$  method. Experiments were conducted in duplicate. The values are presented as means  $\pm$  SEM. Data was analyzed by Kruskal-Wallis test, one-way and two-way ANOVA followed by Tukey's multiple comparison test. Statistical analysis was performed using GraphPad Prism version 9.3 (GraphPad Software, San Diego, California United States, [www.graphpad.com](http://www.graphpad.com)).  $p$ -value  $< 0.05$  is considered a significant value.

## Results

### Effect of Cd exposure on the monitored parameters

Body weight, water, and chow intake of control and Cd-T rats were recorded weekly for 10 weeks (Table 1). Initially, no significant differences were observed in the body weight. However, at week 10 statistically significant difference was observed in the mean body weight between the groups ( $p$ -value  $< 0.001$ ). The weekly water intake in both groups remained stable with slight non-significant fluctuations during the study period, with a significantly reduced intake in the Cd-T

TABLE 1 Body weight, water intake and chow intake during the period of the study.

	Control group		Cd-treated group	
	Initial (Week 1)	Final (Week 10)	Initial (Week 1)	Final (Week 10)
Mean body weight (g)	378.06 ± 4.63	579.32 ± 7.87	358.88 ± 5.04	512.34 ± 10.58***
Mean water intake (mL/rat/week)	276.68 ± 16.47	227.67 ± 30.54	132.78 ± 1.42***	203.12 ± 39.86***
Mean chow intake (g/rat/week)	185.45 ± 2.88	182.65 ± 6.59	158.11 ± 2.66*	180.68 ± 22.21*

\* $p < 0.05$ , \*\*\* $p < 0.001$  when compared to control group at the corresponding time point.

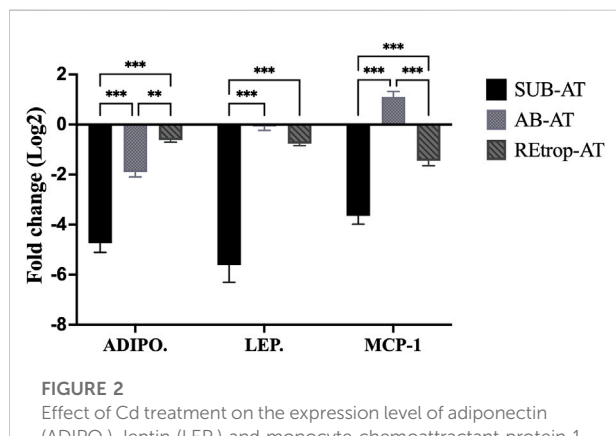


FIGURE 2

Effect of Cd treatment on the expression level of adiponectin (ADIPO.), leptin (LEP.) and monocyte chemoattractant protein 1 (MCP-1) in three different adipose depots of male Sprague-Dawley rats after 10 weeks Cd treatment. Gene expression results were generated using  $2^{-\Delta\Delta Ct}$  method and the mean fold change ( $\log_2$ ) values of the targets mRNA expression were normalized to control samples and the endogenous gene. (significance: more than 2-fold change) and Two-way ANOVA was performed using GraphPad Prism version 9. The significant difference is represented by \*\* $p < 0.01$ , \*\*\* $p < 0.001$ , ( $n = 6$ ).

group ( $p$ -value  $< 0.001$ ). The Cd-T group had a reduced initial water intake of about 52% relative to the control. At the end of the study, the difference in water intake of the Cd-T group was 11 percent lesser than the control. The initial mean chow intake of the Cd-T group was about 15% lesser than the control group, whereas the final mean chow intake of the Cd-T group was found to be like the control group. The differences in weekly chow intake were found to be statistically significant from week 1 until week 10 ( $p$ -value  $< 0.05$ ).

## Accumulation of Cd in adipose depots

The concentration of Cd in the adipose depots was determined by Inductively Coupled Plasma-Optical Emission Spectrometry (ICP-OES). The three adipose depots collected from Cd-T rats exhibited Cd accumulation (Table 2). The increasing order of Cd accumulation was found to be in RETrop-AT  $<$  AB-AT  $<$  SUB-AT. The differences in the mean

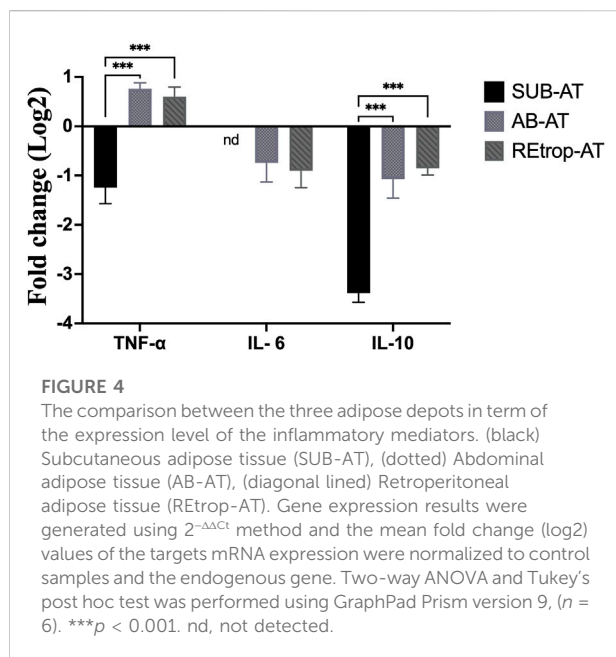
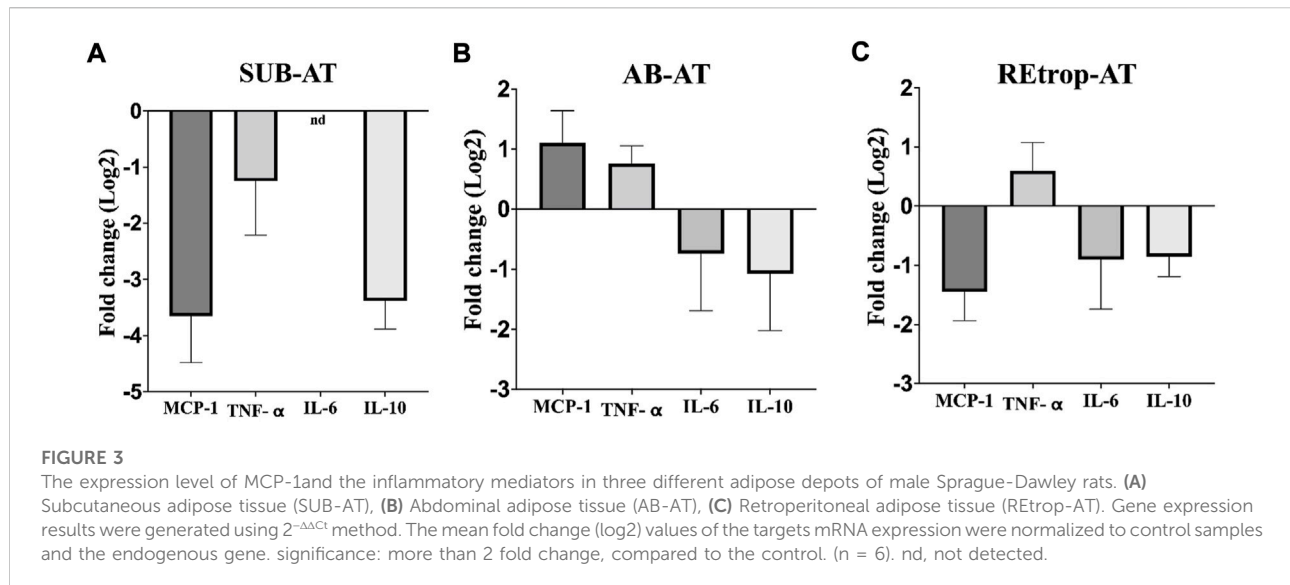
Cd concentrations, considering each depot, was found to be highly significant in SUB-AT ( $p$ -value  $< 0.01$ ) compared to AB-AT and RETrop-AT.

## Evaluation of Cd exposure on adipose tissues

Adipose tissue samples from control and Cd-T rats were analyzed for gene expression to explore the effect of Cd on AT. In Figure 2, the expression patterns of adipokines (adiponectin and leptin) and chemokine (MCP-1) are illustrated in the three fat depots. Subcutaneous adipose tissue exhibited a pattern of downregulated expression for both adiponectin and leptin. Similarly, adiponectin and leptin gene expression were decreased in RETrop-AT and AB-AT. However, the fold change for both adiponectin and leptin in SUB-AT was significant by more than two folds compared to RETrop-AT and AB-AT. For chemokine MCP-1, a downregulation trend is observed in both RETrop-AT and SUB-AT with a significant value ( $-3.8$ -fold) in the latter. Conversely, a trend of up-regulation of MCP-1 was observed in AB-AT.

## Cd exposure and the inflammatory mediators in adipose tissue

After observing differences in MCP-1 among the depots, we investigated the relationship between the expression level of MCP-1 and the inflammatory mediators in each depot under the condition of Cd exposure (Figure 3). Results showed an upregulation trend of TNF- $\alpha$  in AB-AT with no significant fold change. Similar results were observed in RETrop-AT. In contrast, in SUB-AT, TNF- $\alpha$  expression level showed a downregulation trend with no significant fold change. Both IL-6 and IL-10 were downregulated in all AT depots despite varying levels of change of MCP-1. Also, IL-6 was below the detection limit in SUB-AT. Put together, within each AT depot, there was no significant difference between the expression level of MCP-1 and the inflammatory mediators (TNF- $\alpha$ , IL-6, and IL-10). However, when comparing the effect of Cd exposure on the inflammatory mediators between depots (Figure 4),



a significant difference was found between SUB-AT and other depots for TNF- $\alpha$  and IL-10 with a *p*-value < 0.001.

## Discussion

The accumulative properties of Cd in living systems were found to impose adverse effects on tissues and influence their functions (Kumar and Sharma, 2019; Genchi et al., 2020). In this study, the effect of Cd on adipose tissue was investigated in three different depots of adult male SD rats. Our results showed that Cd exposure caused a significant decrease in rats' body weight.

The reduction of the body weight agrees with former studies that recorded Cd exposure caused a downregulation in the body weight of murine (Kawakami et al., 2010; Prabhu et al., 2020). The reduction of the body weight in the Cd-T group is suggestive of either losing adipocytes or dysregulated adipogenesis. Additionally, our results showed a downregulation of adiponectin and leptin mRNA expression levels in all AT depots. This downregulation of adiponectin and leptin mRNA expression level agrees with a previous finding, reporting that acute Cd exposure significantly decreased the mRNA expression level of adiponectin in mice (Kawakami et al., 2010). Another study conducted by Kawakami et al. (2013) using metallothionein-null mice reported that Cd exposure reduced the expression level of leptin and adiponectin in a dose-dependent manner. In our experimental model, we administered chronic low dose exposure of Cd which resulted in a decline in body weight and the expression level of adiponectin and leptin in Cd-T SD rats. The added value of the current work comes from the experimental design that was established to be realistic and proportional to the population exposure in real life (Das et al., 2021).

Under physiological conditions, the mature differentiated adipocytes produce adiponectin and leptin. Therefore, changes in the production of these adipokines are used as markers to assess changes in adipocytes maturation and functions. Conventionally, the expression patterns of adipokines differ between adipose depots (Lee et al., 2013). Subcutaneous adipose tissue expresses leptin and adiponectin more than visceral adipose tissue (Samaras et al., 2010; Lee et al., 2013; Mazaki-Tovi et al., 2016). This aligns with our results where the expression level of adiponectin and leptin is greater in SUB-AT than AB-AT and RETrop-AT.

However, Cd exposure caused a decrease in the gene expression of adiponectin and leptin and was significantly

downregulated by more than two folds in SUB-AT (Figure 2). These changes in the mRNA expression pattern of adiponectin and leptin can be linked with the disruption of adipogenesis including adipocytes maturation. Reaching the maturation stage and achieving the healthy expansion for adipocytes are regulated by critical factors such as peroxisome proliferator-activator receptor gamma (PPAR $\gamma$ ) and CCAAT/enhancer-binding protein alpha (C/EBP $\alpha$ ). A previous study reported that Cd adversely affects the differentiation of preadipocytes by downregulating the expression level of PPAR $\gamma$  and C/EBP $\alpha$  in 3T3-L1 adipocytes (Lee et al., 2012). This also accords with studies by Kawakami et al. (2010) and Kawakami et al. (2013) where results showed that Cd exposure altered the expression level of the critical regulators of adipogenic differentiation, PPAR $\gamma$  and C/EBP $\alpha$  in mice models. Alterations of adiponectin and leptin expression levels indicate the abnormal adipocytes which could be attributed to disrupted maturation process.

The level of Cd accumulation differs in the three adipose depots. The Cd accumulation results (Table 2) showed that the SUB-AT has the highest amount of Cd among other depots, elucidating its vital role as a sink for storage and buffering of Cd. These accumulated Cd levels resulted in a significant downregulation of adiponectin, leptin and MCP-1 expression levels in SUB-AT compared to other depots (Figure 2). According to literature, MCP-1 production and the macrophages' infiltration are enhanced by leptin which is a pro-inflammatory adipokine (Mancuso, 2016). However, in the current work, leptin is downregulated, which could explain the downregulated trend of MCP-1. Moreover, leptin and MCP-1 expression levels are correlated with adiposity (Bruun et al., 2005; De Victoria et al., 2009). Thus, the reduced body weight could negatively affect their expression level. A prior study investigated the inflammatory infiltration patterns in different AT depots and reported that visceral AT had more macrophages than subcutaneous AT (Jonas et al., 2015). Moreover, visceral AT is associated with inflammatory events. This could explain the upregulated trend of MCP-1 and TNF- $\alpha$  in AB-AT of our study (Figure 3).

The link between the abnormal adipocytes and the induction of inflammation, such as in the case of obesity, is extensively reported (Rull et al., 2010; Greevenbroek et al., 2016). This link is characterized by the presence of activated macrophages and inflammatory cytokines such as TNF- $\alpha$  and IL-6. These cytokines mediate the inflammatory response and are

produced by macrophages. Moreover, MCP-1 is responsible for the recruitment of monocytes/macrophages and the induction of inflammatory cytokines in the states of AT abnormality. Therefore, inflammatory cytokines can be used as markers for the activity of macrophages. Additionally, macrophages' function is determined by macrophages' quantity, activation state, and metabolic phenotypes (Li et al., 2020). Under pathological conditions, adipose tissue macrophages (ATM) can exhibit mixed phenotypes in response to the local environment (Wang et al., 2021). Furthermore, studies found that preadipocytes have the ability to differentiate into macrophages which highlights the plasticity of AT under different conditions (Charrière et al., 2003; Thomas and Apovian, 2017). Based on the literature, Cd adversely affects the differentiation capacity into macrophages and interferes with the immune cells' development (Wang et al., 2021). As mentioned earlier, Cd can disrupt the differentiation of preadipocytes through diminishing the transcription factor PPAR $\gamma$ . Another vital role of PPAR $\gamma$  is promoting the differentiation of macrophages into the M2 phenotype (Thomas and Apovian, 2017). Adipose tissue-derived MCP-1 was found to be associated with resident macrophages content, stromal vascular cells, and AT location under both conditions (Bruun et al., 2005). Our results show a trend of downregulation of both IL-6 and IL-10 in all AT depots (Figure 4). However, TNF- $\alpha$  showed a trend of upregulation in AB-AT and REtop-AT but not in SUB-AT (Figure 4). Thus, the downregulation of both anti-inflammatory and pro-inflammatory mediators further supports the hypothesis of impaired macrophages. Likewise, the impaired differentiation capacity of preadipocytes could explain the downregulation of MCP-1 and the inflammatory cytokines.

According to the literature, former studies showed that Cd significantly reduced the phagocytic activity and decreased the inflammatory responses of murine macrophages in a dose-dependent manner (Loose et al., 1978; Jin et al., 2016). Moreover, a subtoxic Cd dose (10  $\mu$ M) was found to inhibit the expression level of both IL-10 and IL-6 in murine macrophages (Riemschneider et al., 2015). Furthermore, Cox et al. (2016) proposed that Cd can induce immune dysfunction in macrophages and confirmed it with the lipopolysaccharide treatment after Cd exposure to find that macrophages' transcription and cytokine release abilities were disrupted (Cox et al., 2016). A single-cell transcriptomic study reported that chronic Cd exposure induces phenotypic alterations in the immune system and reduces the number of monocytes when comparing the circulating immune cells with the plasma Cd level (Lu et al., 2021). Taken together with the current work, chronic Cd exposure disrupts the function of immune cells, especially macrophages.

Former studies that investigated the macrophages infiltration patterns in different AT depots reported that in normal-weight and obese conditions, visceral AT was found to have more macrophages than subcutaneous AT (Jonas et al., 2015). Subcutaneous AT acts as a metabolic sink that stores excess

TABLE 2 Accumulation of cadmium in the different white adipose depots.

Cd concentration ( $\mu$ g/g tissue wt.)	Cadmium-treated group ( $n = 8$ )
Subcutaneous adipose tissue	2.285 $\pm$ 0.600**
Abdominal adipose tissue	0.255 $\pm$ 0.070
Retroperitoneal adipose tissue	0.189 $\pm$ 0.097

Concentration is represented as mean  $\pm$  S.E.M. Data was analyzed using Kruskal-Wallis test. \*\*:  $p < 0.01$  when compared between the adipose depots.

free fatty acids and glycerol in the form of triglycerides. Visceral AT accumulates when the capacity of SUB-AT is exceeded due to chronic stress (Ibrahim, 2010). Also, visceral AT is associated with inflammatory events. This could explain the upregulation trend of MCP-1 and TNF- $\alpha$  in AB-AT of our study. Although the MCP-1 expression level was found to be disrupted, the inflammatory markers were found to be downregulated which suggests that chronic exposure to low-dose Cd is not an inflammatory promotor. It is possible that Cd exposure negatively affected SUB-AT but not to the level that causes significant lipid accumulation in visceral AT.

On the other hand, Kawakami et al. (2013) reported an increment in the number of macrophages and elevation of the mRNA expression level of MCP-1 in the MT-null mice model in a dose-dependent manner. A recent study reported that acute exposure of Cd has a pro-inflammatory effect on human adipocytes (Gasser et al., 2022). An additional study reported acute Cd exposure caused an upregulation of MCP-1 mRNA expression levels in glioblastoma cell lines (Kasemsuk et al., 2020). Moreover, chronic low dose exposure to Cd was found to induce inflammatory infiltration in hepatocytes with an upregulation of MCP-1 mRNA expression level in the pubertal mice model (Li et al., 2021). However, as mentioned earlier, our study followed a different experimental design, including different conditions, tissues, and models which explain the different outcomes regarding MCP-1. This was evident in an *in vitro* study comparing mouse and rat macrophage cell lines which reported that mouse macrophage cell lines were more sensitive to Cd exposure than rat macrophages cell lines (García-Mendoza et al., 2019). Despite the dose, acute exposure of Cd caused an upregulation of MCP-1 mRNA expression level within the first 24h, but the longer time of Cd exposure caused downregulation of MCP-1 expression level for two rats strains (Harstad, 2002). This suggests a different response based on the duration of Cd exposure. Thus, the downregulation of MCP-1 after 10 weeks of exposure to low Cd dose in the current study is the response of ATs of the SD model to the chronic Cd exposure treatment. Of note, the expression of TNF- $\alpha$  was not significant, which may indicate that low-dose Cd is not a pro-inflammatory factor in AT. This is in accordance with previous studies reporting that the pro-inflammatory cytokines were downregulated in the condition of low-dose Cd (Låg et al., 2010; Messner and Bernhard, 2010).

## Conclusion

In conclusion, the current work reported that chronic low-dose Cd exposure leads to accumulation of cadmium in AT depots and the most accumulated amounts were detected in SUB-AT. This altered the gene expression profile of adiponectin and leptin which resulted in its downregulation. The dysregulation of these vital adipokines indicates a toxic effect of Cd that influences

adipocyte functions. To the best of our knowledge, the present study is the first to investigate the effect of chronic low-dose Cd on different white adipose depots. Further investigation is required to study the effect of chronic low-dose Cd on the protein level to explore whether Cd induces posttranscriptional alterations that change the functionality of AT proteins. In addition, a histopathological study is required to study the structural changes of each depot. The outcomes of these experiments could further elucidate the role that Cd plays through adipocytes in developing various metabolic complications.

## Data availability statement

The original contributions presented in the study are included in the article/supplementary materials, further inquiries can be directed to the corresponding author.

## Ethics statement

The animal study was reviewed and approved by the Institutional Animal Care and Use Committee, Qatar University.

## Author contributions

SA: Conceptualization, writing—original draft, investigation, formal analysis, data curation, visualization. SD: Investigation, formal analysis, data curation, writing—review and editing, visualization. KV: Review, editing, methodology, supervision. HA-N: Conceptualization, methodology, data curation, writing—review and editing, visualization, funding acquisition, supervision.

## Funding

This study was funded by the internal Qatar University grants QUCP-CAS-BES-15/16, and QUST-2-LARC-2020-1.

## Acknowledgments

The assistance for resources provided by Dr. Muralitharan Shanmugakonar was greatly appreciated.

## Conflict of interest

The authors declare that the research was conducted in the absence of any commercial or financial relationships that could be construed as a potential conflict of interest.

## Publisher's note

All claims expressed in this article are solely those of the authors and do not necessarily represent those of their affiliated

organizations, or those of the publisher, the editors and the reviewers. Any product that may be evaluated in this article, or claim that may be made by its manufacturer, is not guaranteed or endorsed by the publisher.

## References

- Al-Naemi, H. A., and Das, S. C. (2020). Cadmium-induced endothelial dysfunction mediated by asymmetric dimethylarginine. *Environ. Sci. Pollut. Res.* 27, 16246–16253. doi:10.1007/s11356-020-08116-5
- Andjelkovic, M., Buha Djordjevic, A., Antonijevic, E., Antonijevic, B., Stanic, M., Kotur-Stevuljevic, J., et al. (2019). Toxic effect of acute cadmium and lead exposure in rat blood, liver, and kidney. *Int. J. Environ. Res. Public Health* 16 (2), 274. doi:10.3390/ijerph16020274
- ATSDR (2019). ATSDR's substance priority list. Available at: <https://www.atsdr.cdc.gov/spl/#>.
- Attia, S. M., Varadharajan, K., Shanmugakonar, M., Das, S. C., and Al-Naemi, H. A. (2022). Cadmium: An emerging role in adipose tissue dysfunction. *Expo. Heal.* 14, 171–183. doi:10.1007/s12403-021-00427-3
- Badimon, L., and Cubedo, J. (2017). Adipose tissue depots and inflammation: Effects on plasticity and resident mesenchymal stem cell function. *Cardiovasc. Res.* 113, 1064–1073. doi:10.1093/cvr/cvx096
- Bernhoft, R. A. (2013). Cadmium toxicity and treatment. *Sci. World J.* 2013, 7, doi:10.1155/2013/394652
- Bruun, J. M., Lihn, A. S., Pedersen, S. B., and Richelsen, B. (2005). Monocyte chemoattractant protein-1 release is higher in visceral than subcutaneous human adipose tissue (AT): implication of macrophages resident in the AT. *J. Clin. Endocrinol. Metab.* 90, 2282–2289. doi:10.1210/jc.2004-1696
- Buha, A., Matovic, V., Antonijevic, B., Bulat, Z., Curcic, M., Renieri, E. A., et al. (2018). Overview of cadmium thyroid disrupting effects and mechanisms. *Int. J. Mol. Sci.* 19 (5), 1501. doi:10.3390/ijms19051501
- Chait, A., and den Hartigh, L. J. (2020). Adipose tissue distribution, inflammation and its metabolic consequences, including diabetes and cardiovascular disease. *Front. Cardiovasc. Med.* 7, doi:10.3389/fcvm.2020.00022
- Chandrasekar, B., Boylston, W. H., Venkatachalam, K., Webster, N. J. G., Prabhu, S. D., and Valente, A. J. (2008). Adiponectin blocks interleukin-18-mediated endothelial cell death via APPL1-dependent AMP-activated protein kinase (AMPK) activation and IKK/NF- $\kappa$ B/PTEN suppression. *J. Biol. Chem.* 283, 24889–24898. doi:10.1074/jbc.M804236200
- Charrière, G., Cousin, B., Arnaud, E., André, M., Bacou, F., Pénicaud, L., et al. (2003). Preadipocyte conversion to macrophage. *J. Biol. Chem.* 278, 9850–9855. doi:10.1074/jbc.M210811200
- Choe, S. S., Huh, J. Y., Hwang, I. J., Kim, J. I., and Kim, J. B. (2016). Adipose tissue remodeling: Its role in energy metabolism and metabolic disorders. *Front. Endocrinol. (Lausanne)* 7, 1–16. doi:10.3389/fendo.2016.00030
- Chunhabundit, R. (2016). Cadmium exposure and potential health risk from foods in contaminated area, Thailand. *Toxicol. Res.* 32, 65–72. doi:10.5487/TR.2016.32.1.065
- Cox, J. N., Rahman, M. A., Bao, S., Liu, M., Wheeler, S. E., and Knoell, D. L. (2016). Cadmium attenuates the macrophage response to LPS through inhibition of the NF- $\kappa$ B pathway. *Am. J. Physiol. Lung Cell. Mol. Physiol.* 311, L754–L765. doi:10.1152/ajplung.00022.2016
- Das, S. C., Varadharajan, K., Shanmugakonar, M., and Al-Naemi, H. A. (2021). Chronic cadmium exposure alters cardiac matrix metalloproteinases in the heart of sprague-dawley rat. *Front. Pharmacol.* 12, 663048. doi:10.3389/fphar.2021.663048
- De Victoria, E. O. M., Xu, X., Koska, J., Francisco, A. M., Scalise, M., Ferrante, A. W., et al. (2009). Macrophage content in subcutaneous adipose tissue: Associations with adiposity, age, inflammatory markers, and whole-body insulin action in healthy pima Indians. *Diabetes* 58, 385–393. doi:10.2337/db08-0536
- Echeverría, R., Vrhovnik, P., Salcedo-Bellido, I., Iribarne-Durán, L. M., Fiket, Ž., Dolenc, M., et al. (2019). Levels and determinants of adipose tissue cadmium concentrations in an adult cohort from southern Spain. *Sci. Total Environ.* 670, 1028–1036. doi:10.1016/j.scitotenv.2019.03.114
- egger, A. E., Grabmann, G., Gollmann-Tepeköylü, C., Pechriggl, E. J., Artner, C., Türkcan, A., et al. (2019). Chemical imaging and assessment of cadmium distribution in the human body. *Metalomics* 11, 2010. doi:10.1039/C9MT00178F
- Fasshauer, M., and Blüher, M. (2015). Adipokines in health and disease. *Trends Pharmacol. Sci.* 36, 461–470. doi:10.1016/j.tips.2015.04.014
- Fatima, G., Raza, A. M., Hadi, N., Nigam, N., and Mahdi, A. A. (2019). Cadmium in human diseases: It's more than just a mere metal. *Indian J. Clin. Biochem.* 34, 371–378. doi:10.1007/s12291-019-00839-8
- Ficková, M., Eybl, V., Kotyzová, D., Mičková, V., Möstböck, S., and Brtko, J. (2003). Long lasting cadmium intake is associated with reduction of insulin receptors in rat adipocytes. *BioMetals* 16, 561–566. doi:10.1023/a:1023485130767
- García-Mendoza, D., Han, B., Berg, H. J. H. J., and Brink, N. W. (2019). Cell-specific immune-modulation of cadmium on murine macrophages and mast cell lines *in vitro*. *J. Appl. Toxicol.* 39, 992–1001. doi:10.1002/jat.3788
- Gasser, M., Lenglet, S., Bararpour, N., Sajic, T., Wiskott, K., Augsburger, M., et al. (2022). Cadmium acute exposure induces metabolic and transcriptomic perturbations in human mature adipocytes. *Toxicology* 470, 153153. doi:10.1016/j.tox.2022.153153
- Genchi, G., Sinicropi, M. S., Lauria, G., Carocci, A., and Catalano, A. (2020). The effects of cadmium toxicity. *Int. J. Environ. Res. Public Health* 17, 3782. doi:10.3390/ijerph17113782
- Ghosh, K., N. I., and Indra, N. (2018). Cadmium treatment induces echinocytosis, DNA damage, inflammation, and apoptosis in cardiac tissue of albino Wistar rats. *Environ. Toxicol. Pharmacol.* 59, 43–52. doi:10.1016/J.ETAP.2018.02.009
- Greevenbroek, M. M. J., Schalkwijk, C. G., and Stehouwer, C. D. A. (2016). Dysfunctional adipose tissue and low-grade inflammation in the management of the metabolic syndrome. *Curr. Pract. Future AdvancesF1000Research* 5, 2515. doi:10.12688/f1000research.8971.1
- Harstad, E. B. (2002). Analysis of strain difference in sensitivity to cadmium-induced hepatotoxicity in fischer 344 and sprague-dawley rats. *Toxicol. Sci.* 67, 329–340. doi:10.1093/toxsci/67.2.329
- Henriques, F., Bedard, H., and Luiz Batista Júnior, M. (2019). Adipose tissue - an update. *Adipose Tissue Inflamm. Metabolic Disord.*, 13. doi:10.5772/intechopen.88631
- Hui, H. X., and Feng, T. (2018). *Adipose tissue as an endocrine organ*. Vienna: Intechopen, 13. doi:10.5772/57353
- Ibrahim, M. M. (2010). Subcutaneous and visceral adipose tissue: Structural and functional differences. *Obes. Rev.* 11, 11–18. doi:10.1111/j.1467-789X.2009.00623.x
- Ishak, I., Rosli, F. D., Mohamed, J., and Mohd Ismail, M. F. (2015). Comparison of digestion methods for the determination of trace elements and heavy metals in human hair and nails. *Malays. J. Med. Sci.* 22, 11–20. Available at: <https://pubmed.ncbi.nlm.nih.gov/28223880>.
- Jacobo-Estrada, T., Santoyo-Sánchez, M., Thévenod, F., and Barbier, O. (2017). Cadmium handling, toxicity and molecular targets involved during pregnancy: Lessons from experimental models. *Int. J. Mol. Sci.* 18, 1590. doi:10.3390/ijms18071590
- Jin, Y., Liu, L., Zhang, S., He, R., Wu, Y., Chen, G., et al. (2016). Cadmium exposure to murine macrophages decreases their inflammatory responses and increases their oxidative stress. *Chemosphere* 144, 168–175. doi:10.1016/j.chemosphere.2015.08.084
- Jonas, M. I., Kurylowicz, A., Bartoszewicz, Z., Lisik, W., Jonas, M., Wierzbicki, Z., et al. (2015). Interleukins 6 and 15 levels are higher in subcutaneous adipose tissue, but obesity is associated with their increased content in visceral fat depots. *Int. J. Mol. Sci.* 16, 25817–25830. doi:10.3390/ijms161025817
- Kahn, C. R., Wang, G., and Lee, K. Y. (2019). Altered adipose tissue and adipocyte function in the pathogenesis of metabolic syndrome. *J. Clin. Invest.* 129, 3990–4000. doi:10.1172/JCI129187
- Kasemsuk, T., Phuagkhaopong, S., Yubolphan, R., Rungreangplangkool, N., and Vivithanaporn, P. (2020). Cadmium induces CCL2 production in glioblastoma cells via activation of MAPK, PI3K, and PKC pathways. *J. Immunotoxicol.* 17, 186–193. doi:10.1080/1547691X.2020.1829211
- Kawakami, T., Sugimoto, H., Furuichi, R., Kadota, Y., Inoue, M., Setsu, K., et al. (2010). Cadmium reduces adipocyte size and expression levels of adiponectin and Pparg1/Mest in adipose tissue. *Toxicology* 267, 20–26. doi:10.1016/j.tox.2009.07.022

- Kawakami, T., Nishiyama, K., Kadota, Y., Sato, M., Inoue, M., and Suzuki, S. (2013). Cadmium modulates adipocyte functions in metallothionein-null mice. *Toxicol. Appl. Pharmacol.* 272, 625–636. doi:10.1016/j.taap.2013.07.015
- Kumar, S., and Sharma, A. (2019). Cadmium toxicity: Effects on human reproduction and fertility. *Rev. Environ. Health* 34, 327–338. doi:10.1515/reveh-2019-0016
- Låg, M., Rodionov, D., Øvrevik, J., Bakke, O., Schwarze, P. E., and Refsnes, M. (2010). Cadmium-induced inflammatory responses in cells relevant for lung toxicity: Expression and release of cytokines in fibroblasts, epithelial cells and macrophages. *Toxicol. Lett.* 193, 252–260. doi:10.1016/j.toxlet.2010.01.015
- Lee, E., Moon, J. Y., and Yoo, B. S. (2012). Cadmium inhibits the differentiation of 3T3-L1 preadipocyte through the C/EBP $\alpha$  and PPAR $\gamma$  pathways. *Drug Chem. Toxicol.* 35, 225–231. doi:10.3109/01480545.2011.591401
- Lee, M., Wu, Y., and Fried, S. K. (2013). Adipose tissue heterogeneity: Implication of depot differences in adipose tissue for obesity complications. *Mol. Asp. Med.* 34, 1–11. doi:10.1016/j.mam.2012.10.001
- Li, Y., Yun, K., and Mu, R. (2020). A Review on the biology and properties of adipose tissue macrophages involved in adipose tissue physiological and pathophysiological processes. *Lipids Health Dis.* 19, 164. doi:10.1186/s12944-020-01342-3
- Li, X., Li, H., Cai, D., Li, P., Jin, J., Jiang, X., et al. (2021). Chronic oral exposure to cadmium causes liver inflammation by NLRP3 inflammasome activation in pubertal mice. *Food Chem. Toxicol.* 148, 111944. doi:10.1016/j.fct.2020.111944
- Loose, L. D., Silkworth, J. B., and Simpson, D. W. (1978). Influence of cadmium on the phagocytic and microbicidal activity of murine peritoneal macrophages, pulmonary alveolar macrophages, and polymorphonuclear neutrophils. *Infect. Immun.* 22, 378–381. doi:10.1128/iai.22.2.378-381.1978
- Lu, Y., Wu, J., Gu, W., Huang, Z., Shu, Z., Huang, M., et al. (2021). Single-cell transcriptomics uncovers phenotypic alterations in the monocytes in a Chinese population with chronic cadmium exposure. *Ecotoxicol. Environ. Saf.* 211, 111881. doi:10.1016/j.ecoenv.2020.111881
- Mancuso, P. (2016). The role of adipokines in chronic inflammation. *ImmunoTargets Ther.* 5, 47. doi:10.2147/ITT.S73223
- Mazaki-Tovi, M., Bolin, S. R., and Schenck, P. A. (2016). Differential secretion of adipokines from subcutaneous and visceral adipose tissue in healthy dogs: Association with body condition and response to troglitazone. *Vet. J.* 216, 136–141. doi:10.1016/j.tvjl.2016.08.002
- Messner, B., and Bernhard, D. (2010). Cadmium and cardiovascular diseases: Cell biology, pathophysiology, and epidemiological relevance. *BioMetals* 23, 811–822. doi:10.1007/s10534-010-9314-4
- Novotny, D., Vaverkova, H., and Karasek, D. (2012). Lipoproteins - role in health and diseases, *Adiponectin A Perspective Adipose Tissue Marker Antiinflammatory Antiaterogenic Potencial*, 13. Vienna: InTech. doi:10.5772/47754
- Ordovas, J. M., and Corella, D. (2008). Metabolic syndrome pathophysiology: The role of adipose tissue. *Kidney Int.* 74. doi:10.1038/ki.2008.517
- Ouchi, N., Parker, J. L., Lugus, J. J., and Walsh, K. (2011). Adipokines in inflammation and metabolic disease. *Nat. Rev. Immunol.* 11, 85–97. doi:10.1038/nri2921
- Prabhu, R., Ribeiro, M., and Kajdacsy-Balla, A. (2020). The toxic effect of environmental cadmium on visceral adipose tissue. *FASEB J.* 34, 1. doi:10.1096/fasebj.2020.34.s1.06577
- Rahimzadeh, M. R., Rahimzadeh, M. R., Kazemi, S., and Moghadamnia, A. A. (2017). Cadmium toxicity and treatment: An update. *Casp. J. Intern. Med.* 8, 135–145. doi:10.22088/cjim.8.3.135
- Reagan-Shaw, S., Nihal, M., and Ahmad, N. (2008). Dose translation from animal to human studies revisited. *FASEB J.* 22, 659–661. doi:10.1096/fj.07-9574slf
- Riemschneider, S., Herzberg, M., and Lehmann, J. (2015). Subtoxic doses of cadmium modulate inflammatory properties of murine RAW 264.7 macrophages. *Biomed. Res. Int.* 2015, 295303. doi:10.1155/2015/295303
- Rull, A., Camps, J., Alonso-Villaverde, C., and Joven, J. (2010). Insulin resistance, inflammation, and obesity: Role of monocyte chemoattractant protein-1 (orCCL2) in the regulation of metabolism. *Mediat. Inflamm.* 2010, 1–11. doi:10.1155/2010/326580
- Samaras, K., Botelho, N. K., Chisholm, D. J., and Lord, R. V. (2010). Subcutaneous and visceral adipose tissue gene expression of serum adipokines that predict type 2 diabetes. *Obesity* 18, 884–889. doi:10.1038/oby.2009.443
- Stern, J. H., Rutkowski, J. M., and Scherer, P. E. (2016). Adiponectin, leptin, and fatty acids in the maintenance of metabolic homeostasis through adipose tissue crosstalk. *Cell Metab.* 23, 770–784. doi:10.1016/j.cmet.2016.04.011
- Thomas, D., and Apovian, C. (2017). Macrophage functions in lean and obese adipose tissue. *Metab. Clin. Exp.* 72, 120–143. doi:10.1016/j.metabol.2017.04.005
- USGS (2020). Cadmium. Available at: <https://pubs.usgs.gov/periodicals/mcs2020/mcs2020-cadmium.pdf>.
- Vasiliauskaitė-brooks, I., Sounier, R., Rochoaix, P., and Bellot, G. (2017). Europe PMC Funders Group Structural insights into adiponectin receptors suggest ceramidase activity. *Nature*, 544, 120–123. doi:10.1038/nature21714.Structural
- Wang, Z., Sun, Y., Yao, W., Ba, Q., and Wang, H. (2021). Effects of cadmium exposure on the immune system and immunoregulation. *Front. Immunol.* 12, 695484. doi:10.3389/fimmu.2021.695484
- Zhang, Y., Proenca, R., Maffei, M., Barone, M., Leopold, L., and Friedman, J. M. (1994). Positional cloning of the mouse obese gene and its human homologue. *Nature* 372, 425–432. doi:10.1038/372425a0



## OPEN ACCESS

EDITED BY  
Alex Boye,  
University of Cape Coast, Ghana

REVIEWED BY  
Afrina Mustari,  
Bangladesh Agricultural University,  
Bangladesh  
Milton Prabu,  
Annamalai University, India  
Abdallah Ghonimy,  
Yellow Sea Fisheries Research Institute  
(CAFS), China

\*CORRESPONDENCE  
Ola A. Habotta,  
ola\_ali@mans.edu.eg  
Ahmed Abdeen,  
ahmed.abdeen@fvtm.bu.edu.eg

<sup>†</sup>These authors have contributed equally  
to this work

SPECIALTY SECTION  
This article was submitted to Predictive  
Toxicology,  
a section of the journal  
Frontiers in Pharmacology

RECEIVED 23 August 2022  
ACCEPTED 28 September 2022  
PUBLISHED 14 October 2022

CITATION  
Habotta OA, Wang X, Othman H,  
Aljali AA, Gewaily M, Dawood M,  
Khafaga A, Zaineldin AI, Singla RK,  
Shen B, Ghamry HI, Elhussieny E,  
El-Mleeh A, Ibrahim SF and Abdeen A  
(2022), Selenium-enriched yeast  
modulates the metal bioaccumulation,  
oxidant status, and inflammation in  
copper-stressed broiler chickens.  
*Front. Pharmacol.* 13:1026199.  
doi: 10.3389/fphar.2022.1026199

COPYRIGHT  
© 2022 Habotta, Wang, Othman, Aljali,  
Gewaily, Dawood, Khafaga, Zaineldin,  
Singla, Shen, Ghamry, Elhussieny, El-  
Mleeh, Ibrahim and Abdeen. This is an  
open-access article distributed under  
the terms of the [Creative Commons  
Attribution License \(CC BY\)](https://creativecommons.org/licenses/by/4.0/). The use,  
distribution or reproduction in other  
forums is permitted, provided the  
original author(s) and the copyright  
owner(s) are credited and that the  
original publication in this journal is  
cited, in accordance with accepted  
academic practice. No use, distribution  
or reproduction is permitted which does  
not comply with these terms.

# Selenium-enriched yeast modulates the metal bioaccumulation, oxidant status, and inflammation in copper-stressed broiler chickens

Ola A. Habotta<sup>1\*†</sup>, Xiaoyan Wang<sup>2†</sup>, Hamzah Othman<sup>3</sup>,  
Abdulrahman A. Aljali<sup>4</sup>, Mahmoud Gewaily<sup>5</sup>,  
Mahmoud Dawood<sup>6,7</sup>, Asmaa Khafaga<sup>8</sup>, Amr I. Zaineldin<sup>9</sup>,  
Rajeev K. Singla<sup>10,11</sup>, Bairong Shen<sup>10</sup>, Heba I. Ghamry<sup>12</sup>,  
Eman Elhussieny<sup>13</sup>, Amany El-Mleeh<sup>14</sup>, Samah F. Ibrahim<sup>15</sup> and  
Ahmed Abdeen<sup>16,17\*</sup>

<sup>1</sup>Department of Forensic Medicine and Toxicology, Faculty of Veterinary Medicine, Mansoura University, Mansoura, Egypt, <sup>2</sup>Department of Pathology, Clinical Medical College and the First Affiliated Hospital of Chengdu Medical College, Chengdu, China, <sup>3</sup>Department of Pathology and Clinical Pathology, Faculty of Veterinary Medicine, Omar Al-Mukhtar University, Al-Bayda, Libya, <sup>4</sup>Department of Pharmacology, Toxicology and Forensic Medicine, Faculty of Veterinary Medicine, Omar Al-Mukhtar University, Al-Bayda, Libya, <sup>5</sup>Department of Anatomy and Embryology, Faculty of Veterinary Medicine, Kafrelsheikh University, Kafrelsheikh, Egypt, <sup>6</sup>Department of Animal Production, Faculty of Agriculture, Kafrelsheikh University, Kafrelsheikh, Egypt, <sup>7</sup>The Centre for Applied Research on the Environment and Sustainability, The American University in Cairo, Cairo, Egypt, <sup>8</sup>Department of Pathology, Faculty of Veterinary Medicine, Alexandria University, Edfina, Egypt, <sup>9</sup>Animal Health Research Institute (AHRI-DOKI), Agriculture Research Center, Kafrelsheikh, Egypt, <sup>10</sup>Institutes for Systems Genetics, Frontiers Science Center for Disease-Related Molecular Network, West China Hospital, Sichuan University, Chengdu, China, <sup>11</sup>School of Pharmaceutical Sciences, Lovely Professional University, Punjab, India, <sup>12</sup>Department of Home Economics, College of Home Economics, King Khalid University, Abha, Saudi Arabia, <sup>13</sup>Department of Veterinary Pharmacology, Faculty of Veterinary Medicine, University of Sadat City, Sadat City, Egypt, <sup>14</sup>Department of Veterinary Pharmacology, Faculty of Veterinary Medicine, Menoufia University, Shebin Elkoum, Egypt, <sup>15</sup>Clinical Sciences Department, College of Medicine, Princess Nourah bint Abdulrahman University, Riyadh, Saudi Arabia, <sup>16</sup>Department of Forensic Medicine and Toxicology, Faculty of Veterinary Medicine, Benha University, Toukh, Egypt, <sup>17</sup>Center of Excellence in Screening Environmental Contaminants (CESEC), Benha University, Toukh, Egypt

Copper (Cu) could be seriously hazardous when present at excessive levels, despite its vital contribution to various cellular processes. Selenium-enriched yeast (SeY) was reported to improve the health and metabolic status in broiler chicken. Hence, our study was endeavored to illustrate the mitigating efficacy of SeY on Cu-induced hepatic and renal damage. Cobb chicks aged 1 day were allocated into four experimental groups and offered a basal diet, SeY (0.5 mg/kg), CuSO<sub>4</sub> (300 mg/kg), or SeY plus CuSO<sub>4</sub> in their diets for 42 days. Our results revealed that SeY supplement antagonized significantly the Cu accumulation in livers and kidneys of exposed birds. Marked declines were also detected in the AST, ALT, urea, and creatinine levels, besides marked increases in total protein, glycerides, and cholesterol in the SeY-supplemented group. Moreover, enhancement of cellular antioxidant biomarkers (superoxide dismutase, CAT, GPx, and GSH) along with lowered MDA contents were achieved by SeY in hepatic and renal tissues. Further, SeY exerted a

noteworthy anti-inflammatory action as indicated by decreased inflammatory biomarkers (IL-1 $\beta$  and TNF- $\alpha$ ) and NO levels in both organs. Noticeable histopathological alterations of both organs further validated the changes in the markers mentioned above. To sum up, our findings indicate that SeY can be considered a potential feed supplement for alleviating Cu-induced hepatic and renal damage in broilers, possibly *via* activation of antioxidant molecules and lessening the inflammatory stress.

#### KEYWORDS

copper residue, selenium yeast, oxidative stress, inflammatory cytokines, broiler chicken

## 1 Introduction

Heavy metals are naturally distributed inorganic compounds, that can be discharged from various sources and negatively affect the health of living organisms (Habotta et al., 2022). Among these hazardous environmental metals, copper (Cu) is an element of concern owing to its wide distribution and high toxicity (Zhao et al., 2018). Cu is widely incorporated in many agrochemicals as pesticides, including cupric sulfate (CuSO<sub>4</sub>), which is toxic to different living organisms. In addition, increased Cu release to the environment may happen through melting, mining, industrial, and waste removal activities (Yang et al., 2020). Since it is highly soluble in water, CuSO<sub>4</sub> can easily disseminate to the environment; therefore, Cu exposure is inevitable to animals *via* polluted food or water (Liu et al., 2018a). Notably, it contributes substantially to cellular metabolism and numerous physiological processes such as hematopoiesis, mitochondrial respiration, antioxidation, and immunity (Yang et al., 2020). Despite its valuable physiological functions, former studies had reported that excess Cu could evoke toxicity and damage to hepatic, renal, nervous, and digestive systems (Hashem et al., 2021a; Liao et al., 2021). Cu can impair the respiratory enzyme complexes that stimulate the over-generation of highly reactive radicals and cellular oxidative injury (Hashem et al., 2021a).

The metabolism of Cu is controlled principally by the hepatic tissue, where it accumulates upon excess exposure with no noticeable signs. When the exposed Cu overwhelms the hepatic storage capability, hepatocellular lesions are developed together with release into the circulation causing damage to other tissues (Lu et al., 2010). Dietary exposure to CuSO<sub>4</sub> elicited notable elevations in serum aminotransferases, alkaline phosphatase together with declines in total protein, albumin, globulins, triglycerides, total cholesterol, low-density lipoprotein-cholesterol, and high-density lipoprotein-cholesterol levels in broilers (Hashem et al., 2021b). Likewise, dietary supplementation of inorganic Cu at a dose of 150 mg/kg significantly decreased liver and meat lipids, cholesterol, plasma lipids, triglycerides and cholesterol, beside increasing plasma AST and ALT in exposed ducks (Attia et al., 2012). Further, Cu-intoxicated chickens had higher serum levels of urea, creatinine,

and uric acid in comparison with the control group (Elazab et al., 2021). The deleterious effects of Cu are associated with reactive oxygen species (ROS) formation that surpasses the antioxidant defense system (Liu et al., 2018a). The cellular oxidative stress is accompanied by augmented inflammatory reaction by triggering the proinflammatory mediators (Liu et al., 2018b; Abdeen et al., 2021; Ismail et al., 2022). Liu et al. showed that dietary Cu exposure encouraged oxidative damage and peroxidation of lipid in chicken liver (Liu et al., 2018a). Notable suppression was observed in the antioxidant enzymes with triggered inflammatory responses in immune organs (Yang et al., 2020) and kidneys (Wang et al., 2017) of chicken fed with a Cu-contaminated diet. Further, Cu-induced oxidative damage was reported to trigger mitochondrial fragmentation leading to leakage of cytochrome-c, which in turn facilitates the cell death (Zhao et al., 2018).

Selenium is another essential element crucial for maintaining the intracellular redox balance *via* scavenging the harmful reactive radicals, thus alleviating cellular oxidative injury (Li et al., 2022). Selenium-enriched yeast (SeY) is an organic form of selenium that is lower in toxicity with higher digestibility and bioavailability than sodium selenide (Arnaut et al., 2021). Yeast cells can bind with selenium's organic and inorganic forms and incorporate them permanently into their cell structure. Yeast can bioaccumulate and convert inorganic selenium (sodium selenate and sodium selenite) into organic forms (SeY) (Kieliszek et al., 2015). Supplementation of *Oreochromis niloticus* for SeY over a period of 60 days counteracted hypoproteinemia, elevated serum aminotransferases, urea, and creatinine induced by organophosphorus intoxication (Hassan et al., 2022). Se-enriched yeast reduced creatinine, and blood urea nitrogen levels in the kidneys of chromium-exposed broilers (Zhao et al., 2022). SeY was reported to counteract ochratoxin A-mediated suppression in the levels of antioxidant enzymes and genes in the hepatic and renal tissues of treated chickens (Li et al., 2020b; Li et al., 2020a). Former results unveiled that SeY protected against hepatic and renal oxidative stress and necroptosis elicited by cadmium toxicity in chicken (Wang et al., 2020a; Chen et al., 2021). Furthermore, SeY exerted a remarkable anti-inflammatory effect induced by lead by downregulating the gene transcription levels of inflammatory mediators in skeletal muscles such as interleukin (IL)-1 $\beta$ , IL-4,

and IL-10 of exposed chicken (Liu et al., 2019). Similarly, dietary supplementation of chicken by 0.5 mg/kg SeY lessened markedly the expression levels of gene and protein related to hepatic inflammatory markers like iNOS, NF- $\kappa$ B, TNF- $\alpha$ , and prostaglandins (Wang et al., 2020b).

Up to our knowledge, the mitigating efficiency of SeY against Cu-evoked organ injury in broiler chickens has not been investigated. Therefore, this study was designed to explore the potential protective action of SeY as a feed supplement against Cu-induced oxidative and inflammatory stresses in liver and kidney tissues. Hence, this study appraises the protective impact of SeY against excess dietary inclusion of Cu and enriches its application for improvement of health status in young broiler chicks.

## 2 Materials and methods

### 2.1 Materials

Copper (II) sulphate pentahydrate ( $\text{CuSO}_4 \cdot 5\text{H}_2\text{O}$ ; CAS number 7758-99-8) was purchased from Sigma Aldrich Co. (St. Louis, MO, United States). Selenium yeast (Se, 2000 ppm) was provided by Angel Yeast (Hubei, China; purity >99.5%). All other used chemicals and reagents were of high analytical grade.

### 2.2 Experimental birds and protocol

One day old chicks of Cobb strain broilers were attained from the Faculty of Agriculture, Mansoura University, Egypt. They were raised in clean, well-ventilated floor pens under complete hygienic measures, one replicate per each pen (three birds/replication). Chicks were offered a balanced commercial ration and tap water *ad libitum*. The ideal temperature was changed; for example, it was set at 32°C for the first week and then dropped by 1°C each following week to reach 25°C. The lighting system was 24 h per day for the first week, then changed to 16 h of light and 8 h of darkness starting on day 7 and lasting until the completion of the experiment. The relative humidity was held between 60 and 70%. The basic diet was developed in accordance with Cobb 500 broilers' Broiler Performance and Nutrition Supplement. From day 1 through day 10, birds were given a beginning diet; from day 11 through day 22 they were given a growing diet; from day 23 to the completion of the experiment, they were given a finisher diet. At 7 and 14 days old, all birds received vaccinations against Newcastle disease; at 11 and 22 days old, they received vaccinations against Gumboro disease (Giambrone and Clay, 1986). Table 1 lists the feed components and chemical makeup of the basic diet. The experiment design, procedures and techniques were done in accordance with the guidelines of the Institutional Animal Care and Use Committee of Faculty of Veterinary Medicine, Mansoura University (R/133).

TABLE 1 Proximate and chemical composition of the basal diets (%).

	Experimental diets		
	Starter	Grower	Finisher
<b>Ingredients (%)</b>			
Corn, yellow	59.39	63.41	69.17
Soybean meal 48% crude protein	30.00	26.83	18.92
Corn gluten 60% crude protein	4.53	3	6.30
Soybean oil	2.60	3.4	2.60
Lime stone	1.90	1.83	1.74
Dicalcium phosphate	0.41	0.33	0.20
Common salts	0.30	0.3	0.30
Vit. Premix*	0.25	0.25	0.25
DL Lysine HCL	0.39	0.35	0.38
DL methionine	0.13	0.15	0.08
L-Threonine	0.08	0.08	0.06
L-Valine	0.02	0.02	0
<b>Chemical composition (%)</b>			
Calculated crude protein	21.50	19.50	18.50
Calculated metabolized energy (Kcal/kg)	3034	3107	3180
Analyzed crude protein*	21.32	19.40	18.41
Analyzed ether extract*	5.40	5.82	5.80
Analyzed Ash	5.97	6.36	5.00
Calcium	0.9	0.84	0.76
Available Available phosphate	0.46	0.43	0.38

\*Vitamins and minerals premix used to cover the required vitamins and minerals per each kilogram diet (Vit. A, 10,000 I.U.; Vit. D3, 1,500 I.U.; Vit. E, 10 mg; Vit. K3, 2 mg; Vit. B1, 2 mg; Vit. B2, 5 mg; Vit. B6, 3 mg; Vit. B12, 0.01 mg; Niacin, 27 mg; Folic acid, 1 mg; Biotin, 0.05 mg; Pantothenic acid, 10 mg; Mn, 60 mg; Zn, 50 mg; Cu, 10 mg; I, 0.1 mg; Se, 0.1 mg; Co, 0.1 mg; Fe, 50 mg).

### 2.3 Experimental protocol and sampling

The chicks were haphazardly allocated into four groups of 15 each, with 5 replicates in each group (3 birds x 5 replicates), as follows;

- 1 The first group (Con) received a daily, additive-free basal diet.
- 2 The second group (Cu) was dietary administered with 300 mg/kg  $\text{CuSO}_4$  following the method of Cinar et al. (Cinar et al., 2014; Hashem et al., 2021b).
- 3 The third group (selenium yeast; SeY) received a SeY-supplemented diet at a dose of 0.5 mg/kg (Wang et al., 2020a; Chen et al., 2021).
- 4 The last group (Cu+SeY) was administered basal diets supplemented with  $\text{CuSO}_4$ /kg diet plus SeY at previously mentioned doses.

All birds were carefully observed for any abnormal signs during the experimental time, which lasted for 42 days. Six

randomly chosen birds from each group had blood drawn from their wing veins, which were then centrifuged at 3000 x g for 10 min. Sera were then separated and kept at -20°C in deep freezing until further biochemical analyses. Following the recommendations of the American Veterinary Medical Association (Schaumburg, IL, United States), the birds were killed *via* cervical dislocation (Leary et al., 2016). Liver and kidney tissue were divided into different portions to evaluate antioxidant enzymes, inflammatory biomarkers, Cu and Se residues in both tissues, and histological alterations.

## 2.4 Assessment of Cu and Se concentrations in liver and kidney

Following the mineral measurement method (AOAC) (Chemists and Chemists, 1925), 3 ml of concentrated nitric acid and 1.5 ml of concentrated perchloric acid were used to digest 0.5 gm of liver or kidney tissue. The digestion process was then finished by incubating the samples in a water bath adjusted at 53°C/overnight. The resulting mixture was filtered, left to cool to room temperature, and then 20 ml of deionized water was added for dilution. The concentrations of Cu and Se were determined using a flame atomic absorption spectrophotometer (Buck Scientific 210 VGP, Inc., Norwalk, Connecticut, CT, United States).

## 2.5 Hepatic function parameters

As directed by the manufacturer, serum samples were utilized to calculate hepatic and renal damage indications. According to Reitman and Frankel, the enzymatic activity of alanine aminotransferase (ALT) and aspartate aminotransferase (AST) were estimated (Reitman and Frankel, 1957). Following the protocol of Lowry et al., the serum level of total protein was examined (Lowry et al., 1951). In addition, Roeschlau et al. (1974) and McGowan et al. (1983) were used to estimate the total serum cholesterol and triglycerides levels, respectively.

## 2.6 Renal function biomarkers

According to Coulombe and Favreau's (Coulombe and Favreau, 1963) and Larsen's (Larsen, 1972), we evaluated the renal function markers, urea and creatinine.

## 2.7 Hepatorenal oxidative stress markers

The peroxidation of lipids was assessed spectrophotometrically by measurement of its secondary

metabolite, malondialdehyde (MDA), in liver and kidney homogenates, according to Ohkawa et al. (1979). Depending on the reducing ability of glutathione to 5,5'-dithiobis (2-nitrobenzoic acid) to give yellow-colored 5-thionitrobenzoic acid, glutathione (GSH) was analyzed spectrophotometrically at 405 nm as stated by Ellman (1959).

## 2.8 Hepatorenal antioxidant enzymes activities

The activity of superoxide dismutase (SOD) was evaluated depending on the nitroblue tetrazolium dye reduction rate to diformazan following the method established by Sun et al. (1988). Catalase (CAT) activity was assessed based on the depletion of H<sub>2</sub>O<sub>2</sub> into H<sub>2</sub>O and molecular O at 240 nm, as mentioned by Aebi (1984). Additionally, the evaluation of glutathione peroxidase (GPx) activity was assessed by Paglia and Valentine (1967).

## 2.9 Hepatorenal inflammatory biomarkers

Griess reagent was utilized to estimate nitrite/nitrate (Nitric oxide; NO) levels as stated by Green et al. (1982). The concentrations of IL-1 $\beta$  (Cat number MBS261118) and TNF- $\alpha$  (Cat number MBS2509660) were analyzed using specific ELISA assay kits (MyBioSource, CA, United States).

## 2.10 Histopathological investigations

Liver and kidney specimens were fixed in 10% neutral buffered formalin for 24 h, dehydrated, cleared with xylene, and embedded in molten paraplast. For microscopical examination, a 5  $\mu$ m thick paraffin section was stained with hematoxylin and eosin.

## 2.11 Statistical analyses

Obtained data were analyzed by one-way analysis of variance (ANOVA) followed by *post hoc* Duncan's multiple range test to decide the significance among groups. Data were displayed as mean  $\pm$  standard error (SE). At *p* values <0.05, statistical significance was determined between groups. A multivariate analysis among variables and different treatments was performed through the principal component analysis (PCA) conduction. Together, a clustering heatmap was analyzed by RStudio (R version 4.0.2).

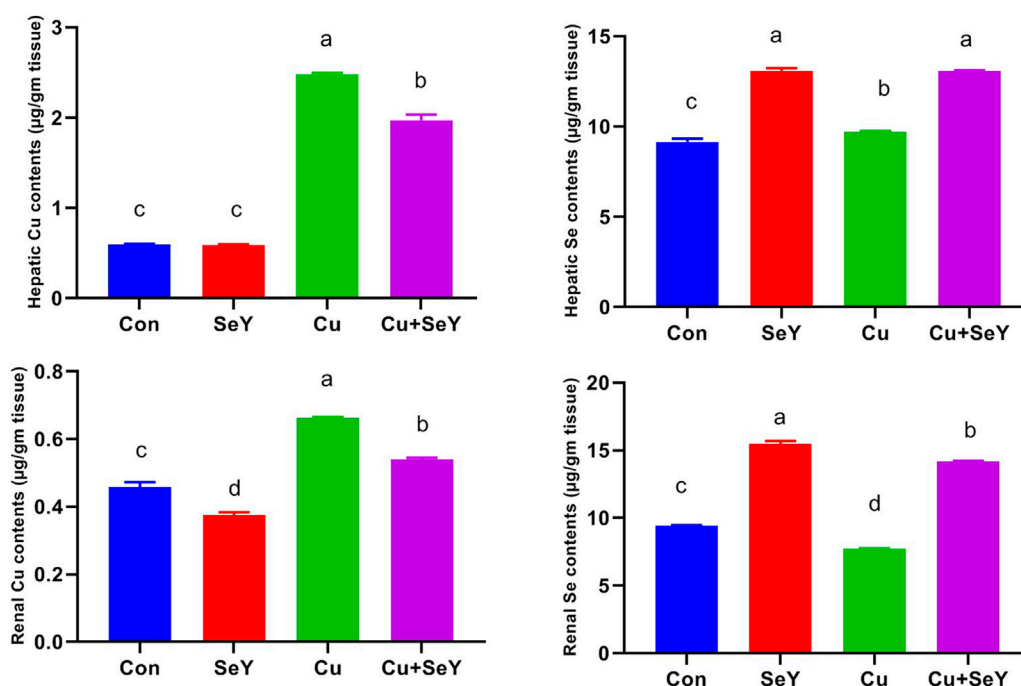


**FIGURE 1**

The copper (Cu) and selenium (Se) residual levels in the hepatic and renal tissues following dietary exposure to copper sulphate (CuSO<sub>4</sub>, 300 mg/kg) and/or selenium yeast (SeY, 0.5 mg/kg) in broiler chicken for 42 days. The values were represented as means ± SE (n = 6). Each bar carrying different letters is significantly different ( $p < 0.05$ ).

## 3 Results

### 3.1 Selenium yeast decreased hepatorenal Cu bioaccumulation

In relation with the control group, significant increases ( $p < 0.05$ ) were seen in the Cu contents in the liver and kidney of chickens that received dietary CuSO<sub>4</sub>, as illustrated in Figure 1. Contrarily, the Cu level in the Cu+SeY group was markedly less than ( $p < 0.05$ ) in the Cu-intoxicated group. Moreover, there was no discernible difference in hepatic Cu levels between the control and SeY groups. SeY group's renal Cu levels were lower than those of the control group.

Additionally, measurements of the Se content in both organs were made across all groups. The Se contents significantly increased ( $p < 0.05$ ) in the Cu+SeY and SeY administered groups but notably diminished ( $p < 0.05$ ) in the Cu-exposed chickens (Figure 1).

### 3.2 Selenium yeast modulated the serum biochemical markers

The indices of liver integrity, including TP, ALT, and AST were measured in serum samples. Noteworthy rises ( $p < 0.05$ )

were noticed in ALT and AST activities with marked decreases in TP in respect to the control group. Adversely, dietary supplementation with SeY markedly reversed ( $p < 0.05$ ) Cu-induced alterations relative to the Cu-treated group (Figure 2). In addition, marked declines ( $p < 0.05$ ) were noticed in serum levels of TC and TG in the Cu-treated group in relation to the sham group, but the supplement of SeY resulted in prominent rises ( $p < 0.05$ ) in their level compared to Cu treated only (Figure 2).

Regarding the effect of SeY on Cu-induced renal functions, serum levels of urea and creatinine were investigated. Our results showed that dietary Cu exposure induced substantial increments ( $p < 0.05$ ) in urea and creatinine levels in relation to the control. However, their levels notably decreased ( $p < 0.05$ ) with the combined treatment with Cu plus SeY (Figure 2).

### 3.3 Selenium yeast decreased Cu-mediated hepatorenal oxidative stress

To investigate the impact of Cu and/or SeY on hepatic oxidative stress, enzymatic and non-enzymatic biomarkers were investigated. As shown in Figure 5, significant depletions were noticed in the contents of SOD, CAT, GPx, and GSH ( $p < 0.05$ ) in the Cu-administered group compared to the control group. These changes were obviously reversed ( $p < 0.05$ ) after

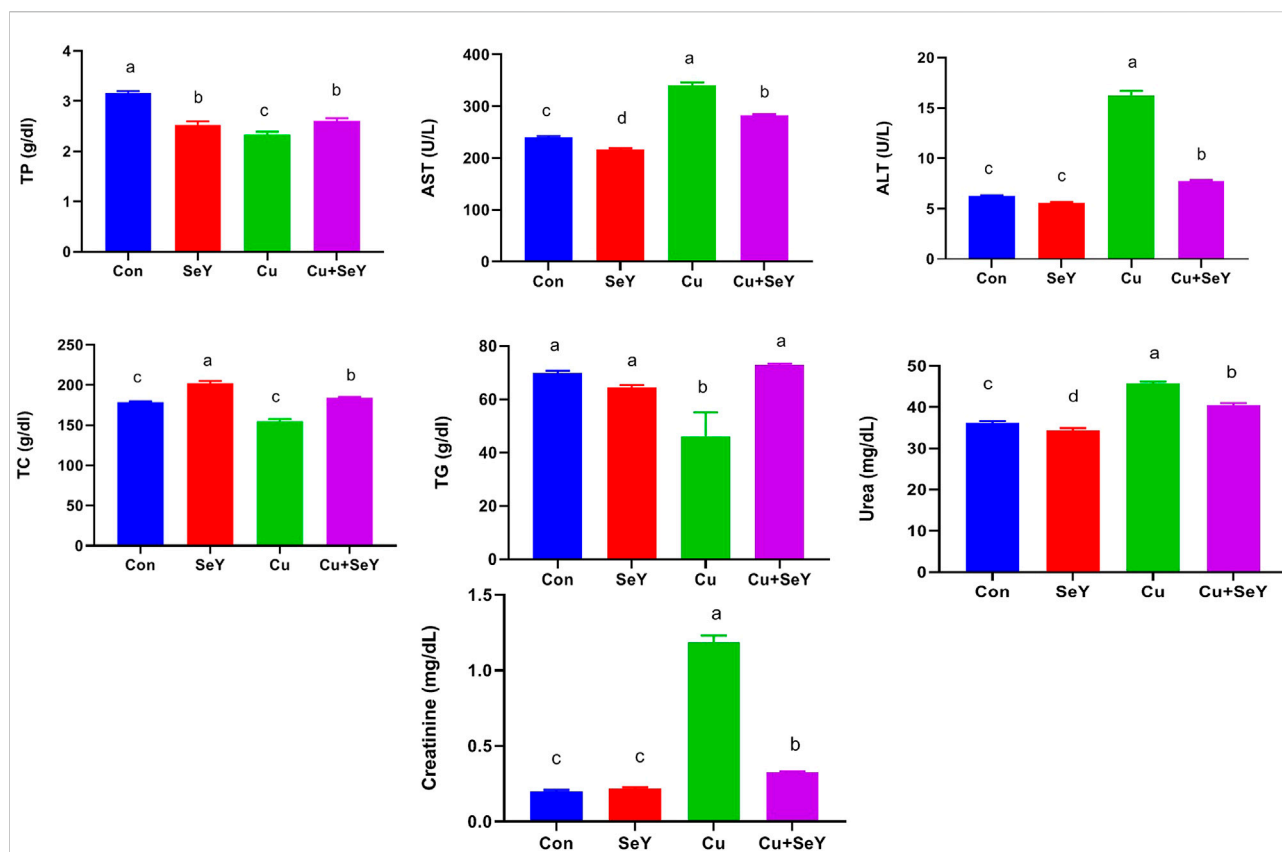


**FIGURE 2**

Serum biochemical markers following dietary exposure to copper sulphate ( $\text{CuSO}_4$ , 300 mg/kg) and/or selenium yeast (SeY, 0.5 mg/kg) in broiler chicken for 42 days. The values were represented as means  $\pm$  SE ( $n = 6$ ). Each bar carrying different letters is significantly different ( $p < 0.05$ ).

dietary supplementation with SeY. The lipid peroxidation expressed in MDA level showed a substantial rise ( $p < 0.05$ ) in hepatic tissue of Cu group in relation to the control. The SeY group had a marked lower MDA level ( $p < 0.05$ ) than that of the group that received Cu only (Figure 3).

The renal contents of SOD, CAT, GPx, and GSH were meaningfully decreased ( $p < 0.05$ ) in  $\text{CuSO}_4$ -exposed chicken compared to the controls. Contrarily, a remarkable decline ( $p < 0.05$ ) was detected in renal MDA level in  $\text{CuSO}_4$  group relative to the sham group. Moreover, the Cu-induced alterations in renal lipid peroxide level and antioxidative biomarkers were counteracted by SeY supplementation compared to the Cu group (Figure 4).

### 3.4 Selenium yeast blocked Cu-mediated hepatorenal inflammation

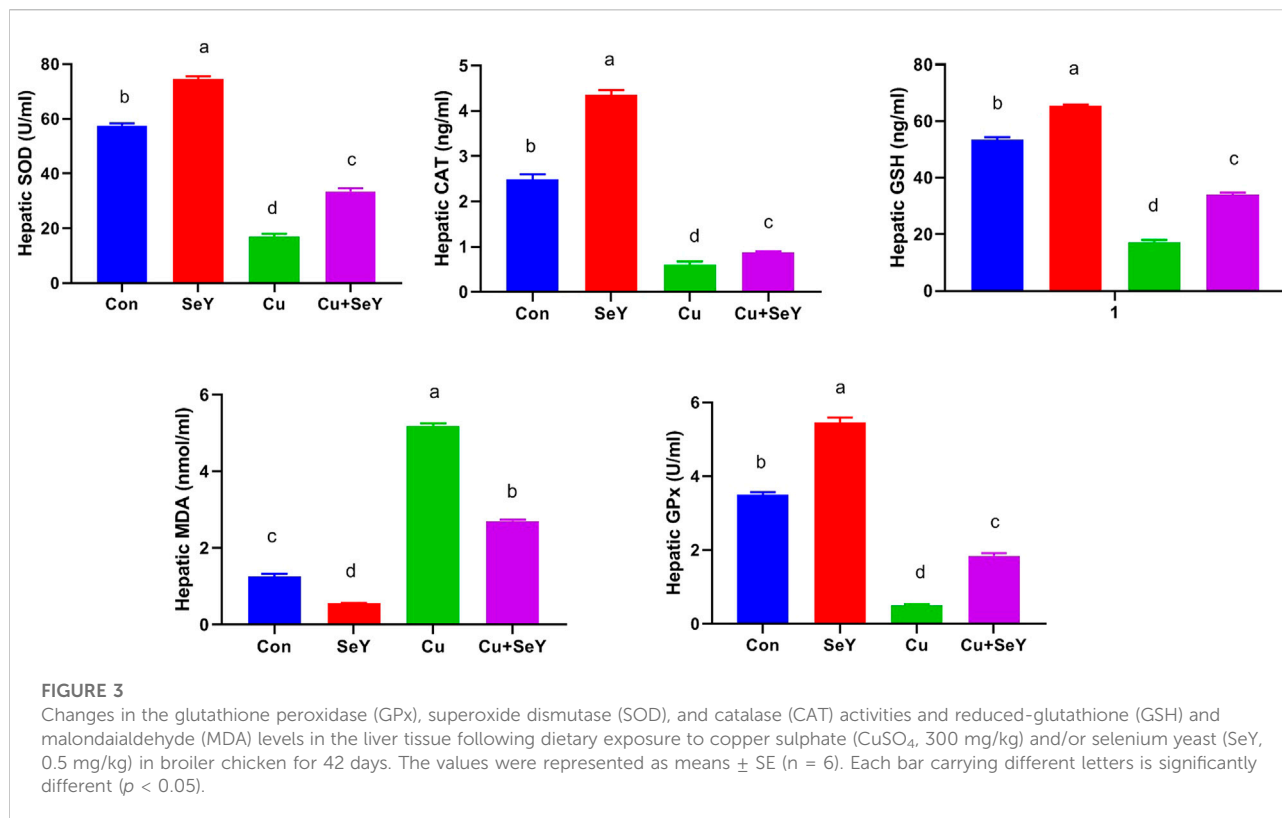
As depicted in Figure 5, the  $\text{CuSO}_4$ -exposed group displayed meaningfully higher levels ( $p < 0.05$ ) of pro-inflammatory cytokines, such as IL-1 $\beta$  and TNF- $\alpha$ , along with NO, in both tissues compared to controls. However, after SeY

supplementation, their levels declined ( $p < 0.05$ ) compared to the Cu-treated group, indicating the anti-inflammatory potential of SeY dietary inclusion.

### 3.5 Selenium yeast alleviated hepatorenal pathological alterations evoked by Cu

Microscopic pictures of hepatic sections from a control group and group that received SeY showed normally arranged hepatocytes in radial plates around central veins with normal sinusoids and portal areas. Further, liver sections in birds received Cu showing portal fibrosis, periportal coagulative necrosis of hepatocytes, and large lymphocyte follicular aggregation. In contrast, mild portal fibrosis with small lymphocytes follicular aggregation was seen in Cu+SeY group (Figure 6).

Microscopical screening of kidney sections from control and SeY groups showing normal tubules, glomeruli, and interstitial tissue. However, those from Cu-intoxicated birds exhibited prominent tubular necrosis, few apoptotic cells, congested inter-tubular blood vessels, and severe



lymphocytic infiltration. On another hand, mild tubular necrosis, congested inter-tubular blood vessels, and mild lymphocytic aggregation in interstitial tissue were recorded after supplementation of SeY to the Cu-exposed chicks (Figure 7).

### 3.6 Variable influence and clustering heatmap

A multivariate analysis (principal component analysis, PCA) was conducted and a smaller set of “summary indices” were elaborated as exhibited in Figure 8A. These data set showed how the studied variables contributed and grouped together along Dimension1 and 2 in response to different treatments. The present PCA indicated that Dimension 1 and 2 had the major contribution (80.7% and 8.2%, respectively). In the same data frame, the PCA score plot revealed that NO, TNF- $\alpha$ , IL-1 $\beta$ , MDA, urea, creatinine, and Cu residues have a tendency to change in the same way in response to Cu toxicity, hence they are grouped oppositely to the Control and SeY groups. Interestingly, the Cu+SeY group is located in the middle between both arms.

Moreover, the clustering heatmap seen in Figure 8B summarizes the concentrations of all determined variables in groups. The heatmap shows the variable concentrations in the

Cu-exposed birds are negatively correlated to the same corresponding concentrations in other treatments.

## 4 Discussion

The current experiment unveiled that SeY was able to reverse the hepatorenal impairment raised by Cu toxicity *via* improving organ functions, enhancing the antioxidant enzymatic activity, and lessening the tissue inflammation in growing broiler chicks. The excess Cu which cannot be digested and absorbed can induce liver injury and negatively affects other organs through circulation (Gaetke et al., 2014). In our study, we measured both Cu and Se levels in hepatic and renal tissues. The results revealed that chicken feeding on a Cu-containing diet resulted in increases in its residues in the liver and kidney compared to the control birds. Former studies showed that hepatic Cu retention increased with dietary Cu supplementation (Kim and Kil, 2015; Wu et al., 2020). Another study employed in chickens indicated that the amount of Cu in the kidney increased somewhat as the amount of time exposed to Cu increased (Elazab et al., 2021). Interestingly, the supplementation with SeY conferred a significant antagonistic action against hepatorenal Cu accumulation in chicken. Lui et al. observed that SeY supplementation at a dose of 0.3 mg/kg for 35 days could

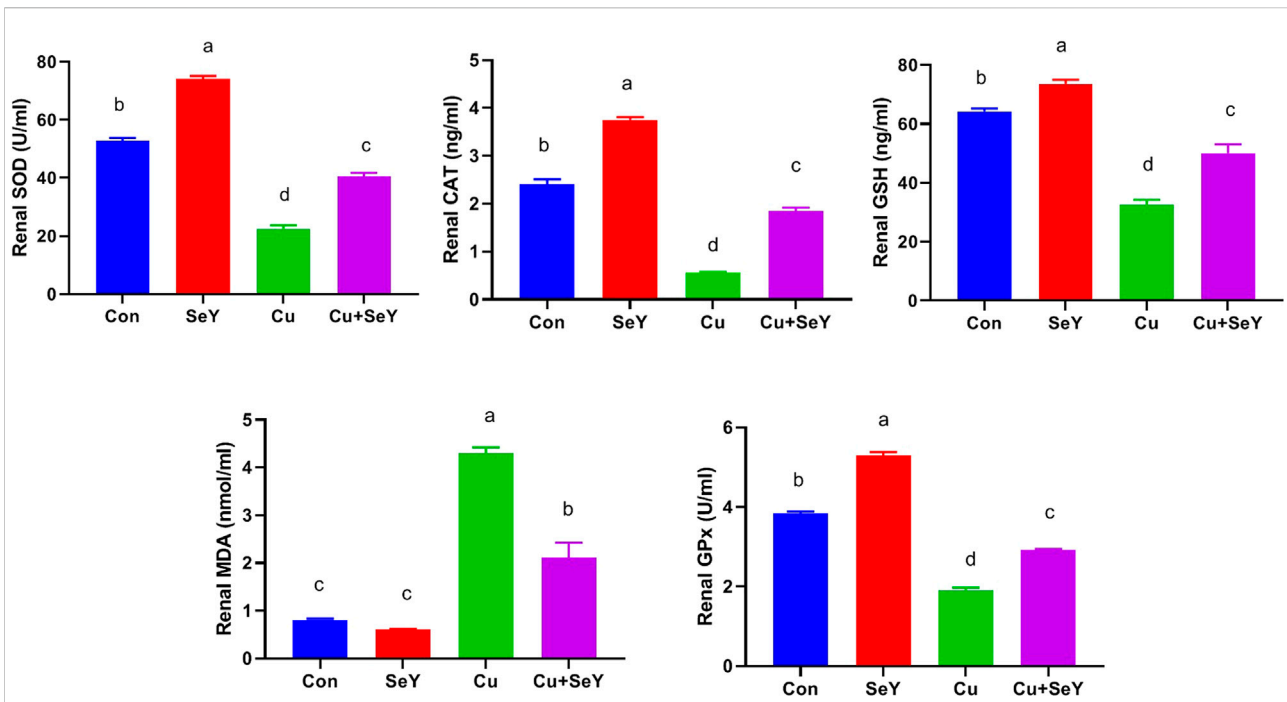


**FIGURE 4**

Changes in the glutathione peroxidase (GPx), superoxide dismutase (SOD), and catalase (CAT) activities and reduced-glutathione (GSH), and malondialdehyde (MDA) levels in the renal tissue following dietary exposure to copper sulphate (CuSO<sub>4</sub>, 300 mg/kg) and/or selenium yeast (SeY, 0.5 mg/kg) in broiler chicken for 42 days. The values were represented as means ± SE (n = 6). Each bar carrying different letters is significantly different (p < 0.05).

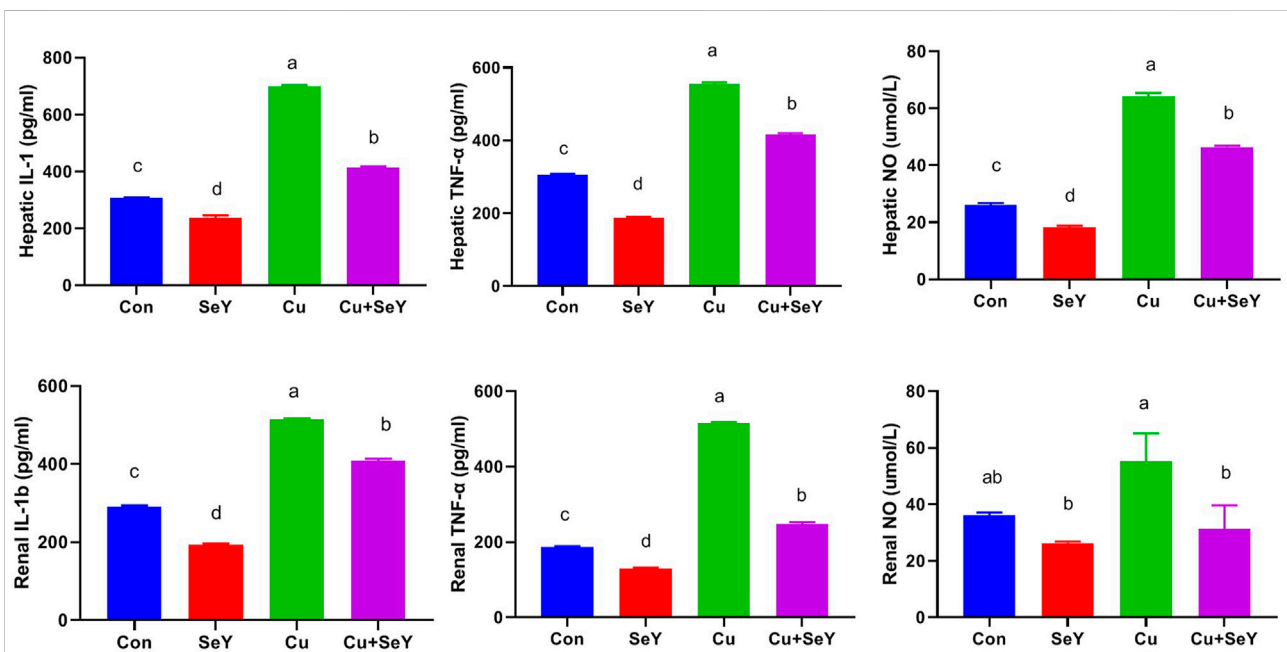


**FIGURE 5**

Hepatic and renal levels of IL-1β, TNF-α, and NO following dietary exposure to copper sulphate (CuSO<sub>4</sub>, 300 mg/kg) and/or selenium yeast (SeY, 0.5 mg/kg) in broiler chicken for 42 days. The values were represented as means ± SE (n = 6). Each bar carrying different letters is significantly different (p < 0.05).

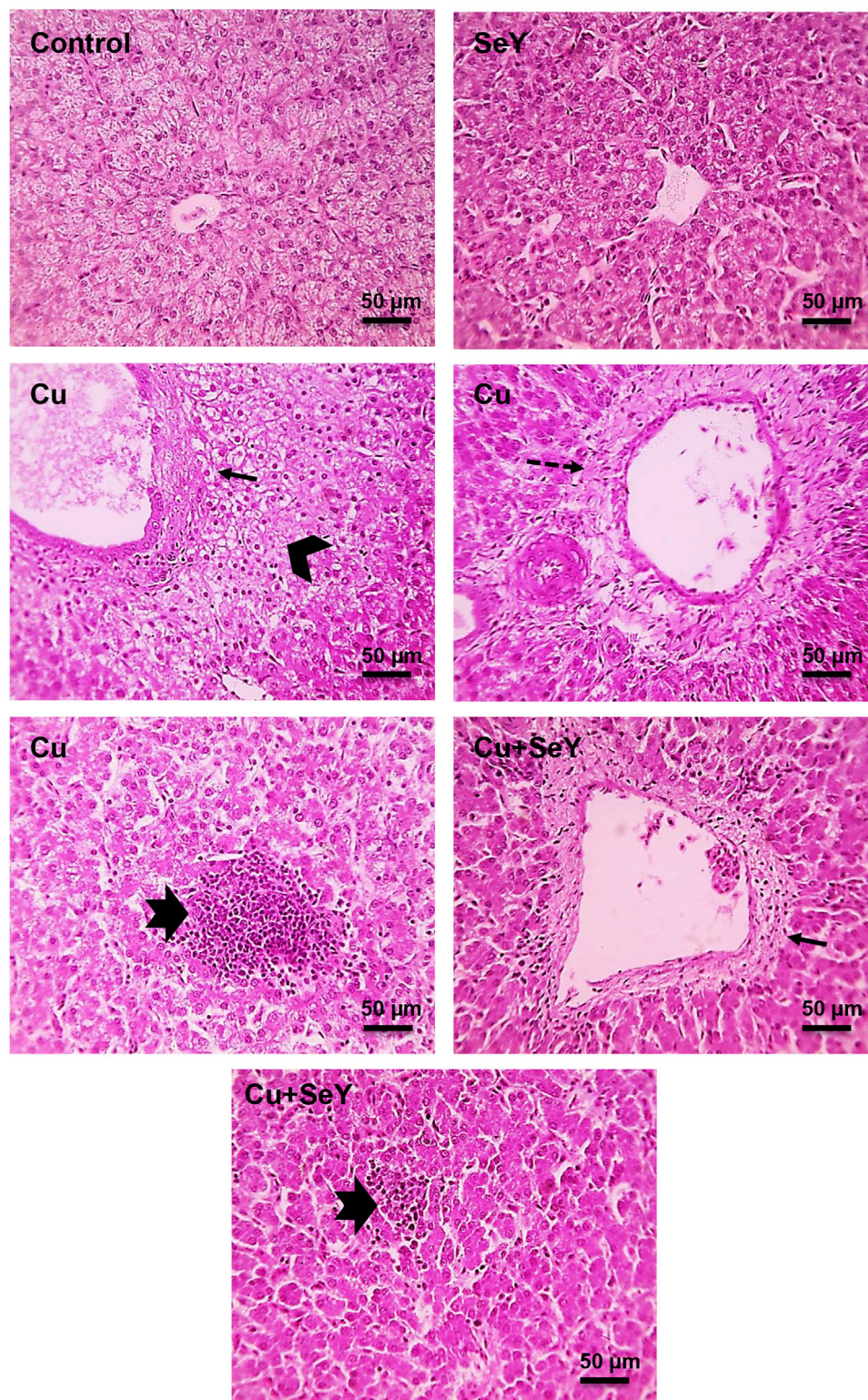


**FIGURE 6**

Microscopic picture of HE-stained liver sections from Control and SeY groups show normally arranged hepatocytes in radial plates around central veins with normal sinusoids and portal areas. However, liver sections from Cu group show portal fibrosis (thin black arrows), periportal coagulative necrosis of hepatocytes (black arrowheads), large lymphocytes follicular aggregation (thick black arrows). Cu+SeY group exhibited mild portal fibrosis (thin black arrows) with small lymphocytes follicular aggregation (thick black arrows). Bars = 50 μm.

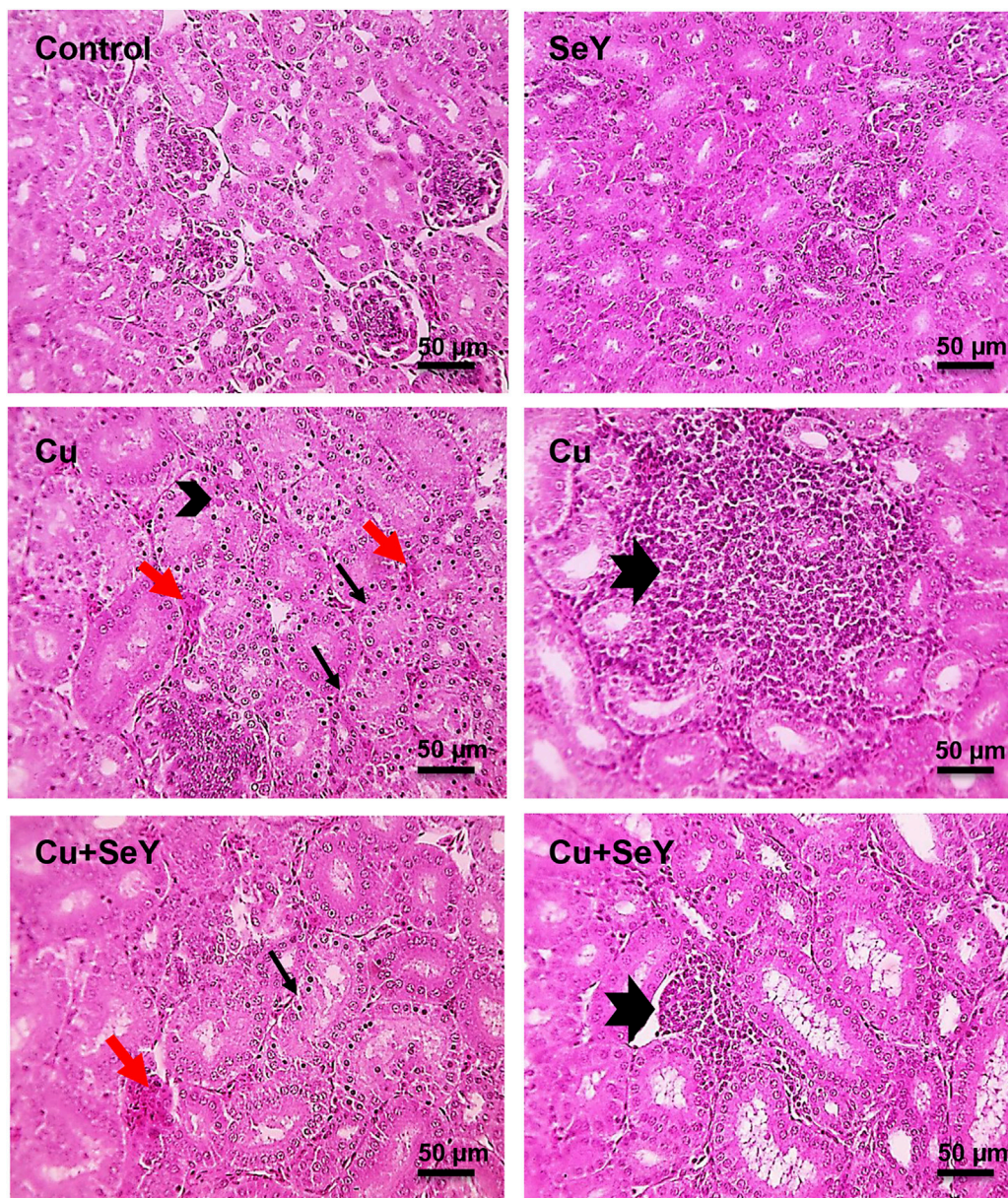


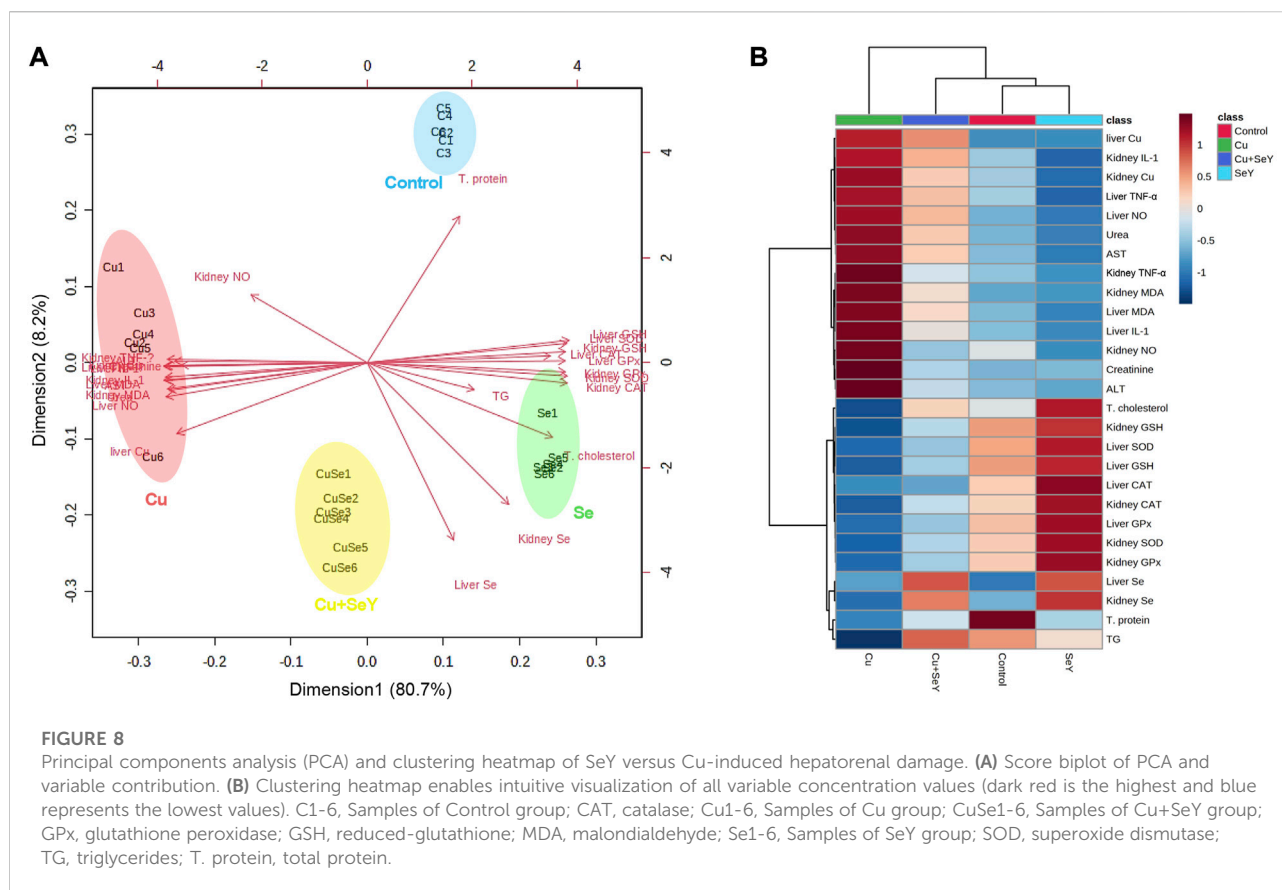
**FIGURE 7**

Microscopic pictures of HE-stained kidney sections from Control group and SeY group show normal tubules, glomeruli, and interstitial tissue. Kidney sections from Cu-treated group exhibit prominent tubular necrosis (thin black arrows), few apoptotic cells (arrowheads), congested inter-tubular blood vessels (red arrows), and large lymphocytes follicular aggregation in interstitial tissue (thick black arrows). Cu+SeY group presents mild tubular necrosis (thin black arrows), congested inter-tubular blood vessels (red arrows), and small lymphocytes follicular aggregation in interstitial tissue (thick black arrows). Bars = 50 µm.

markedly decrease lead overload in the skeletal muscles of intoxicated chickens (Liu et al., 2019). Additionally, raising chicken on 3 mg/kg SeY for 90 days evoked a noticeable reduction in the accumulation of cadmium in the chicken heart (Ge et al., 2021a). These findings indicated that SeY possesses an efficient metal chelation power *via* forming inactive complexes with heavy metals

and enhancing its excretion with subsequent decreases in their concentrations.

The accumulation of excess Cu in both hepatic and renal tissues resulted in disturbance in these organs' functions. Our findings showed significant increases in serum transaminases and decreased serum TP levels in the Cu-exposed group, implying hepatotoxicity because the liver is the central

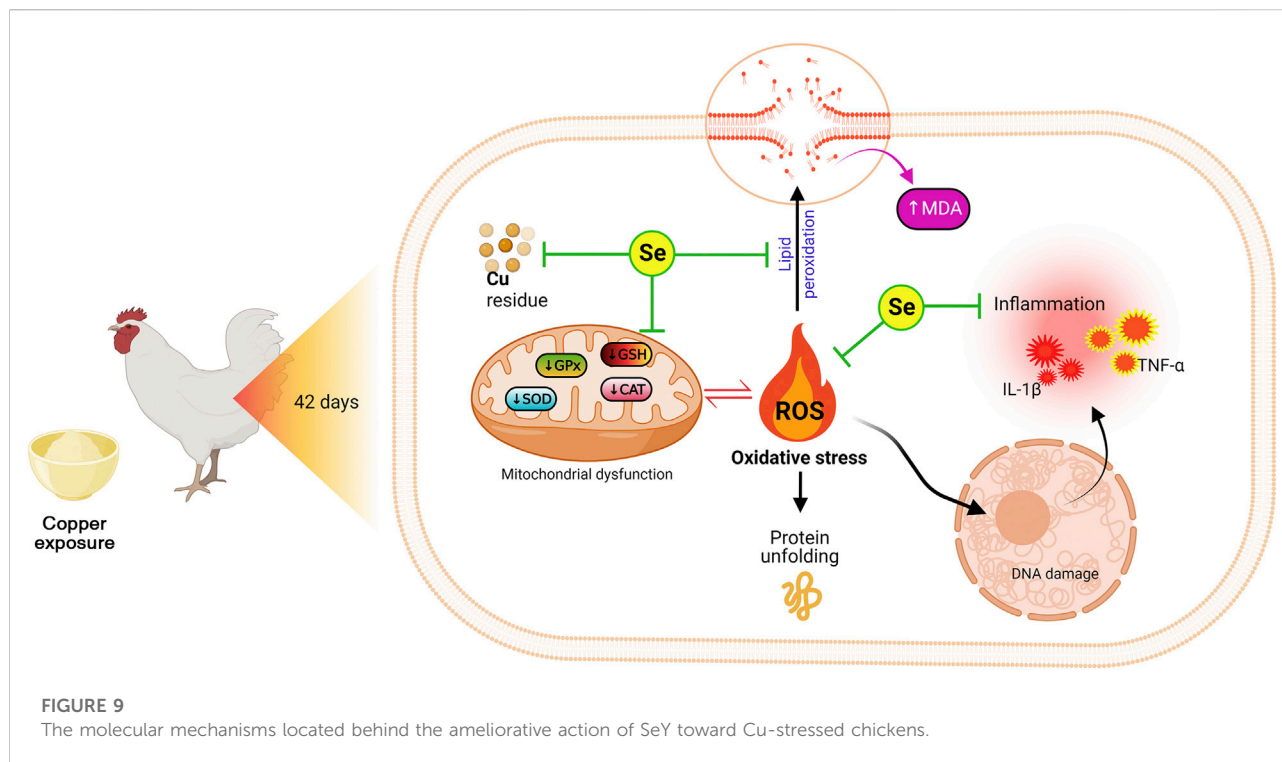


location for Cu accumulation. These findings agree with former studies (Wu et al., 2020; Hashem et al., 2021a). This may be endorsed for the hepatic damage that resulted in excess release of hepatic intracellular enzymes into the bloodstream (Atta et al., 2009). Additionally, the observed hypoproteinemia in our results may refer to the impairment in protein synthesis because of liver damage and/or excess protein loss due to renal insufficiency (Al Aboud et al., 2021). These results are well reinforced by the histopathological findings' periportal coagulative necrosis of hepatocytes. However, supplementation of 450 mg/kg copper proteinate decreased ALT in Bovans laying hens after exposure for 4 weeks, that may be due to the slightly restricted food consumption (Güçlü et al., 2008).

On the contrary, the present study showed that the dietary supplement SeY improved these liver damage biomarkers and decreased the hepatic histological irregularities caused by Cu stress. Similar outcomes were stated by Malyar et al. (2021), who found that selenium-rich *Saccharomyces cerevisiae* restored the liver function biomarkers in rats kept under high heat stress for 42 days. Moreover, SeY protected against ochratoxin-induced elevations in hepatic AST and ALT in chicken exposed to a contaminated diet for 21 days (Li et al., 2020b). Hence, the modulating effect of SeY on liver function markers indicated its

protective effect on the cell membrane of hepatocytes and block the enzyme leak into the blood circulation.

Since the kidney is the leading platform for the excretion of Cu, the renal tubules are vulnerable to Cu harm (Elazab et al., 2021). The analysis of renal function tests unveiled momentous upsurges in serum levels of urea and creatinine in  $\text{CuSO}_4$ -intoxicated birds. As the kidney discharges the nitrogenous end products of the catabolic process, the increases in both biomarkers indicate the impairment in kidney functions (Abdeen et al., 2021; Othman et al., 2021). The histopathological screening of the kidney validated these results characterized by prominent tubular necrosis, few apoptotic cells, congested inter-tubular blood vessels, and large lymphocytes follicular aggregation in the interstitial tissue. These outcomes align with former reports illustrating the adverse renal pathology induced by Cu toxicity in various animal models (Baruah et al., 2018; Hashem et al., 2021b). Wang and colleagues (Wang et al., 2017) reported that chickens exposed to  $\text{CuSO}_4$  at 300 mg/kg food level for 12 weeks also developed atrophied glomeruli and tubular casts. The tubular cells also experienced degeneration and necrosis. Hence, it could be concluded that Cu impaired both glomerular and tubular functions with deteriorations of overall renal performance.



Remarkably, this study's findings showed that SeY obviously counteracted Cu-encouraged renal dysfunction in exposed chicken. Ge et al, (2021b) reported similar results in cadmium-exposed chicken and co-treated with SeY for 90 days. Also, renal function-related biomarkers (creatinine, urea, and uric acid) displayed significant decreases in the SeY-supplemented chicken related to the ochratoxin-intoxicated group (Li et al., 2020a). This nephroprotective effect of SeY refers to its antioxidant effect, and this was confirmed pathologically by the improved renal histoarchitecture.

Our results also showed that birds supplemented with excess  $\text{CuSO}_4$  had marked declines in serum TG and TC compared with the controls, which coincides with previous reports (Idowu et al., 2011; Hashem et al., 2021a). The rate-limiting enzyme in the catabolic process of cholesterol 7-hydroxylase was found to be more active when Cu-supplemented meals were administered (Konjufca et al., 1997). Further, adding Cu to the chicken diet diminished the contents of GSH which suppressed the activity of  $\beta$ -methylglutaryl-CoA reductase with a subsequent decrease in the cholesterol level (Kim et al., 1992). Additionally, dietary Cu caused substantial drops in the hepatic lipogenic enzyme activity, 17 beta-estradiol, and plasma lipid levels (Pearce et al., 1983). Therefore, these reductions in TC and TG of Cu-exposed chickens are caused by reduced cholesterol synthesis, increased lipid degradation, or excretion rate. However, different outcomes were reported by earlier studies. Cinar and collaborators did not find any alteration in plasma total cholesterol levels in copper-exposed broilers (Cinar et al.,

2014). Additionally, marked decreases were reported in plasma triglycerides and cholesterol in Arbor-Acre unsexed broilers exposed to dietary  $\text{CuSO}_4$  or copper proteinate at 50, 100, or 150 mg/kg doses for 56 days (Jegade et al., 2011). These differences may endorse breed, diet components, and the investigational strategy. On the other side, the administration of SeY decreased the opposing effect of Cu on lipid metabolism-related markers. This might be attributed to the capacity of SeY to scavenge free radicals and defense against lipid structure peroxidation.

In addition to the induction of hepatorenal impairments in exposed broilers, Cu elicits over-generation hydroxyl radicals and hydrogen peroxide *via* Fenton and Haber-Weiss reactions (Wang et al., 2018). Many scholars have pointed out that the excess generation of ROS that overwhelm the cellular capacity is one of the hallmarks of heavy metals' harmful actions (Albarakati et al., 2020; Kassab et al., 2020; Al Aboud et al., 2021). These highly reactive radicals could modify the structure or/and function of cellular molecules. The current findings revealed that chickens exposed to dietary Cu developed an imbalance in their liver and kidney's oxidant/antioxidant status. SOD can hamper the superoxide anion and convert it into  $\text{H}_2\text{O}_2$ , which CAT dissociates into water (Albarakati et al., 2020). GPx significantly contributes to the protective function of CAT and is required for the regeneration of GSH. The significant increase in the levels of MDA in both organs indicated that Cu exposure enhanced the formation of  $\text{OH}^\bullet$  which directly interacted with the

polyunsaturated fatty acids in cellular membrane lipid, which led to lipid peroxidation (Wang et al., 2018). Zhao et al. (Zhao et al., 2018) found significant decreases in SOD activity and GSH content in the chicken jejunum in a time-dependent manner after dietary exposure to 300 mg/kg Cu. In another related study, decreases in SOD, CAT, and GPx with increases in MDA in the immune organs were reported in chicken fed on a diet containing Cu at different concentrations for 49 days (Yang et al., 2020). Nevertheless, CuSO<sub>4</sub> exposure for 30 days did not evoke significant differences in total antioxidant capacity in chicken jejunum (Zhao et al., 2018).

In contrast, our data demonstrated that SeY could enhance the hepatorenal antioxidant capacity by decreasing MDA levels and restoring the activity of GPx, SOD, CAT, and GSH concentrations. Se is a crucial cofactor for enzymes involved in scavenging ROS and dietary supplements of sodium selenide, and SeY increases birds' stress tolerance (Arnaut et al., 2021). Li et al. recorded upregulation of hepatic GPx, GLRX2, and MnSOD mRNA expression along with Nrf2 protein expression and its downstream (Keap-1 and HO-1) after dietary inclusion with 0.4 mg/kg SeY in broilers (Li et al., 2020a) suggesting the possible involvement of Nrf2/HO-1/Keap-1 in the protective role of SeY (Li et al., 2020b). Our data were in agreement with those obtained by Cao et al. who reported a reduced aluminum-induced testicular damage in mice after SeY supplementation *via* modifying the redox status (Cao et al., 2020). Elevated ROS can trigger the production of pro-inflammatory cytokines and different inflammatory cells and the release of inflammatory mediators (AL-Megrin et al., 2020). High dietary Cu exposure has been documented to enhance the IL-1 $\beta$  and TNF- $\alpha$  levels in chicken immune organs (Yang et al., 2020) and liver (Liu et al., 2018a). Concurrently, the existing experiment presented that Cu intoxication caused significant elevations in the IL-1 $\beta$  and TNF- $\alpha$ . Interestingly, the proposed findings indicated that SeY could antagonize the Cu-enhanced hepatic and renal inflammatory responses. Se-rich *S. cerevisiae* downregulated the hepatic gene expression of IL-6, TNF- $\alpha$ , COX-2, and NF- $\kappa$ B of heat stressed (Malyar et al., 2021) and aluminium-intoxicated (Luo et al., 2018) Wistar rats. Supporting a former study (Cao et al., 2020), SeY significantly mitigated aluminum-induced testicular toxicity by decreasing the level of NO and NOS activities. Therefore, we strongly assume that SeY might mitigate hepatorenal inflammation induced by Cu exposure *via* down-regulation of the inflammatory mediators.

Moreover, the PCA data indicated that all studied variables are clustered into four zones along Dimension1 (80.7% contribution) and Dimension2 (8.2% contribution). Such distribution was depending on different treatments, where, Cu-intoxicated birds were clustered on the left side and could be markedly discriminated from other treated groups confirming the occurrence of Cu toxicity. PCA also confirmed the protective effects of SeY supplementation since the Cu+SeY group has deviated to the midplane between Cu-intoxicated birds and non-intoxicated ones

(Control and SeY groups). Moreover, the clustering heatmap summarizes the concentration levels of all measured parameters among different groups. The heatmap suggests that the variable concentrations in the Cu-intoxicated group are negatively correlated to the same corresponding concentrations in other groups. The molecular mechanisms located behind the ameliorative action of SeY toward Cu-stressed chickens are illustrated in Figure 9.

## 5 Conclusion

Collectively, this study introduced the alleviating effect of SeY against Cu-induced liver and kidney damage. SeY could reduce the extra-release of inflammatory mediators (IL-1 $\beta$ , TNF- $\alpha$ , and NO) and suppress lipid peroxidation and metal bioaccumulation. These protective mechanisms may be achieved by enhancing the antioxidant enzymatic of SOD, CAT, and GPx, alongside elevating the GSH contents. We strongly suggest that SeY could be a potential feed supplement that offers therapeutic evidence against the Cu-induced liver and kidney injury in chickens. In the future studies, further investigations are required for unveiling the underlying mechanisms for the antagonistic efficacy of Se-Y against heavy metal-induced damage in birds.

## Data availability statement

The original contributions presented in the study are included in the article/supplementary material, further inquiries can be directed to the corresponding authors.

## Ethics statement

The animal study was reviewed and approved by Faculty of Veterinary Medicine Ethical Committee.

## Author contributions

OH: Conceptualization, Data curation, Formal analysis, Investigation, Methodology, Software, Writing—original draft, Writing—review and editing. XW: Conceptualization, Data curation, Formal analysis, Software, Visualization, Supervision, Validation, Writing—original draft, Writing—review and editing. HO and HG: Conceptualization, Data curation, Formal analysis, Writing—review and editing. AA and AZ: Formal analysis, Resources, Software, Validation, Writing—original draft. MG, AK, EE, and AE-M: Data curation, Formal analysis, Investigation, Methodology, Software, Visualization, Writing—original draft. MD, RS, and

BS: Data curation, Formal analysis, Software, Visualization, Writing—original draft. SI: Funding acquisition, Resources, Software, Validation, Visualization, Writing—original draft, Writing—review and editing. Ahmed Abdeen: Conceptualization, Data curation, Formal analysis, Funding acquisition, Investigation, Methodology, Resources, Software, Supervision, Visualization, Writing—review and editing.

## Funding

This research was funded by the Deanship of Scientific Research at King Khalid University through the Large Groups Project under grant number R.G.P2/200/43. This work was also funded by the Princess Nourah bint Abdulrahman University Researchers Supporting Project number (PNURSP2022R127), Princess Nourah bint Abdulrahman University, Riyadh, Saudi Arabia.

## Acknowledgments

The authors are grateful for the resources provided by the Deanship of Scientific Research at King Khalid University through the Large Groups Project under grant number

## References

- Abdeen, A., Samir, A., Elkomy, A., Aboubaker, M., Habotta, O. A., Gaber, A., et al. 2021. The potential antioxidant bioactivity of date palm fruit against gentamicin-mediated hepato-renal injury in male albino rats. *Biomed. Pharmacother.*, 143, 112154. doi:10.1016/j.biopha.2021.112154
- Aebi, H. (1984). Catalase *in vitro*. *Methods Enzymol.* 105, 121–126. doi:10.1016/s0076-6879(84)05016-3
- Al Aboud, D., Baty, R. S., Alsharif, K. F., Hassan, K. E., Zhery, A. S., Habotta, O. A., et al. (2021). Protective efficacy of thymoquinone or ebselen separately against arsenic-induced hepatotoxicity in rat. *Environ. Sci. Pollut. Res. Int.* 28, 6195–6206. doi:10.1007/s11356-020-10955-1
- Al-Megrin, W. A., Metwally, D. M., Habotta, O. A., Amin, H. K., Abdel Moneim, A. E., and El-Khadragy, M. (2020). Nephroprotective effects of chlorogenic acid against sodium arsenite-induced oxidative stress, inflammation, and apoptosis. *J. Sci. Food Agric.* 100, 5162–5170. doi:10.1002/jsfa.10565
- Albarakati, A. J. A., Baty, R. S., Aljoudi, A. M., Habotta, O. A., Elmahallawy, E. K., Kassab, R. B., et al. (2020). Luteolin protects against lead acetate-induced nephrotoxicity through antioxidant, anti-inflammatory, anti-apoptotic, and Nrf2/HO-1 signaling pathways. *Mol. Biol. Rep.* 47, 2591–2603. doi:10.1007/s11033-020-05346-1
- Arnaut, P. R., Da Silva Viana, G., Da Fonseca, L., Alves, W. J., Muniz, J. C. L., Pettigrew, J. E., et al. (2021). Selenium source and level on performance, selenium retention and biochemical responses of young broiler chicks. *BMC Vet. Res.* 17, 151–213. doi:10.1186/s12917-021-02855-4
- Atta, A. H., Fathy, S., Gohar, M., Jan, R., Kamel, G., Mounieir, S. M., et al. (2009). Prolonged administration of high doses of copper nicotinate to rats: Effect on biochemical and cellular constituents of blood and on copper level in serum, liver and muscle. *Int. J. Med. Med. Sci.* 1, 178–183. doi:10.5897/IJMMSS.9000191
- Attia, Y. A., Qota, E. M., Zeweil, H. S., Bovera, F., Abd Al-Hamid, A. E., and Sahledom, M. D. 2012. Effect of different dietary concentrations of inorganic and organic copper on growth performance and lipid metabolism of White Pekin male ducks. *Br. Poult. Sci.*, 53, 77–88. doi:10.1080/00071668.2011.650151

R.G.P2/200/43. Authors also acknowledge the Princess Nourah bint Abdulrahman University Researchers Supporting Project number (PNURSP2022R127), Princess Nourah bint Abdulrahman University, Riyadh, Saudi Arabia. The appreciation is also extended to the Center of Excellence in Screening of Environmental Contaminants (funded by STDF, Egypt) for the support provided to this research.

## Conflict of interest

The authors declare that the research was conducted in the absence of any commercial or financial relationships that could be construed as a potential conflict of interest.

## Publisher's note

All claims expressed in this article are solely those of the authors and do not necessarily represent those of their affiliated organizations, or those of the publisher, the editors and the reviewers. Any product that may be evaluated in this article, or claim that may be made by its manufacturer, is not guaranteed or endorsed by the publisher.

- Baruah, S., Goswami, S., and Kalita, D. (2018). Haematobiochemical and pathological alterations of chronic copper toxicity in ducks. *J. Animal Res.* 8, 283–287. doi:10.30954/2277-940X.04.2018.18
- Cao, C., Zhang, H., Wang, K., and Li, X. 2020. Selenium-rich yeast mitigates aluminum-mediated testicular toxicity by blocking oxidative stress, inhibiting NO production, and disturbing ionic homeostasis. *Biol. Trace Elem. Res.*, 195, 170–177. doi:10.1007/s12011-019-01820-5
- Chemists, A. O. O. A. (1925). *Official methods of analysis of the association of official analytical Chemists*. California, United States: The Association.
- Chen, H., Li, P., Shen, Z., Wang, J., and Diao, L. (2021). Protective effects of selenium yeast against cadmium-induced necroptosis through mir-26a-5p/pten/pi3k/akt signaling pathway in chicken kidney. *Ecotoxicol. Environ. Saf.* 220, 112387. doi:10.1016/j.ecoenv.2021.112387
- Cinar, M., Yildirim, E., Yigit, A. A., Yalcinkaya, I., Duru, O., Kisa, U., et al. 2014. Effects of dietary supplementation with vitamin C and vitamin E and their combination on growth performance, some biochemical parameters, and oxidative stress induced by copper toxicity in broilers. *Biol. Trace Elem. Res.*, 158, 186–96. doi:10.1007/s12011-014-9926-6
- Coulombe, J., and Favreau, L. (1963). A new simple semimicro method for colorimetric determination of urea. *Clin. Chem.* 9, 102–108. doi:10.1093/clinchem/9.1.102
- Elazab, S. T., Elshater, N. S., Kishaway, A. T., and Ei-Emam, H. A. (2021). Cinnamon extract and probiotic supplementation alleviate copper-induced nephrotoxicity via modulating oxidative stress, inflammation, and apoptosis in broiler chickens. *Animals*. 11, 1609. doi:10.3390/ani11061609
- Ellman, G. L. 1959. Tissue sulphydryl groups. *Arch. Biochem. Biophys.*, 82, 70–7. doi:10.1016/0003-9861(59)90090-6
- Gaetke, L. M., Chow-Johnson, H. S., and Chow, C. K. (2014). Copper: Toxicological relevance and mechanisms. *Arch. Toxicol.* 88, 1929–1938. doi:10.1007/s00204-014-1355-y
- Ge, J., Guo, K., Zhang, C., Talukder, M., Lv, M. W., Li, J. Y., et al. 2021a. Comparison of nanoparticle-selenium, selenium-enriched yeast and sodium selenite on the alleviation of cadmium-induced inflammation via NF-kB/IκB

- pathway in heart. *Sci. Total Environ.*, 773, 145442. doi:10.1016/j.scitotenv.2021.145442
- Ge, J., Liu, L. L., Cui, Z. G., Talukder, M., Lv, M. W., Li, J. Y., et al. (2021b). Comparative study on protective effect of different selenium sources against cadmium-induced nephrotoxicity via regulating the transcriptions of selenoproteome. *Ecotoxicol. Environ. Saf.*, 215, 112135. doi:10.1016/j.ecoenv.2021.112135
- Giambrone, J., and Clay, R. P. (1986). Vaccination of day-old broiler chicks against Newcastle disease and infectious bursal disease using commercial live and/or inactivated vaccines. *Avian Dis.* 30, 557–561. doi:10.2307/1590421
- Green, L. C., Wagner, D. A., Glogowski, J., Skipper, P. L., Wishnok, J. S., and Tannenbaum, S. R. (1982). Analysis of nitrate, nitrite, and [15N]nitrate in biological fluids. *Anal. Biochem.* 126, 131–138. doi:10.1016/0003-2697(82)90118-x
- Güçlü, B. K., Kara, K., Beyaz, L., Uyanik, F., Eren, M., and Atasever, A. (2008). Influence of dietary copper proteinate on performance, selected biochemical parameters, lipid peroxidation, liver, and egg copper content in laying hens. *Biol. Trace Elem. Res.*, 125, 1609. doi:10.1007/s12011-008-8164-1
- Habotta, O. A., Elbahnasy, S., and Ibrahim, I. (2022). Neurotoxicity of singular and combined exposure of *Oreochromis niloticus* to methomyl and copper sulphate at environmentally relevant levels: Assessment of neurotransmitters, neural stress, oxidative injury and histopathological changes. *Environ. Toxicol. Pharmacol.* 94, 103935. doi:10.1016/j.etap.2022.103935
- Hashem, M. A., Abd El Hamied, S. S., Ahmed, E., Amer, S. A., and El-Sharnouby, M. E. (2021a). Mitigating the growth, biochemical changes, genotoxic and pathological effects of copper toxicity in broiler chickens by supplementing vitamins C and E. *Animals*, 11, 1811. doi:10.3390/ani11061811
- Hashem, M. A., Abd El Hamied, S. S., Ahmed, E. M. A., Amer, S. A., and Hassan, A. M. (2021b). Alleviating effects of vitamins C and E supplementation on oxidative stress, hematobiochemical, and histopathological alterations caused by copper toxicity in broiler chickens. *Animals*, 11, 1739. doi:10.3390/ani11061739
- Hassan, M. A., Hozien, S. T., Abdel Wahab, M. M., and Hassan, A. M. (2022). Ameliorative effect of selenium yeast supplementation on the physio-pathological impacts of chronic exposure to glyphosate and or malathion in *Oreochromis niloticus*. *BMC Vet. Res.* 18, 159. doi:10.1186/s12917-022-03261-0
- Idowu, O., Ajuwon, O., Fafiolu, A., Oso, A., and Akinloye, O. (2011). Modulation of cholesterol and copper residue levels in muscles and blood serum of finishing broiler chickens fed copper and ascorbic acid supplements. *Pak. J. Nutr.* 10, 781–785. doi:10.3923/pjn.2011.781.785
- Ismail, T., Hegazi, E., Nassef, E., Habotta, O. A., and Gewaily, M. S. (2022). The optimized inclusion level of *Bacillus subtilis* fermented *Azolla pinnata* in Nile tilapia (*Oreochromis niloticus*) diets: Immunity, antioxidative status, intestinal digestive enzymes and histomorphometry, and disease resistance. *Fish. Physiol. Biochem.* 48, 767, 783. doi:10.1007/s10695-022-01076-2
- Jegade, A. V., Oduguwa, O. O., Bamgbose, A. M., Fanimo, A. O., and Nollet, L. (2011). Growth response, blood characteristics and copper accumulation in organs of broilers fed on diets supplemented with organic and inorganic dietary copper sources. *Br. Poult. Sci.*, 52, 133–139. doi:10.1080/00071668.2010.544714
- Kassab, R. B., Lokman, M. S., Daabo, H. M., Gaber, D. A., Habotta, O. A., Hafez, M. M., et al. (2020). Ferulic acid influences Nrf2 activation to restore testicular tissue from cadmium-induced oxidative challenge, inflammation, and apoptosis in rats. *J. Food Biochem.* 44, e13505. doi:10.1111/jfbc.13505
- Kieliszek, M., Błażejak, S., Gientka, I., and Bzducha-Wróbel, A. (2015). Accumulation and metabolism of selenium by yeast cells. *Appl. Microbiol. Biotechnol.* 99, 5373–5382. doi:10.1007/s00253-015-6650-x
- Kim, J. W., and Kil, D. Y. (2015). Determination of relative bioavailability of copper in tribasic copper chloride to copper in copper sulfate for broiler chickens based on liver and feather copper concentrations. *Animal Feed Sci. Technol.* 210, 138–143. doi:10.1016/j.anifeeds.2015.09.022
- Kim, S., Chao, P. Y., and Allen, K. G. (1992). Inhibition of elevated hepatic glutathione abolishes copper deficiency cholesterolemia. *FASEB J.* 6, 2467–2471. doi:10.1096/fasebj.6.7.1563598
- Konjufca, V. H., Pesti, G. M., and Bakalli, R. I. (1997). Modulation of cholesterol levels in broiler meat by dietary garlic and copper. *Poult. Sci.* 76, 1264–1271. doi:10.1093/ps/76.9.1264
- Larsen, K. (1972). Creatinine assay in the presence of protein with LKB 8600 reaction rate analyser. *Clin. Chim. Acta.* 38, 475–476. doi:10.1016/0009-8981(72)90146-5
- Leary, S., Underwood, W., Anthony, R., Corey, D., Grandin, T., Gwaltney-Brant, S., et al. (2016). in *AVMA guidelines for the humane slaughter of animals: 2016 edition*. Editor A. V. M. Association (Schaumburg, Illinois, United States: AVMA), 64.
- Li, K., Cao, Z., Guo, Y., Tong, C., Yang, S., Long, M., et al. (2020a). Selenium yeast alleviates ochratoxin A-induced apoptosis and oxidative stress via modulation of the PI3K/AKT and Nrf2/Keap1 signaling pathways in the kidneys of chickens. *Oxid. Med. Cell. Longev.* 2020, 4048706. doi:10.1155/2020/4048706
- Li, P., Li, K., Zou, C., Tong, C., Sun, L., Cao, Z., et al. (2020b). Selenium yeast alleviates ochratoxin A-induced hepatotoxicity via modulation of the PI3K/AKT and Nrf2/Keap1 signaling pathways in chickens. *Toxins* 12, 143. doi:10.3390/toxins12030143
- Li, X., Hua, J., Wang, S., Hu, Z., Wen, A., and Yang, B. (2022). Genes and signaling pathways involved in the regulation of selenium-enriched yeast on liver metabolism and health of broiler (Gallus gallus). *Biol. Trace Elem. Res.* 2022, 1–16. doi:10.1007/s12011-022-03150-5
- Liao, J., Yang, F., Bai, Y., Yu, W., Qiao, N., Han, Q., et al. (2021). Metabolomics analysis reveals the effects of copper on mitochondria-mediated apoptosis in kidney of broiler chicken (Gallus gallus). *J. Inorg. Biochem.* 224, 111581. doi:10.1016/j.jinorgbio.2021.111581
- Liu, J., Zhao, H., Wang, Y., Shao, Y., Li, J., and Xing, M. (2018a). Alterations of antioxidant indexes and inflammatory cytokine expression aggravated hepatocellular apoptosis through mitochondrial and death receptor-dependent pathways in Gallus gallus exposed to arsenic and copper. *Environ. Sci. Pollut. Res. Int.* 25, 15462–15473. doi:10.1007/s11356-018-1757-0
- Liu, J., Zhao, H., Wang, Y., Shao, Y., Zhang, L., and Xing, M. (2018b). Impacts of simultaneous exposure to arsenic (III) and copper (II) on inflammatory response, immune homeostasis, and heat shock response in chicken thymus. *Int. Immunopharmacol.* 64, 60–68. doi:10.1016/j.intimp.2018.08.021
- Liu, Z., Zhang, F., Lu, P., Zhao, R., Zhang, H., Song, B., et al. (2019). Selenium-yeast alleviated inflammatory damage caused by lead via inhibiting ras/erk pathway and inflammatory factors in chicken skeletal muscles. *Biol. Trace Elem. Res.* 190, 493–500. doi:10.1007/s12011-018-1558-9
- Lowry, O., Rosebrough, N., Farr, A. L., and Randall, R. (1951). Protein measurement with the Folin phenol reagent. *J. Biol. Chem.* 193, 265–275. doi:10.1016/s0021-9258(19)52451-6
- Lu, L., Wang, R. L., Zhang, Z. J., Steward, F. A., Luo, X., and Liu, B. (2010). Effect of dietary supplementation with copper sulfate or tribasic copper chloride on the growth performance, liver copper concentrations of broilers fed in floor pens, and stabilities of vitamin E and phytase in feeds. *Biol. Trace Elem. Res.* 138, 181–189. doi:10.1007/s12011-010-8623-3
- Luo, J., Li, X., Li, X., He, Y., Zhang, M., Cao, C., et al. (2018). Selenium-Rich Yeast protects against aluminum-induced peroxidation of lipid and inflammation in mice liver. *Biometals*, 31, 1051–1059. doi:10.1007/s10534-018-0150-2
- Malyar, R. M., Naseri, E., Li, H., Ali, I., Farid, R. A., Liu, D., et al. (2021). Hepatoprotective effects of selenium-enriched probiotics supplementation on heat-stressed wistar rat through anti-inflammatory and antioxidant effects. *Biol. Trace Elem. Res.* 199, 3445–3456. doi:10.1007/s12011-020-02475-3
- Ohkawa, H., Ohishi, N., and Yagi, K. (1979). Assay for lipid peroxides in animal tissues by thiobarbituric acid reaction. *Anal. Biochem.* 95, 351–358. doi:10.1016/0003-2697(79)90738-3
- Othman, M. S., Khaled, A. M., Al-Bagawi, A. H., Fareid, M. A., Ghany, R. A., Habotta, O. A., et al. (2021). Hepatorenal protective efficacy of flavonoids from *ocimum basilicum* extract in diabetic albino rats: A focus on hypoglycemic, antioxidant, anti-inflammatory and anti-apoptotic activities. *Biomed. Pharmacother.*, 144, 112287. doi:10.1016/j.biopha.2021.112287
- Paglia, D. E., and Valentine, W. N. (1967). Studies on the quantitative and qualitative characterization of erythrocyte glutathione peroxidase. *J. Lab. Clin. Med.* 70, 158–169. doi:10.5555/uri:pii:002214367900765
- Pearce, J., Jackson, N., and Stevenson, M. H. (1983). The effects of dietary intake and of dietary concentration of copper sulphate on the laying domestic fowl: Effects on some aspects of lipid, carbohydrate and amino acid metabolism. *Br. Poult. Sci.* 24, 337–48. doi:10.1080/00071668308416748
- Reitman, S., and Frankel, S. (1957). A colorimetric method for the determination of serum glutamic oxalacetic and glutamic pyruvic transaminases. *Am. J. Clin. Pathol.* 28, 56–63. doi:10.1093/ajcp/28.1.56
- Sun, Y., Oberley, L. W., and Li, Y. (1988). A simple method for clinical assay of superoxide dismutase. *Clin. Chem.* 34, 497–500. doi:10.1093/clinchem/34.3.497
- Wang, Y., Chen, H., Chang, W., Chen, R., Xu, S., and Tao, D. (2020a). Protective effects of selenium yeast against cadmium-induced necroptosis via inhibition of oxidative stress and MAPK pathway in chicken liver. *Ecotoxicol. Environ. Saf.* 206, 111329. doi:10.1016/j.ecoenv.2020.111329
- Wang, Y., Liu, J., Chen, R., Qi, M., Tao, D., and Xu, S. (2020b). The antagonistic effects of selenium yeast (SeY) on cadmium-induced inflammatory factors and the

heat shock protein expression levels in chicken livers. *Biol. Trace Elem. Res.* 198, 260–268. doi:10.1007/s12011-020-02039-5

Wang, Y., Zhao, H., Liu, J., Shao, Y., Li, J., Luo, L., et al. (2018). Copper and arsenic-induced oxidative stress and immune imbalance are associated with activation of heat shock proteins in chicken intestines. *Int. Immunopharmacol.* 60, 64–75. doi:10.1016/j.intimp.2018.04.038

Wang, Y., Zhao, H., Shao, Y., Liu, J., Li, J., and Xing, M. (2017). Copper or/and arsenic induce oxidative stress-cascaded, nuclear factor kappa B-dependent inflammation and immune imbalance, triggering heat shock response in the kidney of chicken. *Oncotarget* 8, 98103–98116. doi:10.18632/oncotarget.21463

Wu, X., Zhu, M., Jiang, Q., and Wang, L. 2020. Effects of copper sources and levels on lipid profiles, immune parameters, antioxidant defenses, and trace element residues in broilers. *Biol. Trace Elem. Res.*, 194, 251–258. doi:10.1007/s12011-019-01753-z

Yang, F., Liao, J., Yu, W., Pei, R., Qiao, N., Han, Q., et al. (2020). Copper induces oxidative stress with triggered NF- $\kappa$ B pathway leading to inflammatory responses in immune organs of chicken. *Ecotoxicol. Environ. Saf.* 200, 110715. doi:10.1016/j.ecoenv.2020.110715

Zhao, H., Wang, Y., Shao, Y., Liu, J., Liu, Y., and Xing, M. 2018. Deciphering the ionic homeostasis, oxidative stress, apoptosis, and autophagy in chicken intestine under copper(II) stress. *Environ. Sci. Pollut. Res. Int.*, 25, 33172–33182. doi:10.1007/s11356-018-3163-z

Zhao, Y., Zhang, H., Hao, D., Wang, J., Zhu, R., Liu, W., et al. 2022. Selenium regulates the mitogen-activated protein kinase pathway to protect broilers from hexavalent chromium-induced kidney dysfunction and apoptosis. *Ecotoxicol. Environ. Saf.*, 239, 113629. doi:10.1016/j.ecoenv.2022.113629

# Frontiers in Pharmacology

Explores the interactions between chemicals and living beings

The most cited journal in its field, which advances access to pharmacological discoveries to prevent and treat human disease.

## Discover the latest Research Topics

[See more →](#)

### Frontiers

Avenue du Tribunal-Fédéral 34  
1005 Lausanne, Switzerland  
[frontiersin.org](http://frontiersin.org)

### Contact us

+41 (0)21 510 17 00  
[frontiersin.org/about/contact](http://frontiersin.org/about/contact)

